WIND-TUNNEL STUDIES OF PRESSURE DISTRIBUTION ON ELEMENTARY BUILDING FORMS

by

Ning Chien, Yin Feng, Hung-Ju Wang,
and Tien-To Siao

Project Sponsored
by the
Office of Naval Research
under
Contract N8onr-500

Iowa Institute of Hydraulic Research
State University of Iowa
Iowa City

1951

Air Infiltration and Ventilation Centre
University of Warwick Science Park
Barclays Venture Centre
Sir William Lyons Road
Coventry CV4 7EZ
Great Britain
Telephone: (0203) 692050
Telex: 312401
Fax: (0203) 410156

22. 6. 91

ınd Tien-To Siao

:search
ı

buildings is essential to the achievement
nethods of securing such knowledge are
:stimates contained in various building
ıs scale-model investigations; and, third,
ilding under consideration. Needless to
ıan overall orders of magnitude. Avail-
ɔ other geometric proportions. Finally,
facilities or sufficient funds to arrange
.lue, therefore, would be a series of in-
:ystematically a considerable range of

ktensive assortment of data, from which
ɔource material of this nature includes a
sts by Dryden and Hill [2] on a model of
·ehensive list of references given by
ıs other papers [4-6]. Each of these
e are fairly broad in their coverage. Only
many investigators, however, could repre-
sentative data be obtained, and even then numerous gaps would remain.

In order to provide a systematic series of test results over a practically useful range of building proportions, the Iowa Institute of Hydraulic Research undertook in 1946 a carefully planned program of wind-pressure investigations. Following an exploratory study conducted in a two-dimensional tunnel as a master's thesis [7], a very extensive thesis project [8] involved tests in a three-dimensional tunnel on a wide assortment of simply-gabled block-type structures. As an Institute project sponsored by the Office of Naval Research, these tests were then extended to thin walls, hangar-type structures, and simple building groups. At the time of writing, another graduate thesis [9] is being prepared on the subject of the effects of parapets. Except for the latter study, all results which have been obtained to date are presented in the following pages.

THEORETICAL CONSIDERATIONS

The distribution of pressure around any body immersed in a moving fluid depends very closely upon the local variation in fluid velocity which the body produces, in accordance with the elementary pressure-velocity relationship [10],

$$p - p_0 = \frac{\rho v_0^2}{2} - \frac{\rho v^2}{2}$$

Evidently, as the velocity v increases above its initial value v_0, the pressure p decreases, and vice versa, in proportion to the density ρ and the square of the velocity. While the decrease in pressure

is not restricted by this equation, its increase is limited to the value $(p - p_0)_{max} = \rho v_0^2/2$ at a point of stagnation or zero velocity. Introduction of the notation $\Delta p = p - p_0$ and division of each term by this reference value $\rho v_0^2/2$ reduces the foregoing equation to the more general dimensionless form

$$\frac{\Delta p}{\rho v_0^2/2} = 1 - \left(\frac{v}{v_0}\right)^2$$

This equation is independent of the dimensional system used, the numerical value of each ratio being the significant factor regardless of the actual magnitude of each individual quantity. For example, at a stagnation point $\Delta p/(\rho v_0^2/2)$ invariably has a magnitude of unity.

Just as the pressure distribution depends upon the velocity variation which the body produces, the velocity variation in turn is related to the pattern of the surrounding flow. Thus, according to the continuity principle, the velocity will decrease where the stream lines are caused to diverge and increase where the stream lines are caused to converge. This flow pattern, finally, is controlled by three independent groups of factors: the geometric dimensions of the body, the kinematic characteristics of the undistrubed flow, and the dynamic properties of the fluid. Thus, the body and its orientation can be fully described by a series of linear dimensions and one or more angles, the oncoming flow by its distribution of velocity, and the fluid by its mass density ρ and viscosity μ. Like the pressure-velocity relationship, these factors may be grouped dimensionlessly for purposes of generalization. In other words, the relative proportions of the body may be represented by a series of geometric ratios (such as length to height L/H, width to height B/H, etc.). The velocity v at any elevation y may be divided by some average value V_0 characteristic of the approaching flow to yield v/V_0 and the elevation may be divided by the body height to yield y/H. Finally, the ratio of the accelerative characteristics to the viscous characteristics of the flow takes the form of the Reynolds number $R = \rho V_0 H/\mu = V_0 H/\nu$.

In general, therefore, the relative pressure distribution around any body - such as a building in a wind - will depend upon the body form, the velocity characteristics of the oncoming flow, and the Reynolds number. If each of these independent dimensionless factors is held constant, the relative distribution of pressure will also remain constant, regardless of changes in the actual magnitudes of the individual variables involved. As a result, a full-scale building may be tested at model scale in either air or water, provided only that the model is geometrically similar to its prototype in form and orientation, the velocity distribution in the approaching flow is kinematically similar, and the mean velocity in the model is such as to yield dynamic similarity - that is, equality of the Reynolds numbers - for the given prototype velocity, model scale, and fluid properties.

Construction of a building model to any given scale involves little difficulty, particularly if it is the effect of the overall proportions which is to be studied rather than that of the small details. Under such circumstances, the details are ordinarily not reproduced. It should be noted, however, that in certain instances such apparently minor factors as surface roughness can play a vital role if the flow is in a critical state between two different regimes.

Simulation of any desired velocity distribution in the approaching flow is also a fairly simple matter, through use of successive upstream screens of the proper height and mesh [11]. A logarithmic function of the form $v = A \log y + B$ (see Fig. 1) satisfactorily reproduces average wind characteristics [3].

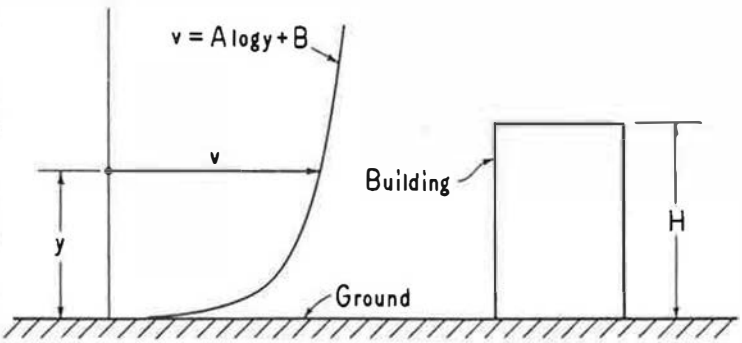

Fig. 1. Definition sketch for vertical distribution of wind velocity.

The fact nevertheless remains that too little is generally known about prototype conditions to select appropriate values of the two constants, since meteorological reports are usually given in terms of the velocity at some arbitrary elevation. Moreover, natural winds are by no means steady, the mean flow being accompanied by gusts of a magnitude which is predictable only statistically. Wind-tunnel tests, therefore, are usually conducted in an air stream of constant velocity corresponding to the nominal meteorological value. This yields higher base pressures than those

in a stream in which the velocity decreases with decreasing elevation; however, it does not include the effects of intermittent gusts, which can only be approximated by applying to the nominal velocity an arbitrary multiplying factor in accordance with local meteorological records.

Complete dynamic similarity between model and prototype is considerably more difficult to attain, because - if the same fluid is used - constancy of the Reynolds number requires a change in velocity which is inversely proportional to the change in linear scale. Since the average model building would have to be reduced at least thirty-fold to be accommodated without constriction effects in the average wind-tunnel, and since winds below 50 miles per hour are seldom of practical interest, this would require a model air speed of at least 1500 miles per hour. Not only is such a value well above the velocity of sound in air, but a rough computation will show that a mean air speed even as low as 250 miles per hour can result in appreciable effects of compressibility. The possibility of conducting tests in a water channel would have the advantage of a ten-fold decrease in viscosity - and hence in velocity - as compared with tests in air, but such water speeds (with comparable cross-sectional dimensions) are practically out of the question.

To compensate for this apparent dilemma is the fortunate circumstance that duplication of the prototype Reynolds number is not directly necessary unless the body under study is well streamlined [12], since only then (for the velocity range in question) do viscous influences generally govern the flow pattern. The extent to which the Reynolds criterion of similarity can be disregarded thus depends largely upon the extent to which the body to be tested departs from the streamlined ideal. Most buildings are so angular that the flow patterns around them (Fig. 2a) are quite independent of viscous influence (assuming the velocity distribution of the approaching flow to be the same), and dynamic similarity between model and prototype will be attained at velocities even well below that which is being simulated.

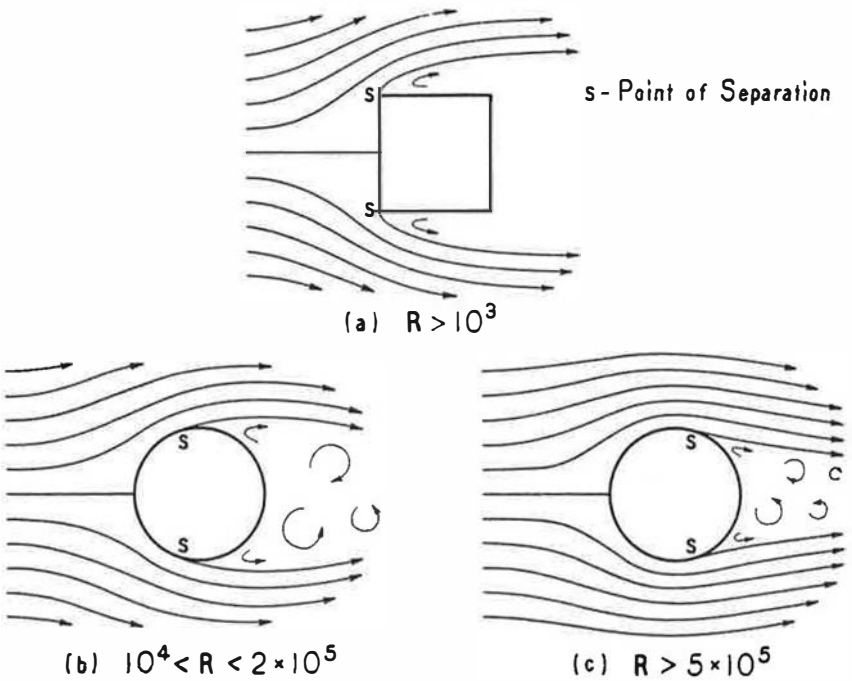

Fig. 2. Patterns of flow past square and circular sections.

Structural forms which are rounded rather than angular, on the other hand, produce a fairly constant average pattern (Fig. 2b) over a considerable range of moderately high Reynolds numbers, and another fairly constant pattern (Fig. 2c) at very high Reynolds numbers, but the borderline between the two is primarily a viscous function. Typical of such forms are cylindrical chimneys and tanks. It is known, however, that roughening the body surface produces a transition from the one type of pattern to the other at a lower Reynolds number [13], and this experimental technique is frequently used to obtain essential similarity without the excessively high test velocities otherwise required.

Once a sufficiently good degree of probable agreement between model and prototype conditions is ensured, the investigation involves simply the measurement either of pressure intensities at all desired locations or, in some instances, of the overall force upon the model. If the local pressure intensities are measured in sufficient detail, of course, their proper summation over the model surface will yield indirectly either the resultant force or its rectilinear components. Reduction of the pressure measurements to the dimensionless form $\Delta p/(\rho V_0^2/2)$ - or of the force measurements to the comparable form $F/(A\rho V_0^2/2)$ - will then result in a generalized series of numerical values from which the corresponding prototype conditions may be determined for any desired wind speed.

EXPERIMENTAL PROCEDURE

The wind-tunnel used in the investigations herein described was of the low-velocity non-recirculating type [14], air being drawn into a large stilling chamber through windows at one end of the Institute laboratory and eventually exhausted through windows at either side. An entrance bell with honeycomb led from the baffled stilling chamber into the channel proper, the test section of which (see Fig. 3) was 4 feet high, 6 feet wide, and 20 feet long. A 60-inch centrifugal fan driven by a $7\frac{1}{2}$-horsepower motor immediately followed the test section. The velocity over the available range from 1 to 25 feet per second was controlled by adjustable louvers at the downstream end of the test section in conjunction with a two-fold change in motor speed. Except for the boundary-layer zone next to the tunnel walls, the velocity of the air stream was within 1 percent of constancy over the test section. In order that the measurements would be essentially free from this boundary-layer influence, instead of being placed on the tunnel floor the models were mounted at the center of a plate of 0.082-inch aluminum 2 feet wide and 3 feet long supported on slender posts 6 inches above the floor. This plate could be turned to simulate any desired wind orientation.

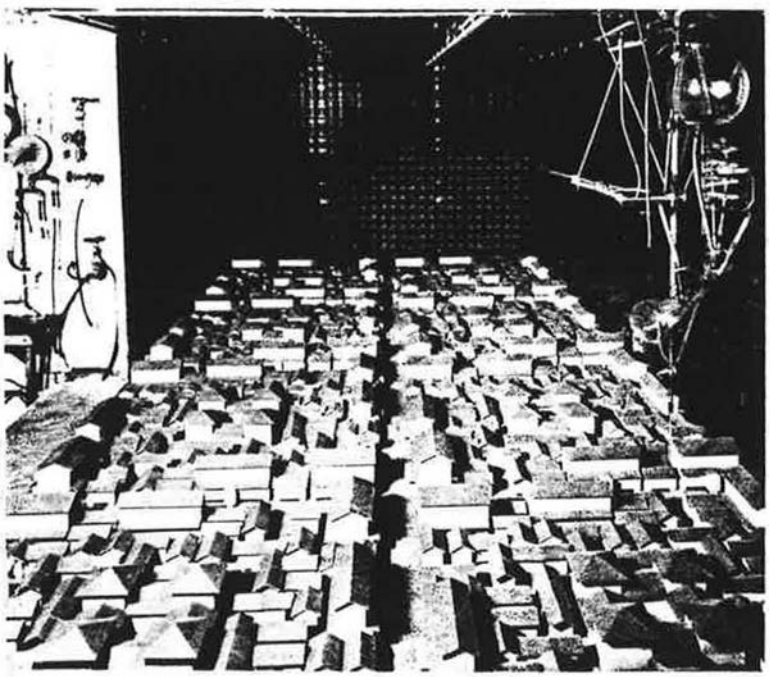

Fig. 3. View of wind-tunnel test section during investigation of gas diffusion in an urban district.

The models themselves were carefully constructed of 1/8-inch sheet plastic (Lucite or Plexiglass) in the series of unit combinations summarized in Fig. 4. For the block forms with gable roofs, the units consisted of 4-by-4-inch and 4-by-8-inch blocks each 2 inches high (the largest composite model being 16 inches long, 4 inches wide, and 6 inches high), and corresponding gables with roof pitches of 15°, 30°, and 45°. The hangar forms consisted of semi-cylinders having a constant diameter of 6 inches and lengths varying from 3 to 24 inches. The single walls were varied systematically from 16 inches long by 2 inches high to 4 inches long by 6 inches high, each being 3/8 inch thick. All units were fastened together in the desired combinations by means of small machine screws and keys, joints being sealed with cellulose tape wherever necessary. Typical model units are shown in Figs. 5, 6, and 7.

Piezometer holes were placed in only a few of the units, and these were then shifted from place to place in the structure until complete pressure-distribution data for the structure as a whole were obtained. In each position the piezometer unit overlapped its neighboring positions, thus ensuring continuity of pressure data and permitting detection of accidental leakage. A typical unit contained as many as 62 piezometer holes, each of which was 1/32 inch in diameter, closely spaced where the gradients

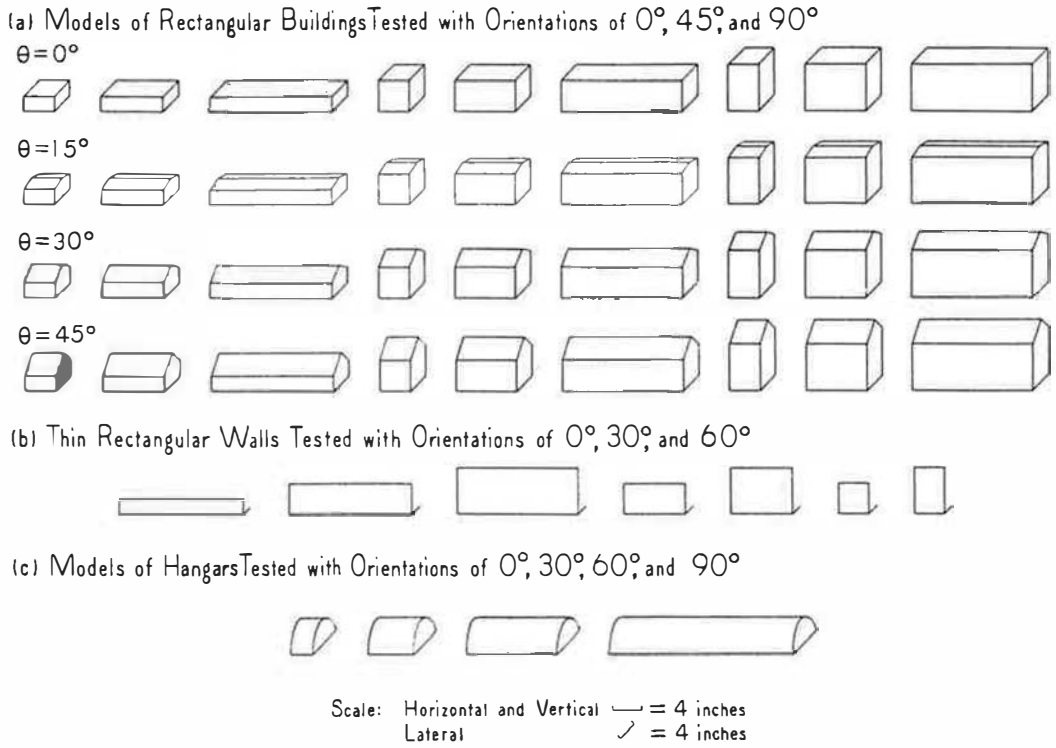

Fig. 4. Summary chart of model proportions.

were expected to be high and farther apart in other zones; no piezometers were closer than 1/16 inch to the edges of the surfaces. The locations of the piezometer holes and details of piezometer construction are shown in Figs. 8, 9, and 10. All pressure leads consisted of 3/16-inch rubber tubing passed through a central hole in the bottom of the aluminum plate and thence downstream to the door of the observation chamber.

Velocity measurements in the undisturbed flow 3 feet upstream from the model location were made by means of a Prandtl-Pitot tube connected to a sensitive differential gage of the Wahlen type reading

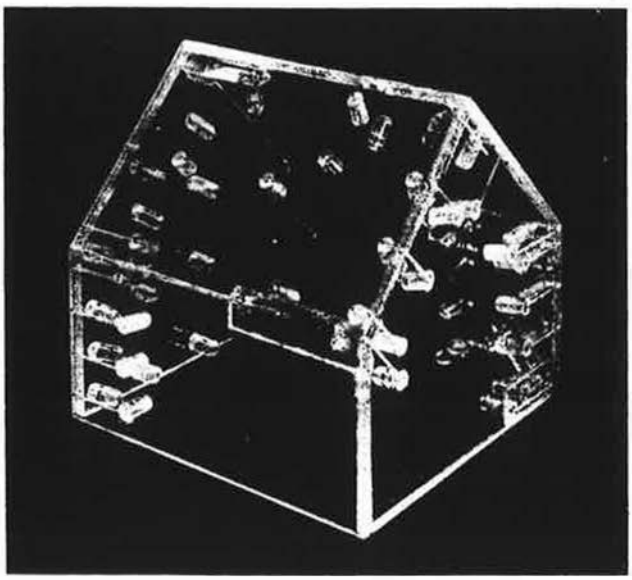

Fig. 5. Model of building with gabled roof.

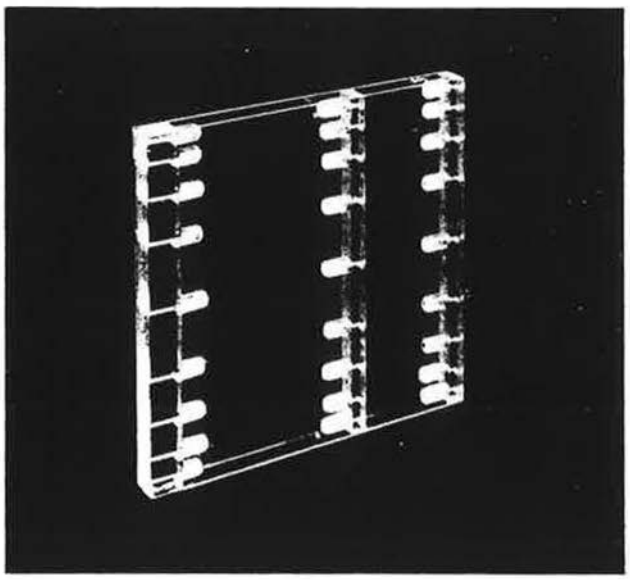

Fig. 6. Model of vertical rectangular wall.

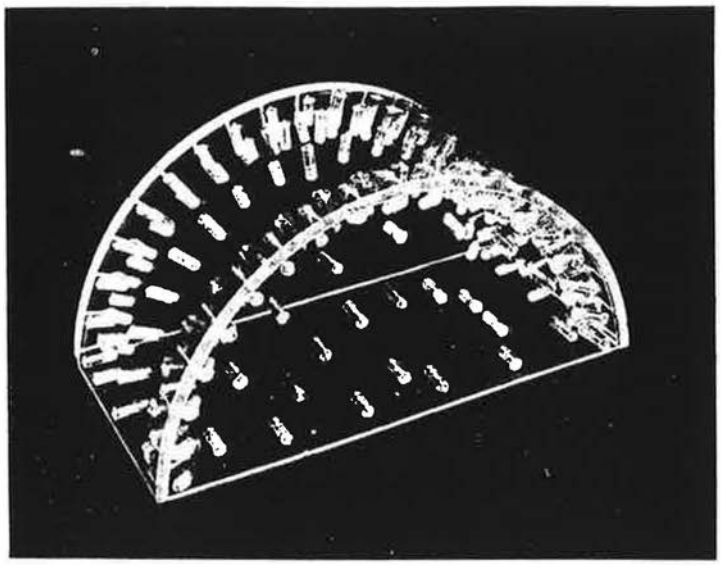

Fig. 7. Model of hangar-type structure.

to 0.001 inch of alcohol [15]. The same gage was used for the measurement of pressure distribution, one leg of the gage then being connected to a reference piezometer in the floor of the test section 3 feet ahead of the model. As the test velocities were invariably greater than 20 feet per second, the sensitivity of the gage reading was about 1 percent of the stagnation pressure. The overall probable error for each point, on the other hand, was on the order of ± 2 percent. However, the method of presenting the results in a generalized fashion tended to minimize local errors, just as passing a smooth curve through any series of point measurements serves to offset their experimental scatter.

The size of most of the models was sufficiently small in comparison with that of the tunnel cross section for the effect of the constriction upon the velocity to be practically negligible. The two largest buildings (the 3 x 24-inch hangar and the 8 x 16-inch block), to be sure, had projected areas which reduced the 4 x 6-foot flow passage by about 2 and 4 percent, respectively. However, the resulting errors in the velocity distribution in the immediate vicinity of such models are about one-fourth the computed change in mean velocity, and hence no corrections were considered necessary.

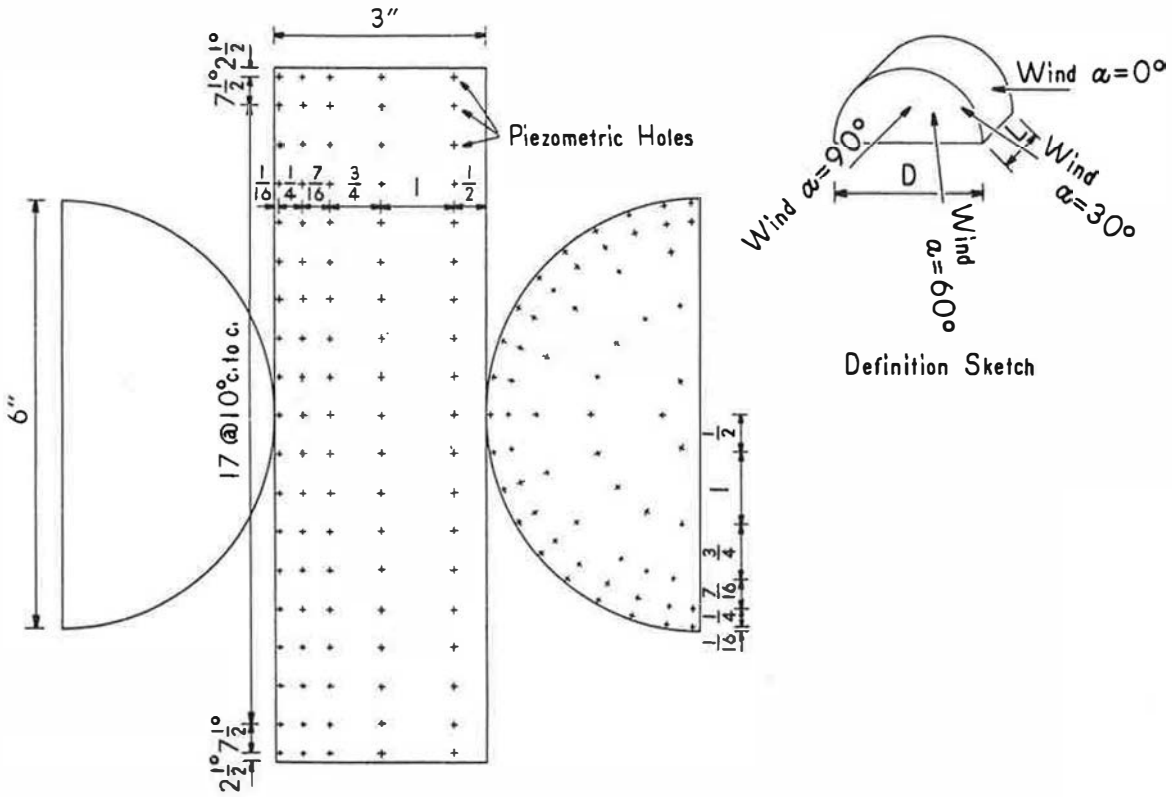

Fig. 8. Arrangement of piezometers on a hangar unit.

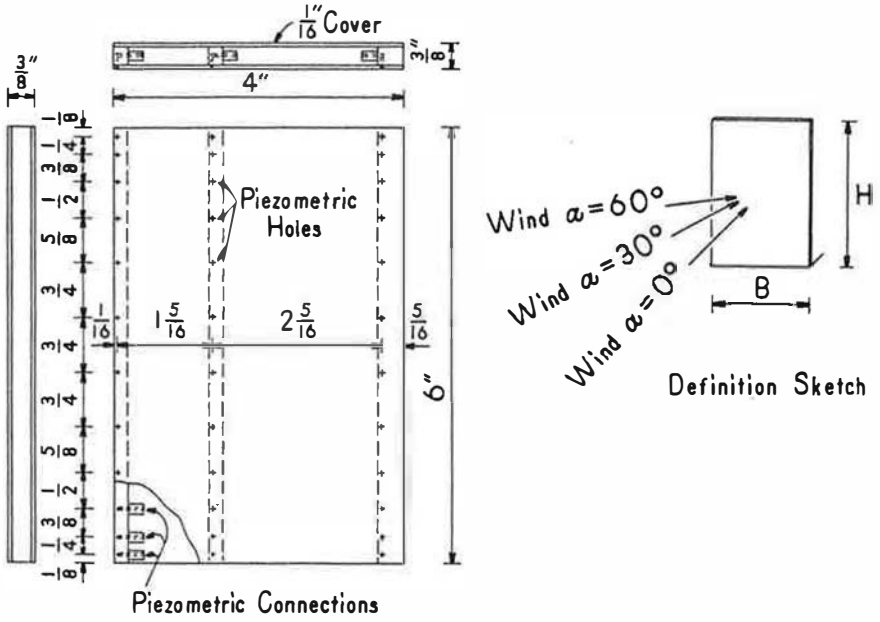

Fig. 9. Arrangement of piezometers on wall unit.

In addition to the pressure readings, observations of the flow patterns were made by means of smoke plumes resulting from the application of titanium tetrachloride. As seen in Fig. 11, this technique clearly reveals the outlines of the eddies produced in zones of separation. These are of three rather distinct types: First, the eddy with transverse axis which forms at the upstream base of a normal structure as the result of boundary resistance (i.e., the reduced boundary velocity of the approaching flow). Second, the eddy with transverse axis which forms beyond the abrupt discontinuity produced by the edge of a wall or roof. Third, the longitudinal vortices which form in combination with the other

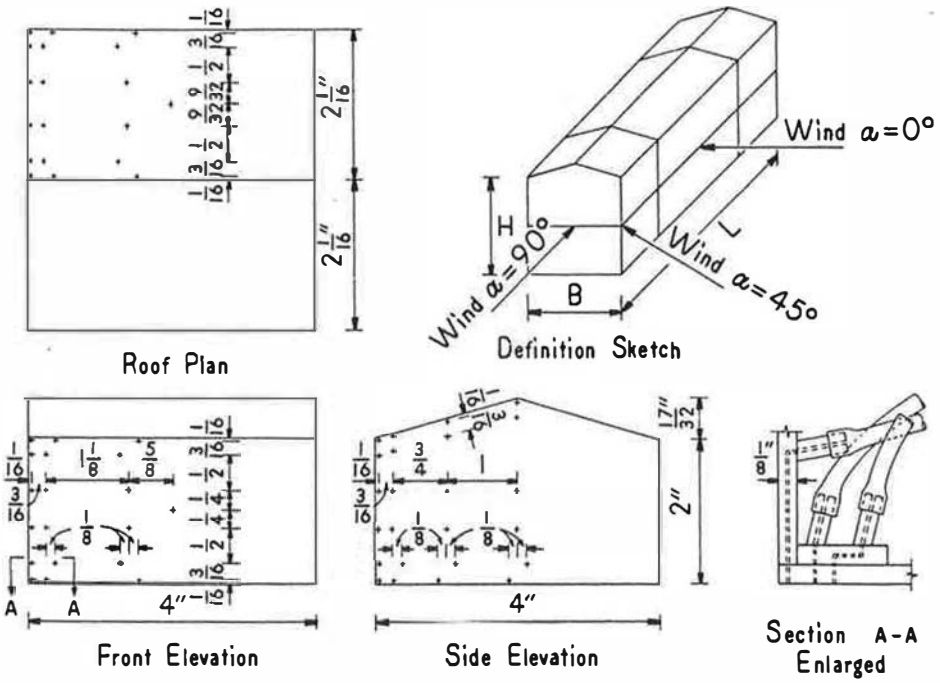

Fig. 10. Arrangement of piezometers on a gabled unit.

types and become particularly intense for certain building orientations - such as the flat-roofed structure in a quartering wind. The first type (Fig. 11a) results in the reduction of the stagnation and other positive pressures (and probably an alleviation of subsequent underpressures) to a degree which depends upon the departure of the approaching wind from constancy with elevation. The second (Fig. 11b) yields a low pressure throughout the eddy zone approximately equal to that at the point of separation. The third type (Fig. 11c) is generally accompanied by large negative pressures at its core and hence in its immediate vicinity.

Evaluation of test results involved first of all the conversion of pressure measurements to the dimensionless form $\Delta p/(\rho V_0^2/2)$, secondly the construction of pressure contours from these point values on the developed building surfaces, and thirdly the integration of the contour areas to yield either component or resultant forces. Determination therefrom of either the local pressures or the overall forces for particular wind speeds and temperatures involves simply the reverse computational procedure, as is illustrated by the following two numerical examples.

Assume for illustration that model measurements indicate a maximum local value of $\Delta p/(\rho V_0^2/2) = -4.5$ and an average of $(F/A)/(\rho V_0^2/2) = -2.7$ for the windward roof of a building, and that the corresponding local pressure intensity and total load are desired on a 20 x 30-foot prototype surface in a 60-mile-per-hour wind at 40° Fahrenheit. It is necessary first of all to know the mass density of the fluid for the given temperature; under average barometric conditions this value may be taken from the following table:

T (deg Fahr)	-20	0	+20	40	60	80	100
ρ (slug/ft^3)	0.0028	0.0027	0.0026	0.0025	0.0024	0.0023	0.0022

The prototype pressure corresponding to the dimensionless model indication will then be:

$$\Delta p = -4.5\,\frac{\rho V_0^2}{2} = -4.5\,\frac{0.0025\left(50\,\frac{5280}{60 \times 60}\right)^2}{2} = -30.2 \text{ psf}$$

The total load, in turn, will have the magnitude:

$$F = -2.7\,A\,\frac{\rho V_0^2}{2} = -2.7 \times 20 \times 30\,\frac{0.0025\left(50\,\frac{5280}{60 \times 60}\right)^2}{2} = -10{,}900 \text{ lb}$$

In the first instance the negative sign indicates a pressure below atmospheric. In the second instance the negative sign indicates a suction or outward force. In both instances, moreover, the values refer only to the external surface in question. If the pressure within the building is atmospheric, these will then also represent the net effect of the wind. If, on the other hand, the internal pressure is not atmospheric but is equal to that on the outside surface at the point of an opening (i.e., an open door or window), then the net effect must be determined by algebraic combination of the two.

ANALYSIS OF RESULTS

Hangar-type Structures

Since structures of the Quonset or hangar class consist in part of curved surfaces, any model study of the flow pattern which they produce must first of all evaluate the degree to which viscous effects govern this pattern. From extensive data on flow past elementary cylinders and model chimneys it might be expected that a rather pronounced change in the pattern - and hence in the pressure distribution - will take place as the flow along the boundary surface changes from the laminar to the turbulent state. This occurs on smooth cylindrical surfaces in a non-turbulent stream at about $R = 4 \times 10^5$, decreasing to perhaps $R = 10^5$ as the surface becomes progressively rougher or the turbulence of the approaching flow increases. While much the same sort of change does occur at approximately the same

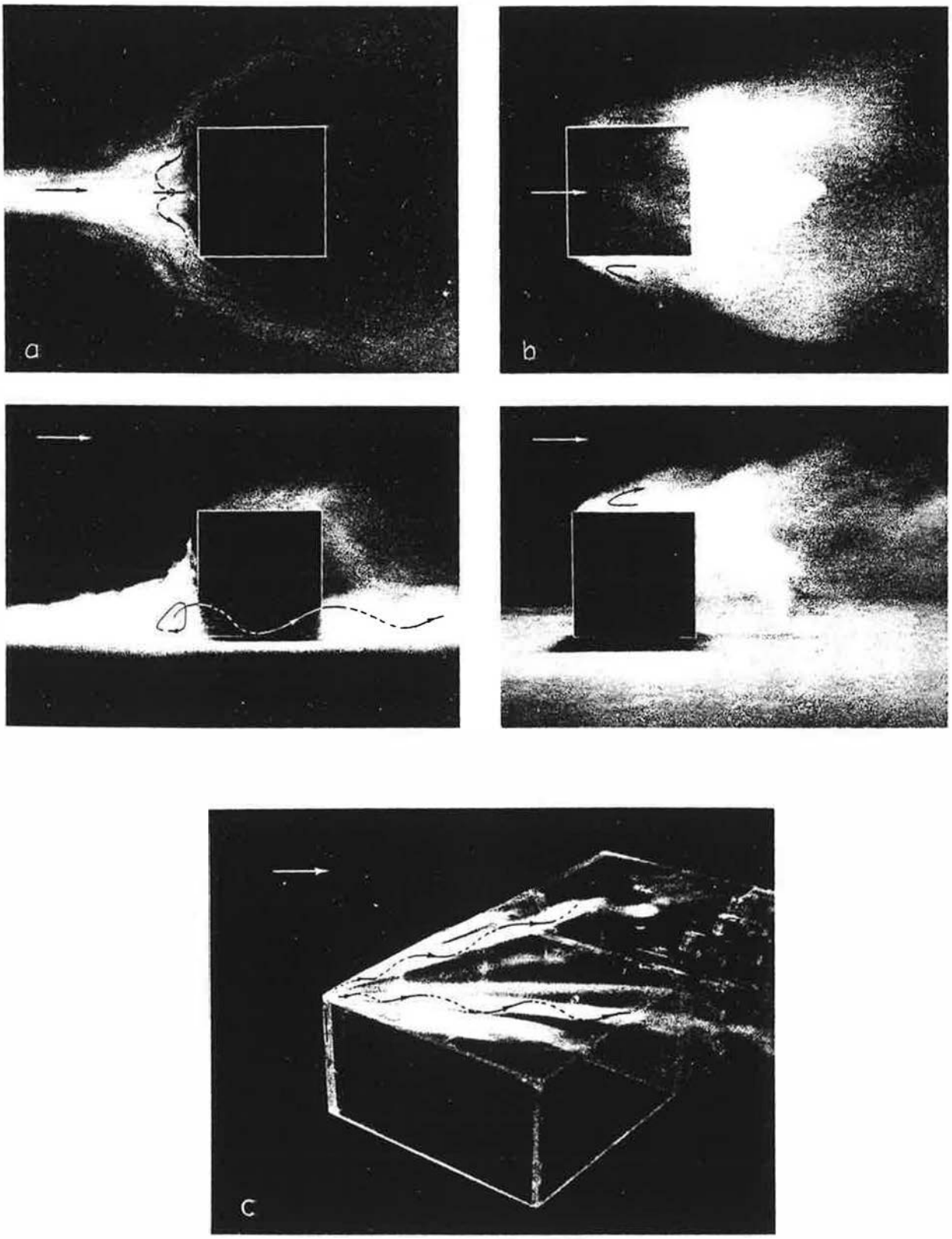

Fig. 11. Eddy patterns produced by block-type structures.

Reynolds number (based upon the diameter), when a semi-cylinder is mounted on a plane boundary with axis normal to the wind, the presence of the boundary also has a modifying effect. In the case of the full cylinder, that is, the wake is free to pendulate laterally as vortices are shed alternately from either side of the plane of symmetry. In the case of the semi-cylinder, on the contrary, the presence of the boundary at the original plane of symmetry completely eliminates this pendulatory motion and thereby alleviates to some degree the pressure change accompanying the change in flow pattern.

In order to ascertain experimentally the relative magnitude of the viscous effect, the longest hangar model (L = 24 inches, D = 6 inches) was tested in two of the Institute tunnels at the highest practicable Reynolds numbers, 8.5×10^4 and 2.0×10^5. Although these were below the critical point, the transition from laminar to turbulent boundary-layer flow was advanced artificially through use in turn of fine trip wires, sand grains cemented to the surface, and turbulence screens. The results are shown in Fig. 12, which also contains for reference purposes the characteristic pressure distributions for the full cylinder. Although a stable flow pattern with turbulent boundary layer was readily obtained, the pressure distribution for the hangar is clearly not as extreme as that for the full cylinder. Owing to tunnel limitations, reproduction of the prototype Reynolds number was wholly out of the question. However, while it is possible that with increasing values of R some further pressure reduction might have resulted, it could not be expected to reach the extreme of the full cylinder.

For lack of further information, it was necessarily assumed that the pressure measurements obtained with artificial stimulation of boundary-layer turbulence represented prototype conditions with sufficient approximation. Such stimulation was hence used in all cases except those in which the orientation of the structure resulted in initial separation from the end face rather than from the curved surface. In this connection it is to be noted that the minimum relative pressures occurred at a wind angle of approximately 30° from the normal.

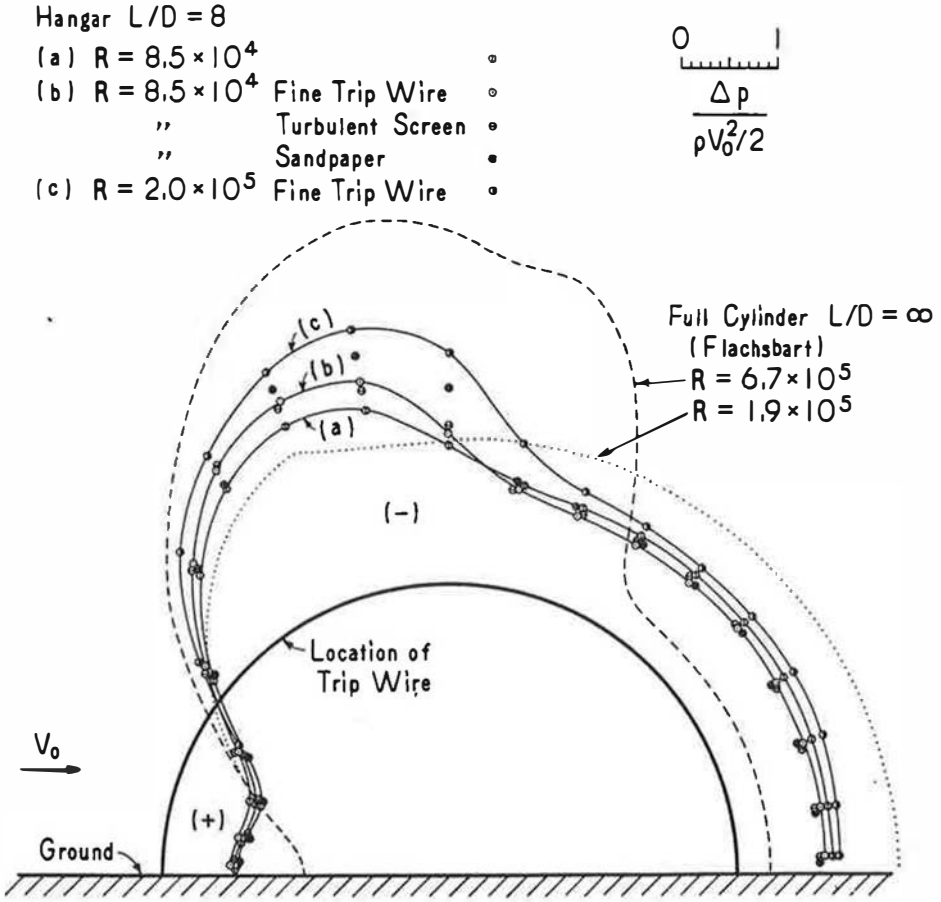

Fig. 12. Pressure distribution at midsection of hangar under various conditions.

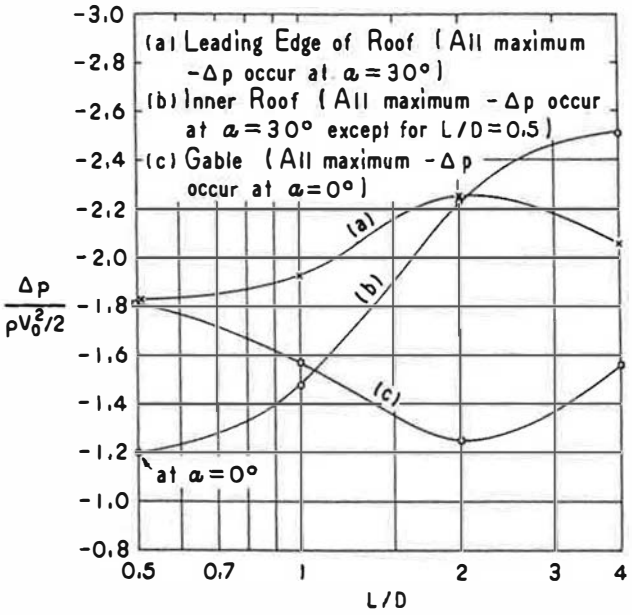

Fig. 13. Maximum local negative pressure on hangars of various length-width ratios.

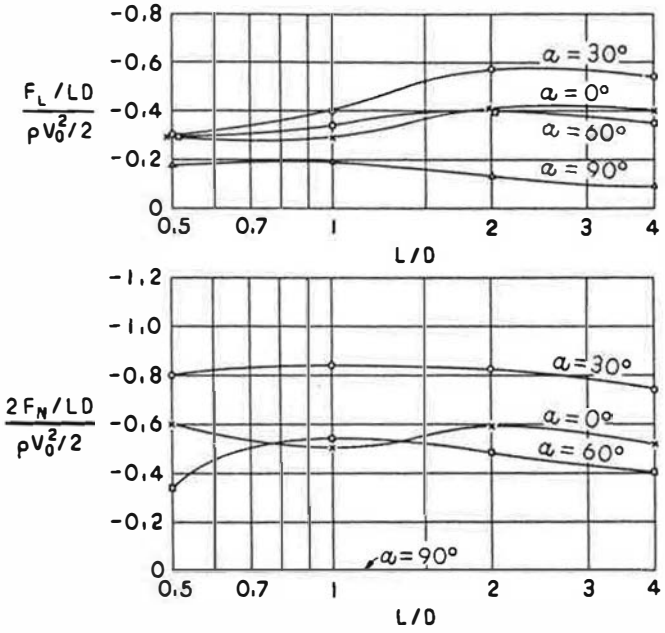

Fig. 14. Coefficients of lift and normal drag for hangars of various length-width ratios at different angles of attack.

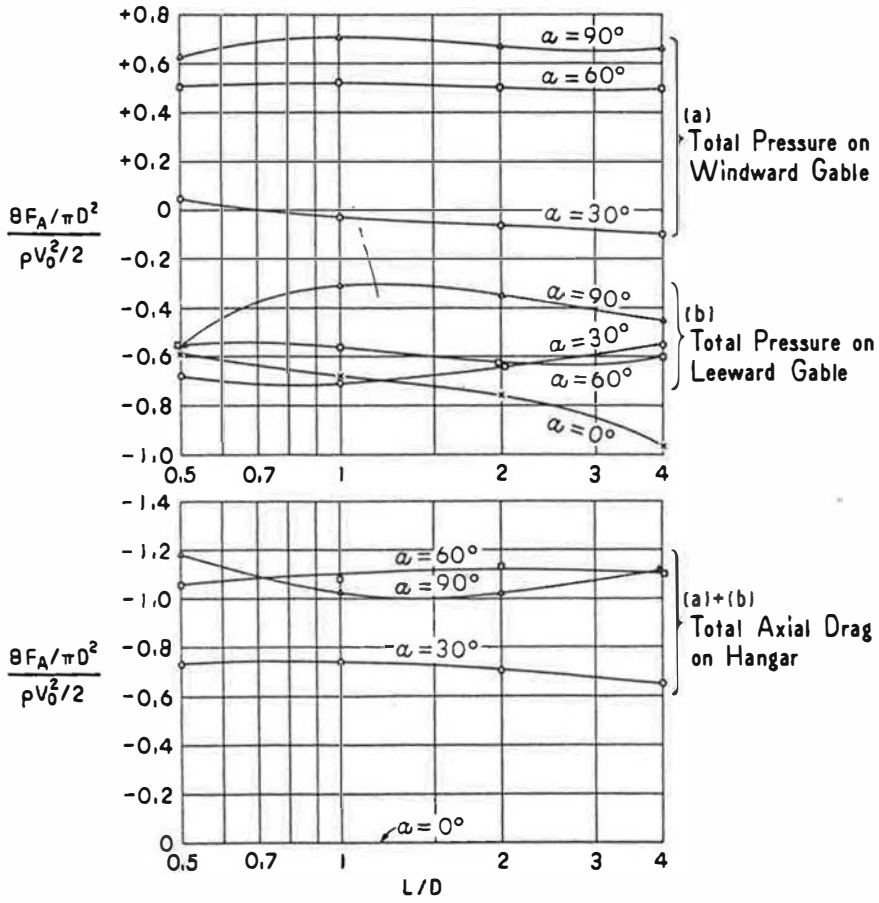

Fig. 15. Coefficient of axial drag for hangars of various length-width ratios at different angles of attack.

Table I

Maximum Local Negative Pressures $\frac{\Delta p}{\rho V_0^2/2}$ on Hangars

	L/D = 1/2			L/D = 1		
α	Leading edge	Inner roof	Gable	Leading edge	Inner roof	Gable
0°		-1.20	-1.81		-1.28	-1.57
30°	-1.83	-0.98	-0.80	-1.93	-1.48	-0.80 (Lee)
60°	-0.97	-0.70	-0.62 (Lee)	-1.29	-0.91	-0.67 (Lee)
90°	-0.86		-0.69 (Lee)	-1.26		-0.33 (Lee)

	L/D = 2			L/D = 4		
α	Leading edge	Inner roof	Gable	Leading edge	Inner roof	Gable
0°		-1.66	-1.25		-1.70	-1.56
30°	-2.25	-2.23	-0.77 (Lee)	-2.16	-2.51	-0.60 (Lee)
60°	-1.44	-1.21	-0.77 (Lee)	-1.58	-1.16	-0.64 (Lee)
90°	-1.31		-0.37 (Lee)	-1.14		-0.49 (Lee)

Table II

1. Lift Coefficient $\frac{F_L/LD}{\rho V_0^2/2}$ for Hangars

L/D	α = 0°	30°	60°	90°
1/2	0.29	0.30	0.29	0.18
1	0.29	0.40	0.34	0.19
2	0.41	0.57	0.40	0.13
4	0.40	0.54	0.35	0.09

2. Normal Drag Coefficient $\frac{2F_N/LD}{\rho V_0^2/2}$ for Hangars

L/D	α = 0°	30°	60°	90°
1/2	0.60	0.80	0.34	0
1	0.50	0.84	0.54	0
2	0.59	0.82	0.48	0
4	0.51	0.74	0.40	0

Table II (Continued)

3. Axial Drag Coefficient $\frac{8F_A/\pi D^2}{\rho V_o^2/2}$ for Hangars

	(a) Total Pressure on Windward Gable				(b) Total Pressure on Leeward Gable				(a) + (b) = Axial Drag on Hangar			
L/D	α = 0°	30°	60°	90°	0°	30°	60°	90°	0°	30°	60°	90°
1/2	-0.59	+0.05	+0.51	+0.63	-0.59	-0.68	-0.55	-0.55	0	0.73	1.06	1.18
1	-0.68	-0.03	+0.52	+0.71	-0.68	-0.71	-0.56	-0.31	0	0.74	1.08	1.02
2	-0.76	-0.06	+0.50	+0.67	-0.76	-0.64	-0.63	-0.35	0	0.70	1.13	1.02
4	-0.97	-0.10	+0.50	+0.66	-0.97	-0.55	-0.60	-0.46	0	0.65	1.10	1.12

Tests on the hangar type of building were conducted at wind angles of 0°, 30°, 60°, and 90°, with the necessarily constant height-width (i.e., radius-diameter) ratio of $\frac{1}{2}$ and the length-width ratios of $\frac{1}{2}$, 1, 2, and 4, thus including 16 separate conditions. Generalized plots of the resulting pressure contours, together with pressure profiles for representative cross sections, are presented in Figs. 27 to 43 of the Appendix. Figure 13 contains a plot of maximum negative pressures taken from these curves and summarized in Table I. In no case, it should be noted, did the pressure reach its full stagnation magnitude, owing to the slight resistance (and resulting base vortex) produced by the table upon which the models were mounted. Since the action of a larger boundary surface (i.e., the considerable variation of actual wind velocity with elevation) would be still greater, so far as this effect is concerned both positive and negative pressures in the model can be considered more extreme than those to be expected at full scale.

Because of the light weight of such structures, their susceptibility to either tipping or sliding must also be considered. Figures 14 and 15 have therefore been prepared to give in dimensionless form the vertical lifting force F_L and the normal and axial components of horizontal drag F_N and F_A. Table II summarizes the data upon which these plots were based. As previously indicated, multiplication of these numerical factors by the appropriate values of the denominators of the parametric terms (in units of feet, seconds, and slugs) will yield the desired force components (in pounds).

Vertical Walls

Compared with the foregoing tests on the hangar-type structures, the tests on the vertical walls were not only perfectly straightforward but productive as well of results which should not differ materially from those for geometrically similar prototypes. Wind angles of 0°, 30°, and 60° were investigated, with supplementary measurements at 10° intervals to determine maximum values; the height-width ratios involved in the tests were $\frac{1}{8}$, $\frac{1}{4}$, $\frac{3}{8}$, $\frac{1}{2}$, $\frac{3}{4}$, 1, and $\frac{3}{2}$, resulting in a total of 21 conditions. The generalized pressure contours for these conditions are shown in Figs. 44 to 64 of the Appendix. The maximum local negative pressure intensities are summarized in Fig. 16 as a function of the wall proportions. The so-called end effects are seen to play a considerable role in alleviating the pressure reduction; for example, the square wall displays only one-fourth the maximum negative pressure produced by the wall in which the ends are farthest apart.

The relative magnitude of the resultant normal force F_D upon a wall of any height-width ratio is indicated by the dimensionless drag values plotted in Fig. 17 and summarized in Table III. The component parts of the net drag are separated in the table so that the positive force exerted on the windward face and the negative force on the leeward face may be evaluated separately to determine the resulting couple. This couple arises from the fact that the centers of pressure on the two faces are not opposite each other except when the wind angle is 0°; consequently a twisting moment is exerted upon the wall at all other angles. To permit ready computation of this moment, the locations of the centers of pressure are shown graphically in Fig. 18 and summarized in Table IV. The wall proportions are seen to have a decided effect, the eccentricity of loading about both the vertical and horizontal axes increasing with decreasing height-width ratio.

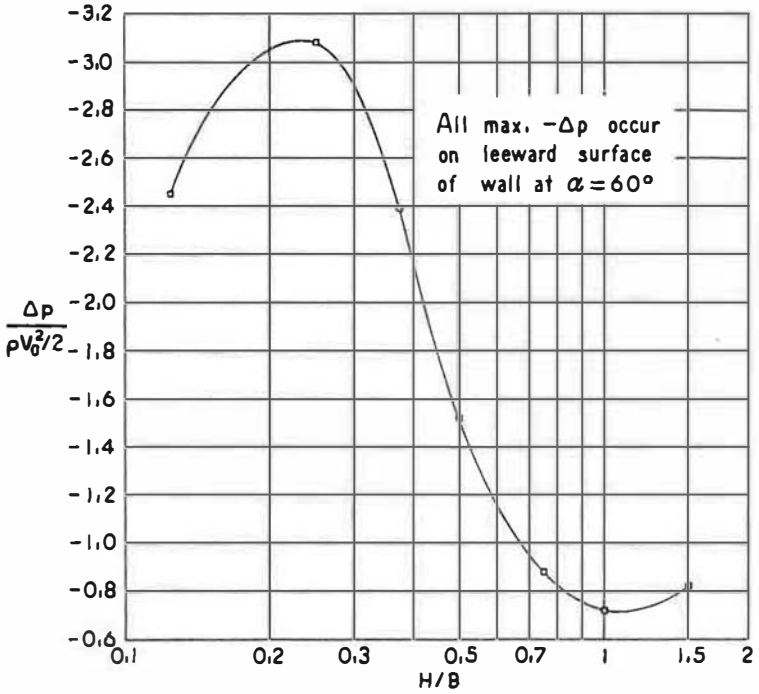

Fig. 16. Maximum local negative pressure on thin rectangular walls.

Table III

Normal Drag Coefficient $\frac{F/BH}{\rho V_0^2/2}$ for Thin Rectangular Walls

	(a) Total Positive Pressure on Windward Surface			(b) Total Negative Pressure on Leeward Surface			(a) + (b) = Total Normal Force on Wall		
H/B	α = 0°	30°	60°	0°	30°	60°	0°	30°	60°
1/8	+0.75	+0.56	+0.21	-0.62	-0.85	-0.82	1.37	1.41	1.03
1/4	+0.73	+0.59	+0.23	-0.55	-0.74	-1.03	1.28	1.33	1.26
3/8	+0.75	+0.61	+0.24	-0.54	-0.70	-1.08	1.29	1.31	1.32
1/2	+0.76	+0.61	+0.26	-0.51	-0.65	-1.04	1.27	1.26	1.30
3/4	+0.76	+0.62	+0.25	-0.47	-0.59	-0.69	1.23	1.21	0.94
1	+0.72	+0.61	+0.23	-0.46	-0.56	-0.58	1.18	1.17	0.81
3/2	+0.79	+0.64	+0.27	-0.53	-0.62	-0.64	1.32	1.26	0.91

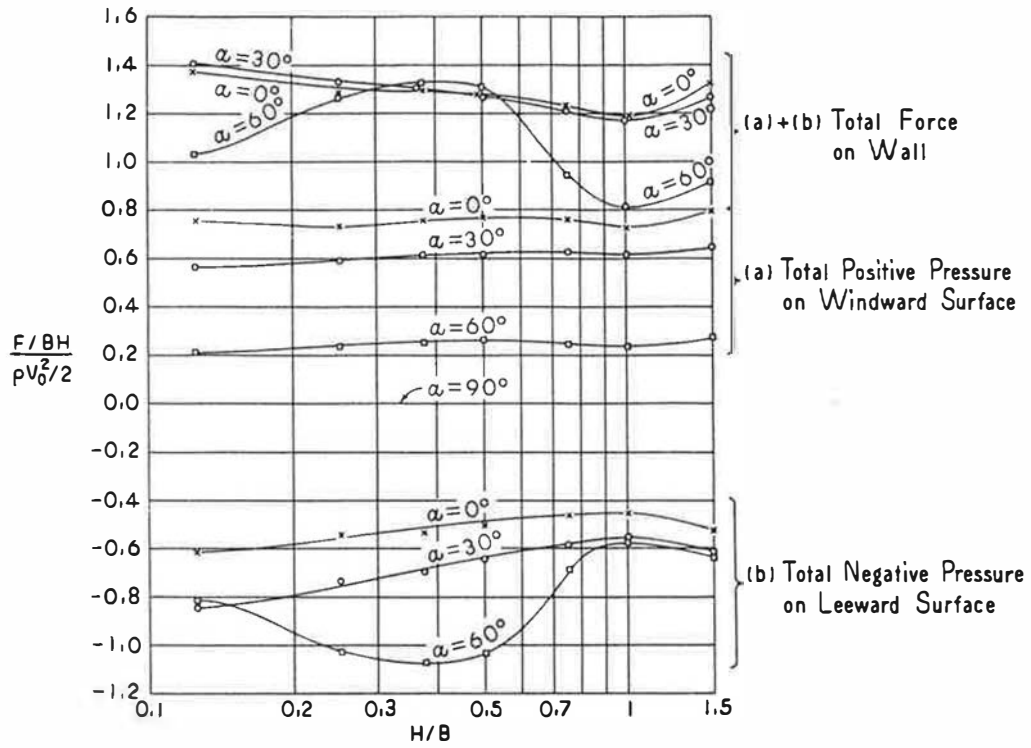

Fig. 17. Normal drag coefficient for vertical walls of various height-width ratios at different angles of attack.

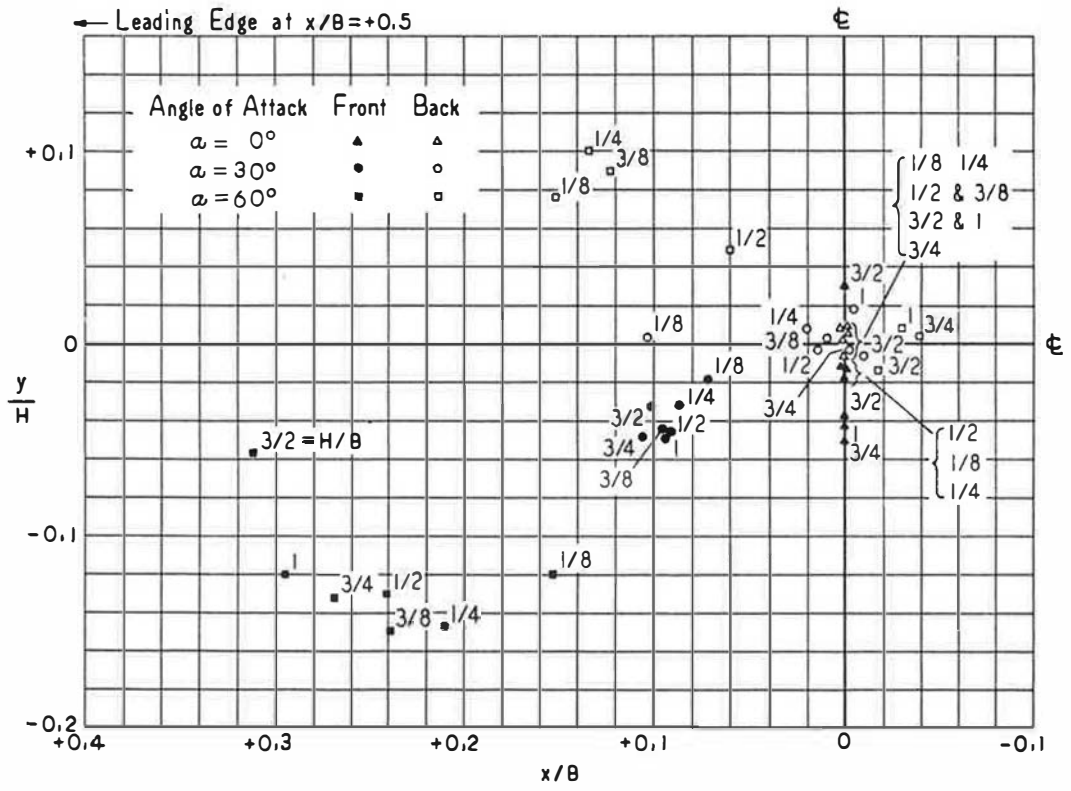

Fig. 18. Location of pressure center on vertical walls of various height-width ratios at different angles of attack.

Table IV

Location of Pressure Centers on Thin Rectangular Walls
(Refer to Fig. 18 for nomenclature)

	$\alpha = 0^0$				$\alpha = 30^0$			
	Windward Surface		Leeward Surface		Windward Surface		Leeward Surface	
H/B	x/B	y/H	x/B	y/H	x/B	y/H	x/B	y/H
1/8	0	-0.012	0	+0.008	+0.071	-0.018	+0.012	+0.003
1/4	0	-0.017	0	+0.008	+0.086	-0.032	+0.020	+0.008
3/8	0	-0.037	0	+0.004	+0.095	-0.044	+0.009	+0.003
1/2	0	-0.011	0	+0.004	+0.092	-0.045	+0.014	-0.003
3/4	0	-0.050	0	-0.006	+0.105	-0.048	-0.002	-0.002
1	0	-0.042	0	+0.003	+0.093	-0.048	-0.008	+0.018
3/2	0	+0.031	0	+0.003	+0.101	-0.032	-0.011	-0.006

$\alpha = 60^0$

	Windward Surface		Leeward Surface	
H/B	x/B	y/H	x/B	y/H
1/8	+0.153	-0.119	+0.151	+0.076
1/4	+0.211	-0.147	+0.134	+0.101
3/8	+0.239	-0.149	+0.123	+0.090
1/2	+0.241	-0.130	+0.060	+0.049
3/4	+0.269	-0.132	-0.039	+0.004
1	+0.296	-0.120	-0.029	+0.008
3/2	+0.312	-0.056	-0.017	-0.013

Block-type Structures

Buildings of the simple block type with gabled roofs were tested under the following conditions: wind angles of 0^0, 45^0, and 90^0; length-width ratios of 1, 2, and 4; height-width ratios of $\frac{1}{2}$, 1, and $\frac{3}{2}$; and roof slopes of 0^0, 15^0, 30^0, and 45^0. A total of 108 separate conditions were thus involved. The resulting generalized pressure contours are reproduced in Figs. 65 to 172 of the Appendix. As was done for the previously described structural forms, these contour plots could be integrated to yield values of the total wind loading. However, in the design of structures of this type it is rather the maximum local pressures and the average pressures over vertical sections which are of primary interest. The summary diagrams for this series of runs are therefore of the latter type.

In Fig. 19 will be found a plot of maximum negative roof pressures as a function of roof angle for the various length-width and height-width ratios. To be noted is the fact that the greatest underpressures generally occur at the smallest roof angles and on the buildings presenting the maximum normal cross section and the least depth in the direction of flow. The peak value of -7.4 would correspond, for the extreme case of stagnation conditions (+1) within the building, to a local intensity of uplift of 78 pounds per square foot in a wind of 60 miles per hour. This is well in excess of usual design figures.

Maximum values of the average positive and negative pressures over vertical sections of the front or windward wall are summarized in Fig. 20 for all wind orientations, the positive values corresponding

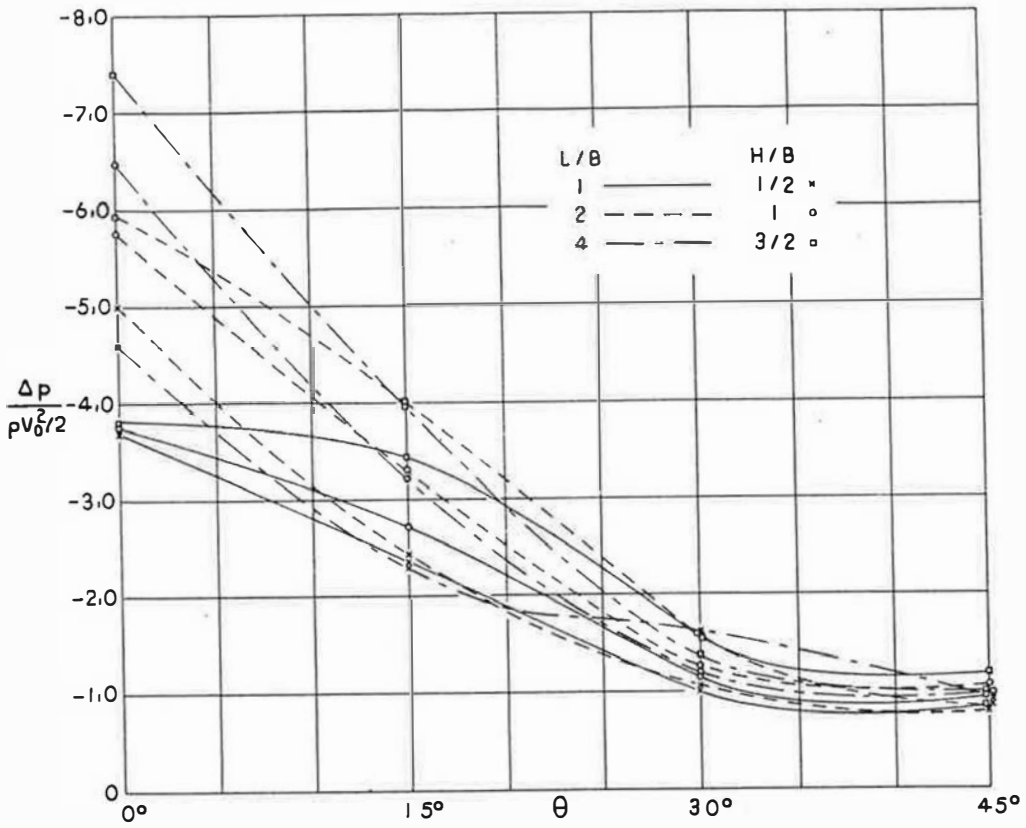

Fig. 19. Maximum local negative pressure on roof of block-type structure.

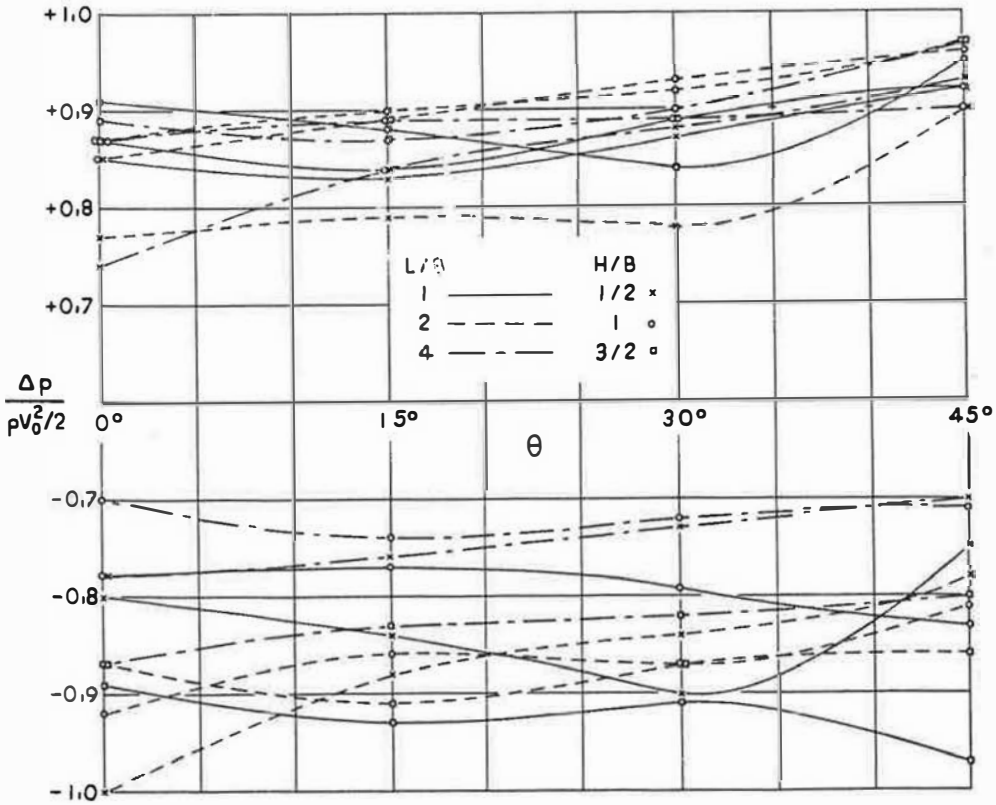

Fig. 20. Maximum average positive or negative pressure on a vertical section of the windward wall.

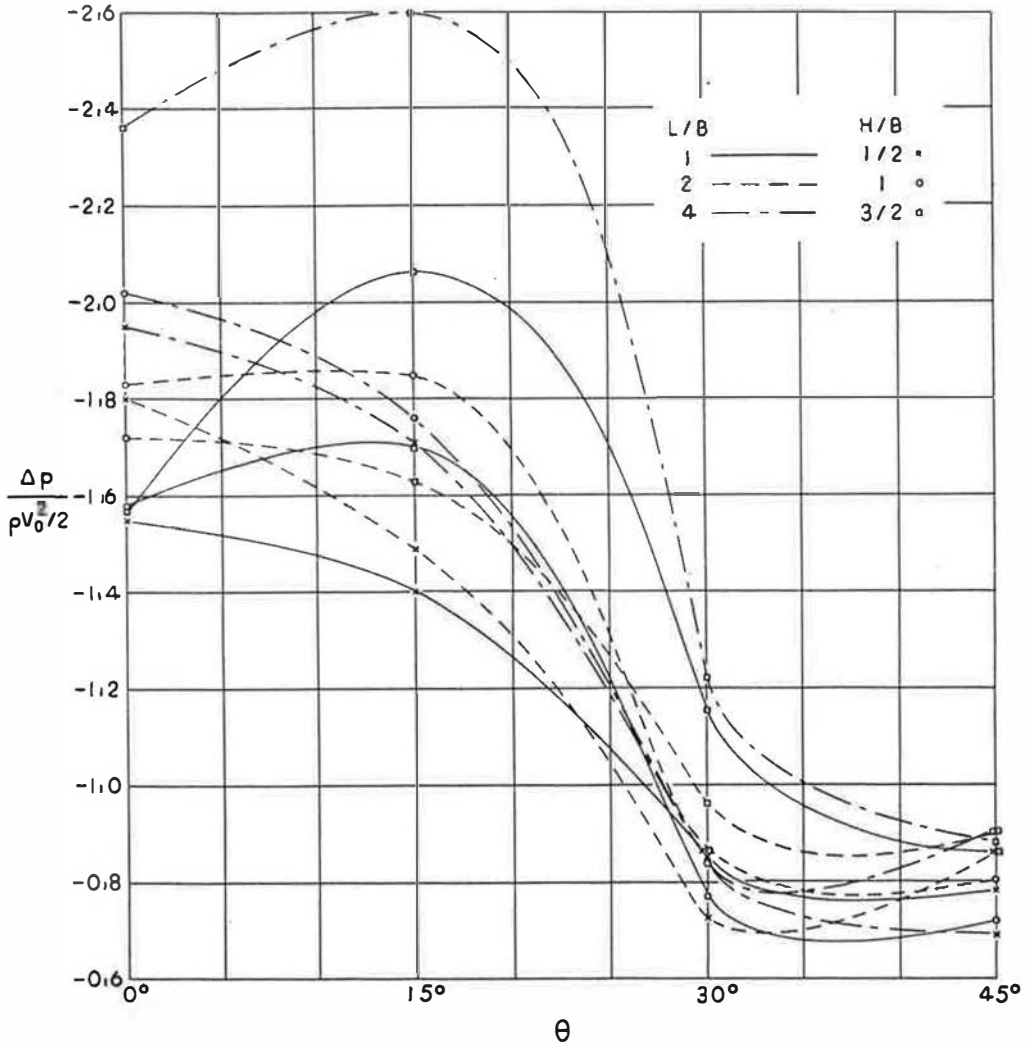

Fig. 21. Maximum average negative pressure on a transverse section of the windward roof.

in general to the midsections and the negative values to those in the edge zones. Comparable plots of the maximum average negative pressures on transverse sections of the windward and leeward roofs will be seen in Figs. 21 and 22. It is apparent herefrom that the roof pressures are greatly affected by the roof inclination. The worst vacuums evidently develop on the windward side at an angle of about 15° and on the leeward side as the angle approaches zero. These values become the more extreme as the width and the height of the building increase with respect to its dimension in the downwind direction. Figure 23 likewise shows maximum values of average negative pressures on the leeward side of the building.

Figure 24 summarizes the average roof pressures over transverse midsections and edge sections as a function of roof angle for the various building proportions. Again apparent is the great effect of roof angle upon the pressure distribution. The A.S.C.E. Code values of 1936 [16] are also plotted in this figure. Whereas the code recommendations are reasonably close to the results of this investigation for the leeward roof at midsection, they appear dangerously low at the midsection of the windward roof and at the edge sections of both.

Effect of Building Proximity

Since even the limited variables considered in the foregoing studies of single buildings were seen to require a considerable number of separate tests, it will be apparent that a comparable study of the effect

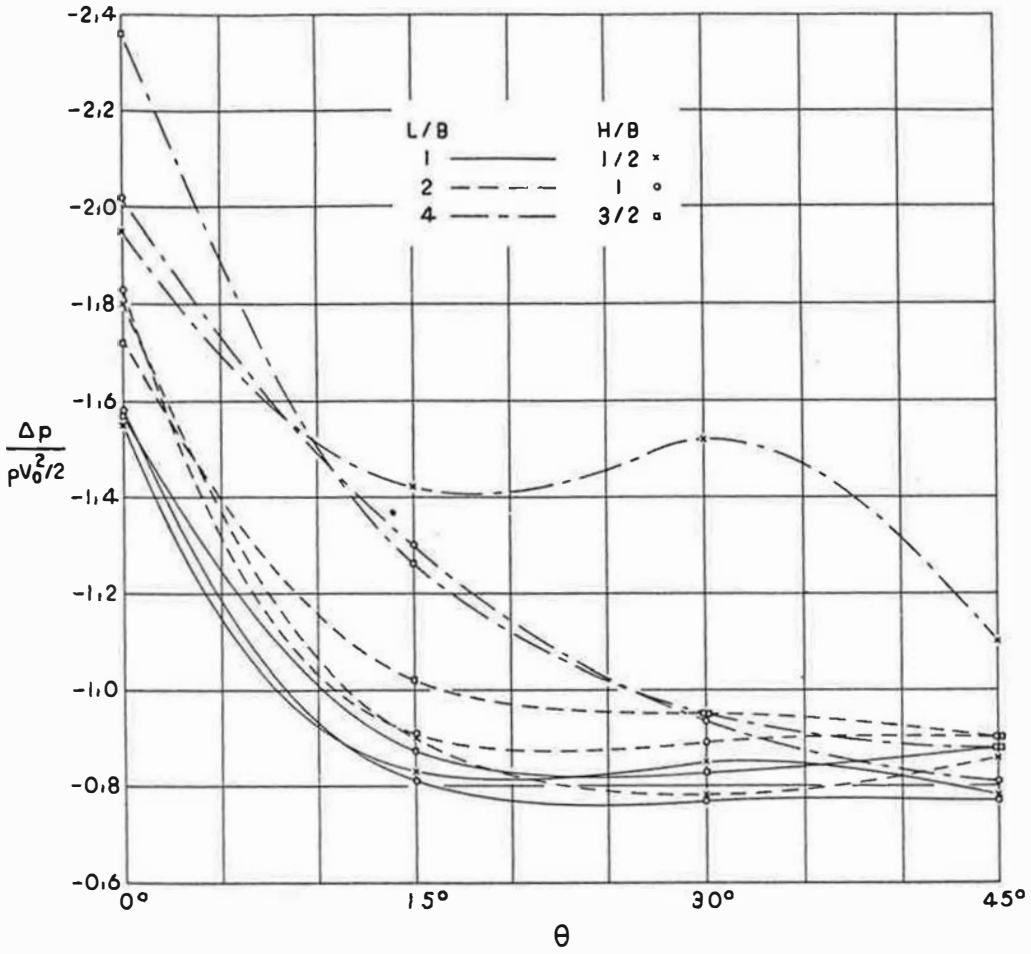

Fig. 22. Maximum average negative pressure on a transverse section of the leeward roof.

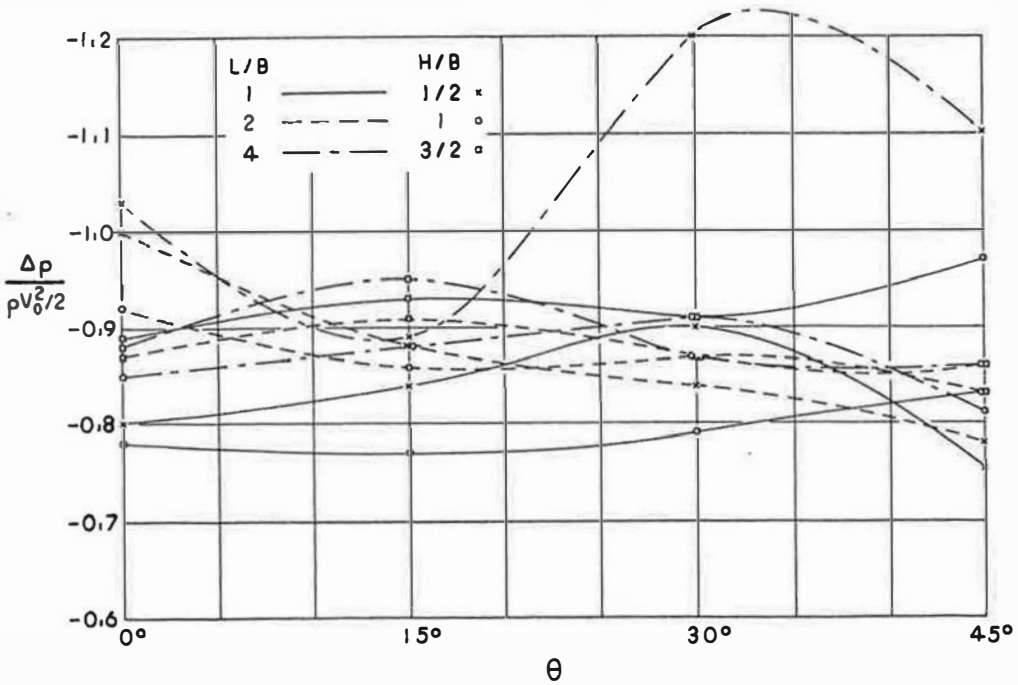

Fig. 23. Maximum average negative pressure on a vertical section of the leeward wall.

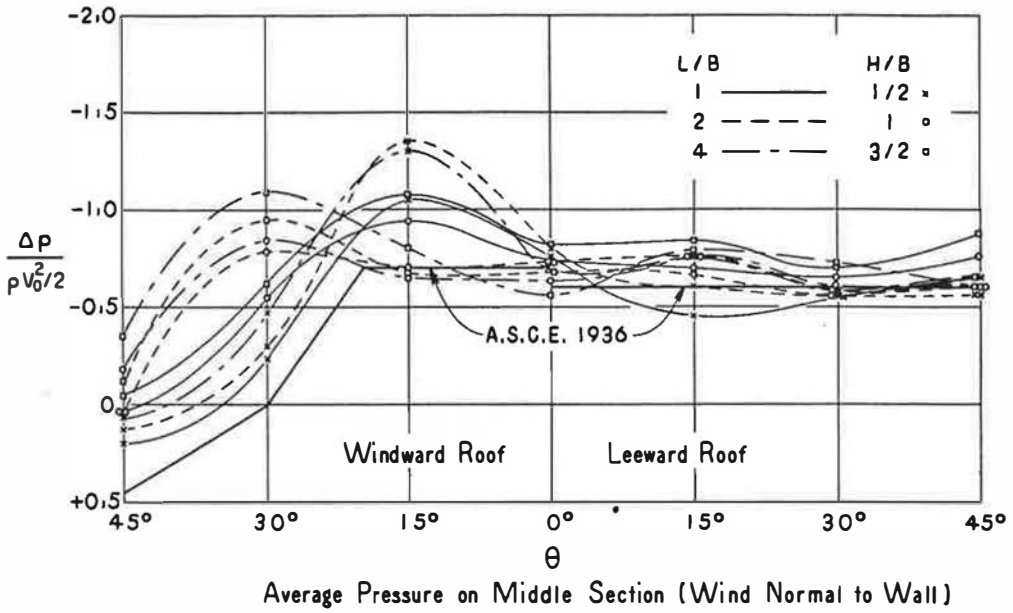

Average Pressure on Middle Section (Wind Normal to Wall)

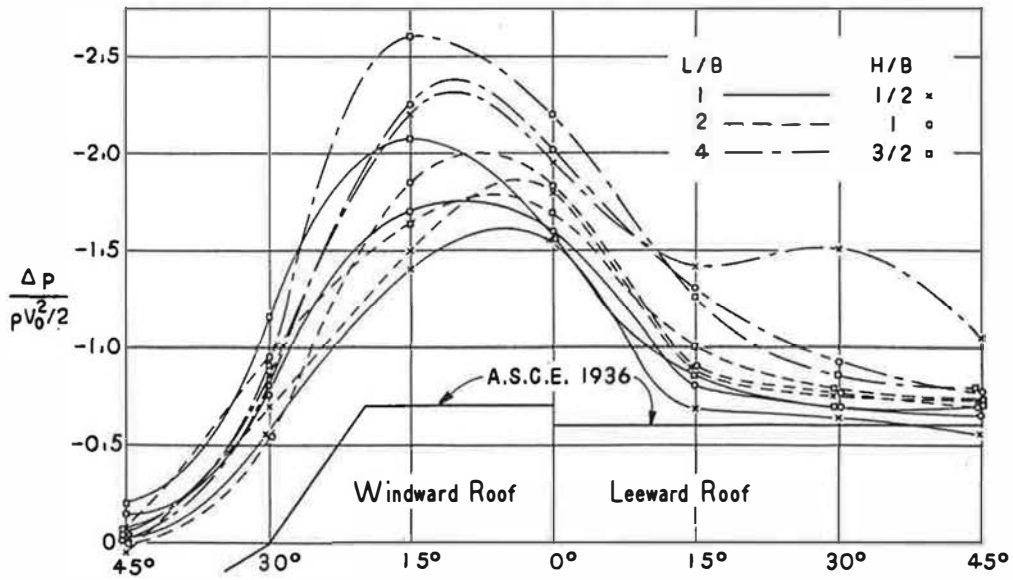

Average Pressure on End Section (45° Wind)

Fig. 24. Average pressure on middle and end sections of roof.

of building proximity could become extremely involved if all possible combinations were investigated. For this reason the study described herein was merely an exploratory one to indicate the order of magnitude of the effect. Two flat-roofed buildings of identical width and height were placed side by side, the sole variables being the equal length of the two in the parallel (i.e., the downwind) direction, the wind angle, and the spacing S. Measurement of the pressure distribution was restricted to one of the parallel faces. Since winds normal to the coplanar (i.e., front) faces resulted in the maximum pressure reductions in all but two cases, the results presented in Fig. 173 of the Appendix are restricted to four values of S/B and four values of L/B with a normal wind, and one value of S/B and four values of L/B with a wind at 30° from the normal.

As was to be expected, the pressure between the buildings at first decreased toward a minimum as the buildings were brought closer together, and then increased toward a maximum as the building spacing

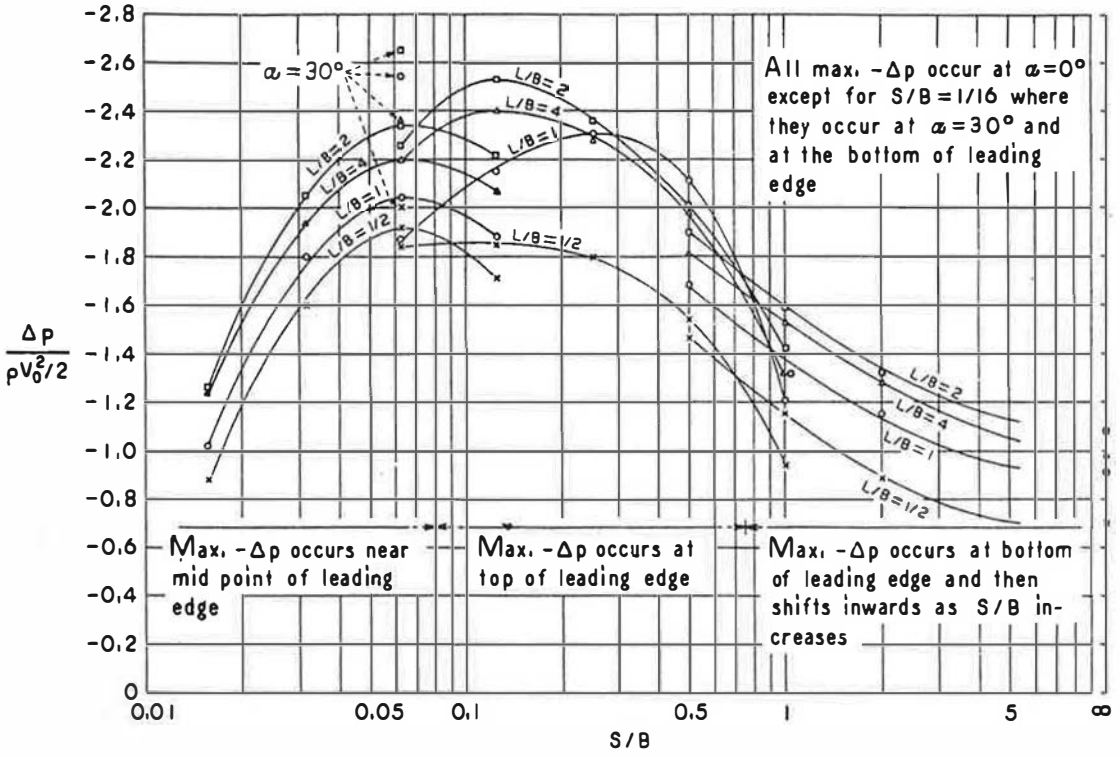

Fig. 25. Maximum local negative pressure on facing walls of two parallel flat-roofed block-type buildings.

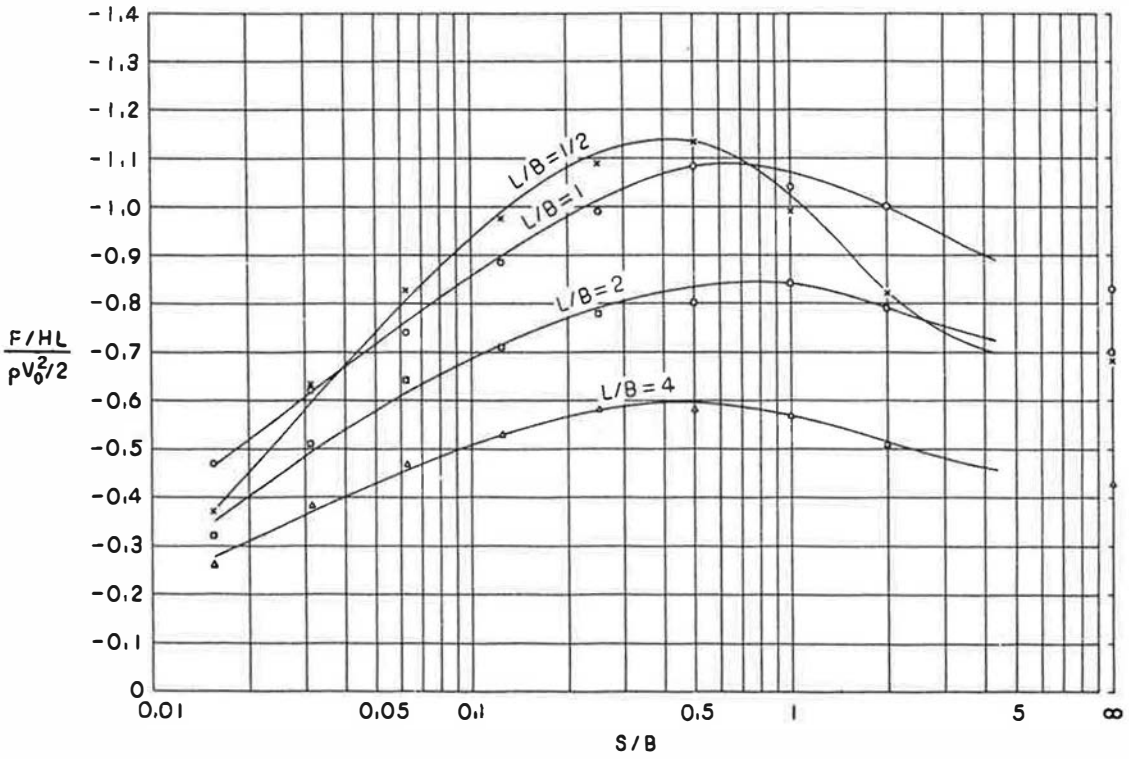

Fig. 26. Total pressure on inner walls of two parallel flat-roofed block-type buildings at angle of attack $\alpha = 0^{\circ}$.

became so small as to restrict the flow through the narrowing passage. In all instances the greatest pressure reduction occurred at the front edge of the passage - sometimes near the top, sometimes near the mid-point, and sometimes near the bottom, depending upon the various characteristic ratios and the wind direction. A plot of the maximum local negative pressures is shown in Fig. 25 and the data are summarized in Table V. In general it may be said that a maximum negative pressure about twice as great as that occurring at the same point on an isolated building is produced when the spacing is about one-tenth that of the building width or height. This general rule is obviously subject to modification if the width and height are not identical.

Integration of the pressure distribution to yield the coefficient of total force upon one of the parallel walls necessarily results in considerably different maximal conditions, since the average pressure is affected greatly by the length of passage. The relative values of this force are plotted in Fig. 26 and summarized in Table VI. From these it will be seen that in general the average suction per unit area reaches a maximum value which is some three times that for a single building when the spacing is about half the building width or height.

Table V

Maximum Local Negative Pressure $\frac{\Delta p}{\rho V_0^2/2}$ on Facing Walls of Two Parallel Flat-Roofed Rectangular Buildings

	L/B = 1/2			L/B = 1		
S/B	Center	Top	Bottom	Center	Top	Bottom
0.0156	-0.88			-1.02		
0.0313	-1.60			-1.80		
0.0625	-1.92	-1.84	-2.00 (α = 30°)	-2.04	-1.87	-2.54 (α = 30°)
0.125	-1.71	-1.85		-1.88	-2.15	
0.250		-1.80			-2.30	
0.500		-1.53	-1.46		-2.11	-1.68
1.0		-0.94	-1.15		-1.21	-1.32
2.0			-0.89			-1.15
∞			-0.70			-0.91

	L/B = 2			L/B = 4		
S/B	Center	Top	Bottom	Center	Top	Bottom
0.0156	-1.26			-1.45		
0.0313	-2.05			-1.94		
0.0625	-2.34	-2.26	-2.65 (α = 30°)	-2.20	-2.20	-2.34 (α = 30°)
0.125	-2.22	-2.53		-2.06	-2.40	
0.250		-2.36			-2.27	
0.500		-2.00	-1.90		-1.98	-1.81
1.0		-1.42	-1.59		-1.32	-1.53
2.0			-1.32			-1.28
∞			-1.08			-0.98

All maxima at leading edge, and (except for S/B = 0.0625) at α = 0°.

Table VI

Total Pressure $\frac{F/HL}{\rho V_o^2/2}$ on Facing Walls of Two Parallel Flat-Roofed Rectangular Buildings at Angle of Attack $\alpha = 0^0$

S/B	L/B = 1/2	L/B = 1	L/B = 2	L/B = 4
0.0156	-0.37	-0.47	-0.32	-0.26
0.0313	-0.63	-0.62	-0.51	-0.38
0.0625	-0.83	-0.74	-0.64	-0.47
0.125	-0.98	-0.88	-0.71	-0.53
0.250	-1.09	-0.99	-0.78	-0.58
0.500	-1.13	-1.08	-0.80	-0.58
1.00	-0.99	-1.04	-0.84	-0.57
2.00	-0.82	-1.00	-0.79	-0.51
∞	-0.68	-0.83	-0.70	-0.43

SUMMARY AND CONCLUSIONS

Described in the foregoing pages are systematic series of pressure measurements on elementary model structures of three different categories - hangars, walls, and buildings with gable roofs - of various proportions and at various wind orientations. The results are presented in the Appendix in the form of 145 different dimensionless plots of the pressure distribution on the developed surfaces for any wind speed and prototype scale. Supplementary plots show the effect of building proximity for 28 different conditions. The geometric characteristics were varied in such a manner that the resulting pressure diagrams permit ready interpolation to intermediate conditions not specifically investigated. In addition to these plots of pressure distribution, both diagrams and tables are presented showing maximum local positive and negative pressures, average positive and negative pressures over vertical sections, and total wind loading both on typical surfaces and over the structures as a whole. The limited number of building-code recommendations applicable to such conditions are plotted for purposes of comparison.

Since positive wind pressures cannot exceed stagnation values, whereas negative pressures may attain at least several times this magnitude, it is almost always the zones of separation with their accompanying underpressures which should govern structural design. Code recommendations do not safely reflect the negative loadings which may occur. Under these circumstances, it would appear advisable either to modify existing codes accordingly or to design structures with careful attention to actual pressure data for the structural geometry under consideration. It is believed that the data presented herein will serve as dependable first approximations to the pressure distributions over more complex structures of a comparable overall geometry. Even for conditions which are not roughly similar to those herein described, the broad and systematic nature of the various plots should nevertheless give a qualitative insight into the types of boundary geometry leading to extreme pressure reduction.

Although the usefulness of model investigations is now too generally accepted to require further testimony at this time, it would appear in order to emphasize the desirability of conducting specific tests on composite structures which are either too complex to analyze thoroughly in terms of elementary forms or too costly to ignore the safety and economy in design which detailed model tests would permit. This is particularly true in the case of building groups. Of a related nature, but beyond the scope of this investigation, is the matter of locating ventilation intakes and exhausts, as well as vents for smoke or toxic fumes; this phase of the design problem is likewise controlled by the flow pattern and hence is equally subject to model investigation.

ACKNOWLEDGMENTS

All experimental studies herein described were conducted in the laboratories of the Iowa Institute of Hydraulic Research. The tests on the single block-type buildings were made by Messrs. Chien, Feng, and Wang as a master's thesis in the Department of Mechanics and Hydraulics, under the direction of Professor J. W. Howe. The remaining tests were made by Messrs. Wang and Siao as an Institute project under the direction of Professor Hunter Rouse and sponsored by the Office of Naval Research through Contract N8onr-500. All drawings for this report were prepared by Mr. Siao, the text was written by Professors Howe and Rouse, and the printing was partially financed by the Office of Naval Research.

REFERENCES

[1] Irminger, I., "Experiments on Wind Pressure," *Engineering*, Vol. 60, Dec. 1895, p. 787.

[2] Dryden, H. L., and Hill, G. C., "Wind Pressure on a Model of the Empire State Building," *Journal of Research*, National Bureau of Standards, Vol. 10, 1933, p. 493. (See also "Wind Pressure on a Model of a Mill Building," Vol. 6, 1931, p. 735.)

[3] Kaufmann, W., *Hydromechanik*, Vol. II, Julius Springer, Berlin, 1934, pp. 269-289.

[4] Pagon, W. W., "Wind Tunnel Studies Reveal Pressure Distribution on Buildings," *Engineering News Record*, Dec. 1934, p. 814; "What Aerodynamics Can Teach the Civil Engineer," March 1934, p. 349.

[5] Klemin, A., Schaefer, E. B., and Beerer, J. G., "Aerodynamics of the Perisphere and Trylon at World's Fair," *Transactions A.S.C.E.*, Vol. 104, 1939, p. 1449.

[6] Bailey, A., and Vincent, N. D. G., "Wind-Pressure on Buildings Including Effects of Adjacent Buildings," *Journal Inst. C. E.*, March 1943, p. 243.

[7] Austin, G. A., Jr., "A Study of the Pressure Distribution on a Series of Two-Dimensional Roof Forms," M. S. Thesis, State University of Iowa, June 1947.

[8] Chien, N., Feng, Y., and Wang, H. J., "Pressure Distribution on Models of Three-Dimensional Buildings Exposed to Moving Air," M. S. Thesis, State University of Iowa, June 1948.

[9] Nacy, P. S., "Modification of Pressure Distribution Around Buildings Due to Parapets," M. S. Thesis, State University of Iowa, June 1951.

[10] Rouse, H., *Elementary Mechanics of Fluids*, John Wiley & Sons, 1946, p. 62.

[11] Baines, W. D., and Peterson, E. G., "An Investigation of Flow Through Screens," *Transactions, A.S.M.E.*, Vol. 73, July 1951.

[12] Rouse, H., "Use of the Low-Velocity Air Tunnel in Hydraulic Research," *Proceedings of the Third Hydraulics Conference*, University of Iowa Studies in Engineering, Bulletin 31, 1947, p. 121.

[13] Goldstein, S., *Modern Developments in Fluid Dynamics*, Vol. II, Oxford University Press, 1938, p. 432.

[14] *The Iowa Institute of Hydraulic Research*, University of Iowa Studies in Engineering, Bulletin 30, 1946, p. 28.

[15] *Engineering Hydraulics*, edited by H. Rouse, John Wiley & Sons, 1950, p. 191.

[16] "Wind-Bracing in Steel Buildings," Fifth Progress Report of Subcommittee No. 31, Committee on Steel of the Structural Division, *Proceedings A.S.C.E.*, March 1936, p. 397.

APPENDIX

Generalized Plots of Pressure Distribution

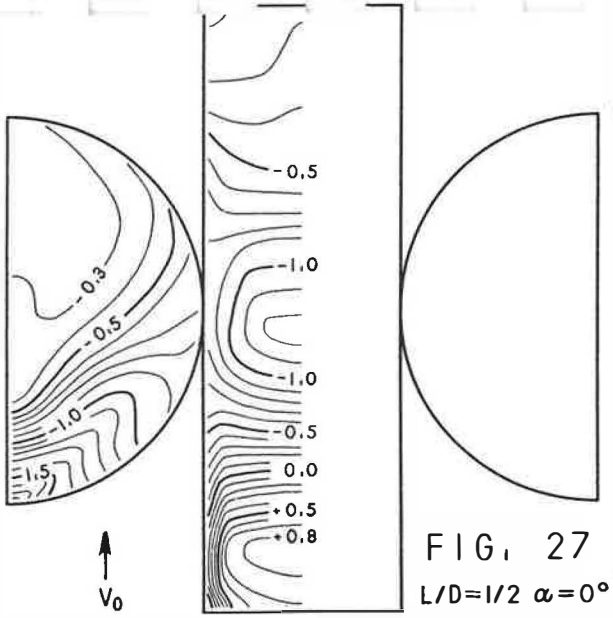

FIG. 27
L/D=1/2 α=0°

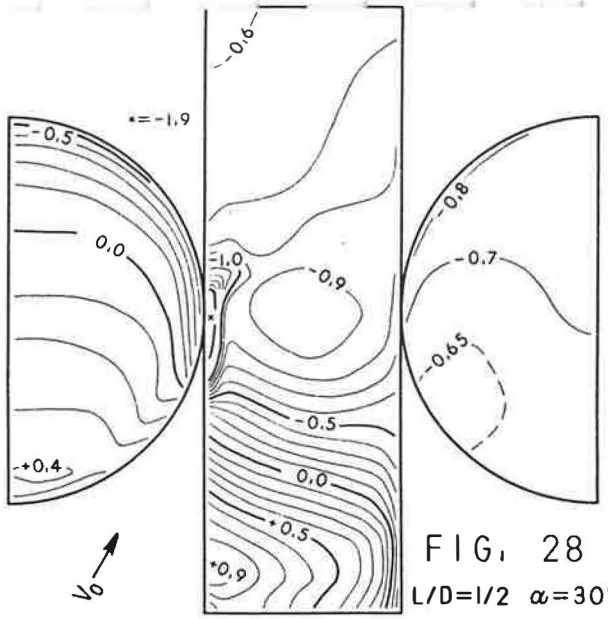

FIG. 28
L/D=1/2 α=30°

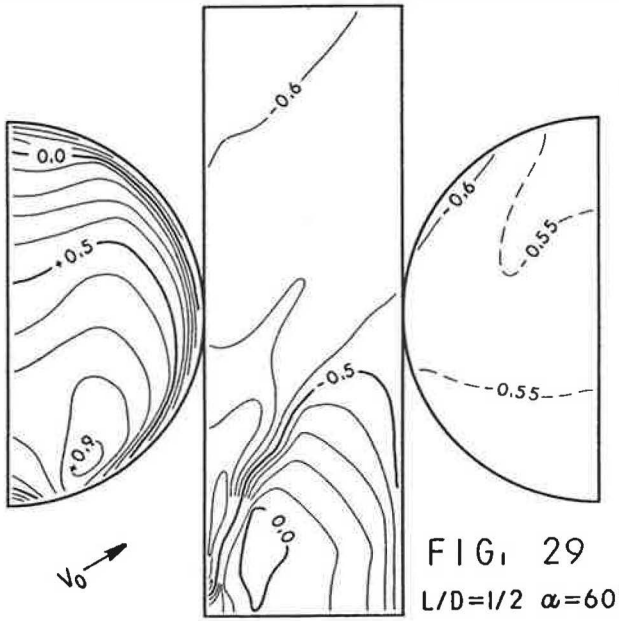

FIG. 29
L/D=1/2 α=60°

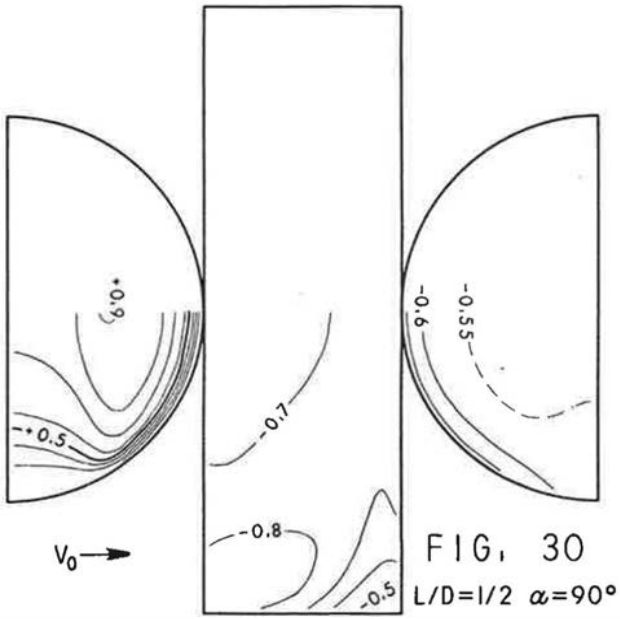

FIG. 30
L/D=1/2 α=90°

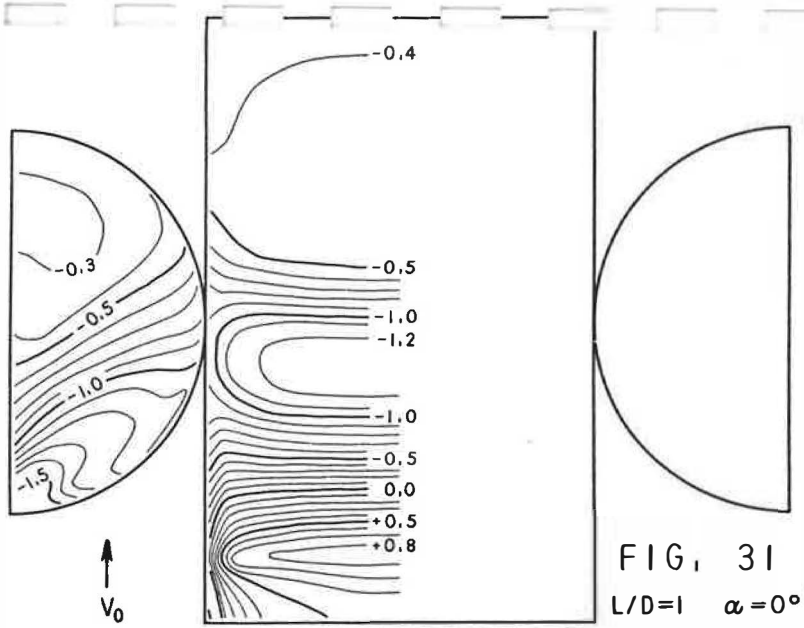

FIG. 31
L/D=1 $\alpha = 0°$

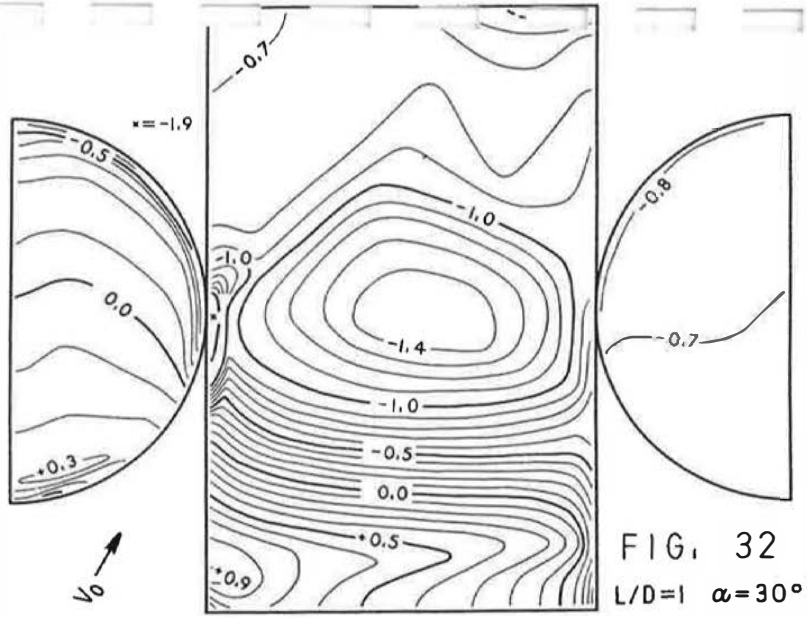

FIG. 32
L/D=1 $\alpha = 30°$

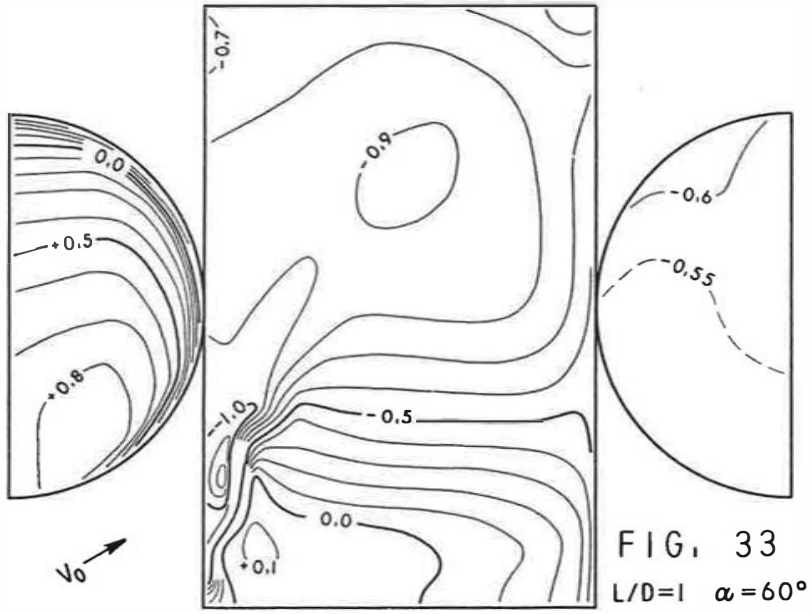

FIG. 33
L/D=1 $\alpha = 60°$

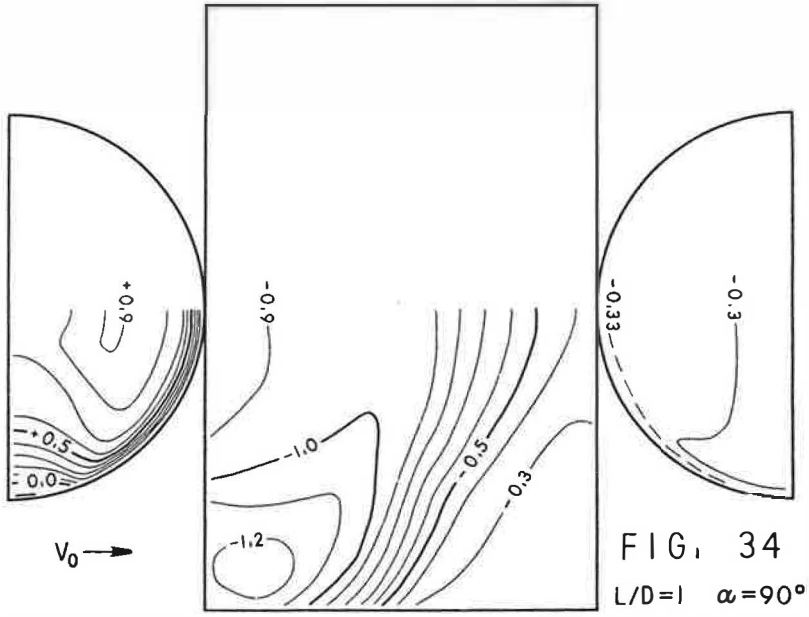

FIG. 34
L/D=1 $\alpha = 90°$

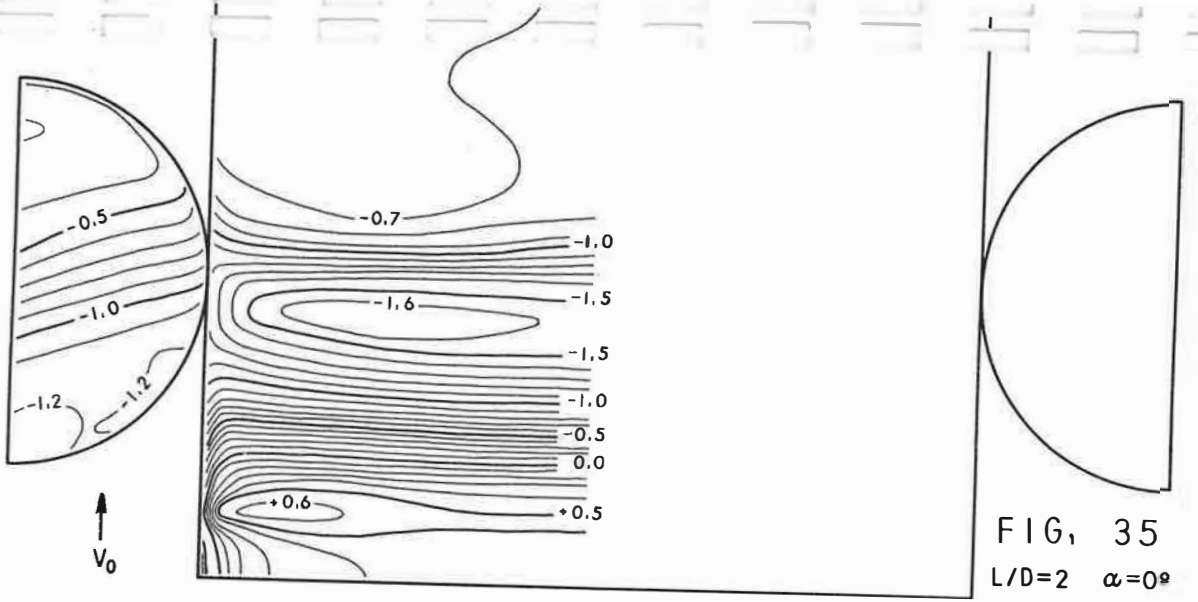

FIG. 35
L/D=2 α=0°

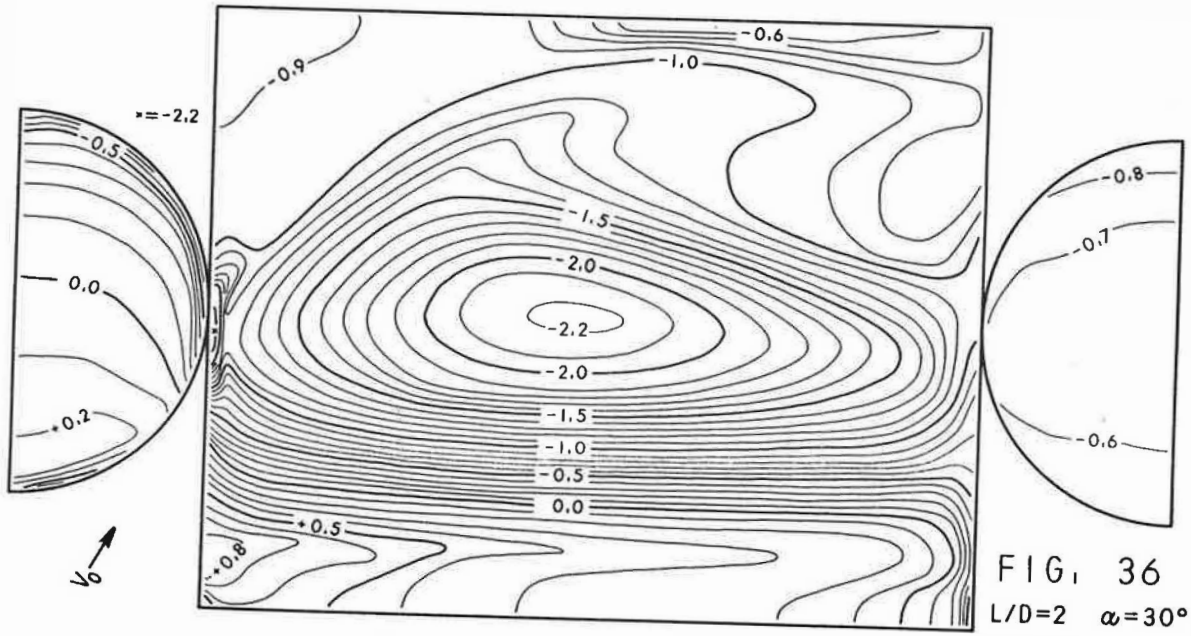

FIG. 36
L/D=2 α=30°

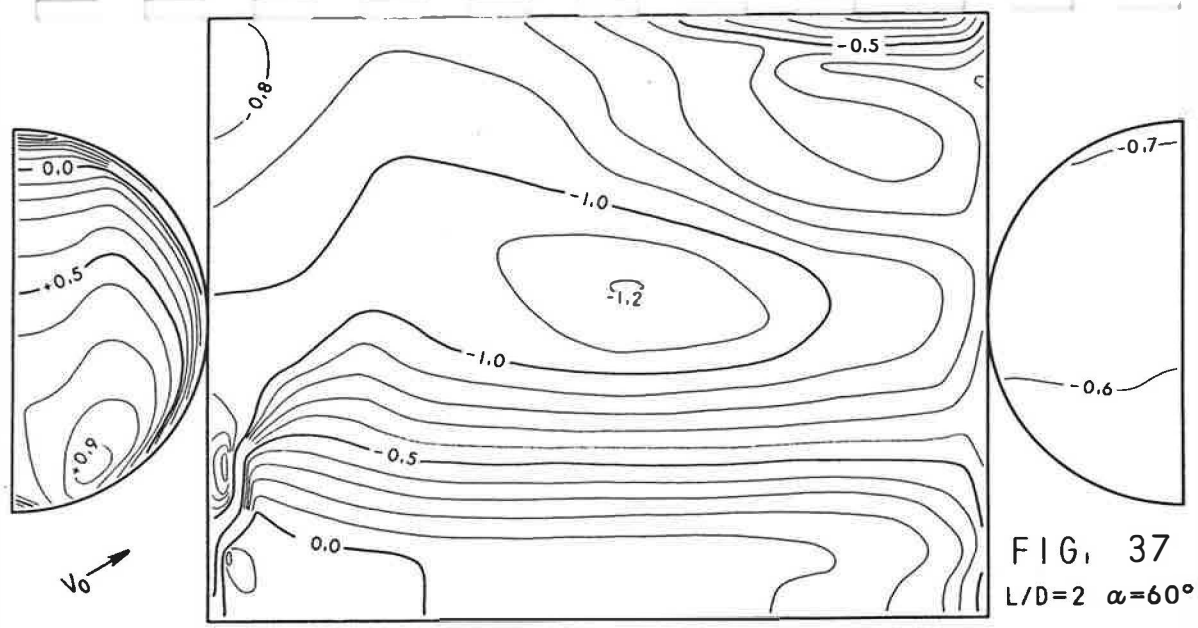

FIG. 37
L/D=2 α=60°

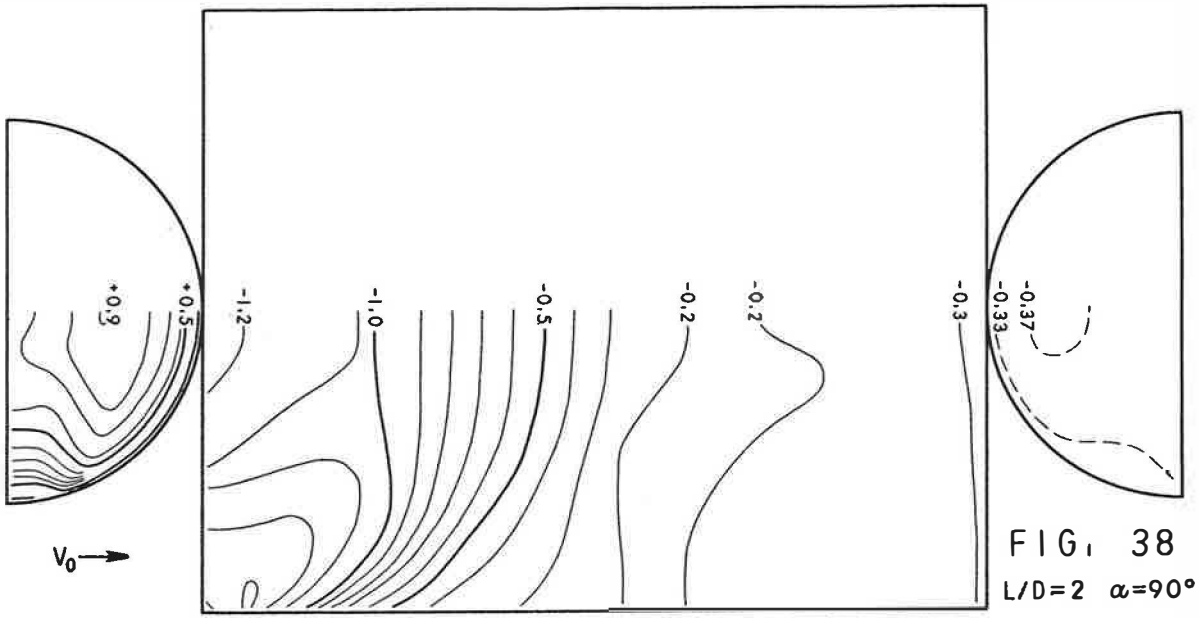

FIG. 38
L/D=2 α=90°

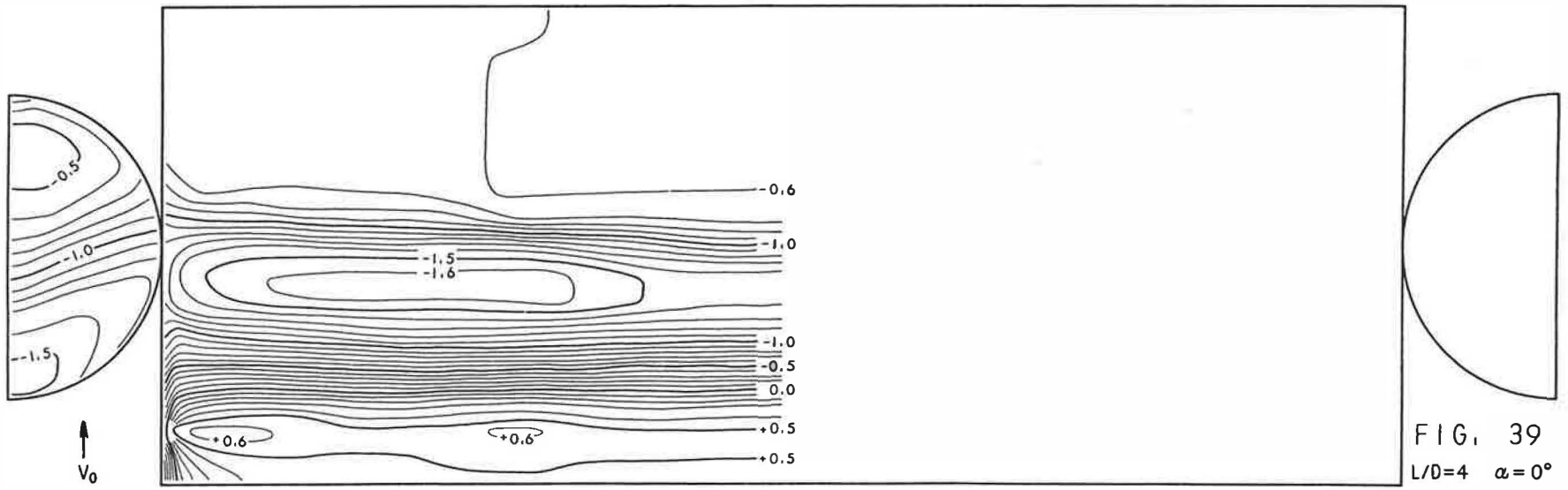

FIG. 39
L/D=4 $\alpha = 0°$

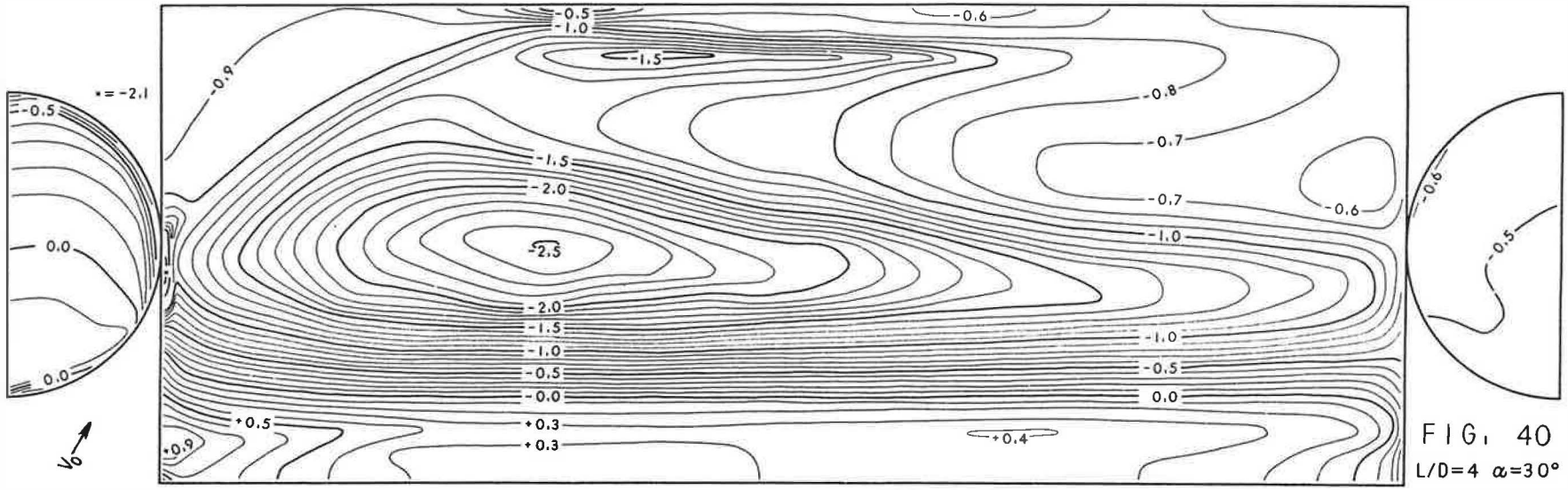

FIG. 40
L/D=4 $\alpha = 30°$

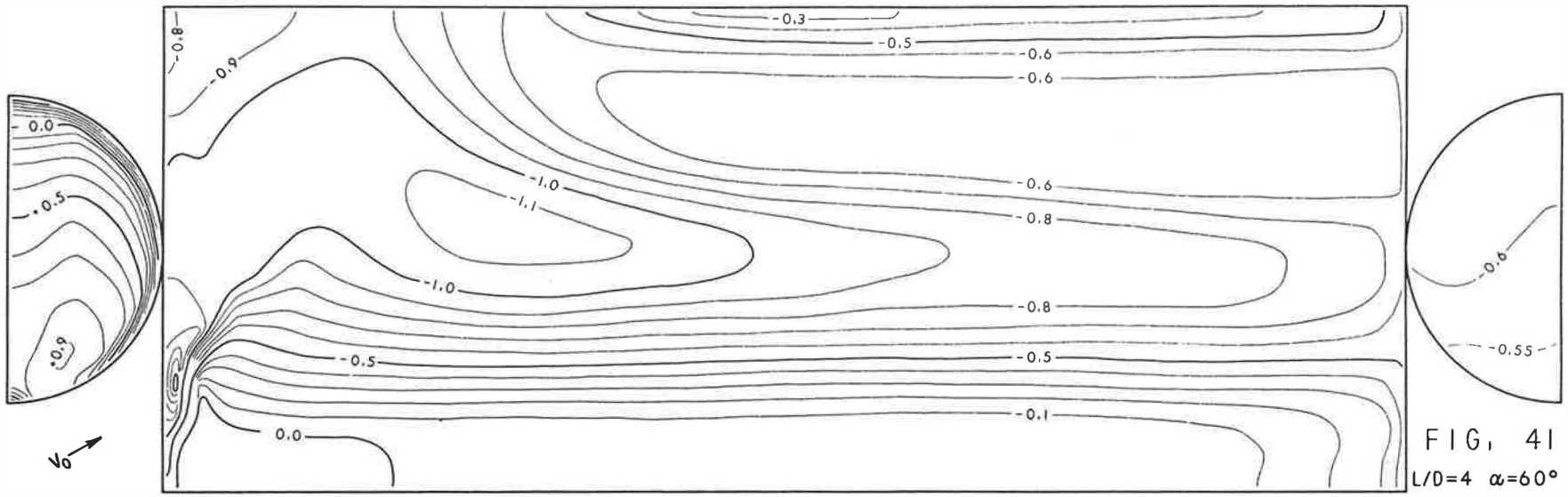

FIG. 41
L/D=4 α=60°

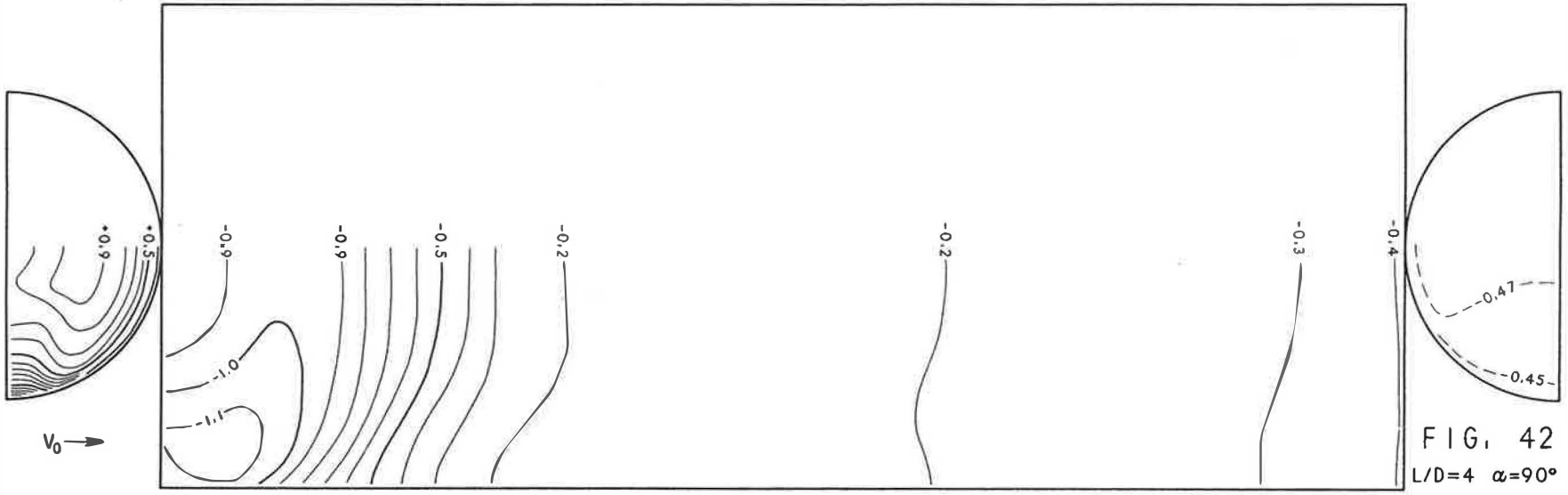

FIG. 42
L/D=4 α=90°

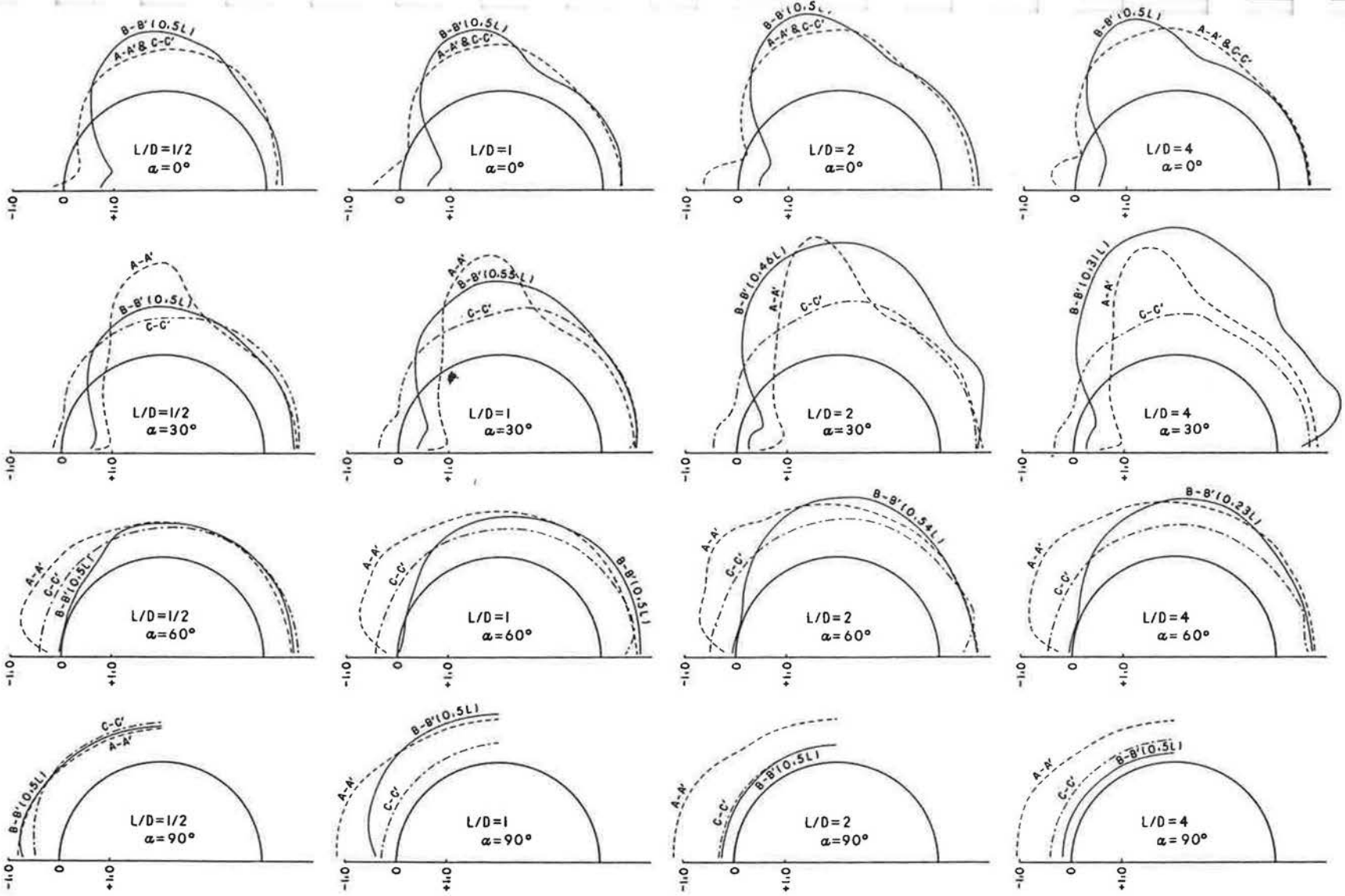

FIG. 43 Pressure Profiles for End and Intermediate Sections of Hangars of Various L/D Ratios at Various Angles of Attack α

A-A' End Section near Upwind Gable

B-B' Intermediate Section through Max. $-\Delta p$ on Roof

C-C' End Section near Downwind Gable

0 1

$$\frac{\Delta p}{\rho V_0^2/2}$$

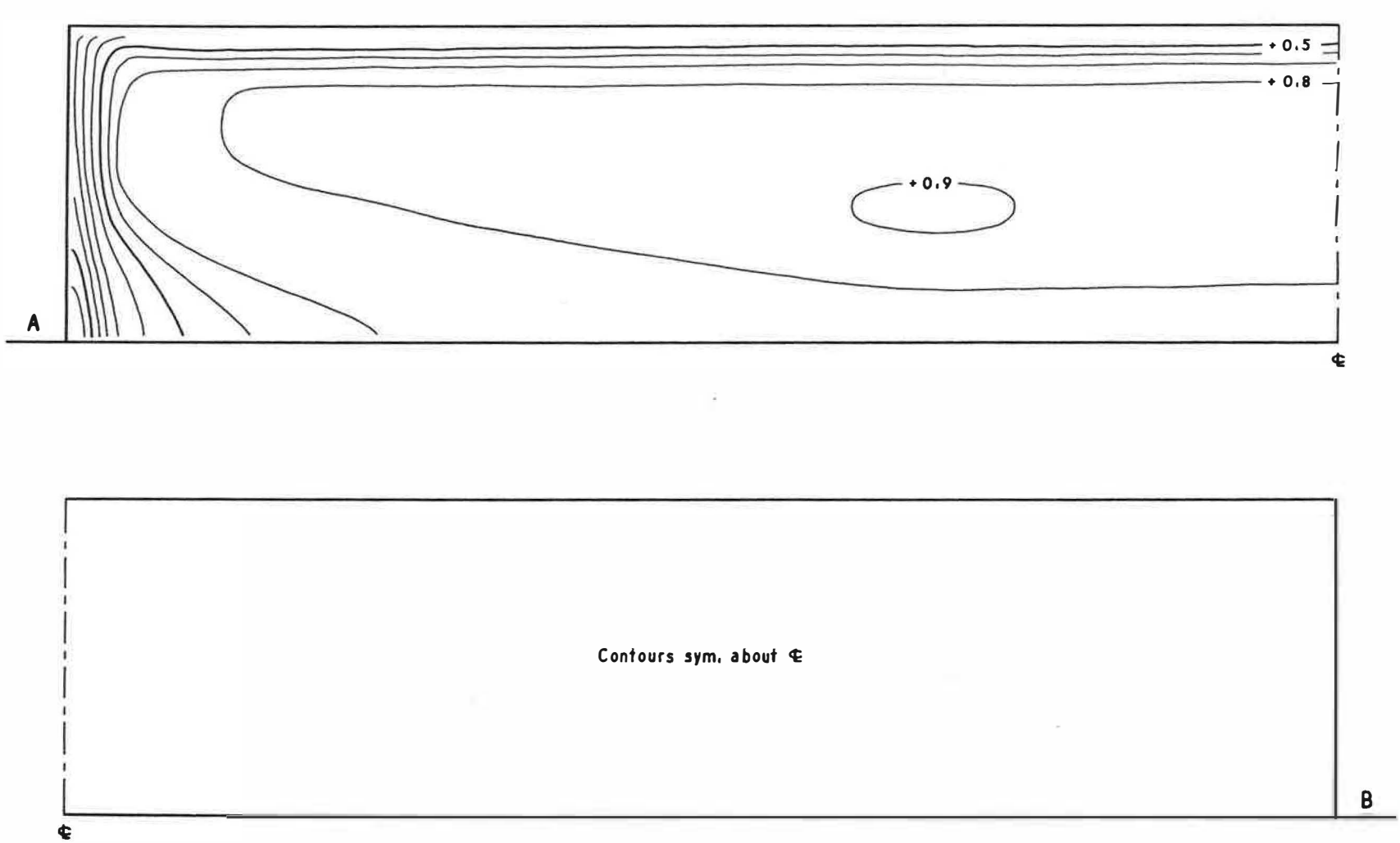

FIG. 44 H/B = 1/8 $\alpha = 0°$

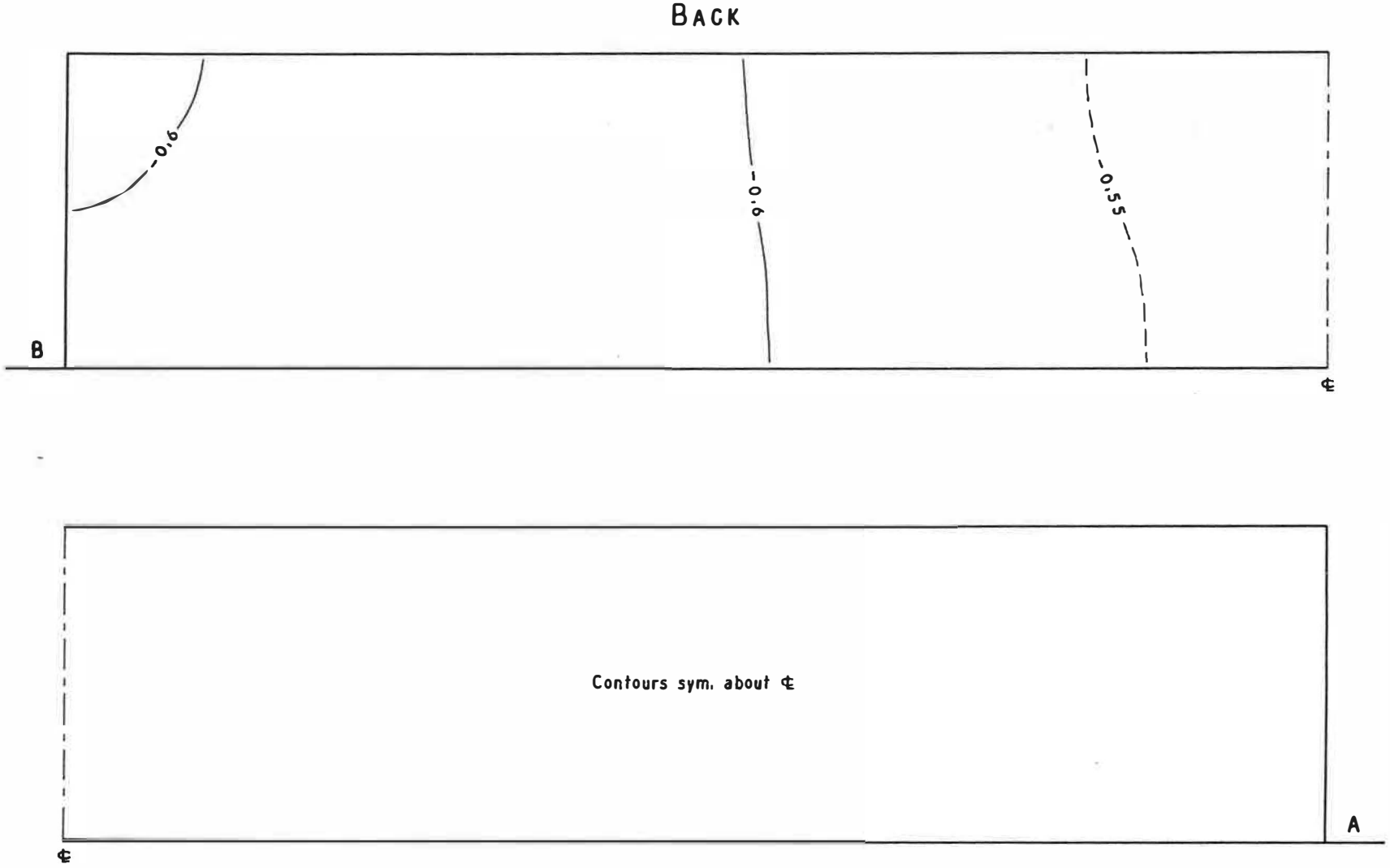

FIG. 44 (CONTINUED)

FRONT

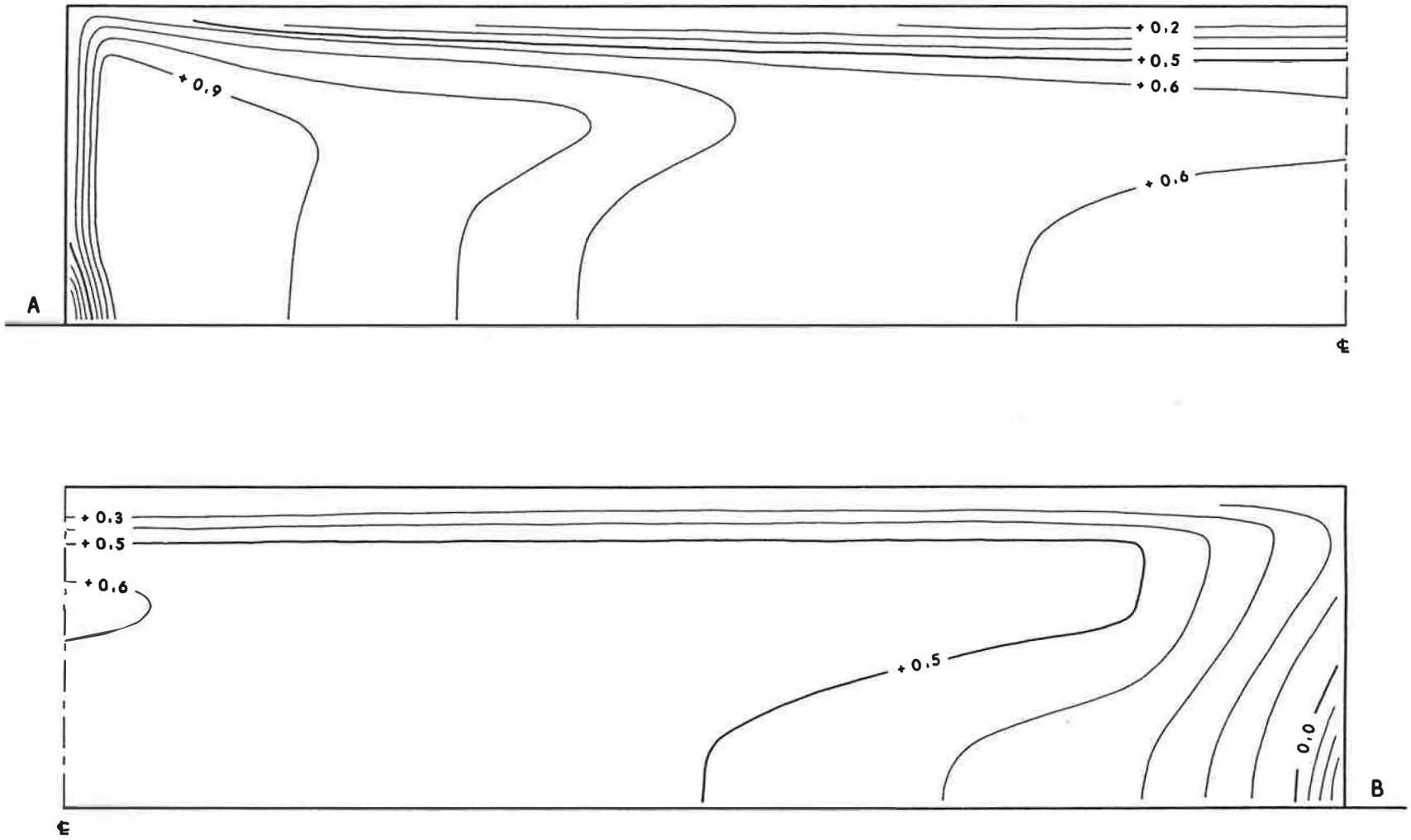

FIG. 45 H/B=1/8 α=30°

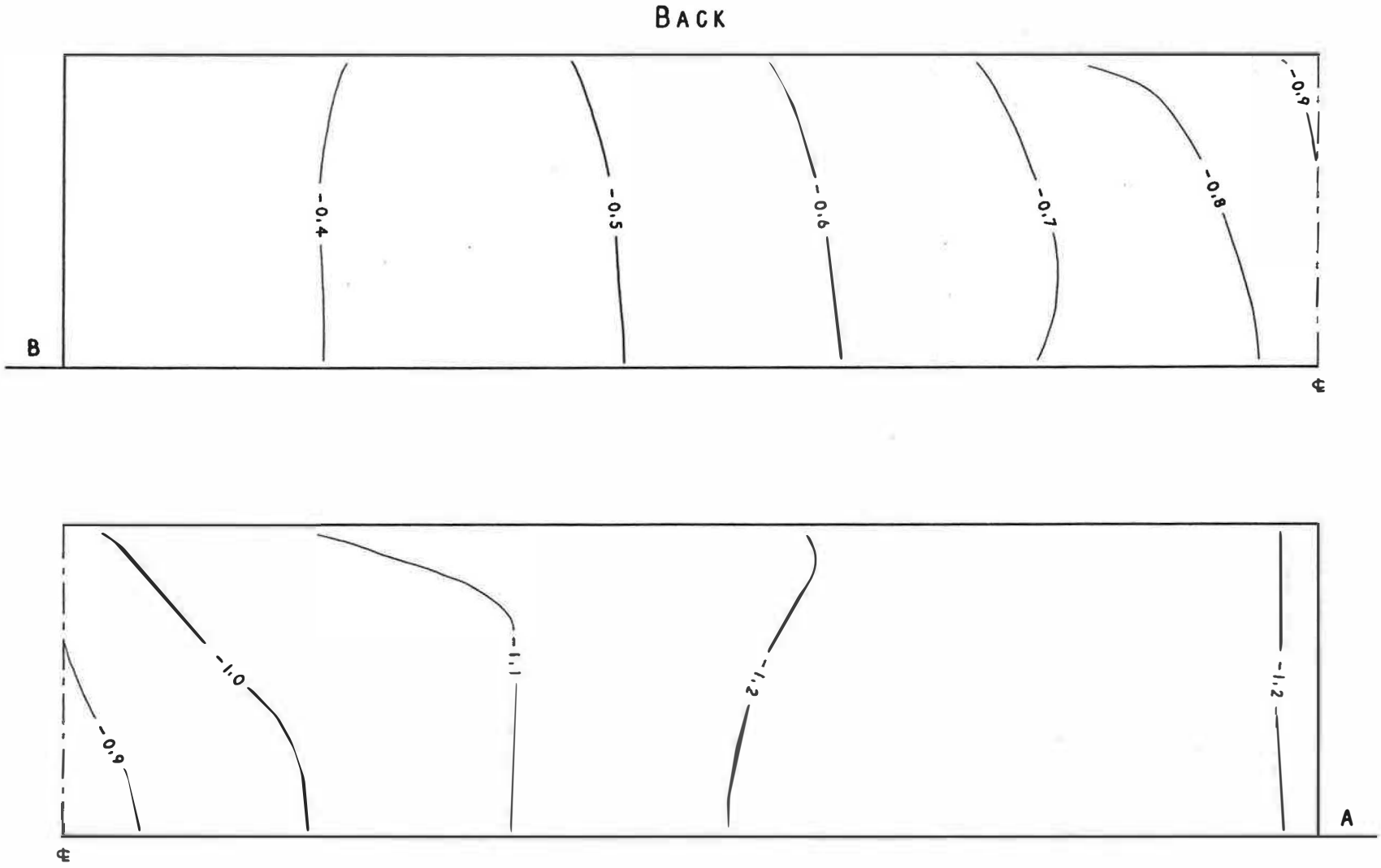

FIG. 45 (CONTINUED)

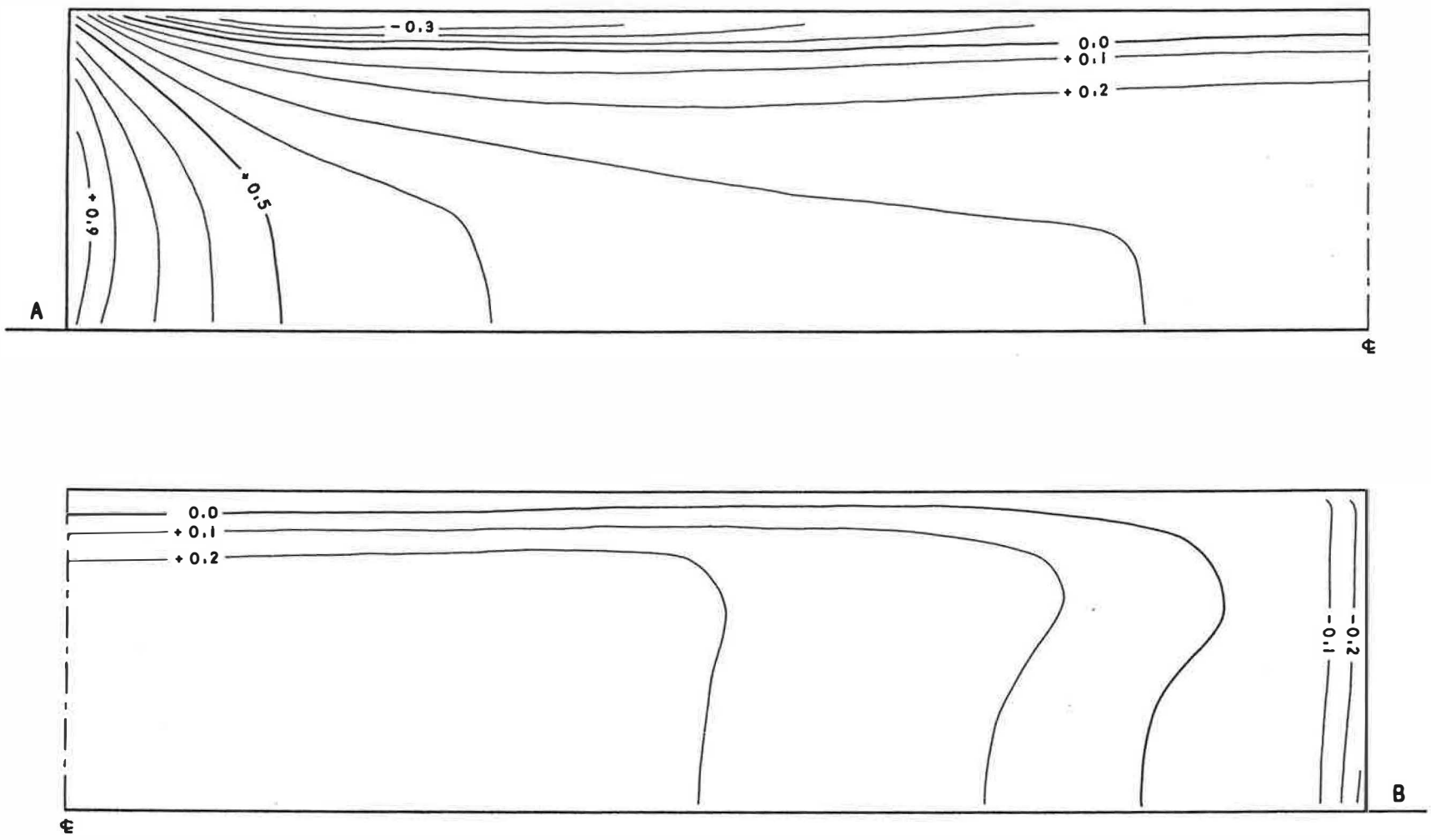

FIG. 46 H/B=1/8 $\alpha = 60°$

BACK

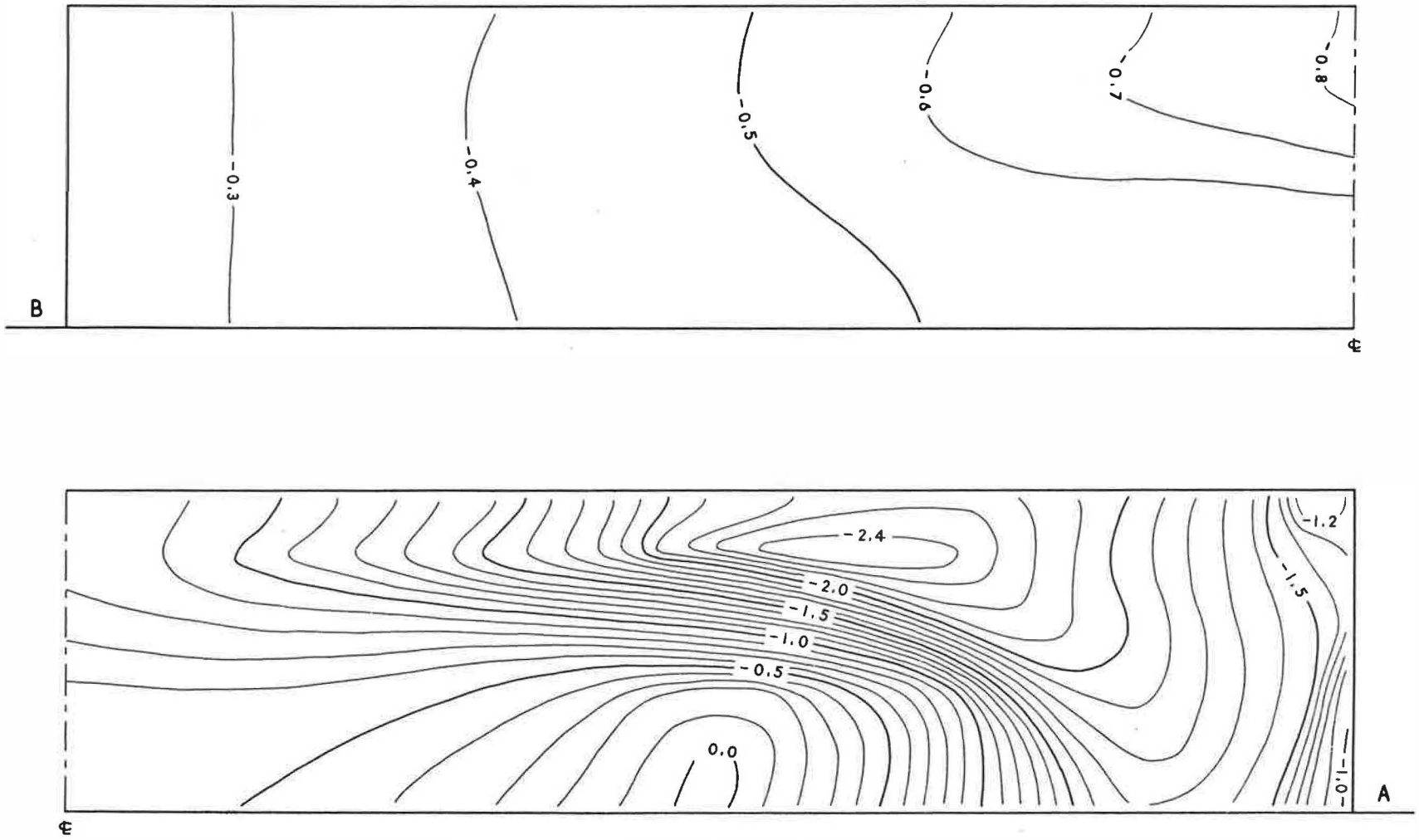

FIG. 46 (CONTINUED)

FRONT

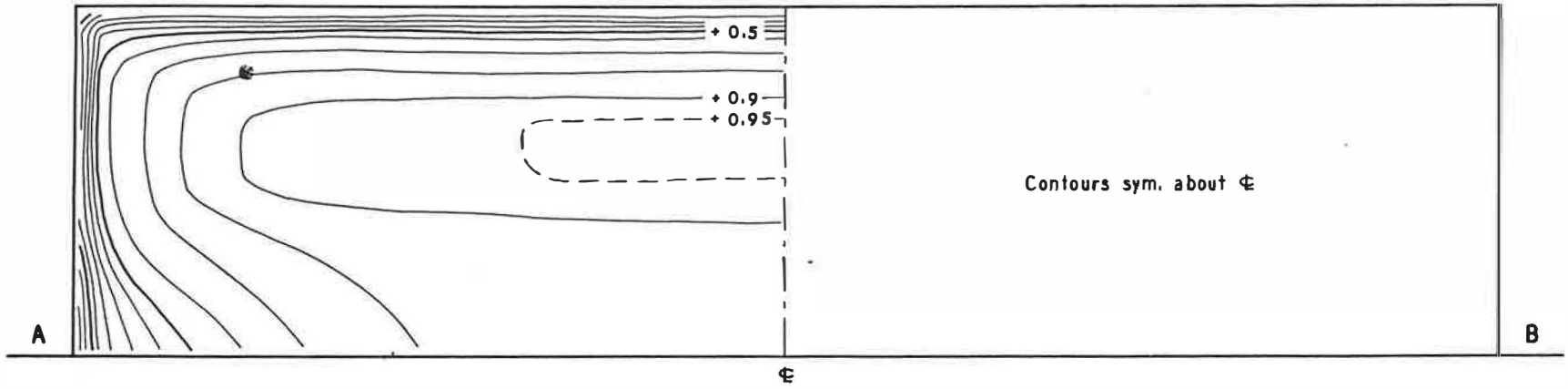

BACK

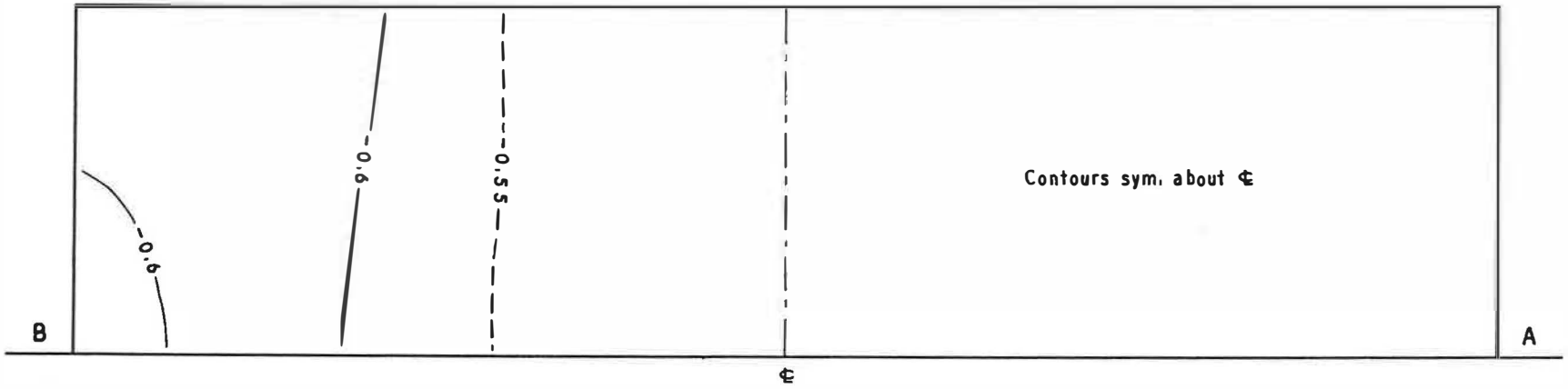

FIG. 47 H/B=1/4 $\alpha = 0°$

FRONT

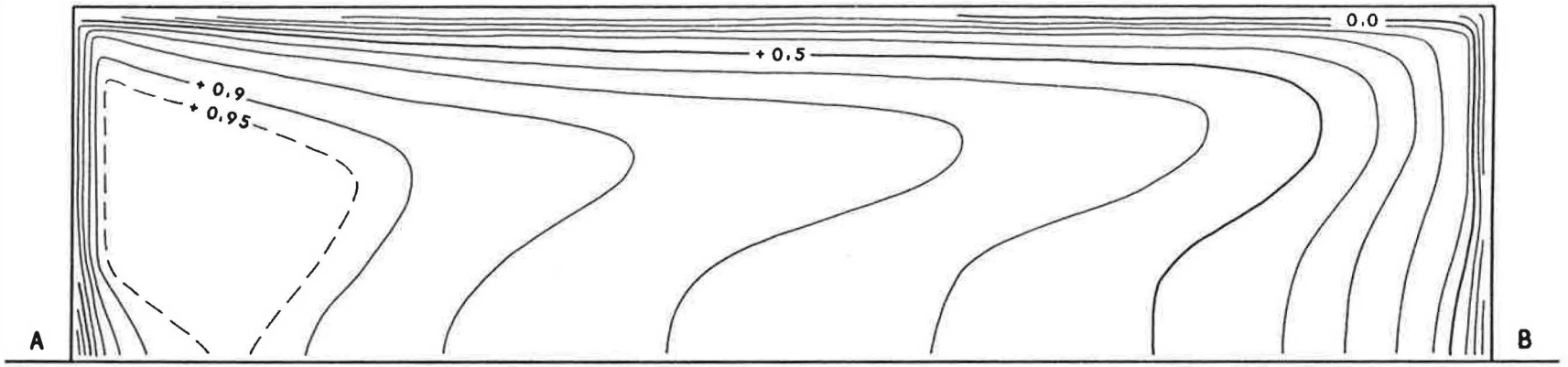

BACK

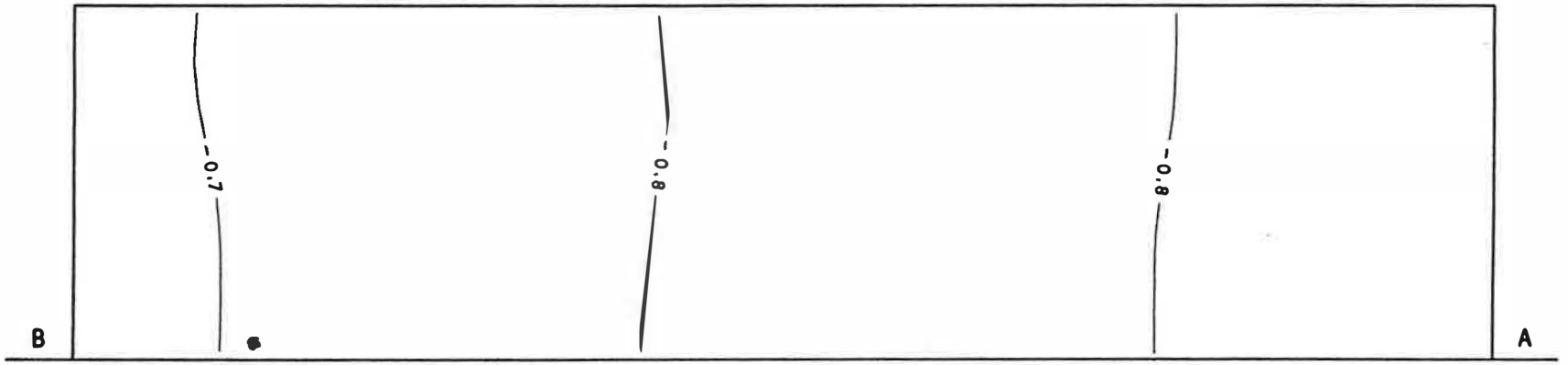

FIG. 48 H/B=1/4 α=30°

FRONT

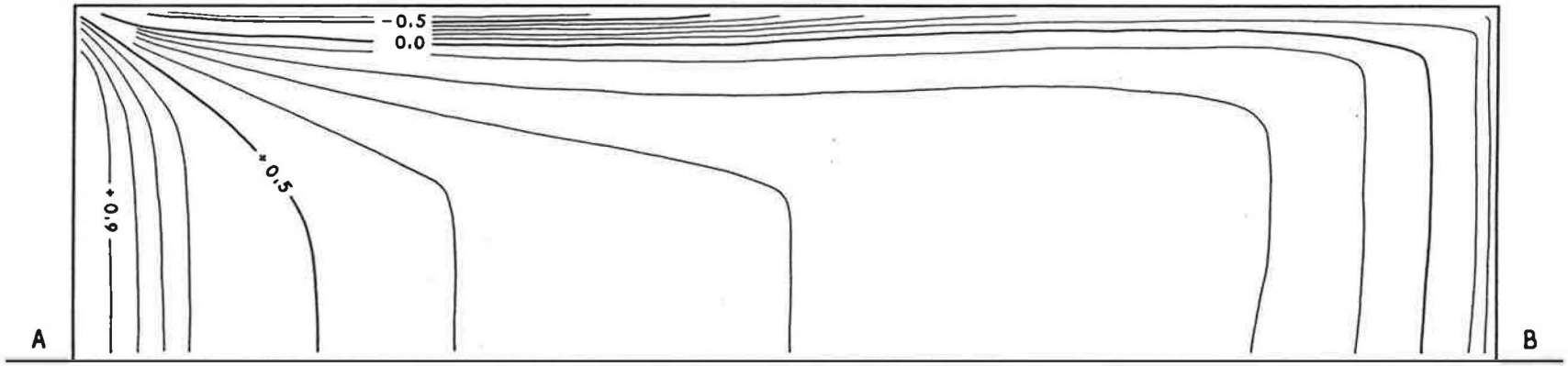

BACK

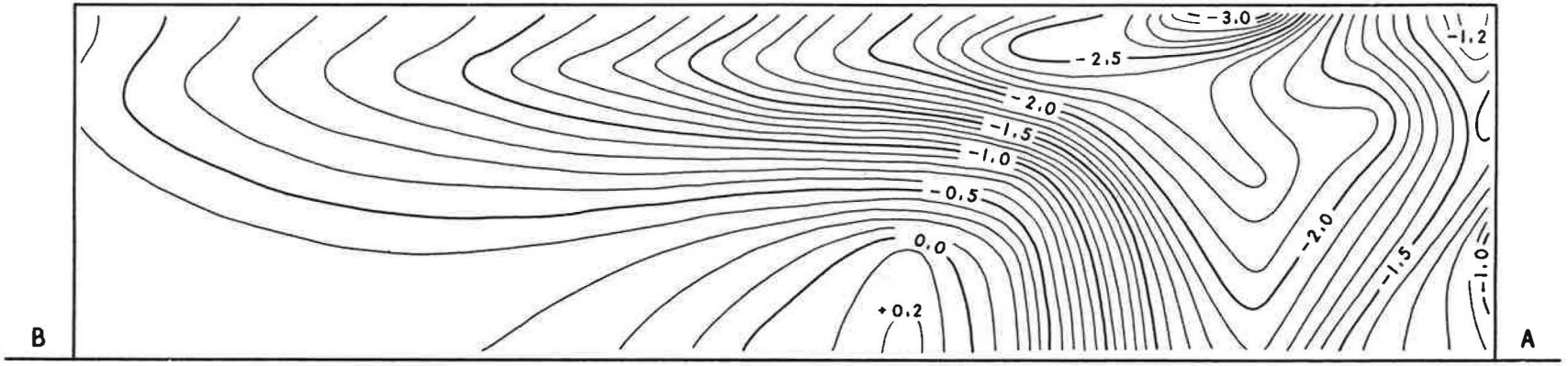

FIG. 49 H/B=1/4 α=60°

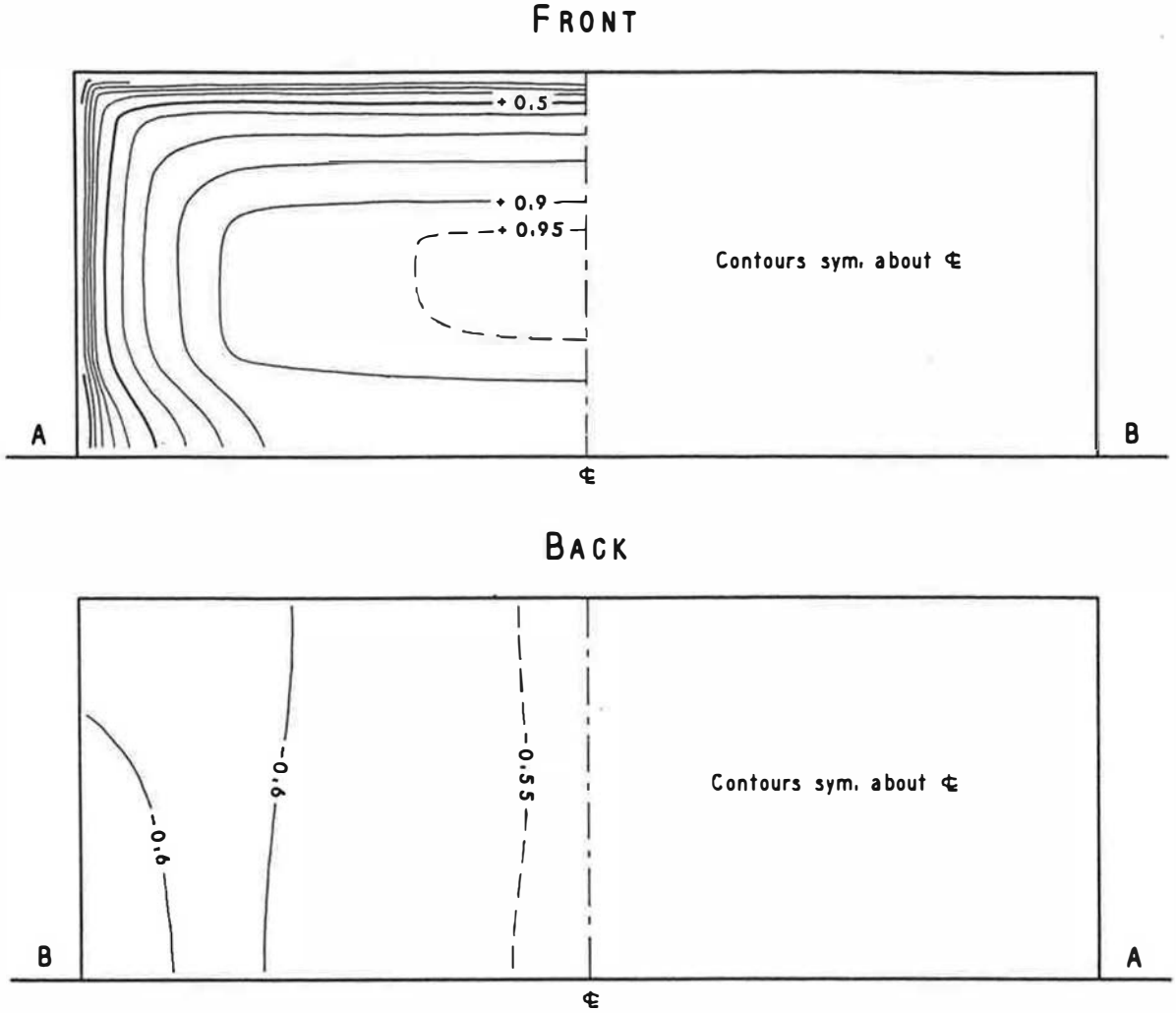

FIG. 50 H/B=3/8 $\alpha = 0°$

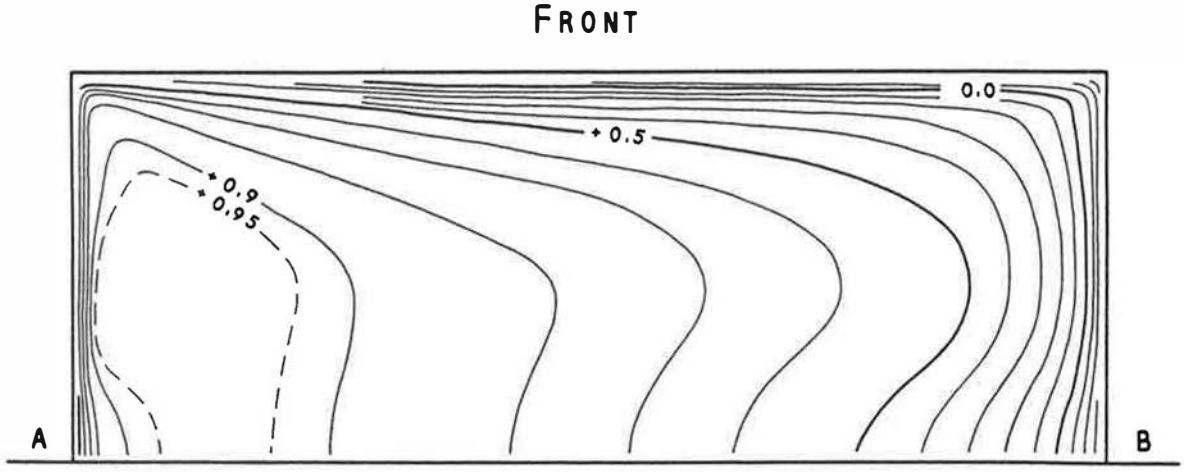

FIG. 51 H/B=3/8 $\alpha = 30°$

BACK

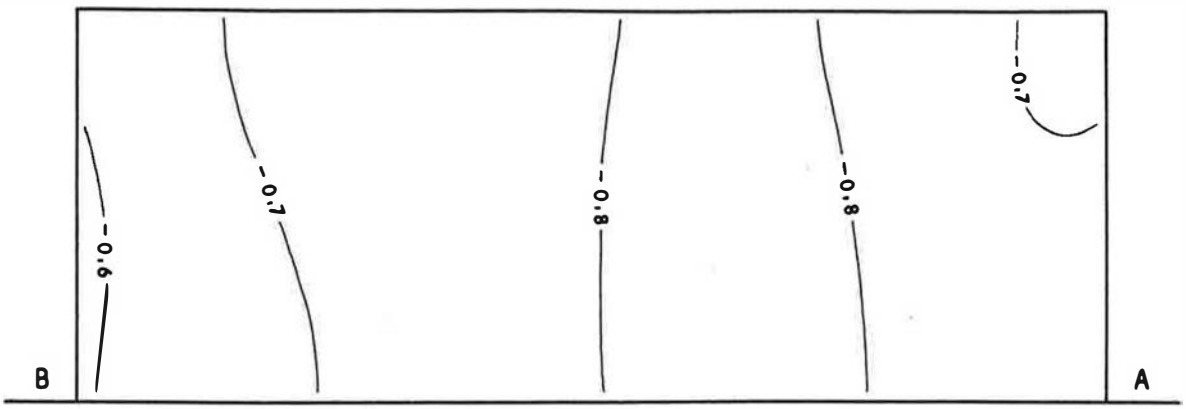

FIG. 51 (CONTINUED)

FRONT

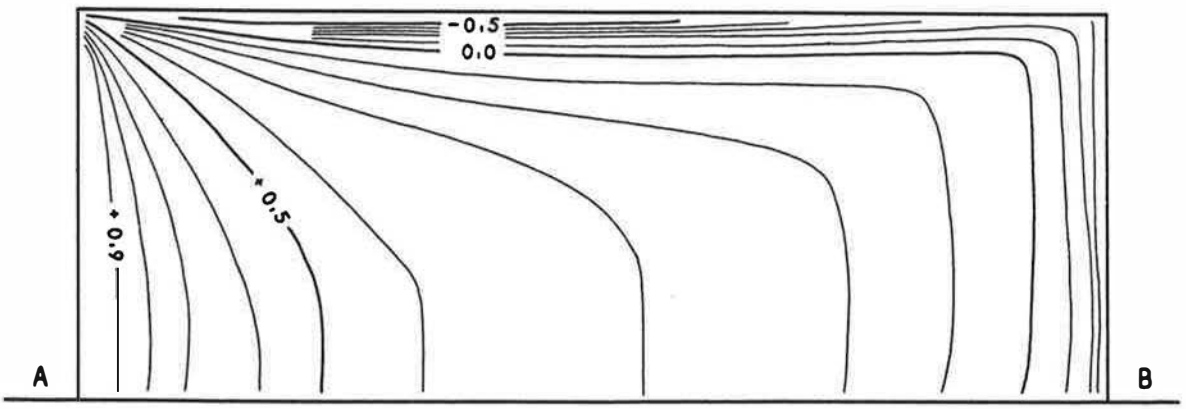

BACK

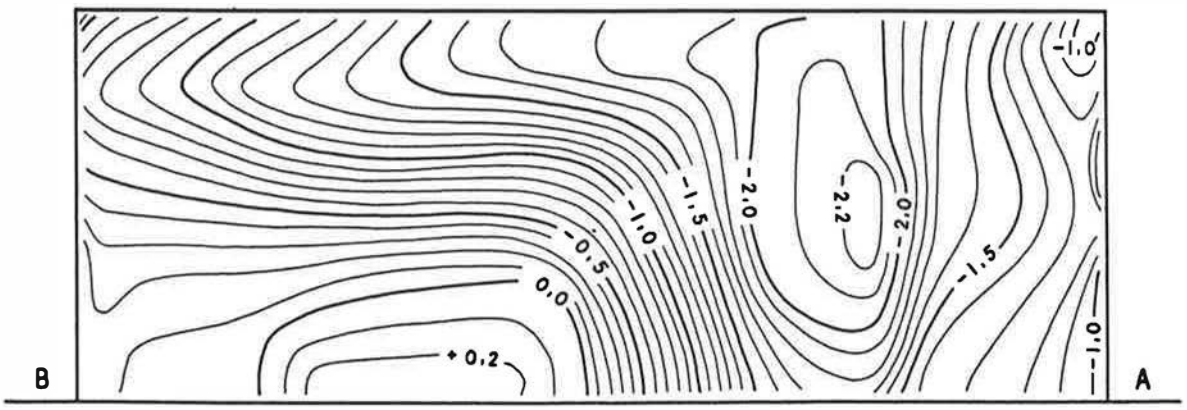

FIG. 52 H/B=3/8 α=60°

FRONT

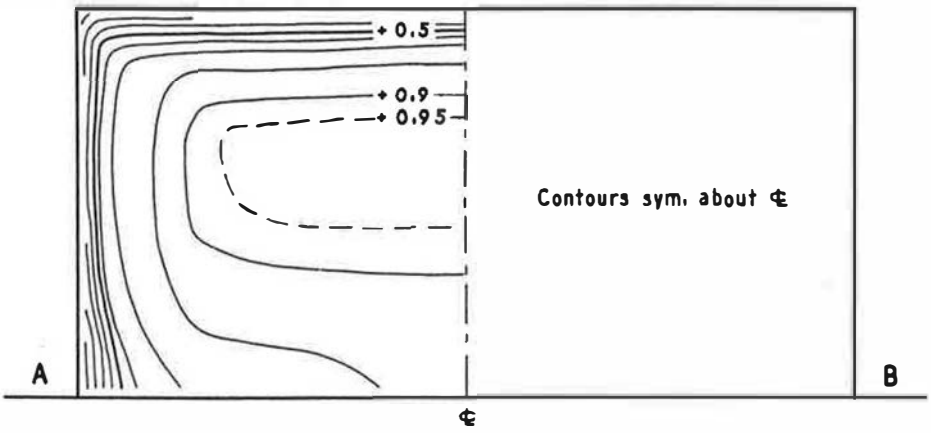

BACK

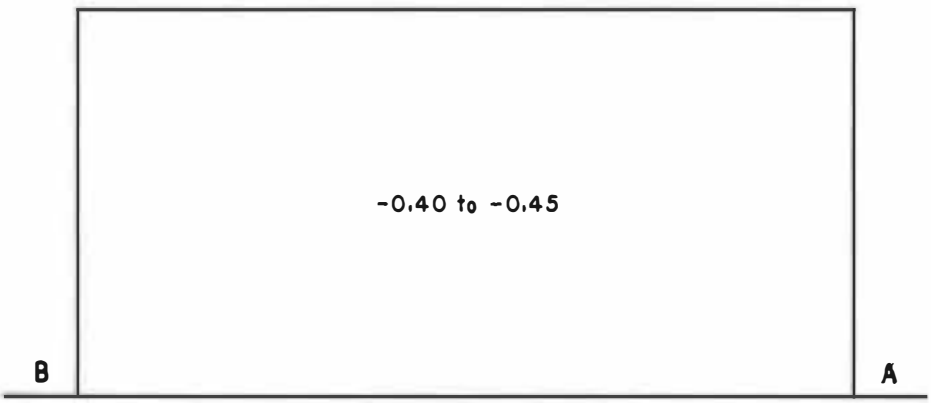

FIG. 53 H/B = 1/2 $\alpha = 0°$

FRONT

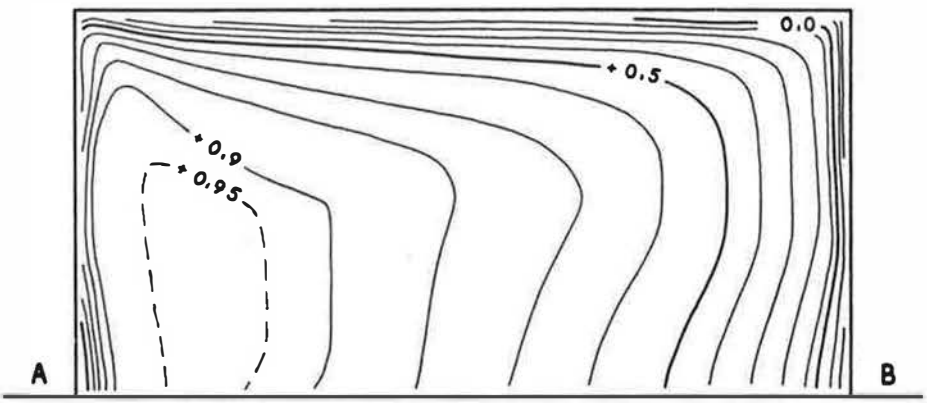

FIG. 54 H/B = 1/2 $\alpha = 30°$

BACK

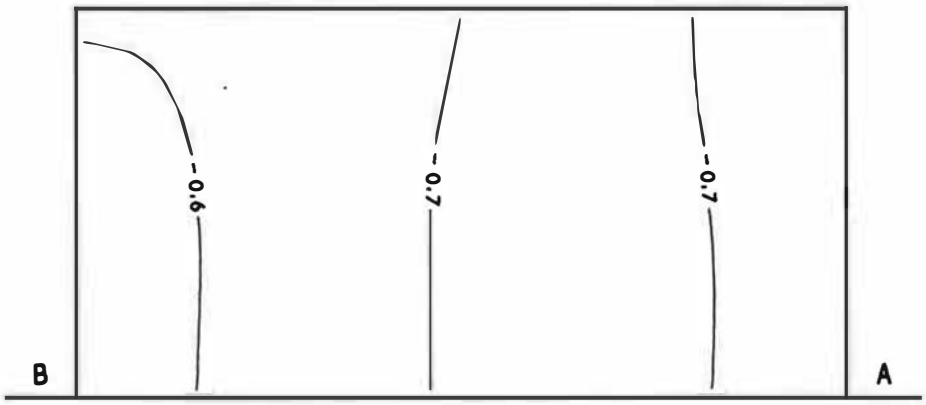

FIG. 54 (CONTINUED)

FRONT

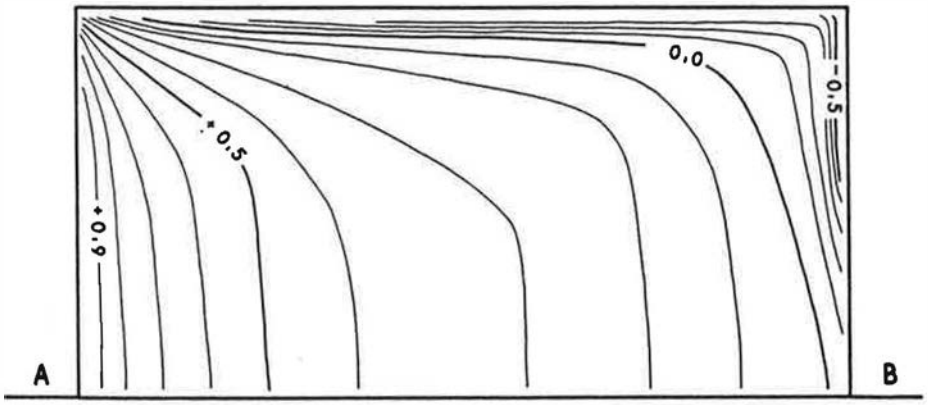

BACK

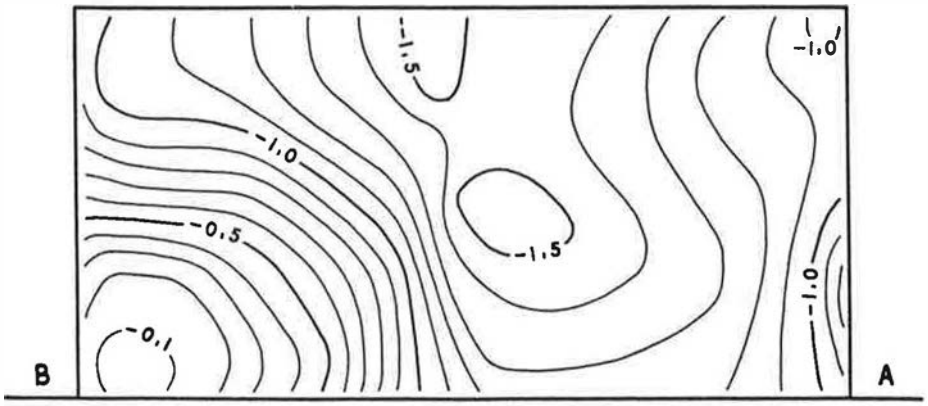

FIG. 55 H/B=1/2 $\alpha=60^{\circ}$

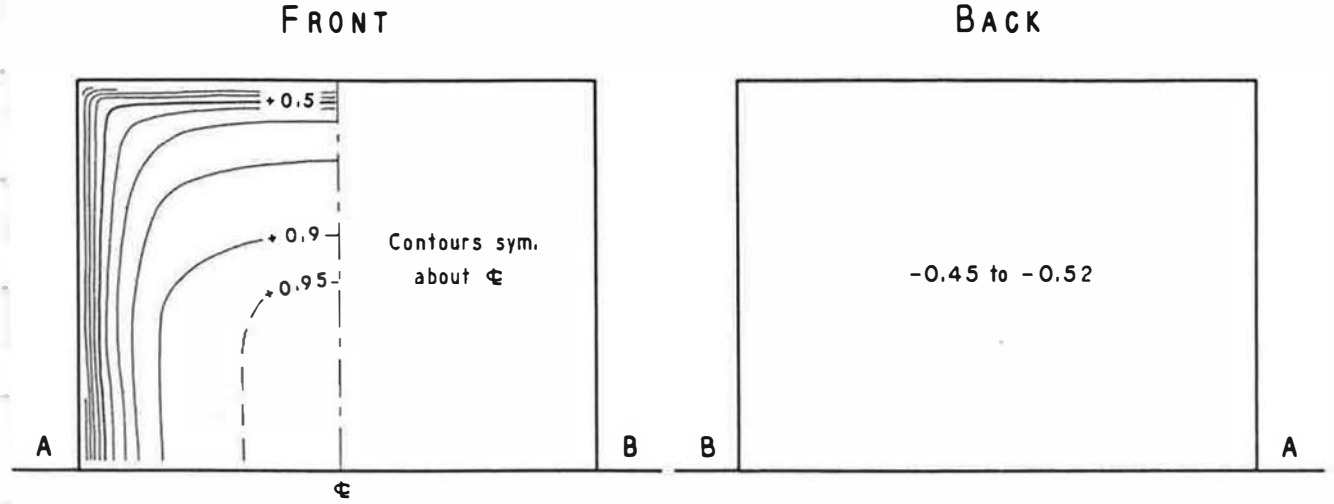

FIG. 56 H/B=3/4 $\alpha = 0°$

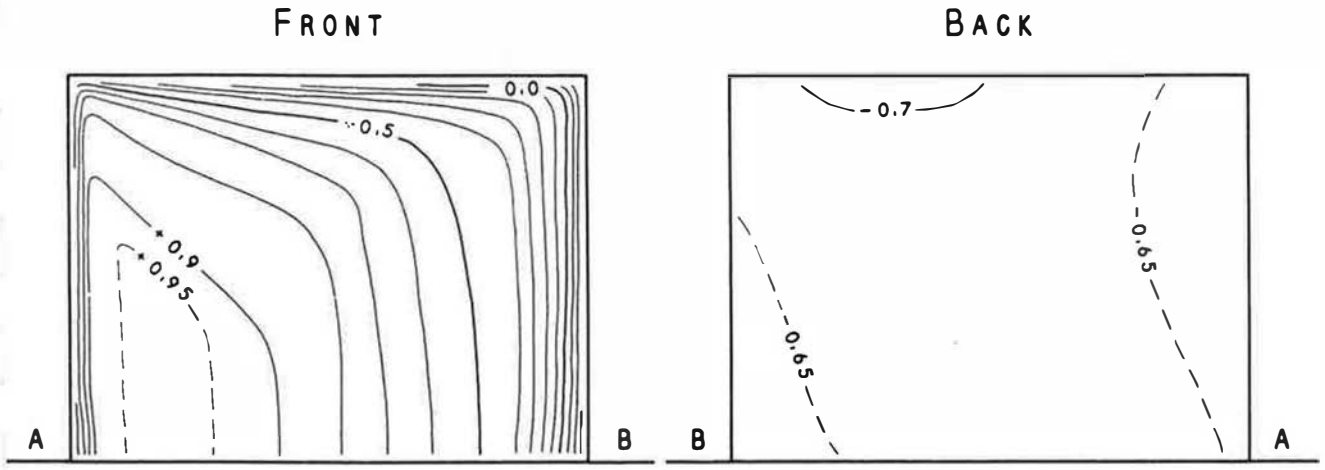

FIG. 57 H/B=3/4 $\alpha = 30°$

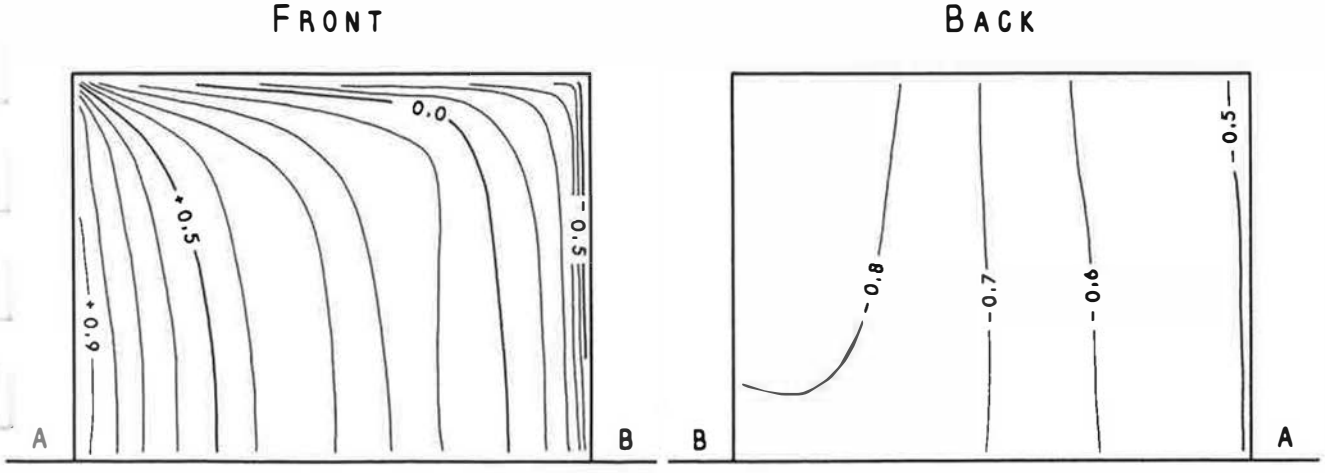

FIG. 58 H/B=3/4 $\alpha = 60°$

FRONT

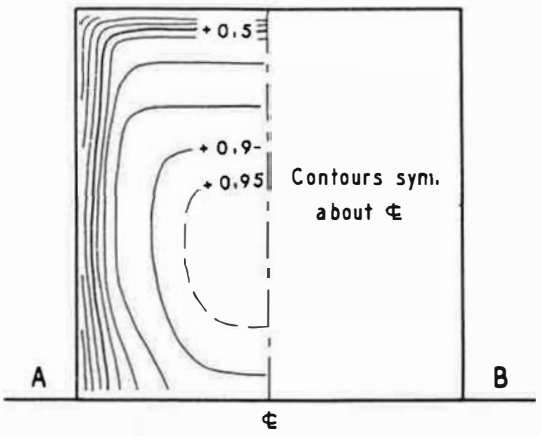

BACK

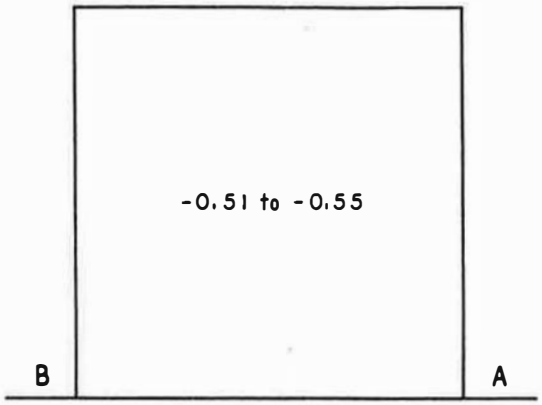

FIG. 59 H/B=1 $\alpha = 0°$

FRONT

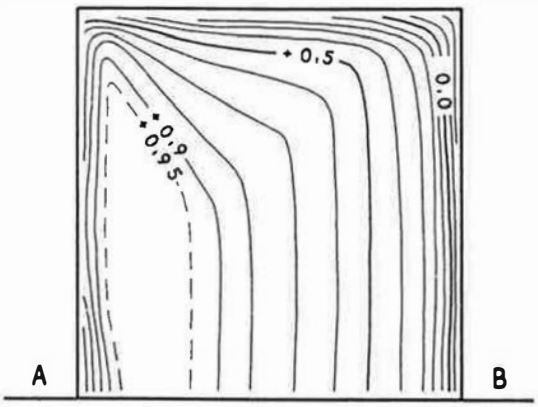

BACK

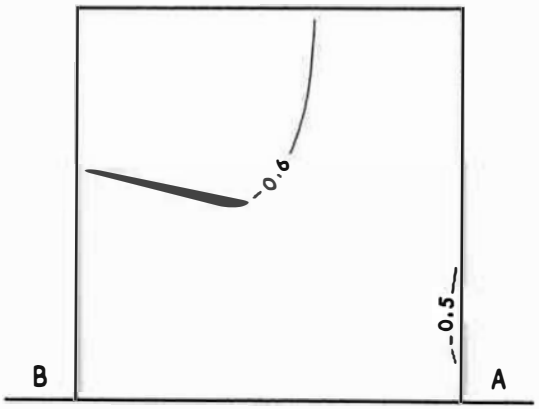

FIG. 60 H/B=1 $\alpha = 30°$

FRONT

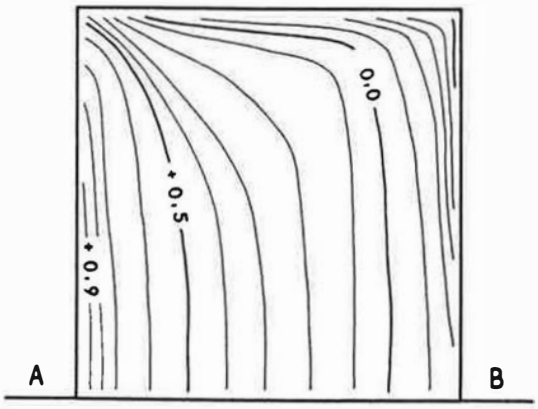

BACK

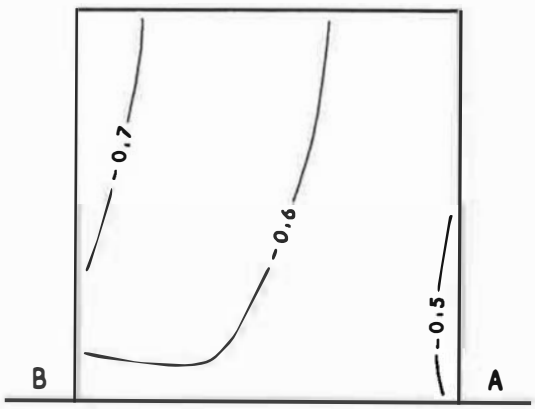

FIG. 61 H/B=1 $\alpha = 60°$

FRONT

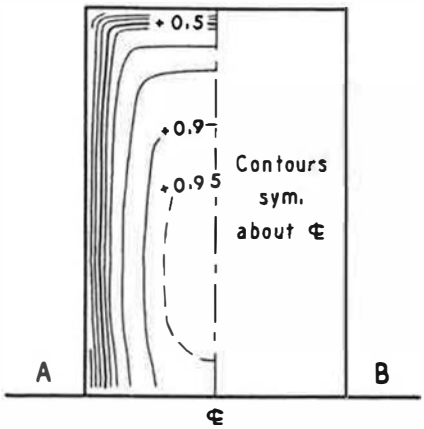

BACK

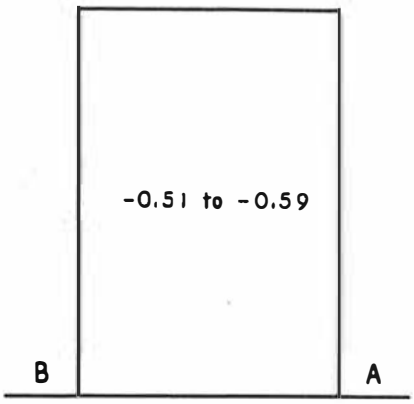

FIG. 62 H/B=3/2 $\alpha=0°$

FRONT

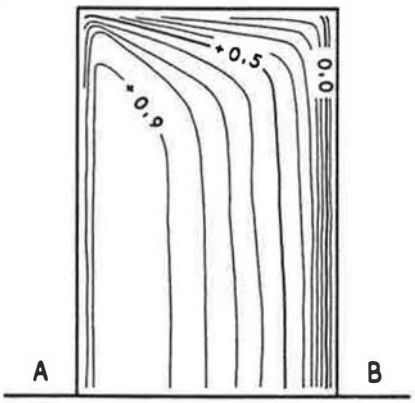

BACK

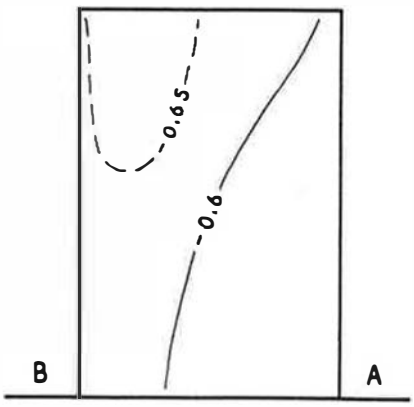

FIG. 63 H/B=3/2 $\alpha=30°$

FRONT

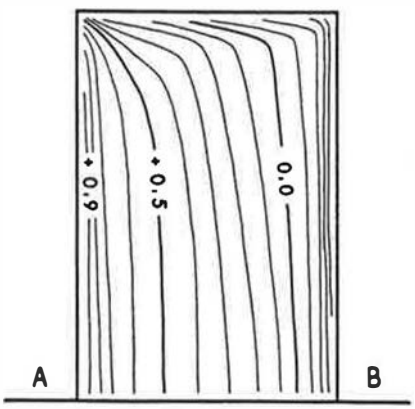

BACK

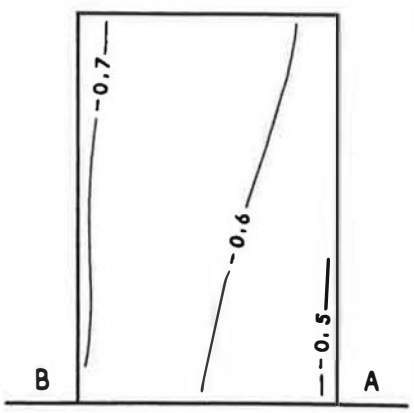

FIG. 64 H/B=3/2 $\alpha=60°$

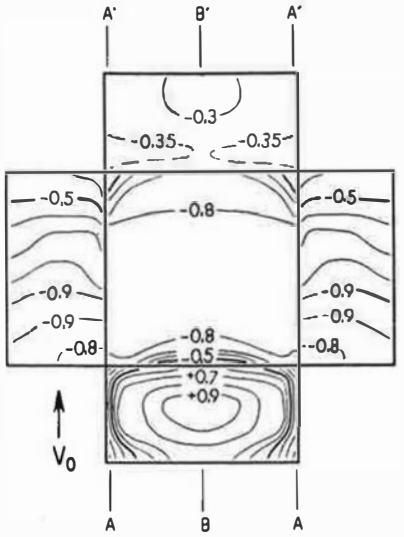

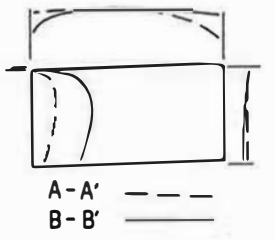

FIG. 65

θ=0°
H/B=1/2 α=0°
L/B=1

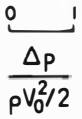

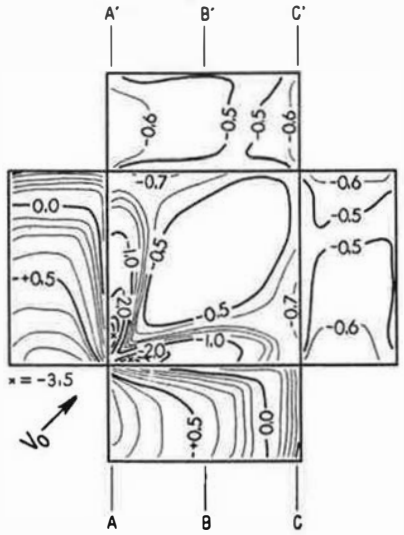

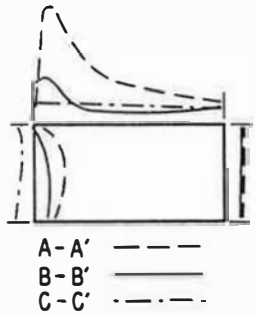

FIG. 66

θ=0°
H/B=1/2 α=45°
L/B=1

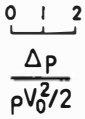

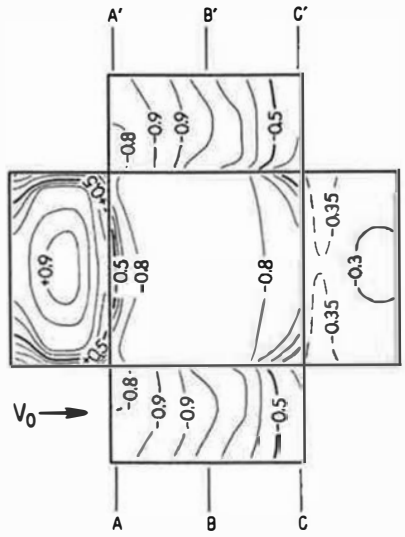

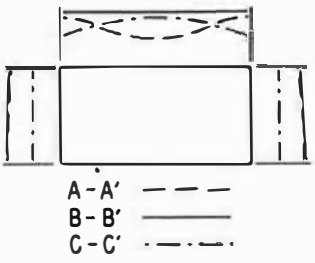

FIG. 67

θ=0°
H/B=1/2 α=90°
L/B=1

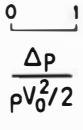

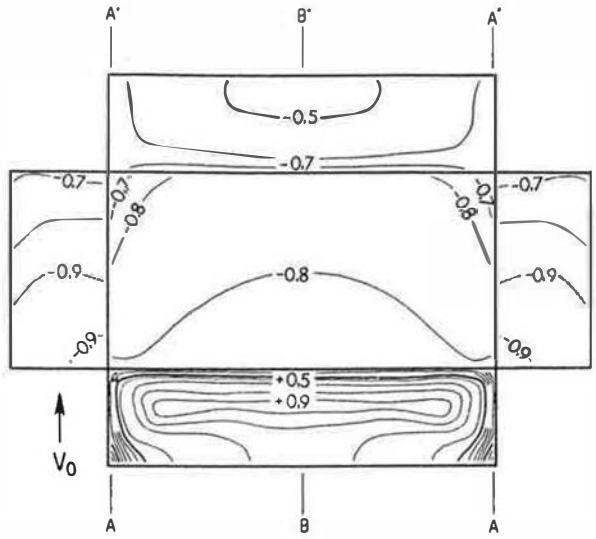

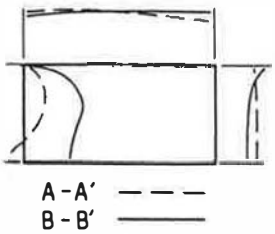

FIG. 68

θ=0°
H/B=1/2 α=0°
L/B=2

$\frac{\Delta P}{\rho V_0^2/2}$ (0 — 1)

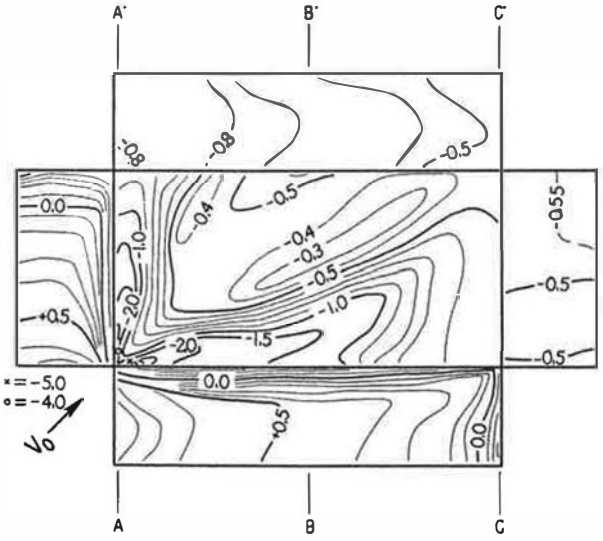

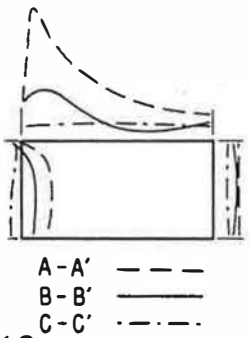

FIG. 69

θ=0°
H/B=1/2 α=45°
L/B=2

$\frac{\Delta P}{\rho V_0^2/2}$ (0 — 1 — 2)

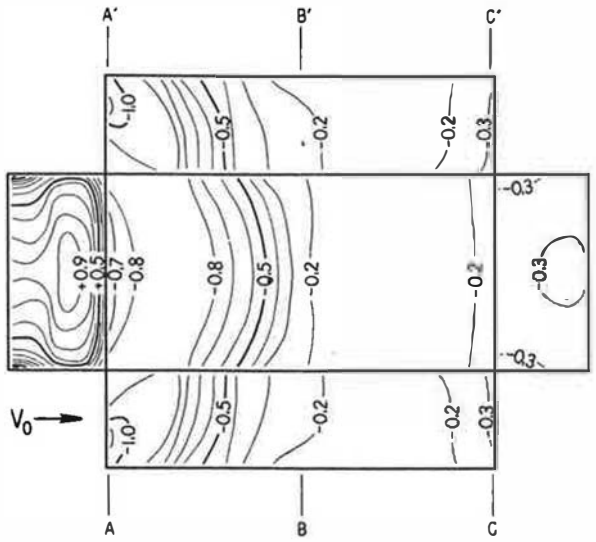

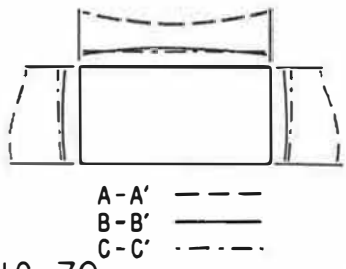

FIG. 70

θ=0°
H/B=1/2 α=90°
L/B=2

$\frac{\Delta P}{\rho V_0^2/2}$ (0 — 1)

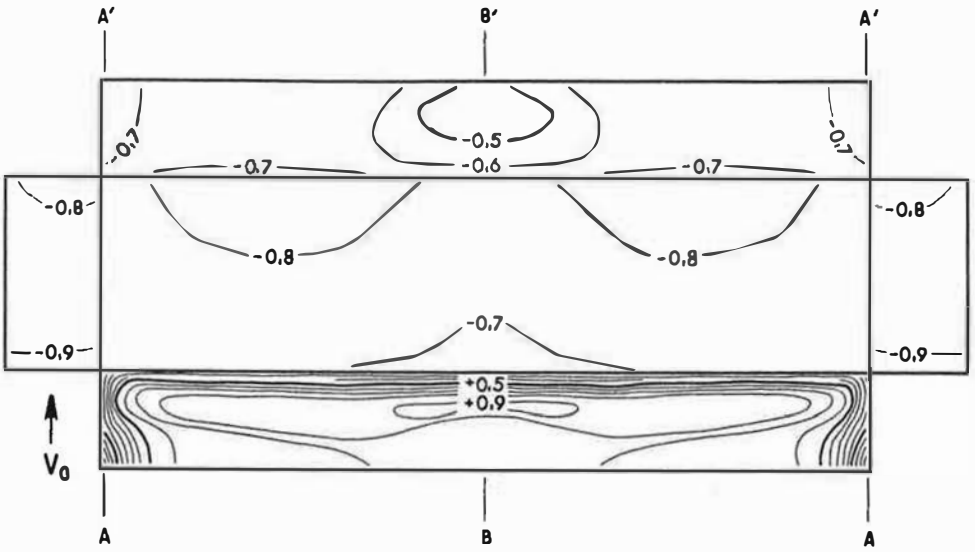

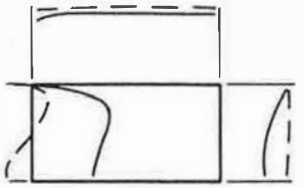

FIG. 71

θ = 0°
H/B = 1/2 α = 0°
L/B = 4

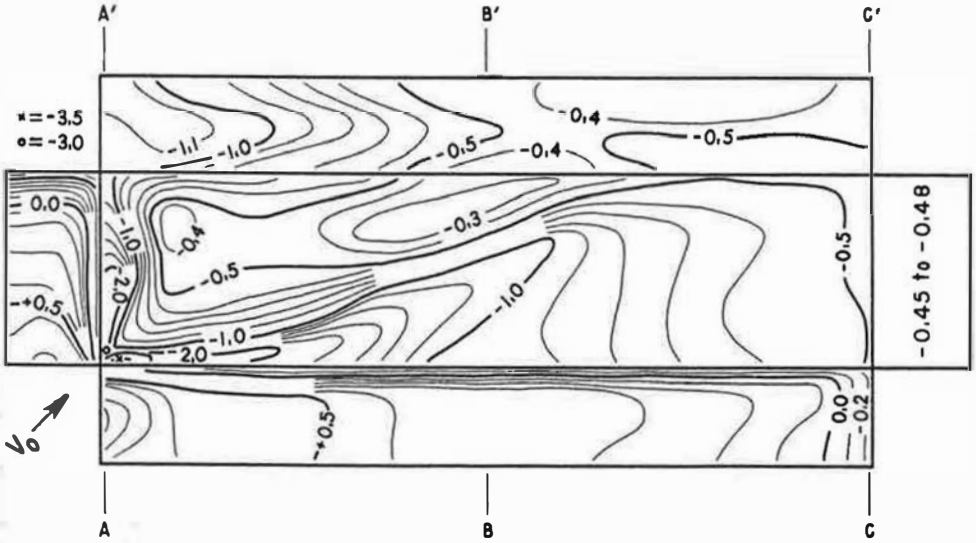

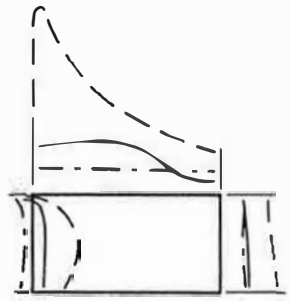

FIG. 72

θ = 0°
H/B = 1/2 α = 45°
L/B = 4

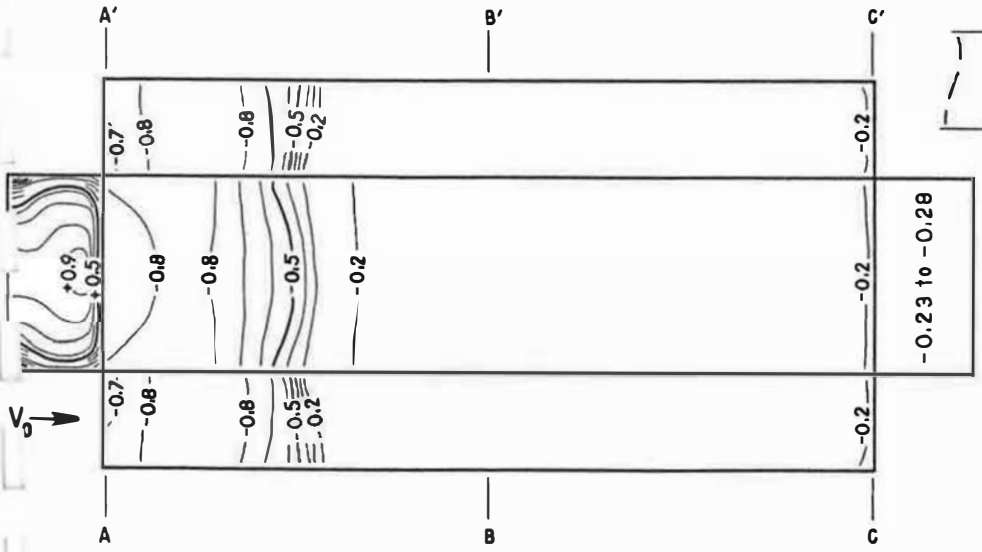

FIG. 73

θ = 0°
H/B = 1/2 α = 90°
L/B = 4

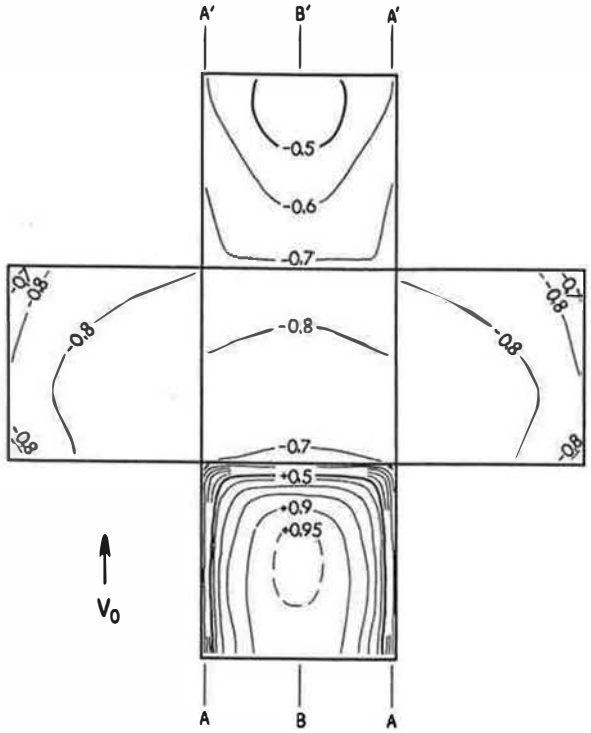

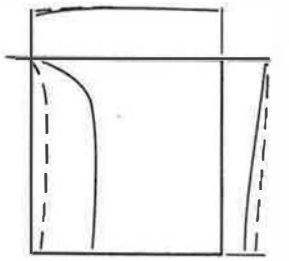

A-A′ — — —
B-B′ ——

0 1

$\frac{\Delta P}{\rho V_0^2/2}$

FIG. 74

θ=0°
H/B=1 α = 0°
L/B=1

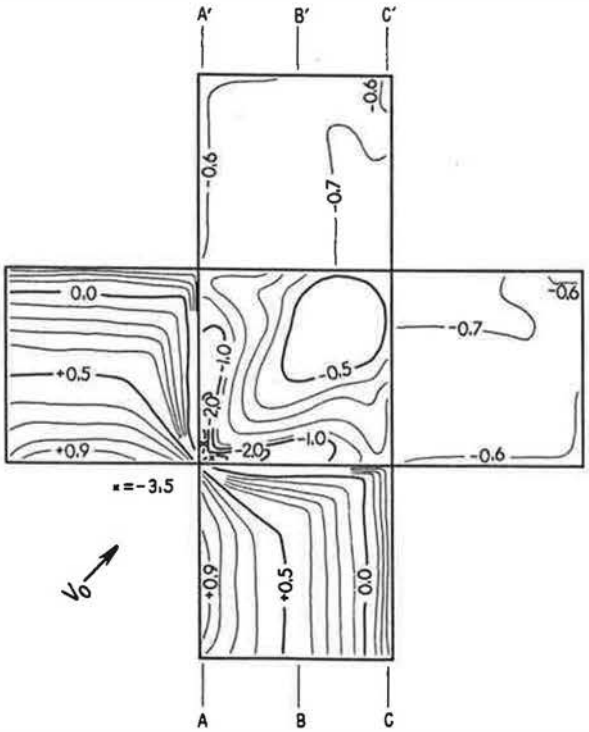

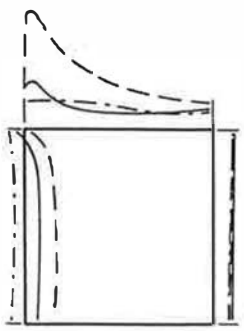

A-A′ — — —
B-B′ ——
C-C′ -·-·-

0 1 2

$\frac{\Delta P}{\rho V_0^2/2}$

FIG. 75

θ=0°
H/B=1 α=45°
L/B=1

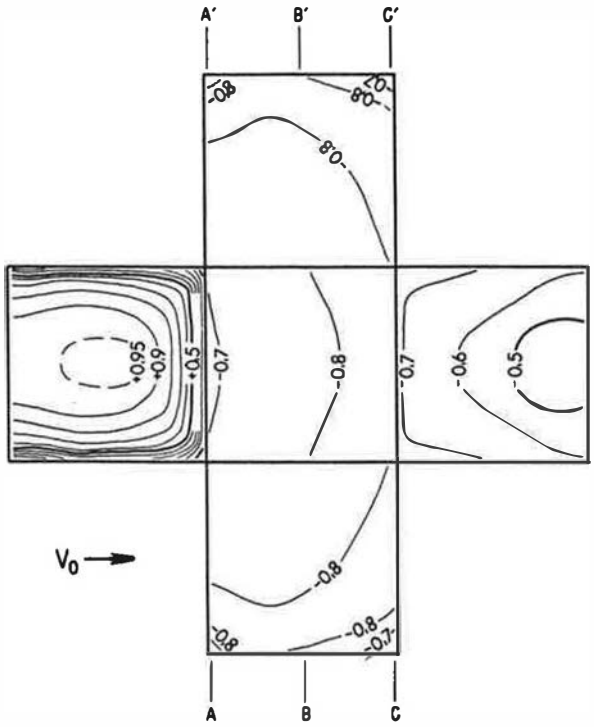

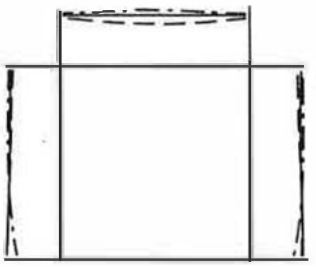

FIG. 76

θ=0°
H/B=1 $\alpha = 90°$
L/B=1

0 1

$\frac{\Delta P}{\rho V_0^2/2}$

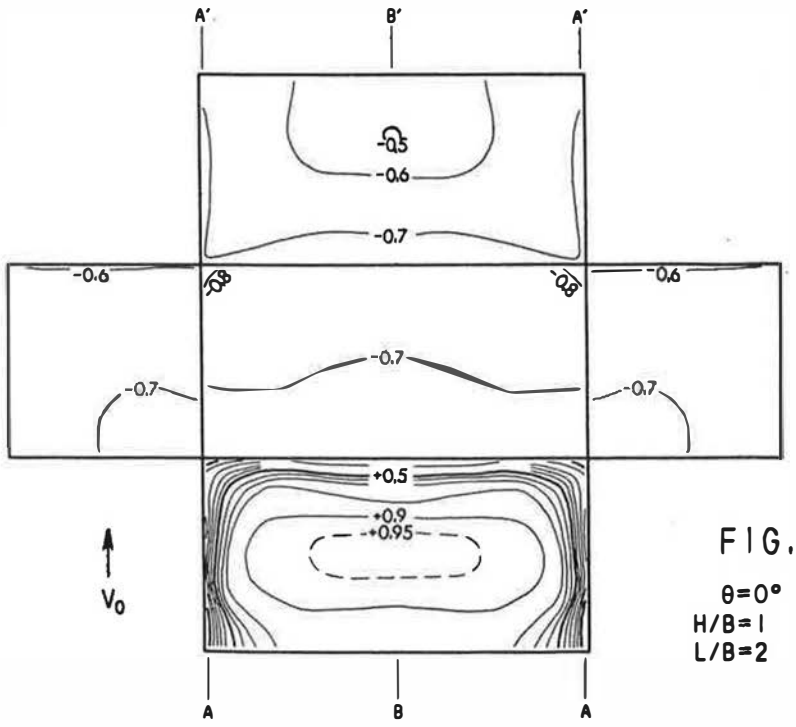

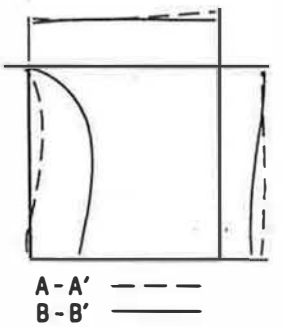

FIG. 77

θ=0°
H/B=1 $\alpha = 0°$
L/B=2

0 1

$\frac{\Delta P}{\rho V_0^2/2}$

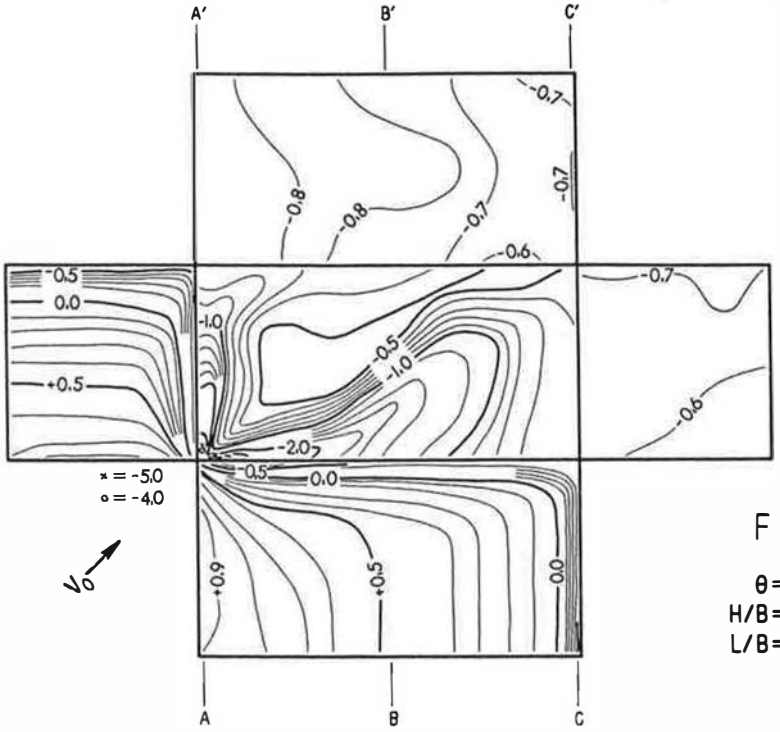

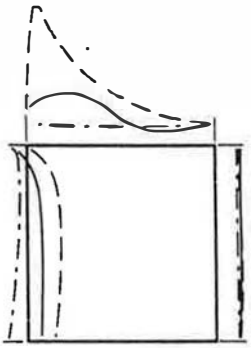

A - A′ — — —
B - B′ ——————
C - C′ -·-·-·-

0 1 2

$\frac{\Delta P}{\rho V_0^2/2}$

FIG. 78

θ=0°
H/B=1 α=45°
L/B=2

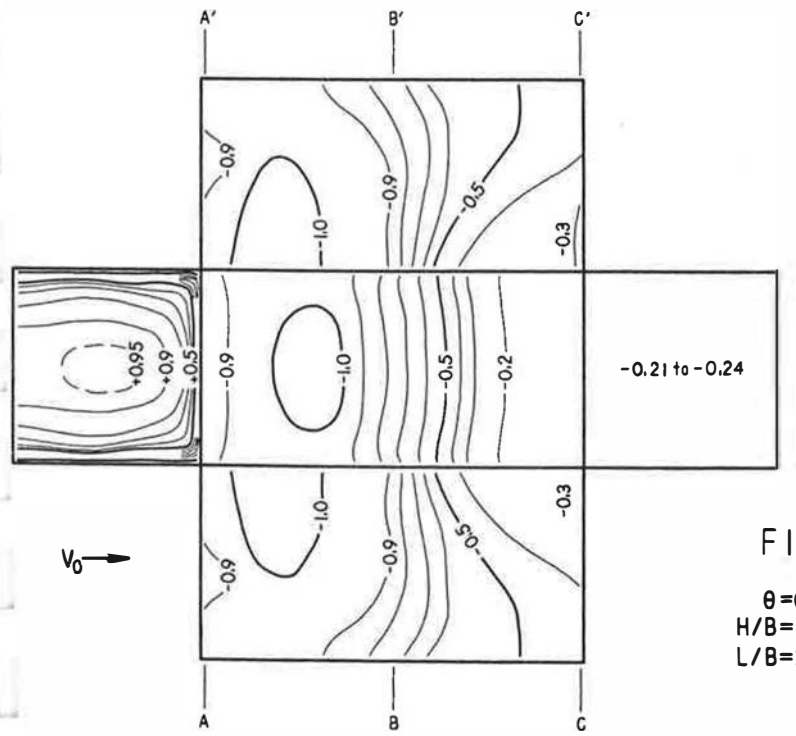

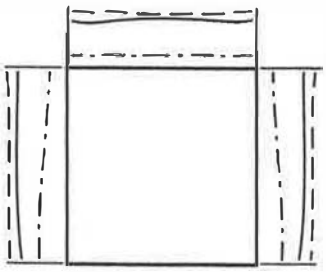

A - A′ — — —
B - B′ ——————
C - C′ -·-·-·-

0 1

$\frac{\Delta P}{\rho V_0^2/2}$

FIG. 79

θ=0°
H/B=1 α=90°
L/B=2

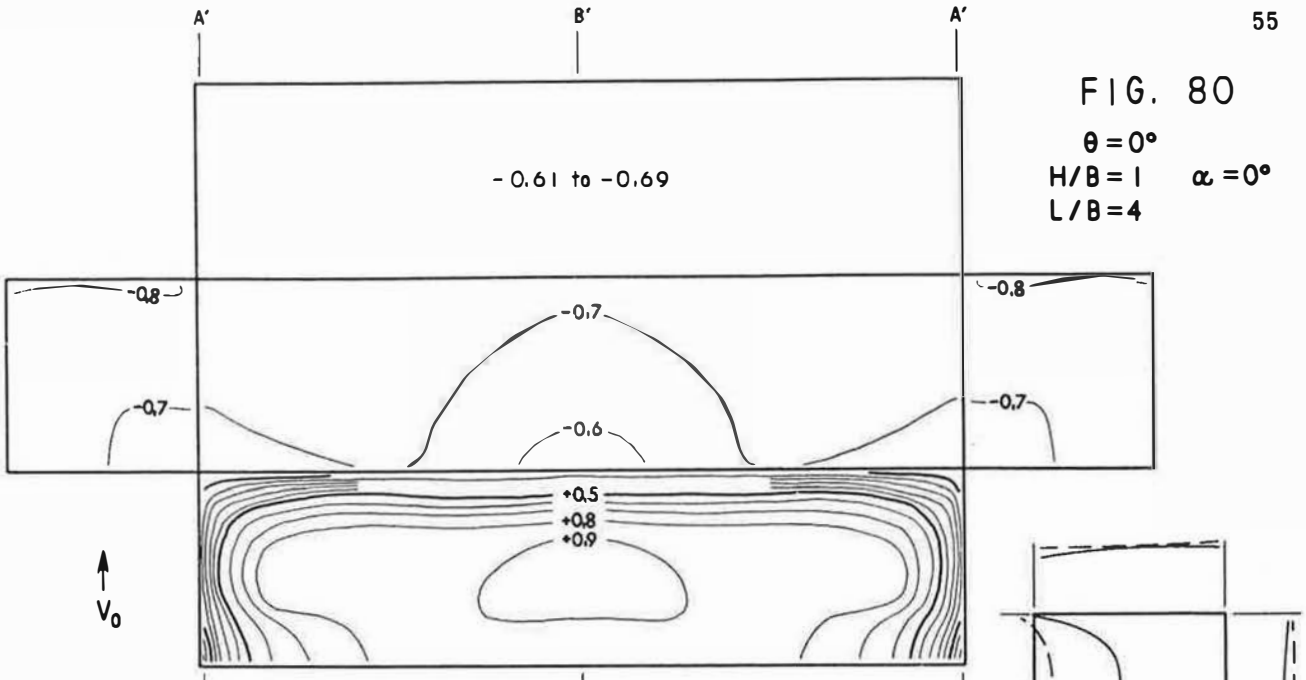

FIG. 80

θ = 0°
H/B = 1 α = 0°
L/B = 4

A - A' — — —
B - B' ———
0 1
$\frac{\Delta P}{\rho V_0^2/2}$

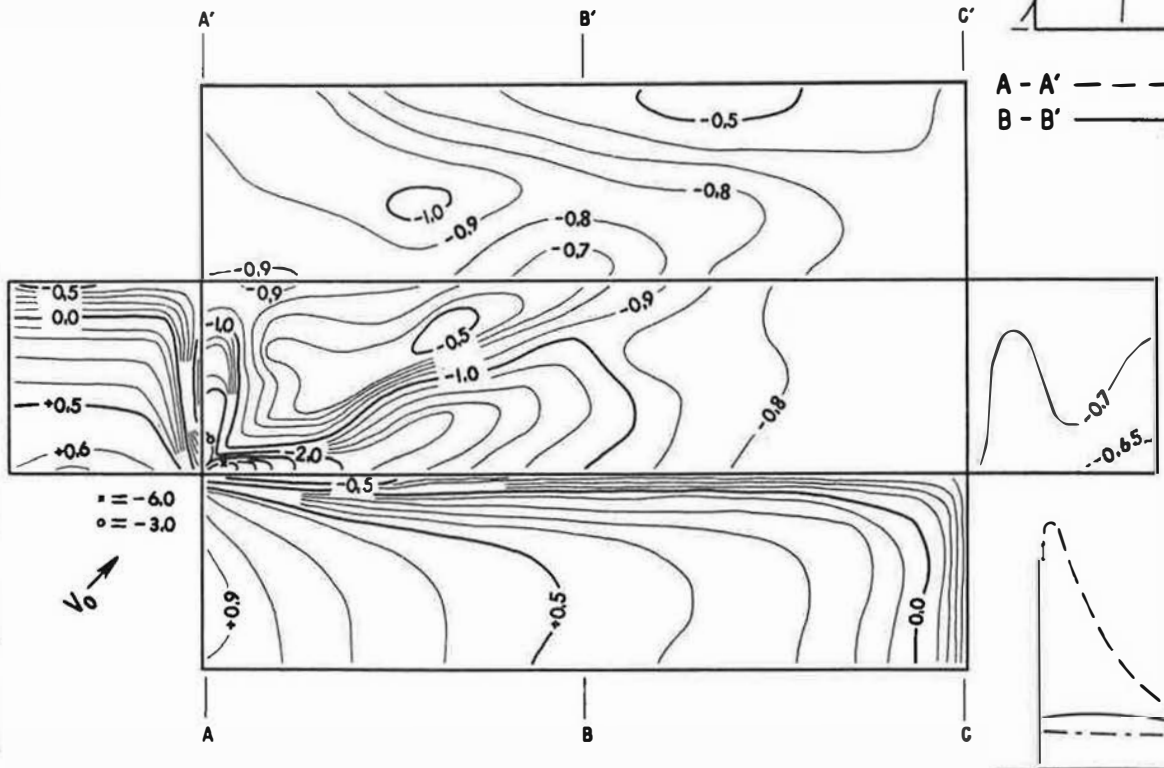

FIG. 81

θ = 0°
H/B = 1 α = 45°
L/B = 4

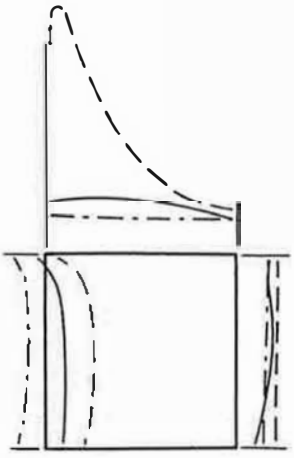

A - A' — — —
B - B' ———
C - C' ·—·—·
0 1 2
$\frac{\Delta P}{\rho V_0^2/2}$

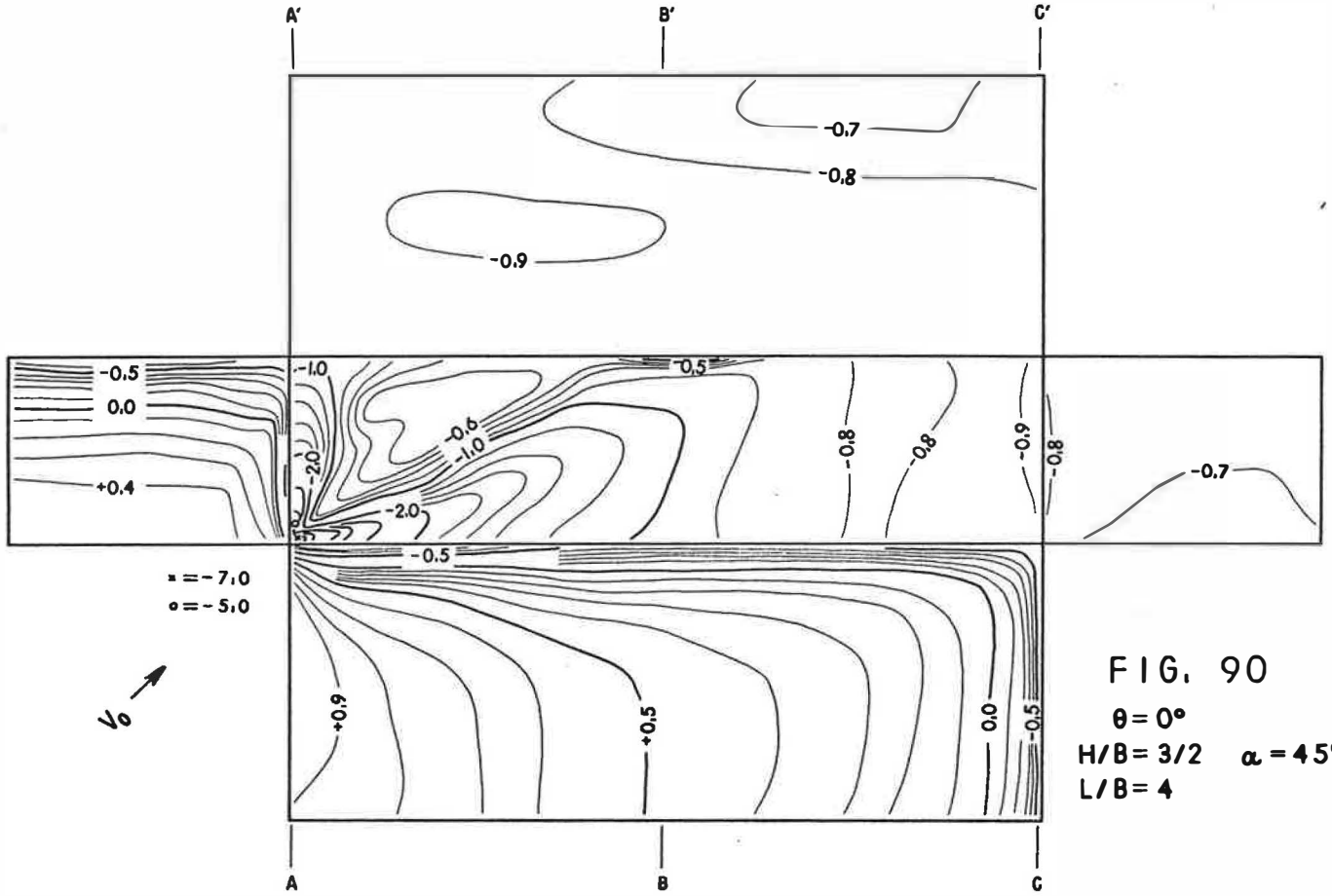

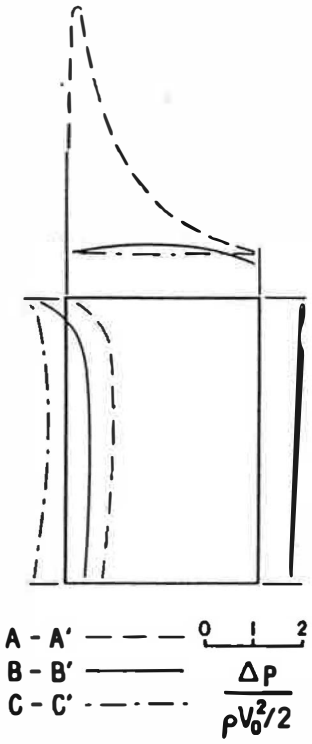

FIG. 90

θ = 0°

H/B = 3/2 α = 45°

L/B = 4

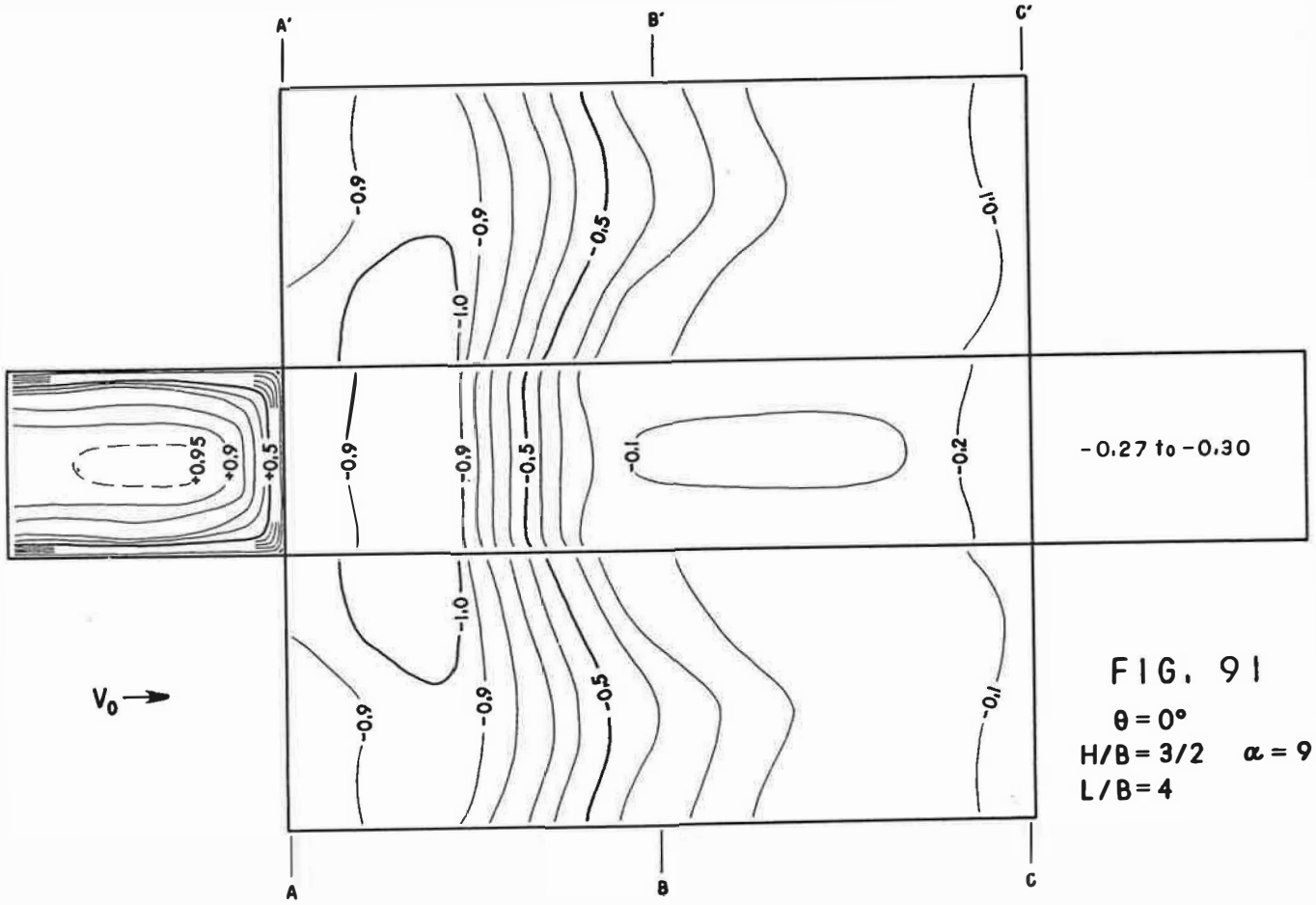

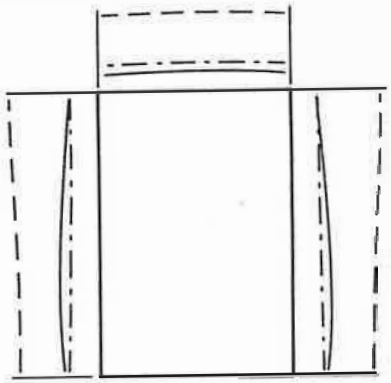

FIG. 91

$\theta = 0°$

$H/B = 3/2 \quad \alpha = 90°$

$L/B = 4$

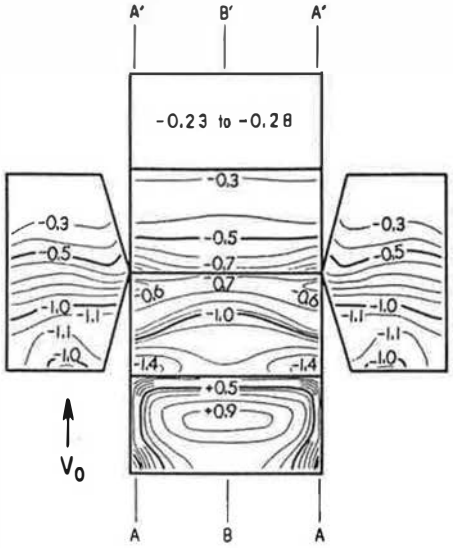

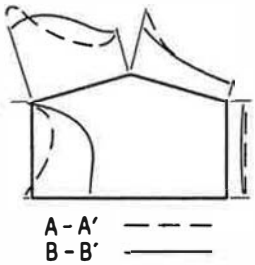

FIG. 92

θ=15°
H/B=1/2 α = 0°
L/B=1

$\frac{\Delta P}{\rho V_0^2/2}$

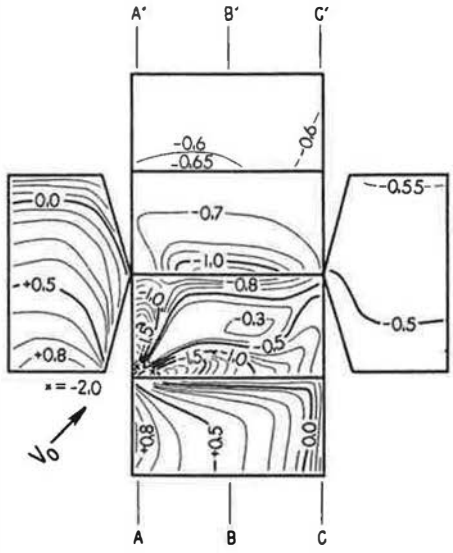

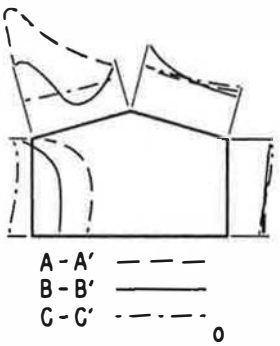

FIG. 93

θ=15°
H/B=1/2 α=45°
L/B=1

$\frac{\Delta P}{\rho V_0^2/2}$

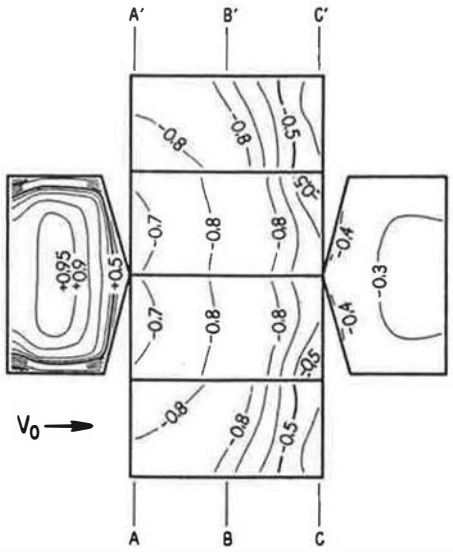

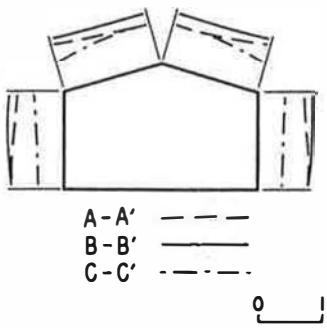

FIG. 94

θ=15°
H/B=1/2 α=90°
L/B=1

$\frac{\Delta P}{\rho V_0^2/2}$

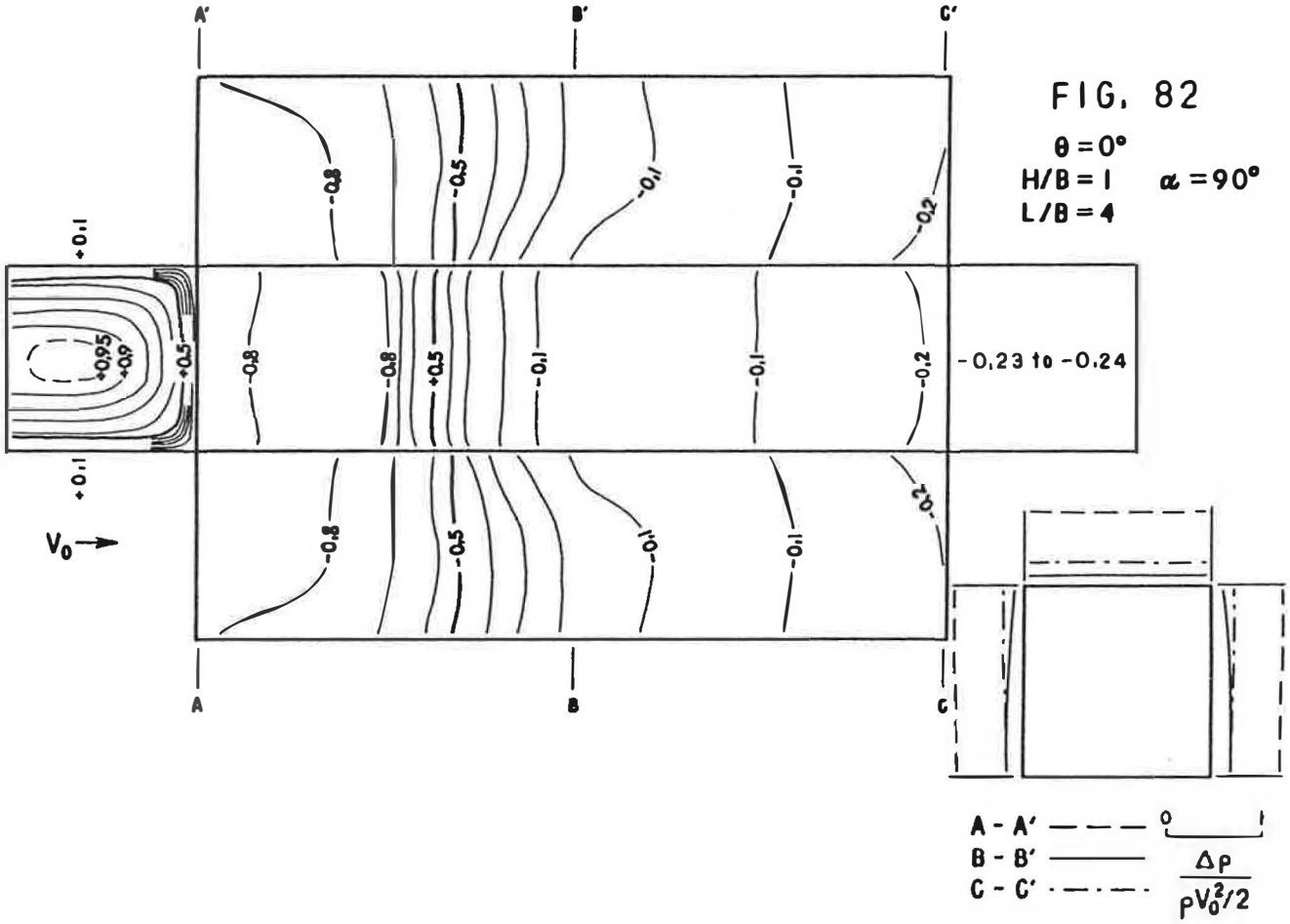

FIG. 82

$\theta = 0°$
$H/B = 1$ $\alpha = 90°$
$L/B = 4$

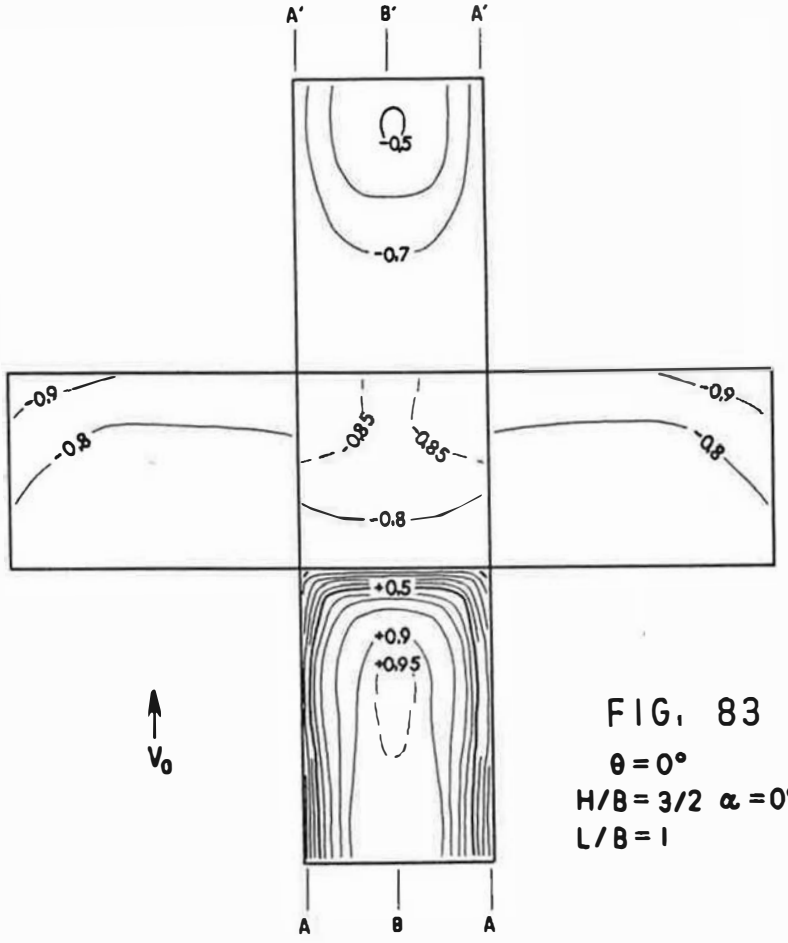

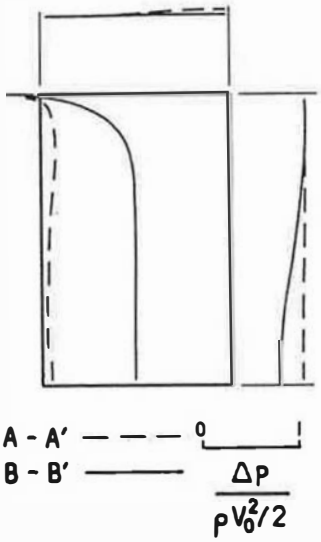

FIG. 83

$\theta = 0°$
$H/B = 3/2$ $\alpha = 0°$
$L/B = 1$

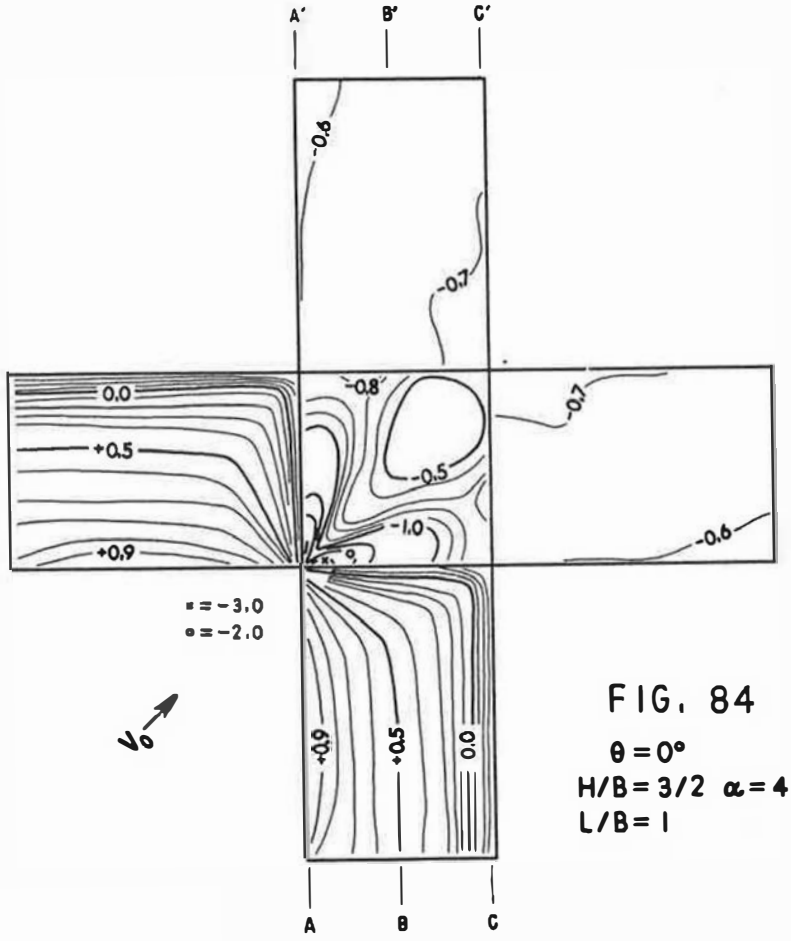

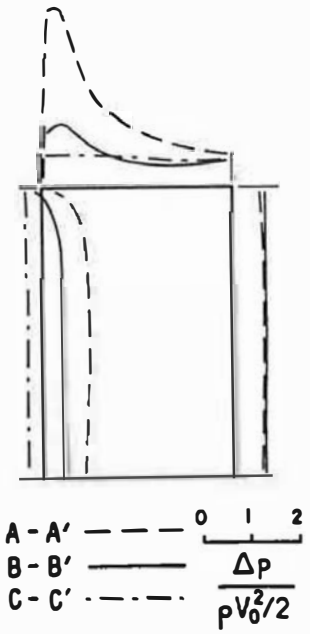

FIG. 84

$\theta = 0°$
$H/B = 3/2$ $\alpha = 45°$
$L/B = 1$

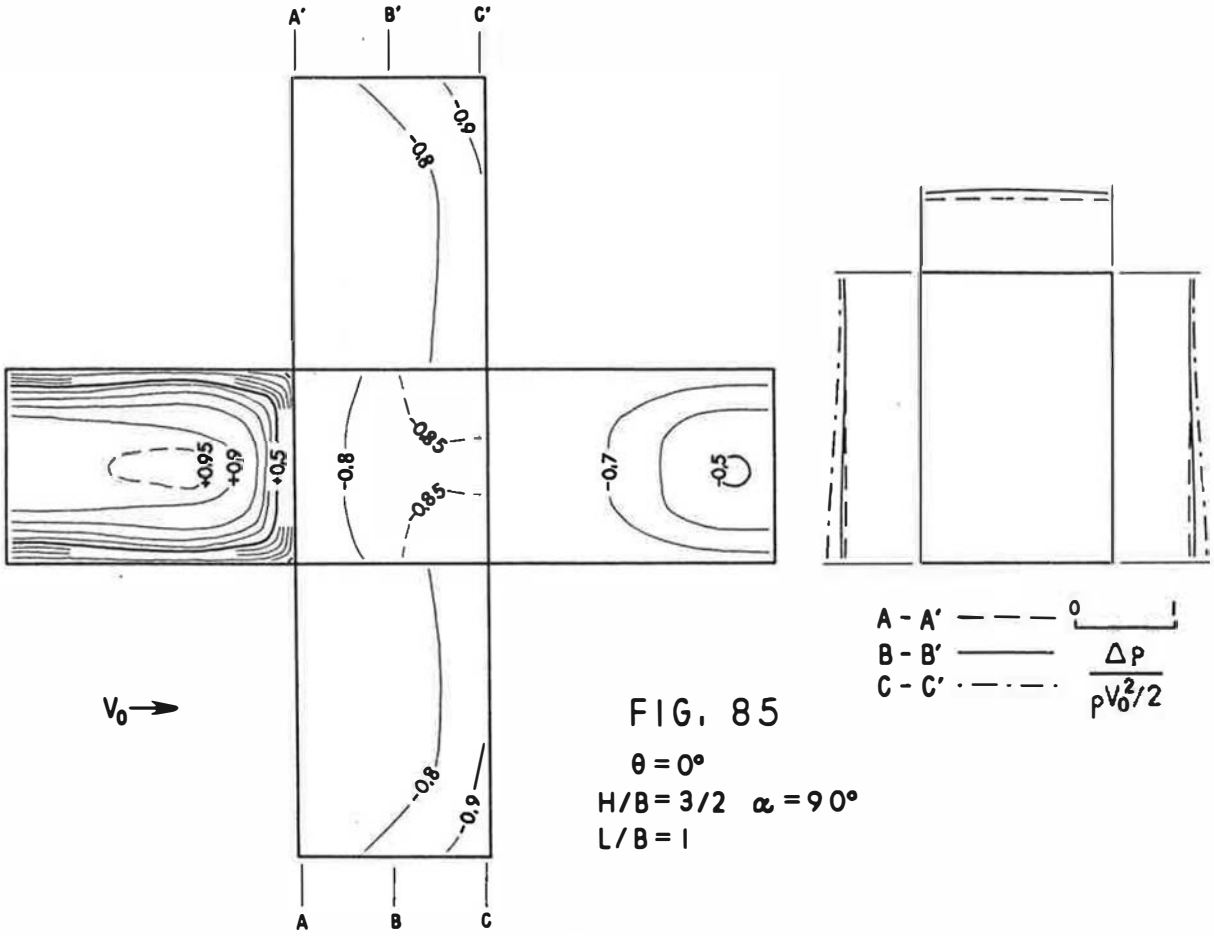

FIG. 85

$\theta = 0°$

$H/B = 3/2 \quad \alpha = 90°$

$L/B = 1$

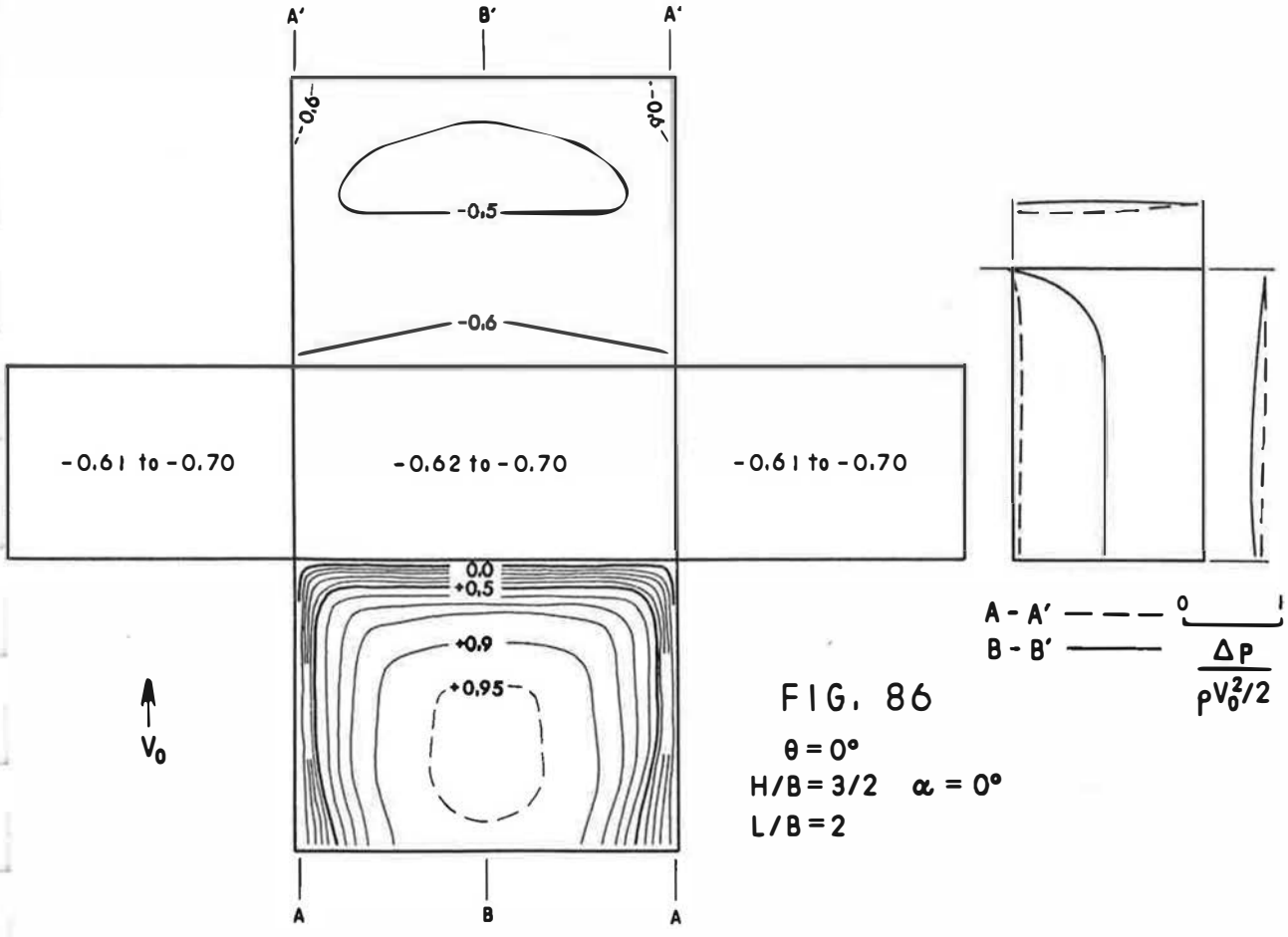

FIG. 86

$\theta = 0°$

$H/B = 3/2 \quad \alpha = 0°$

$L/B = 2$

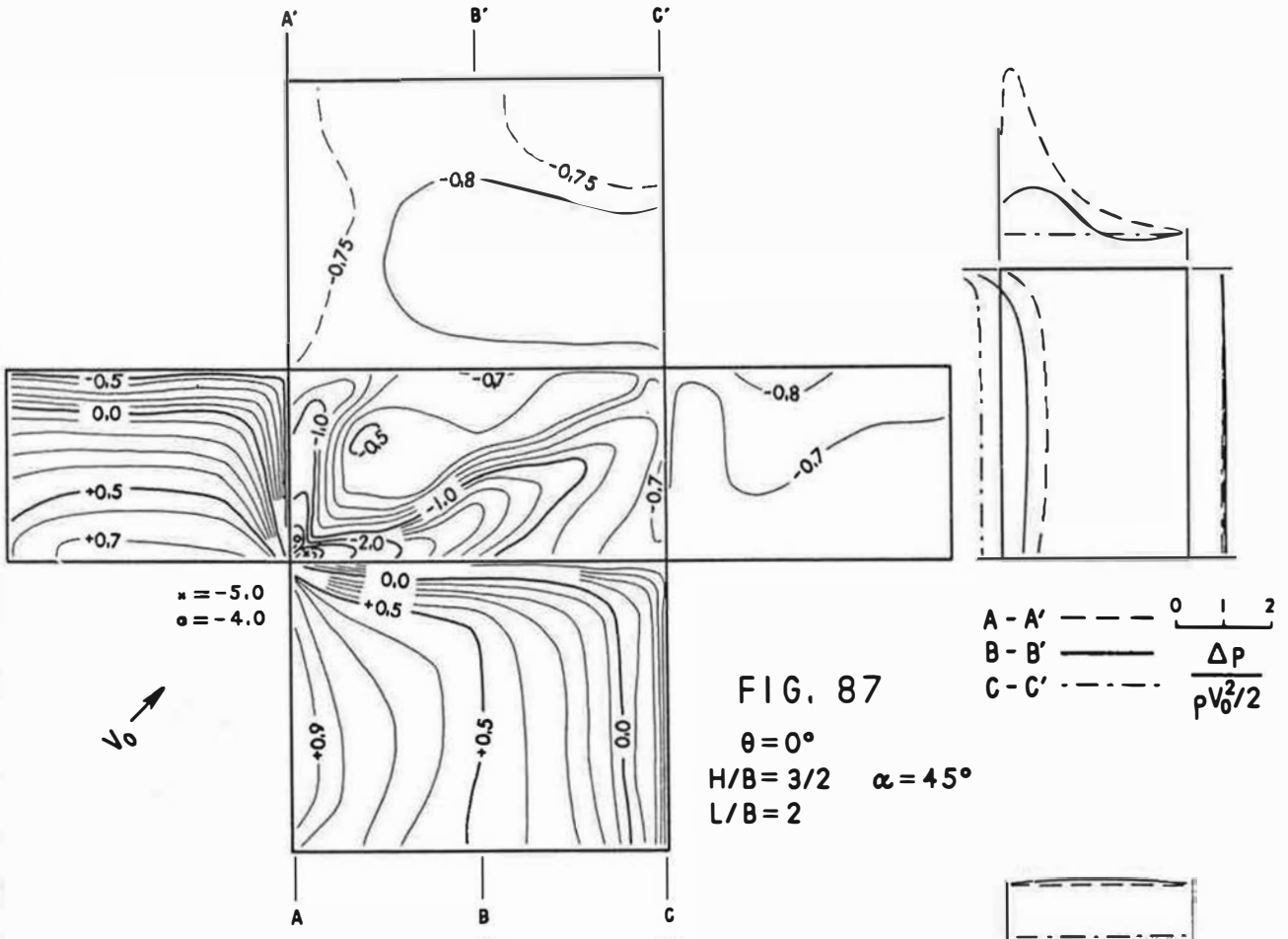

FIG. 87

θ = 0°
H/B = 3/2 α = 45°
L/B = 2

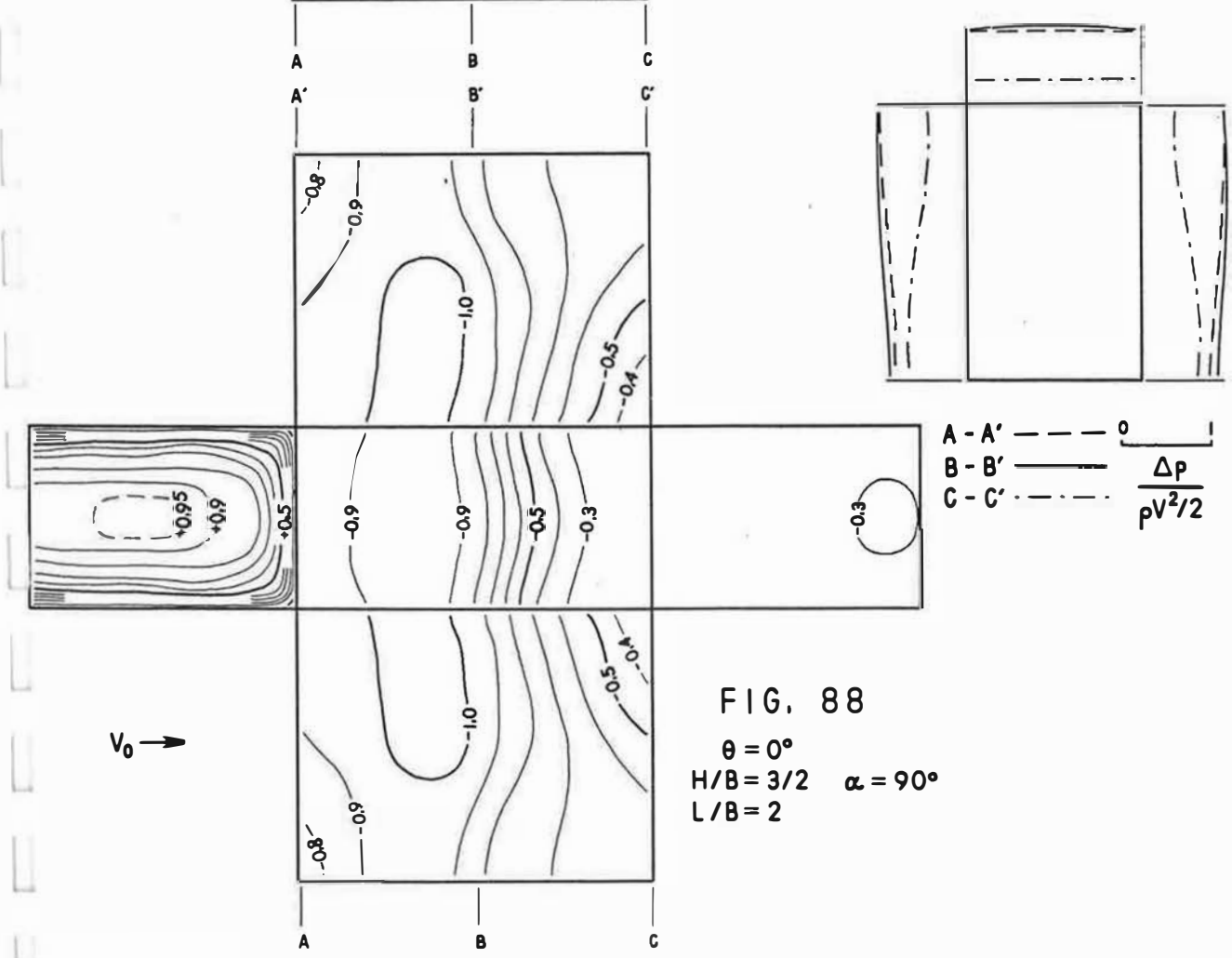

FIG. 88

θ = 0°
H/B = 3/2 α = 90°
L/B = 2

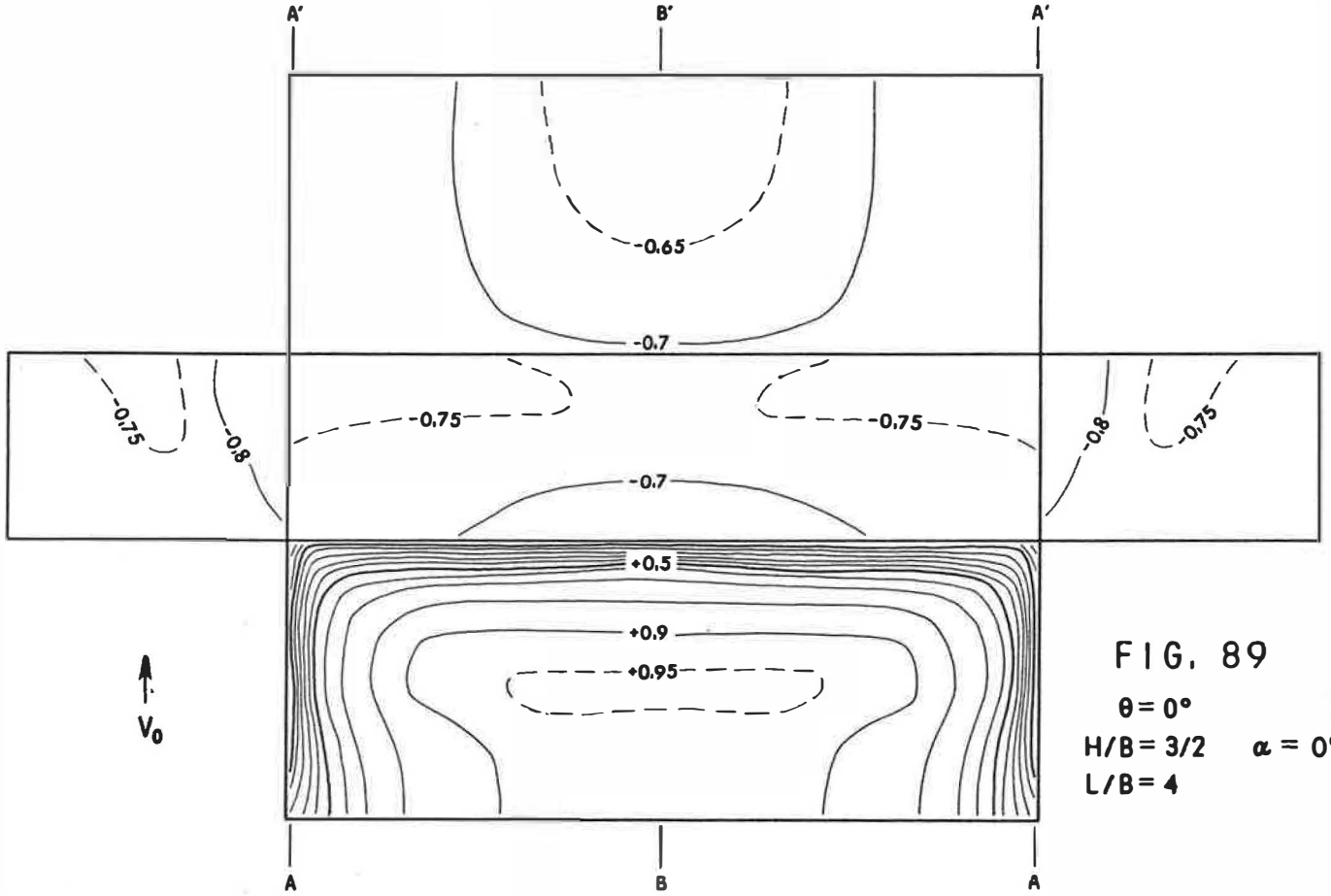

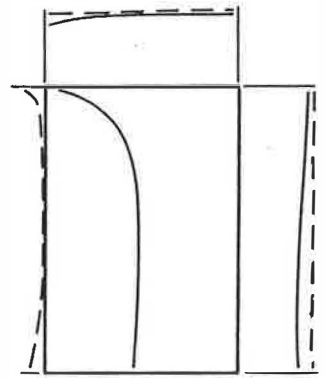

FIG. 89

$\theta = 0°$

$H/B = 3/2 \quad \alpha = 0°$

$L/B = 4$

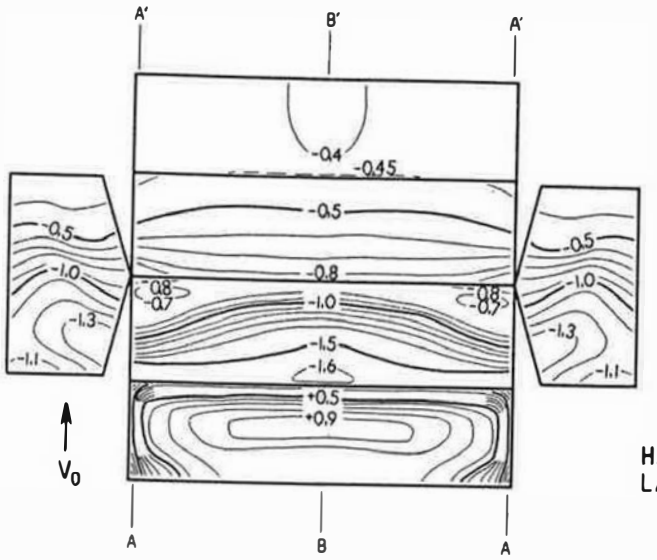

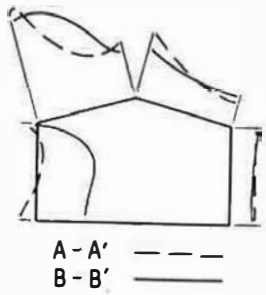

FIG. 95

θ = 15°
H/B = 1/2 α = 0°
L/B = 2

0 ⌊ 1
$\frac{\Delta p}{\rho V_0^2/2}$

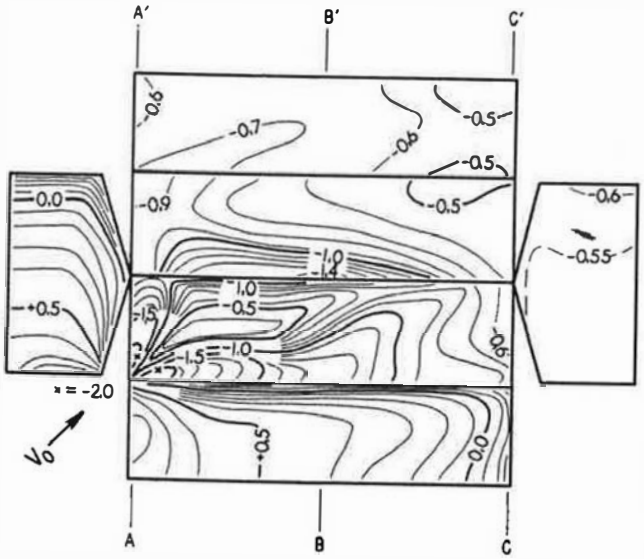

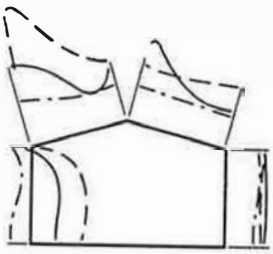

FIG. 96

θ = 15°
H/B = 1/2 α = 45°
L/B = 2

0 ⌊ 1
$\frac{\Delta p}{\rho V_0^2/2}$

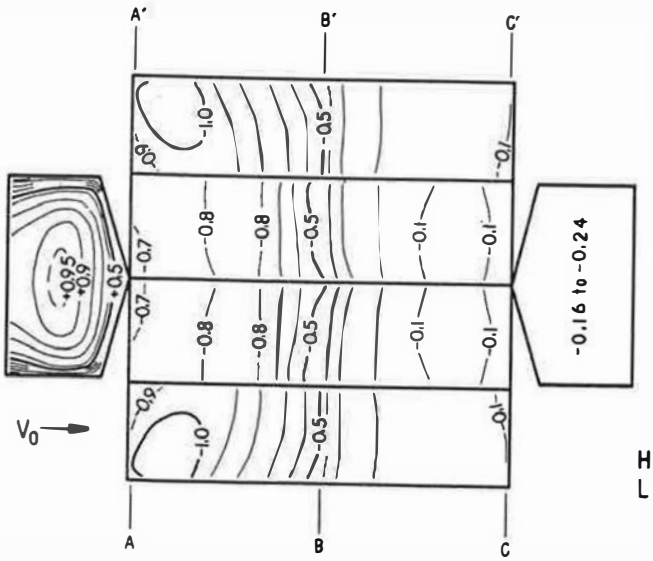

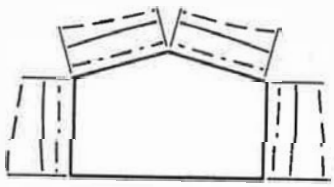

FIG. 97

θ = 15°
H/B = 1/2 α = 90°
L/B = 2

0 ⌊ 1
$\frac{\Delta p}{\rho V_0^2/2}$

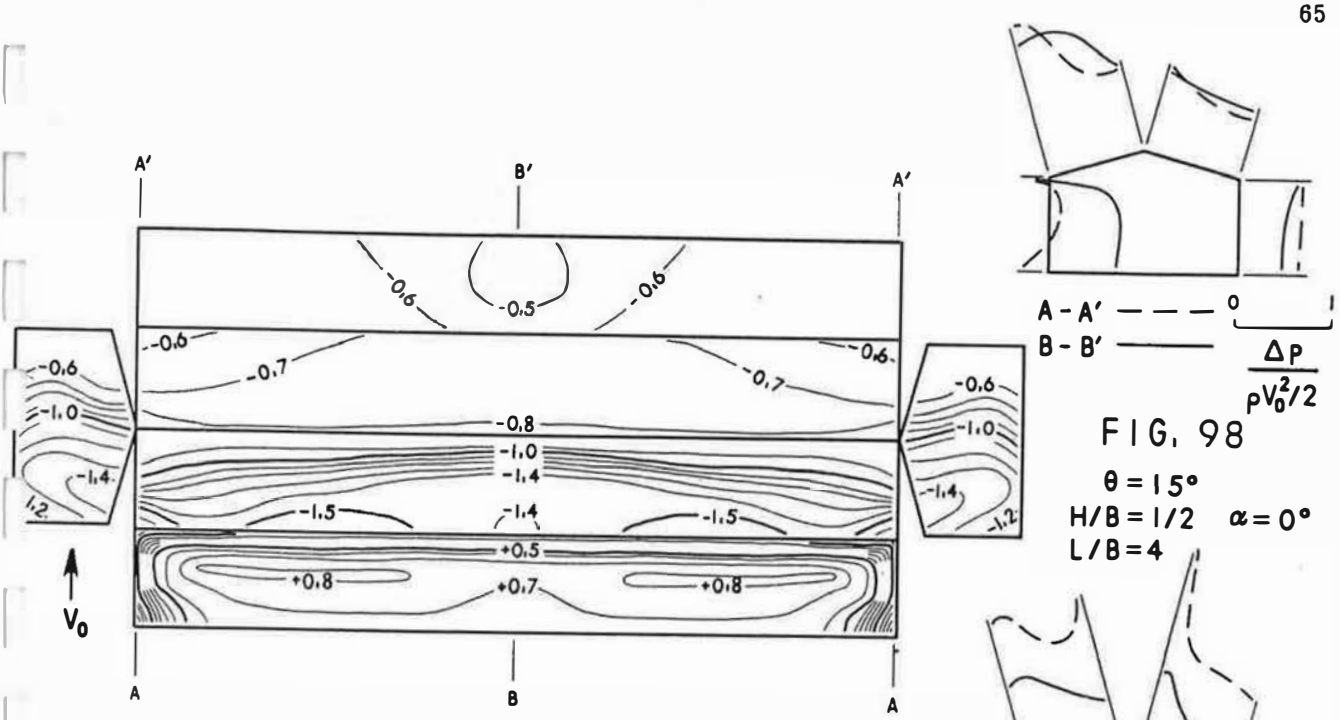

FIG. 98

$\theta = 15°$
$H/B = 1/2$ $\alpha = 0°$
$L/B = 4$

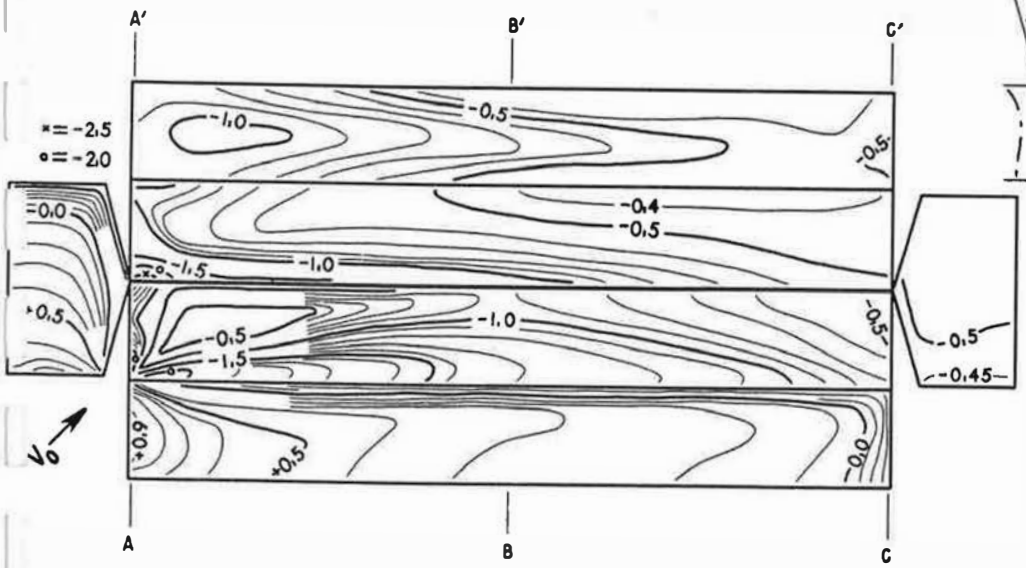

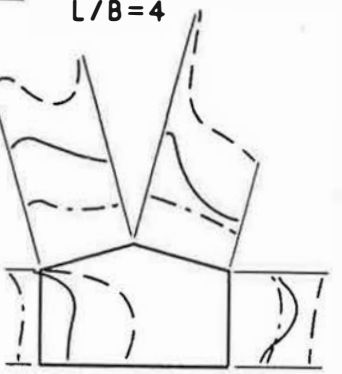

FIG. 99

$\theta = 15°$
$H/B = 1/2$ $\alpha = 45°$
$L/B = 4$

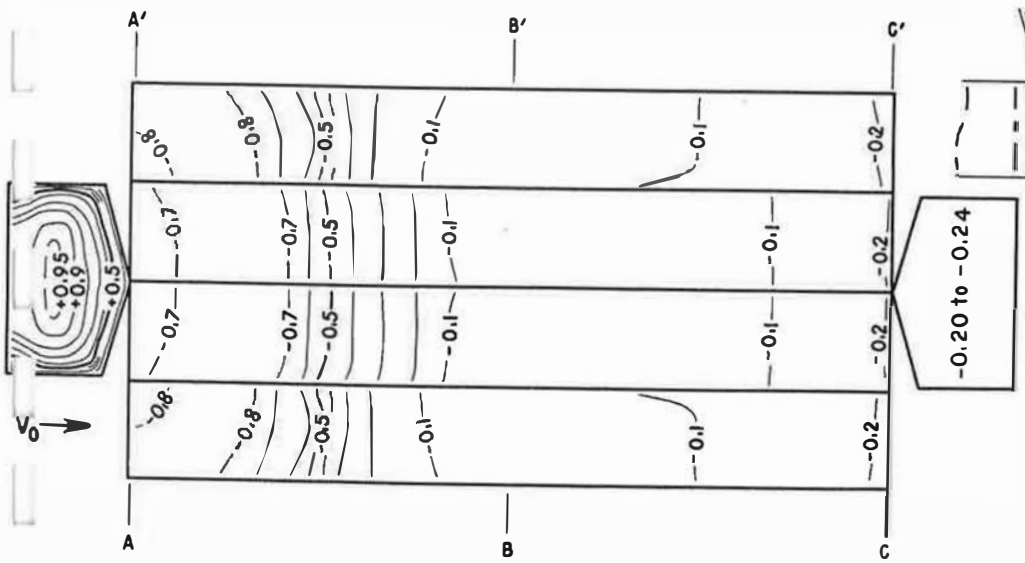

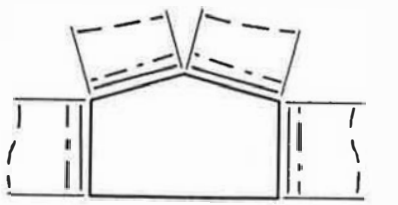

FIG. 100

$\theta = 15°$
$H/B = 1/2$ $\alpha = 90°$
$L/B = 4$

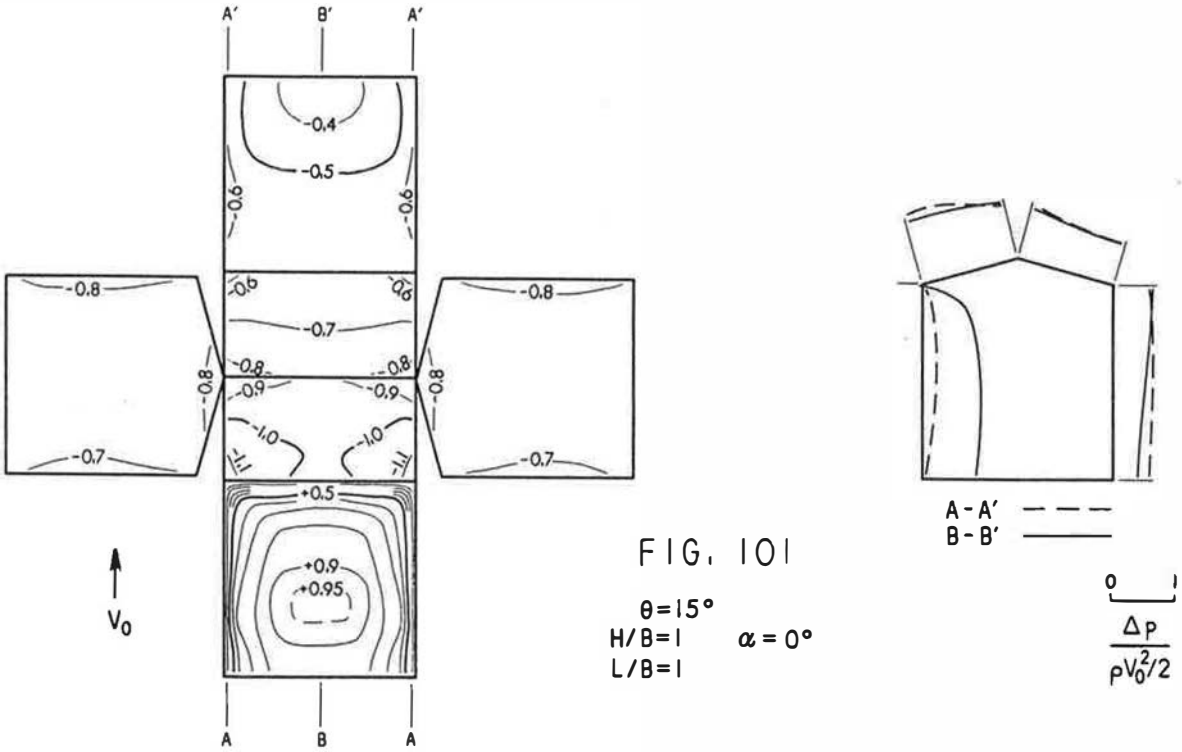

FIG. 101

θ=15°
H/B=1 α=0°
L/B=1

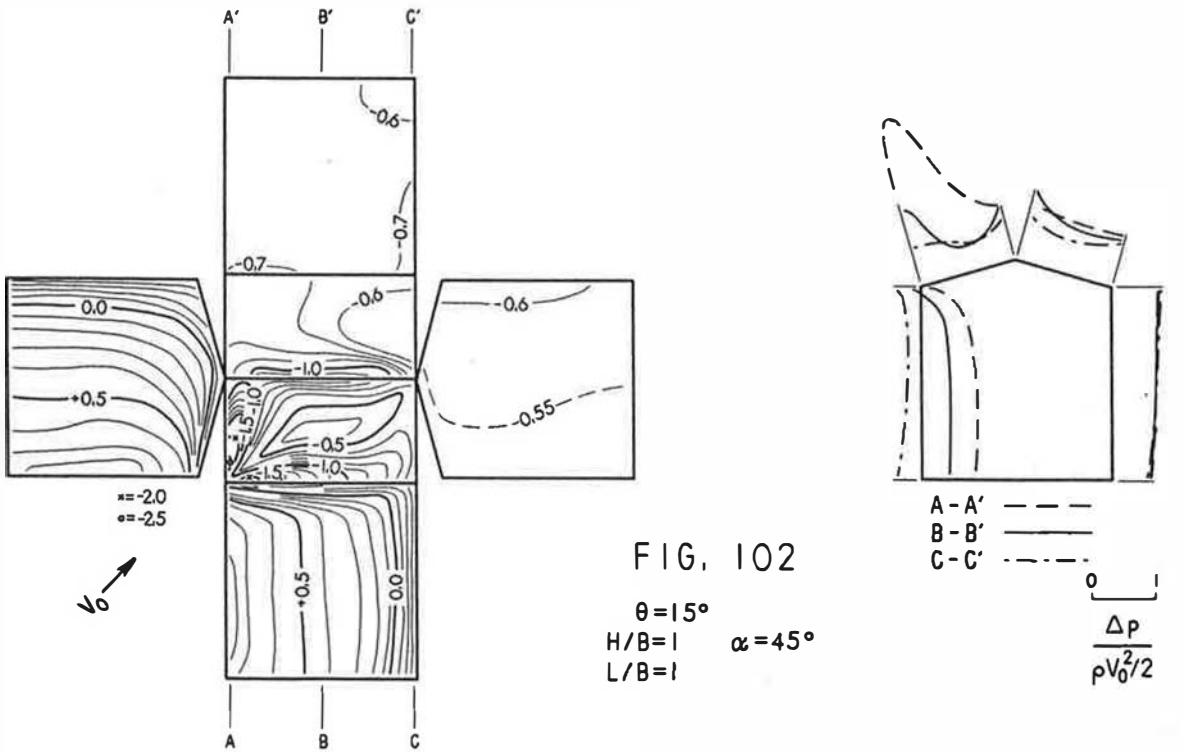

FIG. 102

θ=15°
H/B=1 α=45°
L/B=1

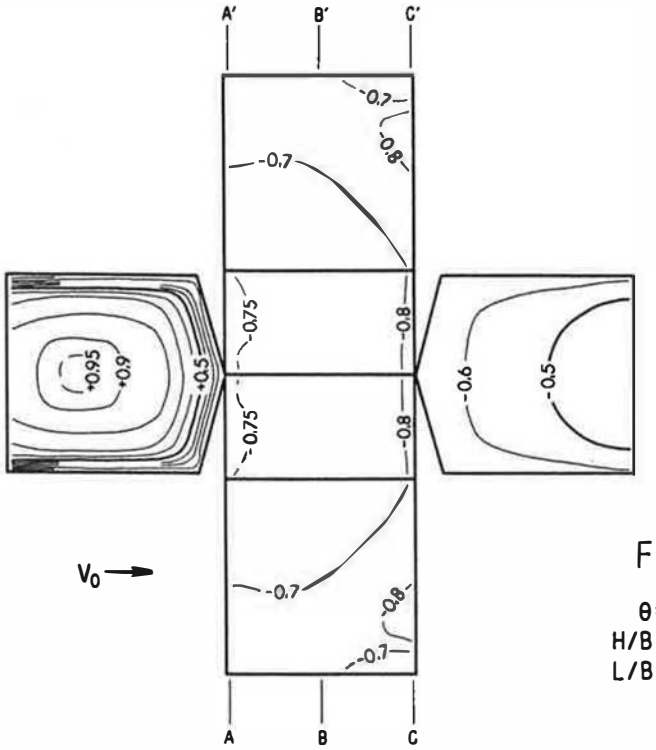

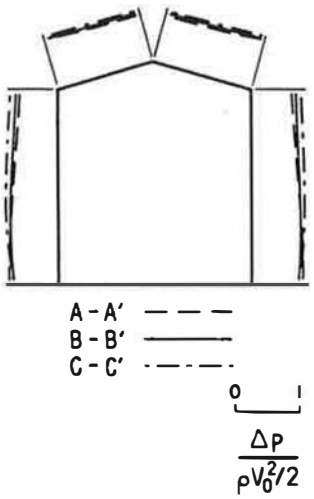

FIG. 103

θ=15°
H/B=1 α=90°
L/B=1

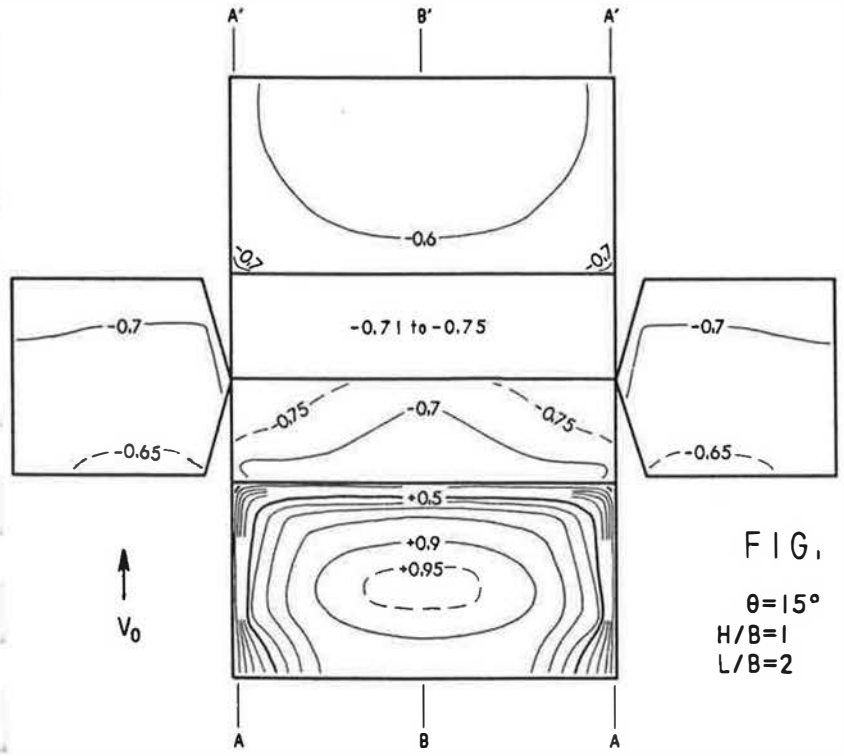

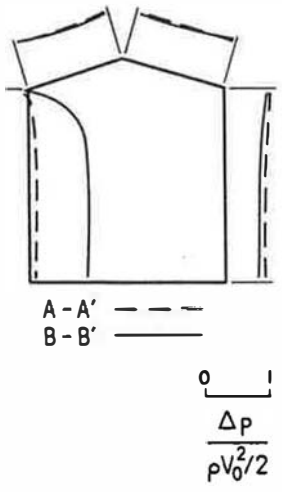

FIG. 104

θ=15°
H/B=1 α=0°
L/B=2

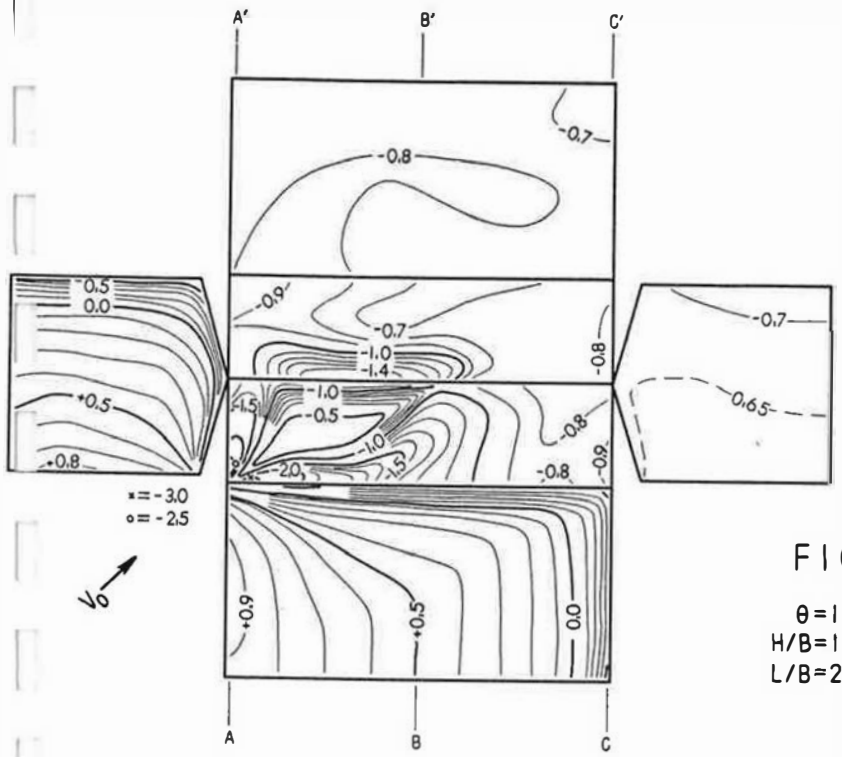

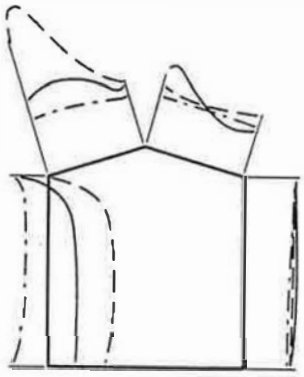

FIG. 105

θ = 15°
H/B = 1 α = 45°
L/B = 2

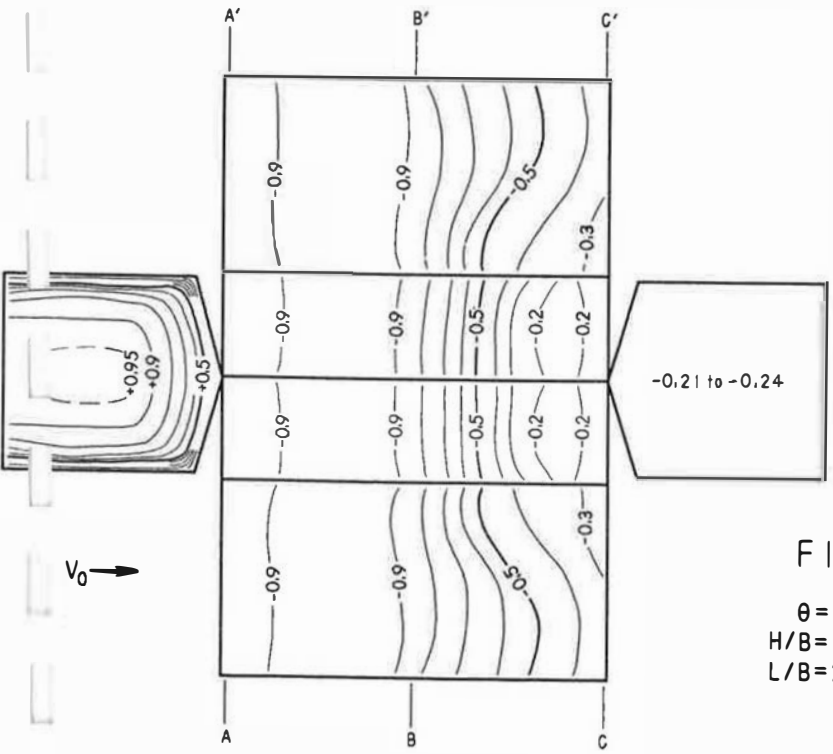

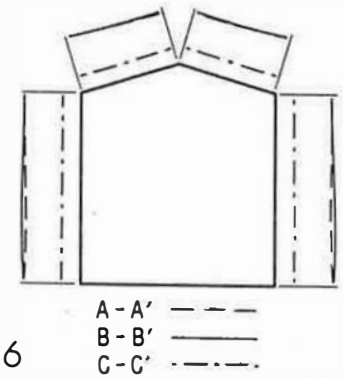

FIG. 106

θ = 15°
H/B = 1 α = 90°
L/B = 2

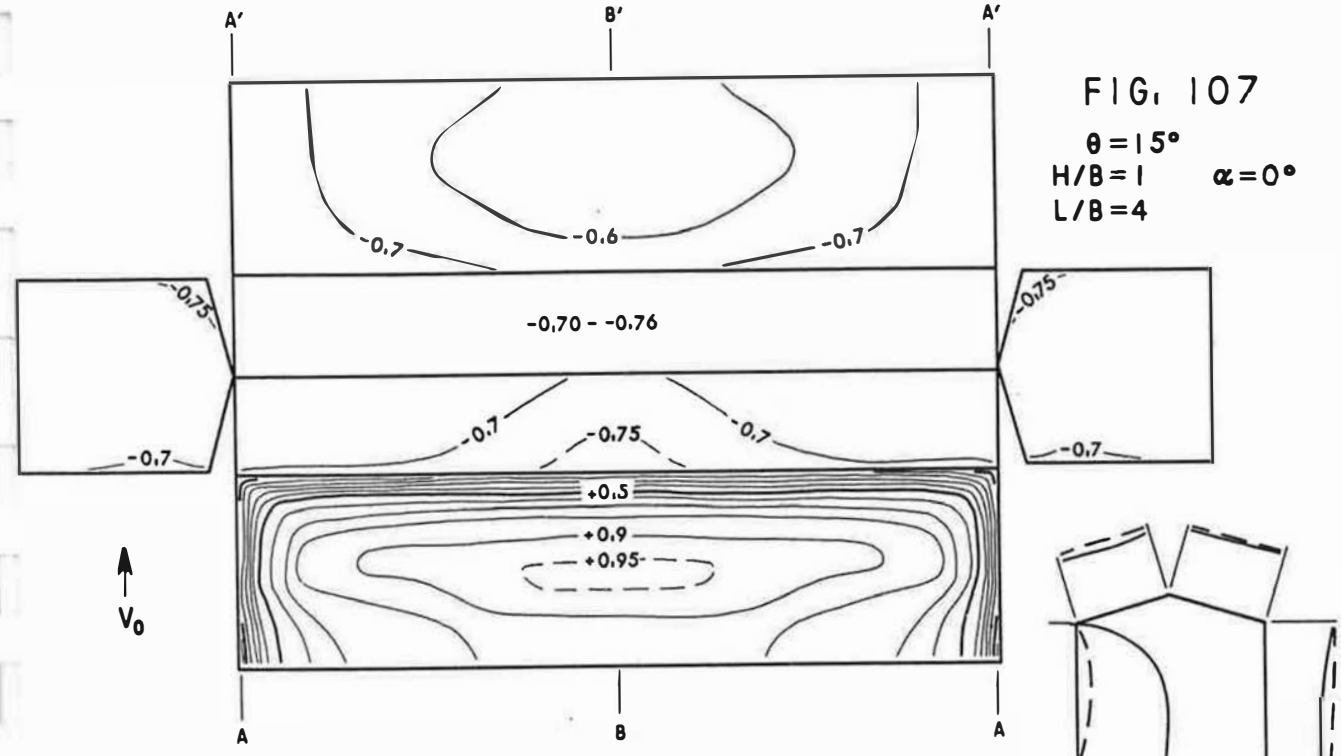

FIG. 107

θ = 15°
H/B = 1 α = 0°
L/B = 4

A - A' — — —
B - B' ———
0 1
ΔP / ρV0²/2

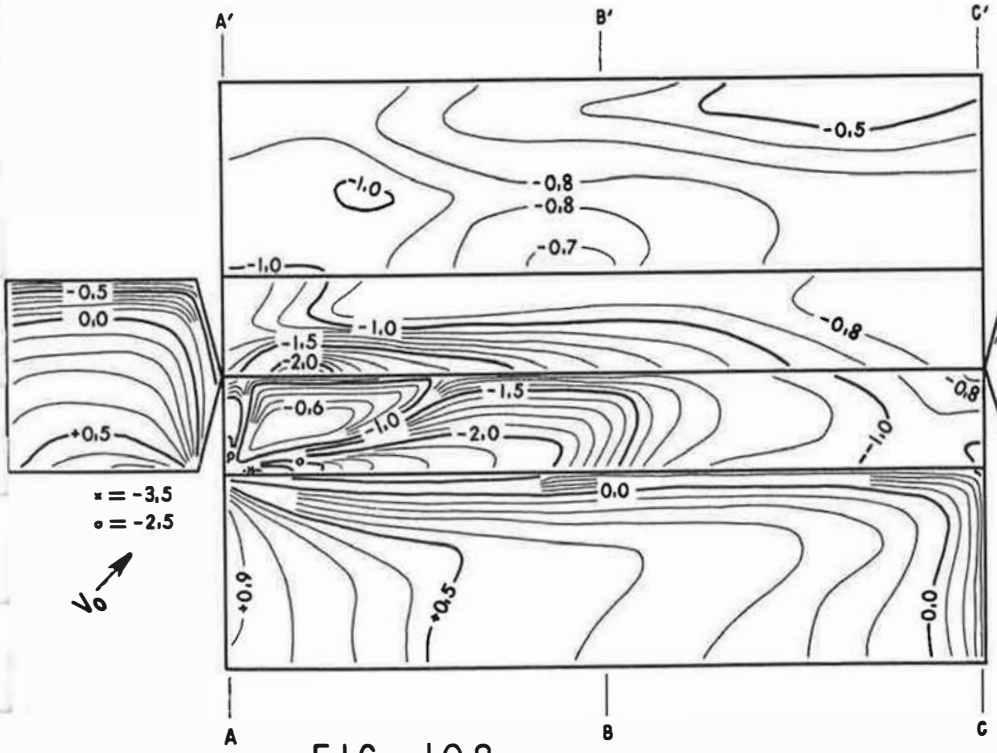

FIG. 108

θ = 15°
H/B = 1 α = 45°
L/B = 4

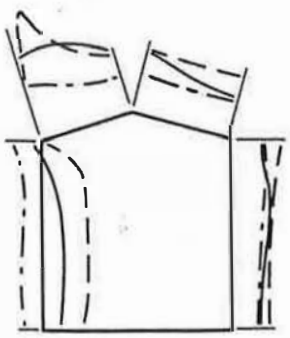

A - A' — — —
B - B' ———
C - C' ·—·—·
0 1 2
ΔP / ρV0²/2

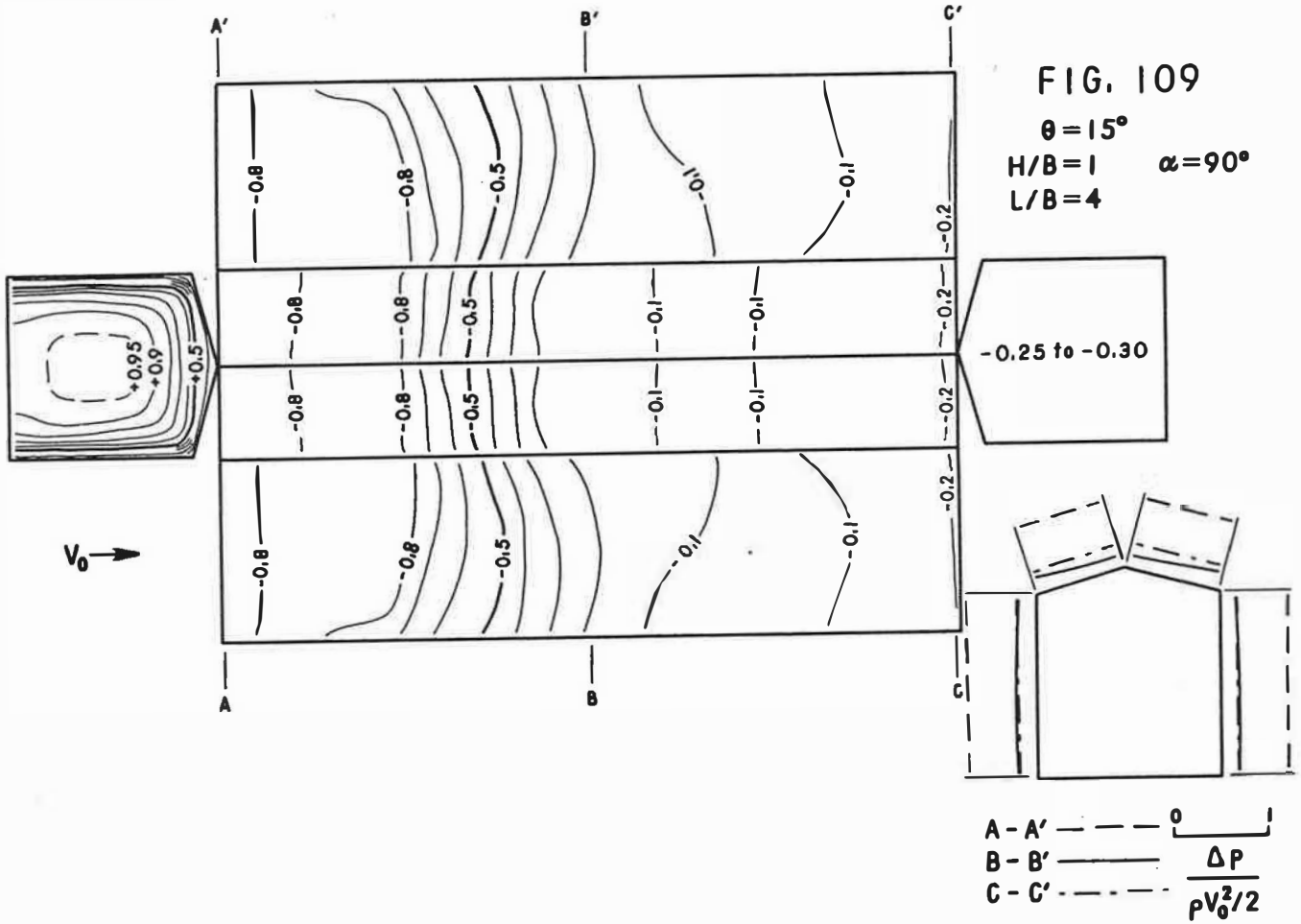

FIG. 109

$\theta = 15°$

H/B = 1 $\alpha = 90°$

L/B = 4

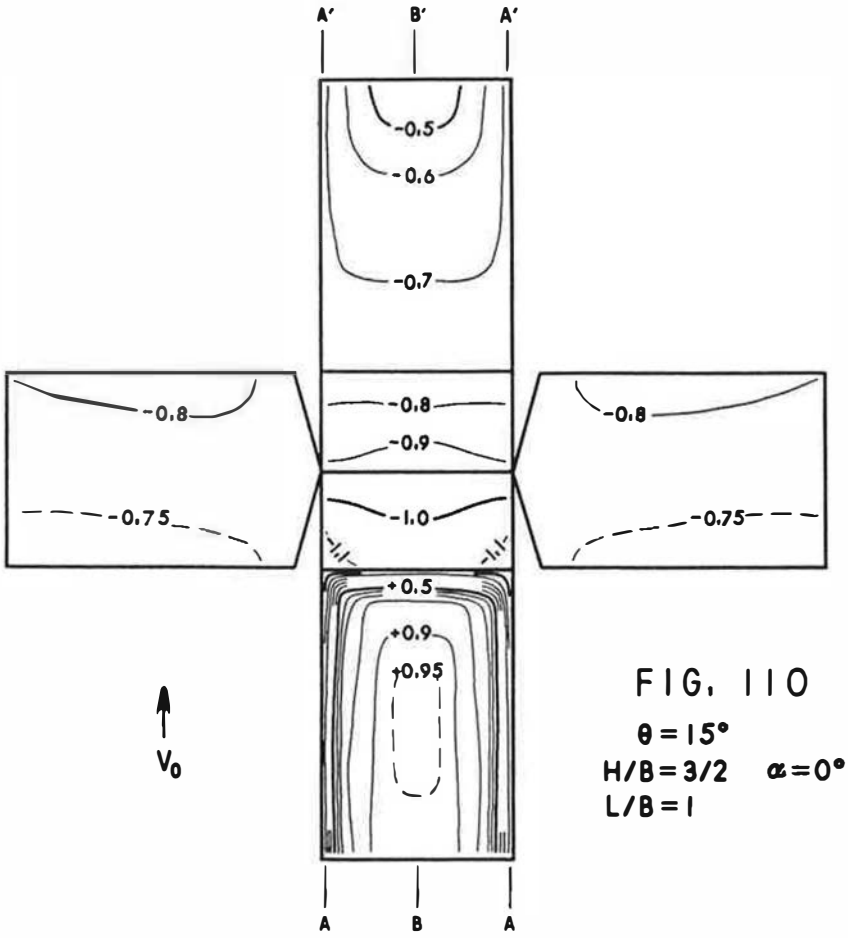

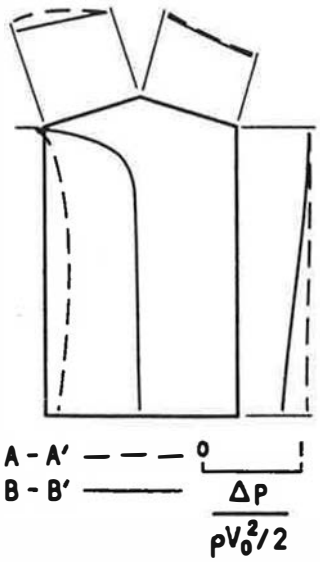

FIG. 110

θ = 15°
H/B = 3/2 α = 0°
L/B = 1

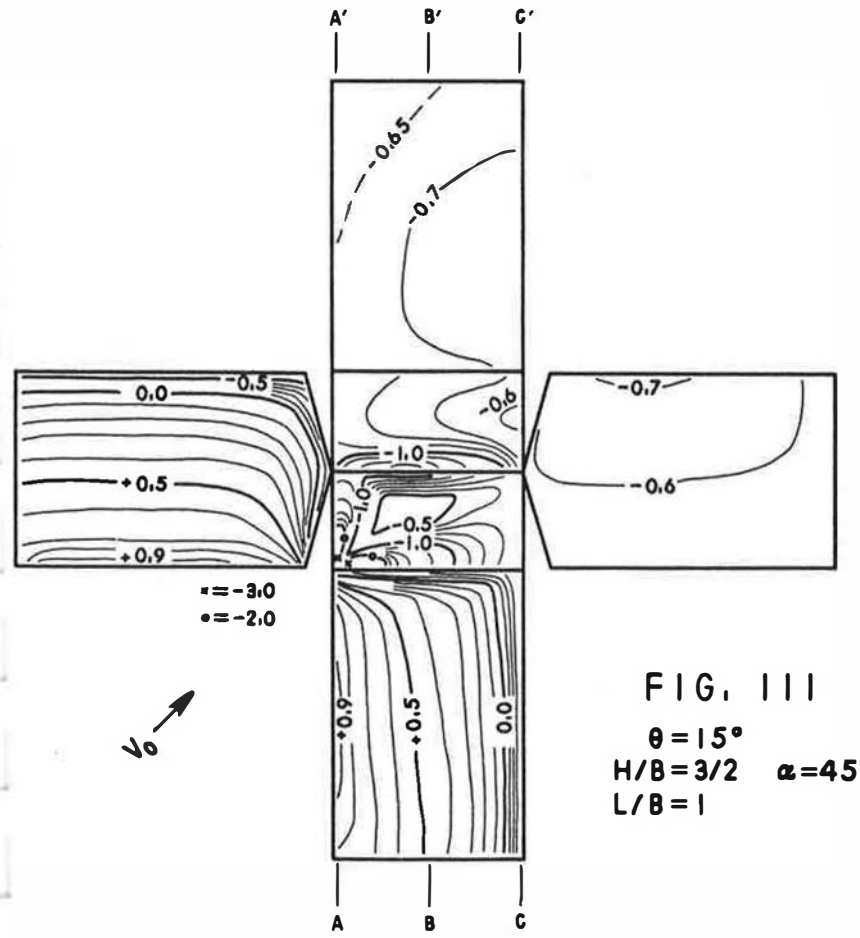

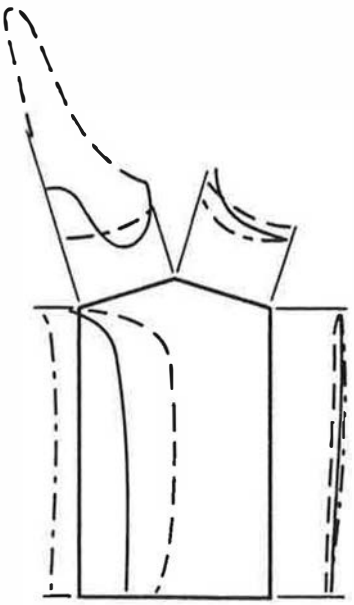

FIG. 111

θ = 15°
H/B = 3/2 α = 45°
L/B = 1

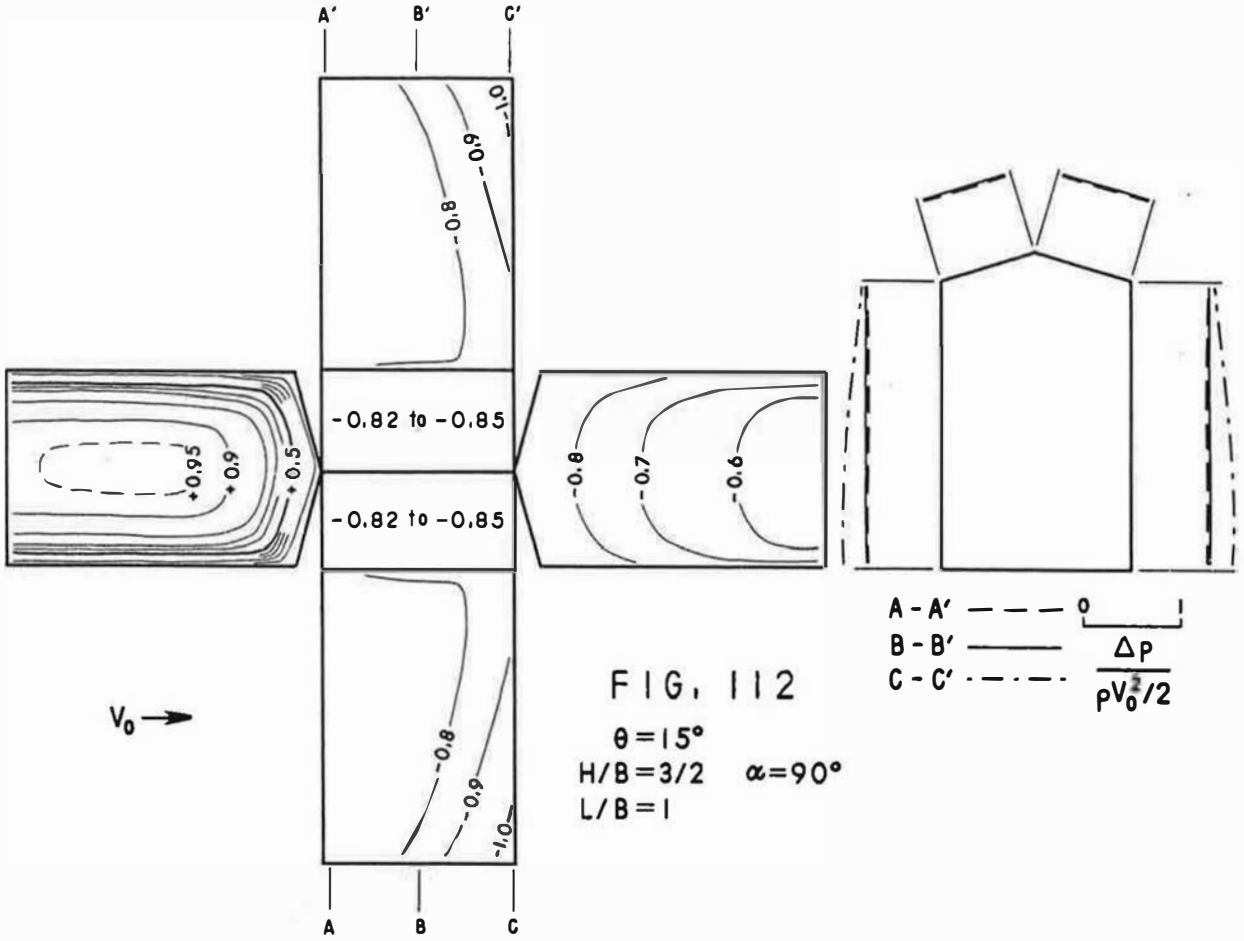

FIG. 112

θ = 15°
H/B = 3/2 α = 90°
L/B = 1

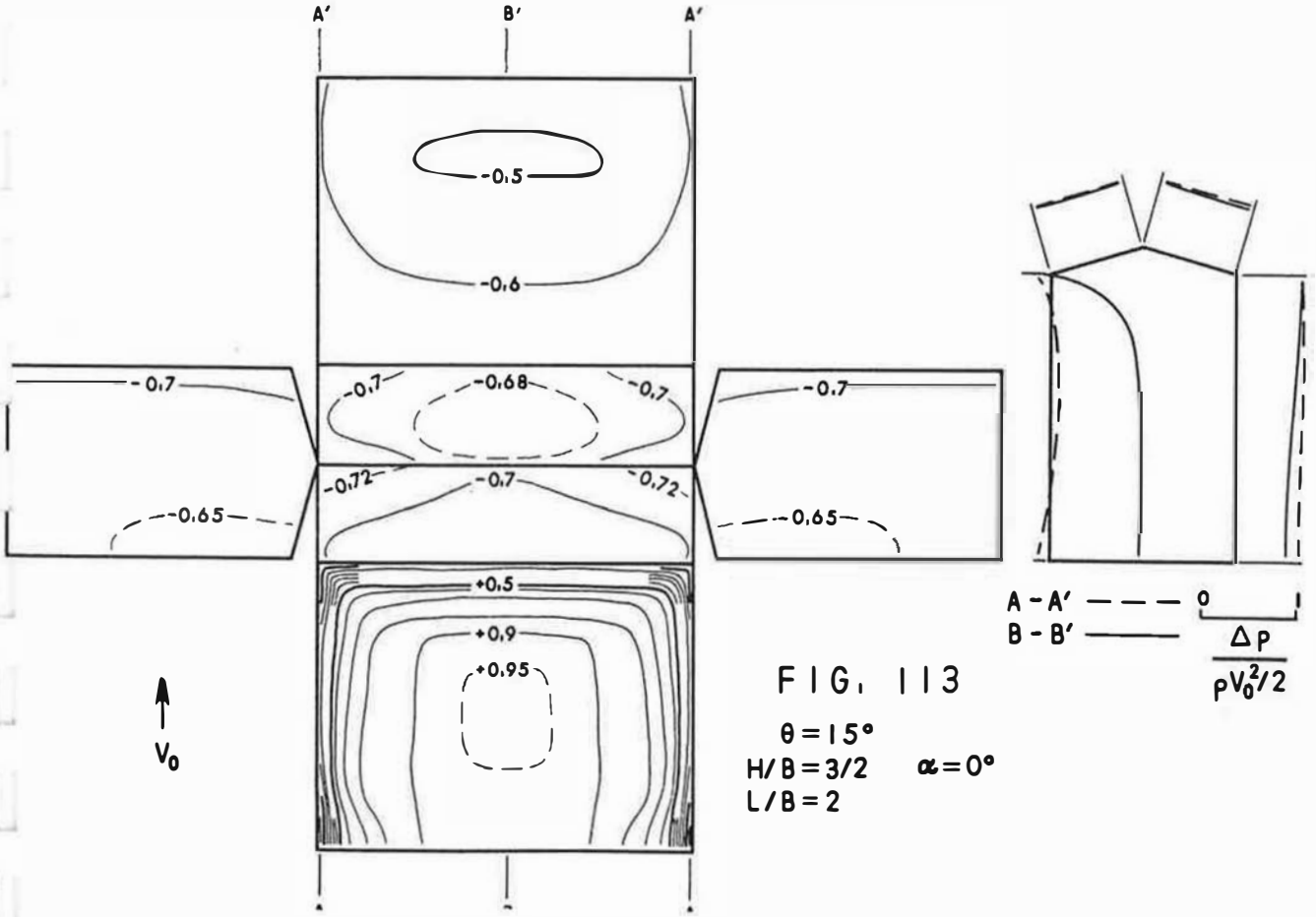

FIG. 113

θ = 15°
H/B = 3/2 α = 0°
L/B = 2

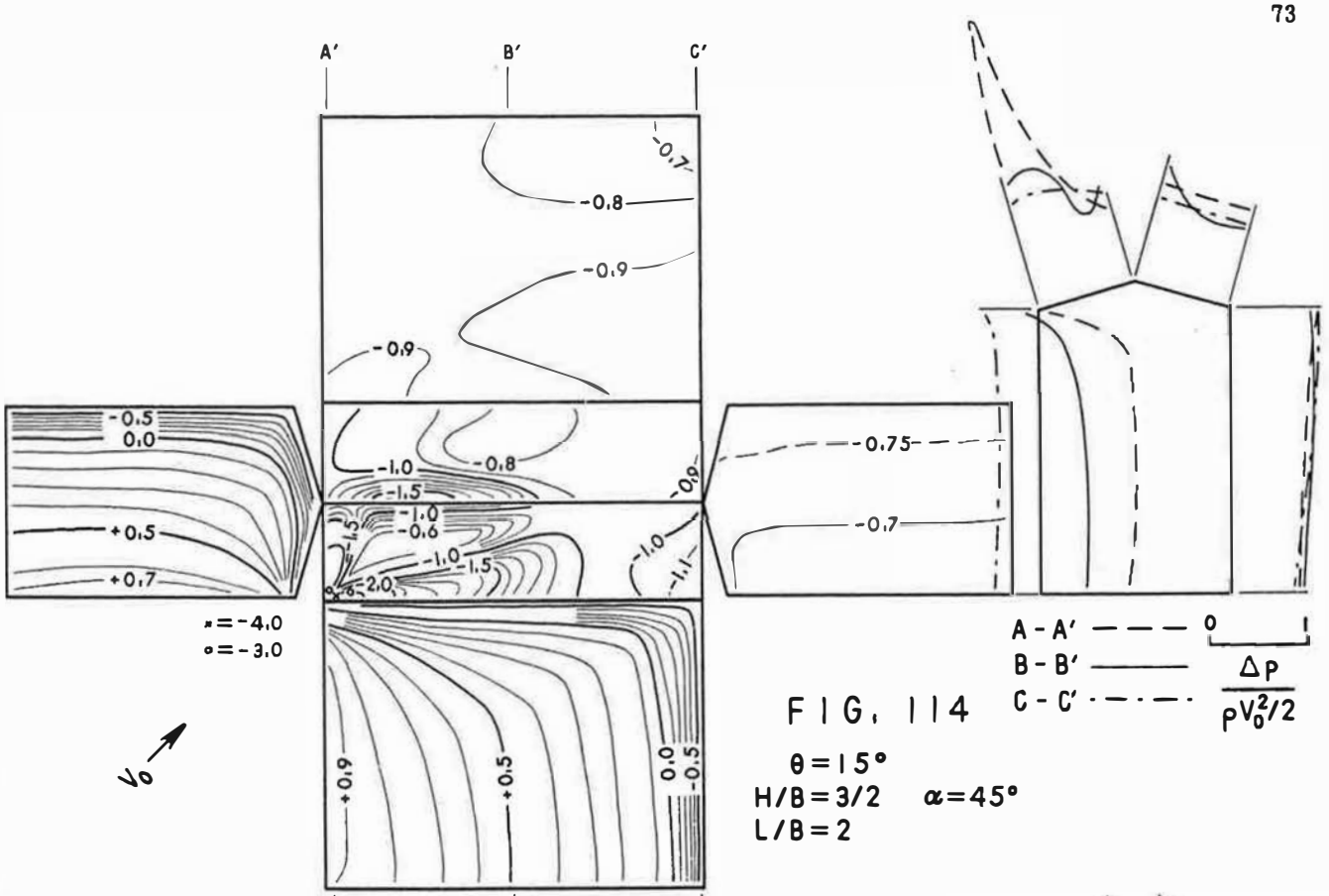

FIG. 114

θ = 15°
H/B = 3/2 α = 45°
L/B = 2

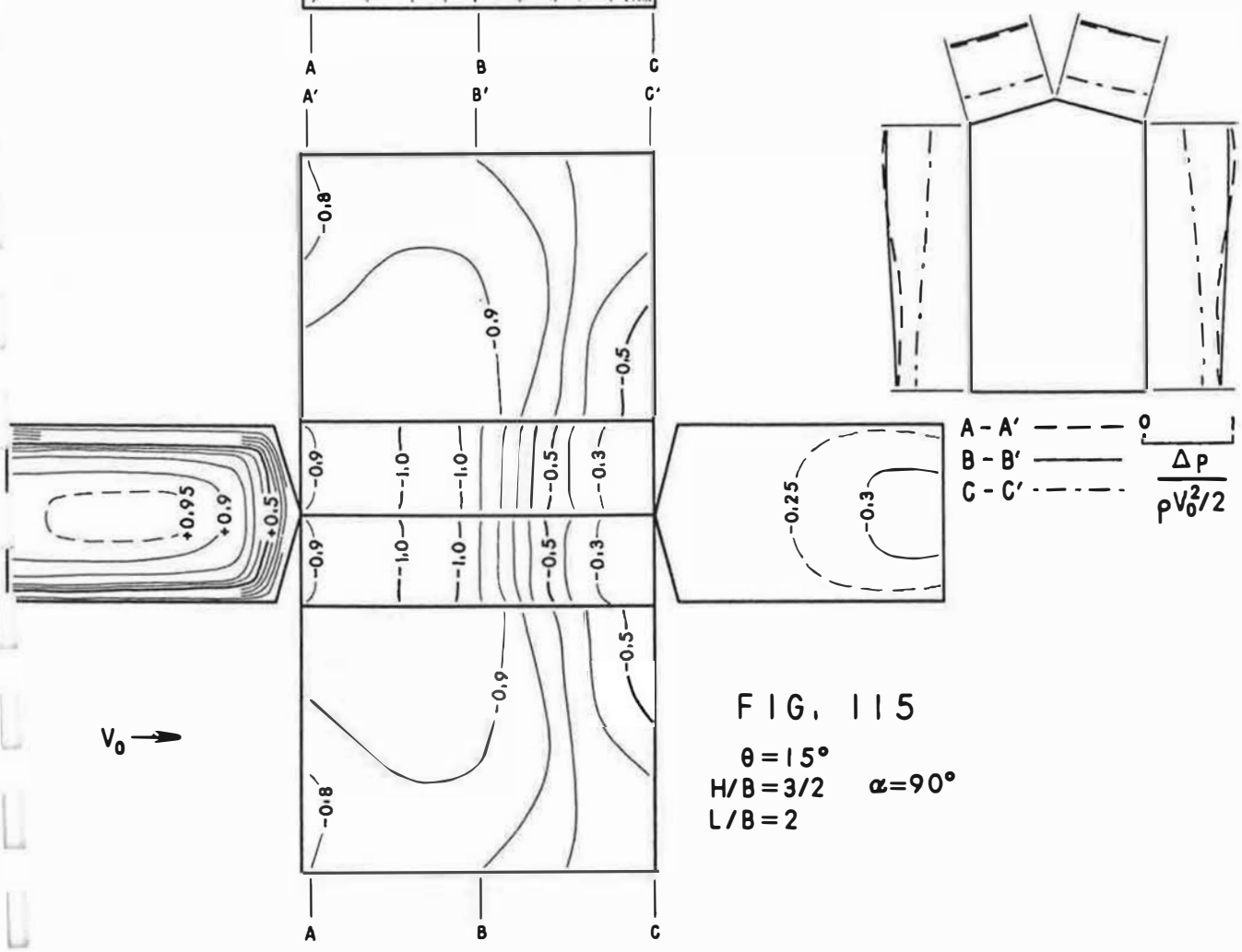

FIG. 115

θ = 15°
H/B = 3/2 α = 90°
L/B = 2

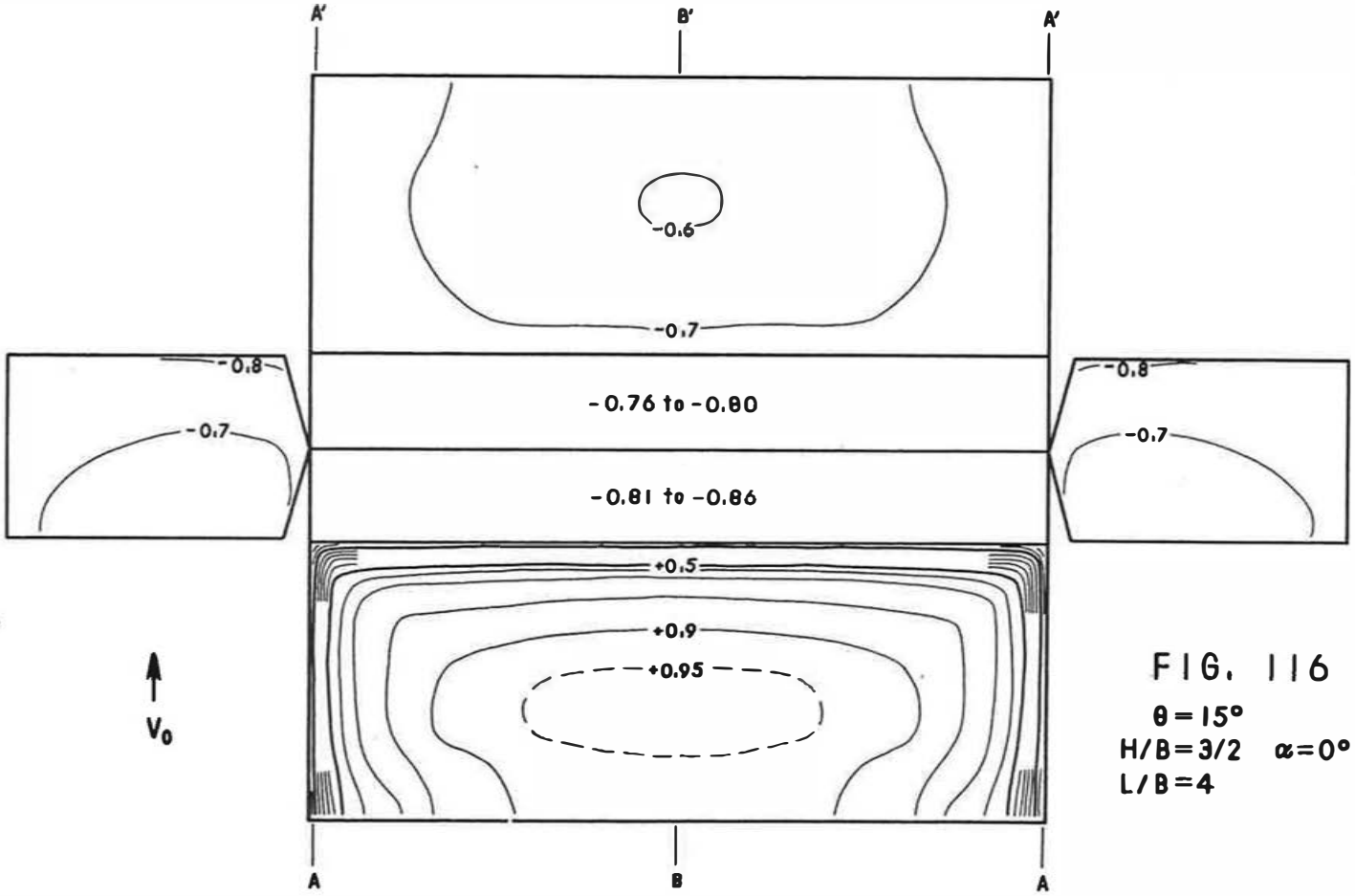

FIG. 116

$\theta = 15°$
$H/B = 3/2 \quad \alpha = 0°$
$L/B = 4$

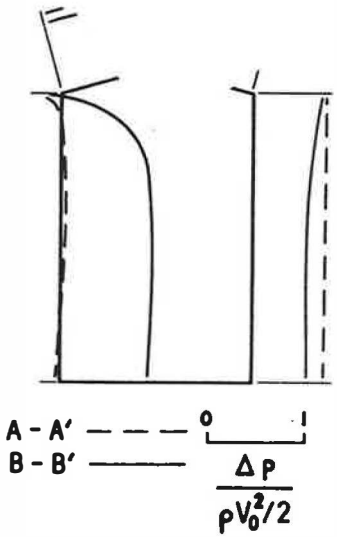

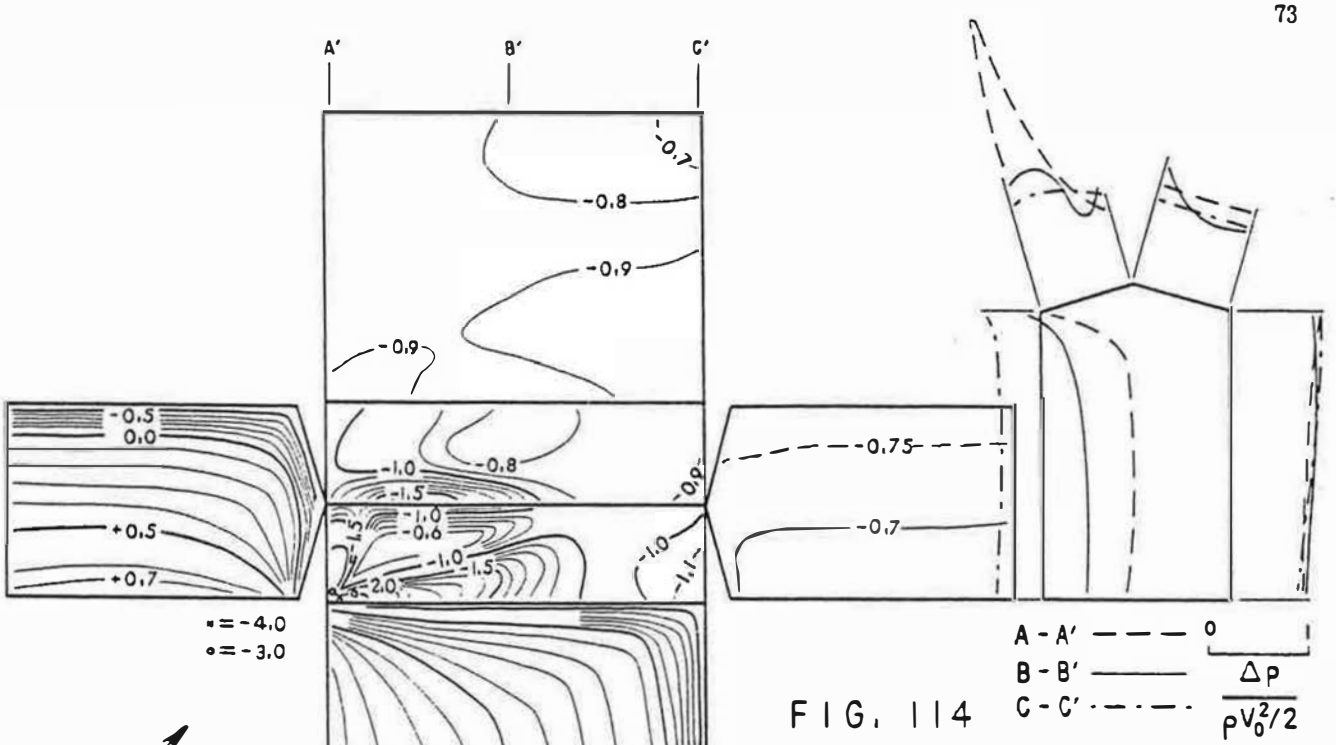

FIG. 114

θ = 15°
H/B = 3/2 α = 45°
L/B = 2

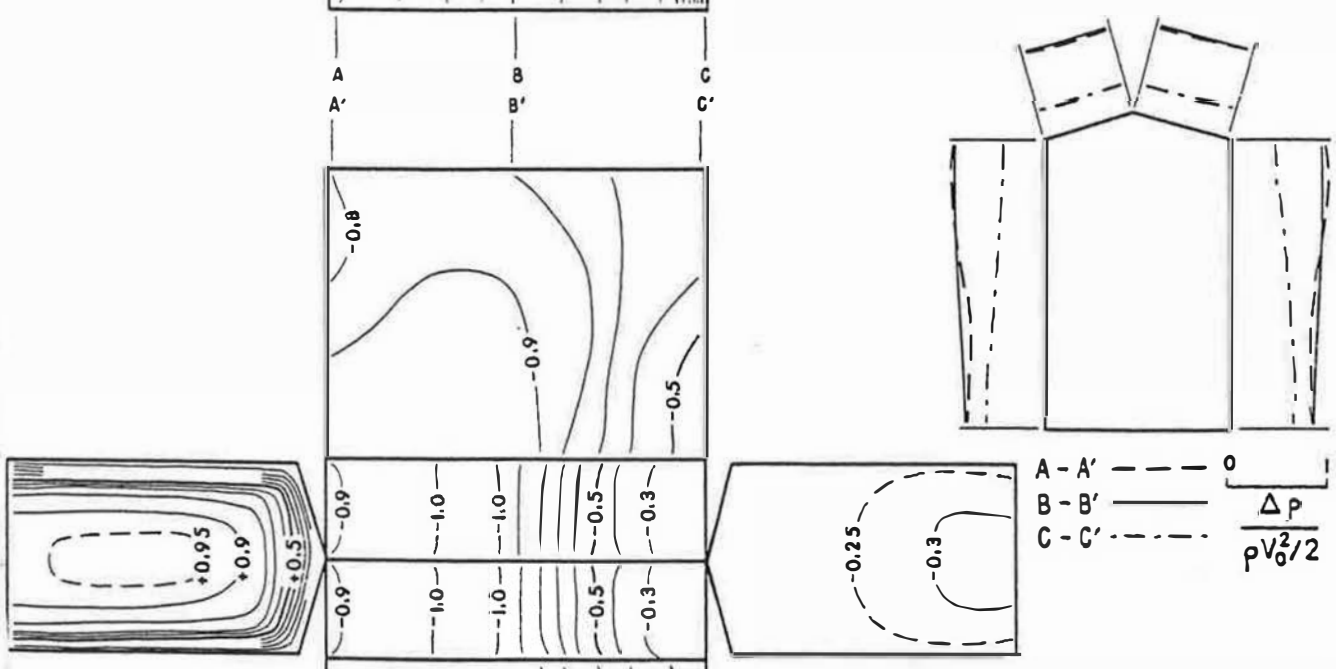

FIG. 115

θ = 15°
H/B = 3/2 α = 90°
L/B = 2

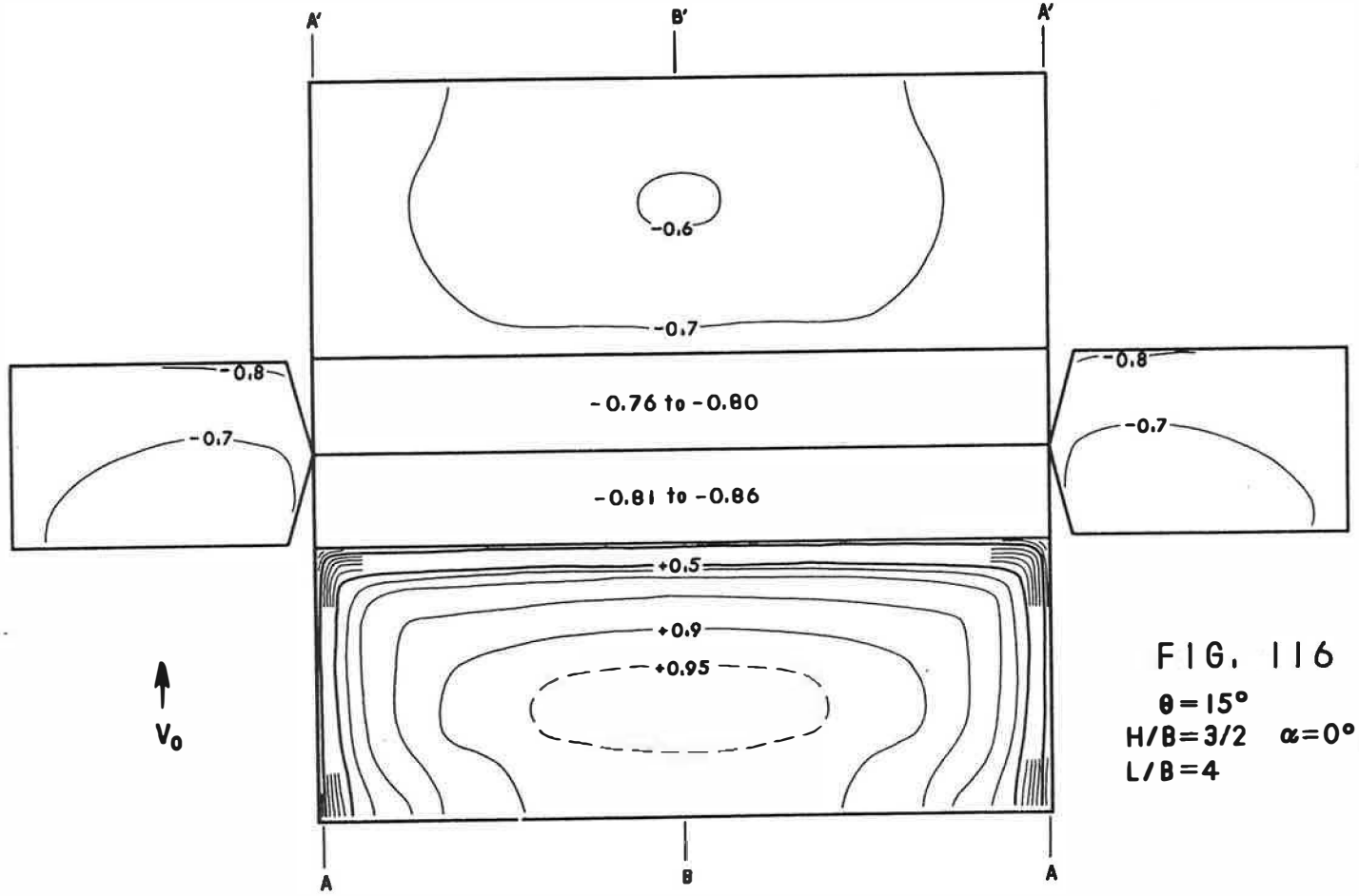

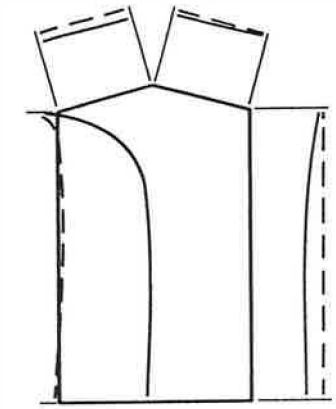

FIG. 116

$\theta = 15°$
$H/B = 3/2 \quad \alpha = 0°$
$L/B = 4$

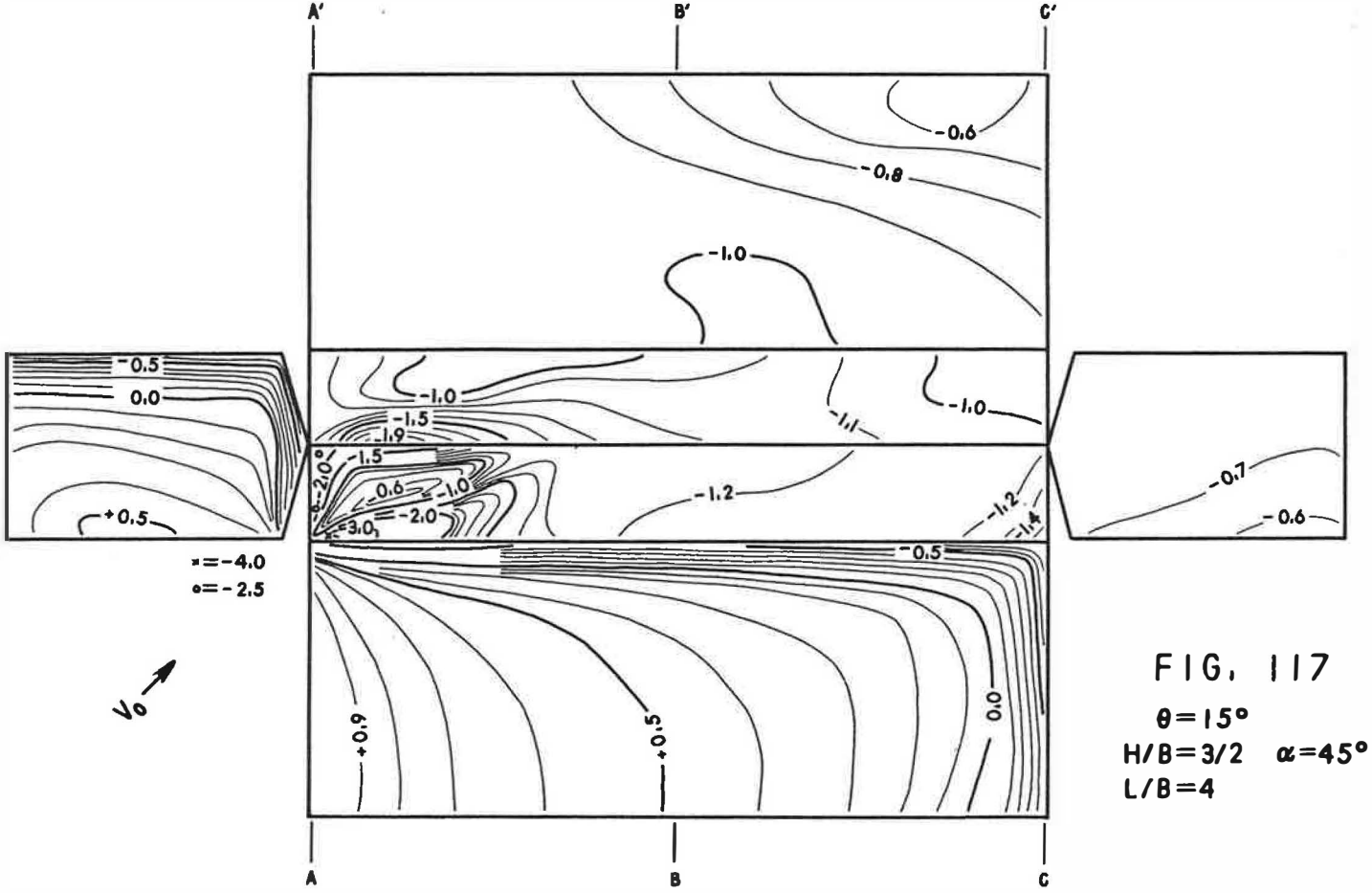

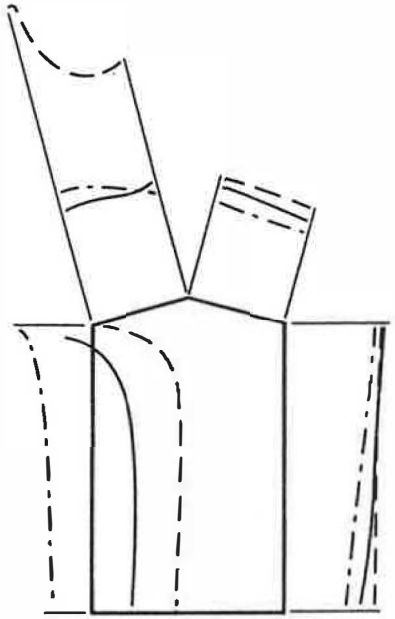

FIG. 117

θ=15°
H/B=3/2 α=45°
L/B=4

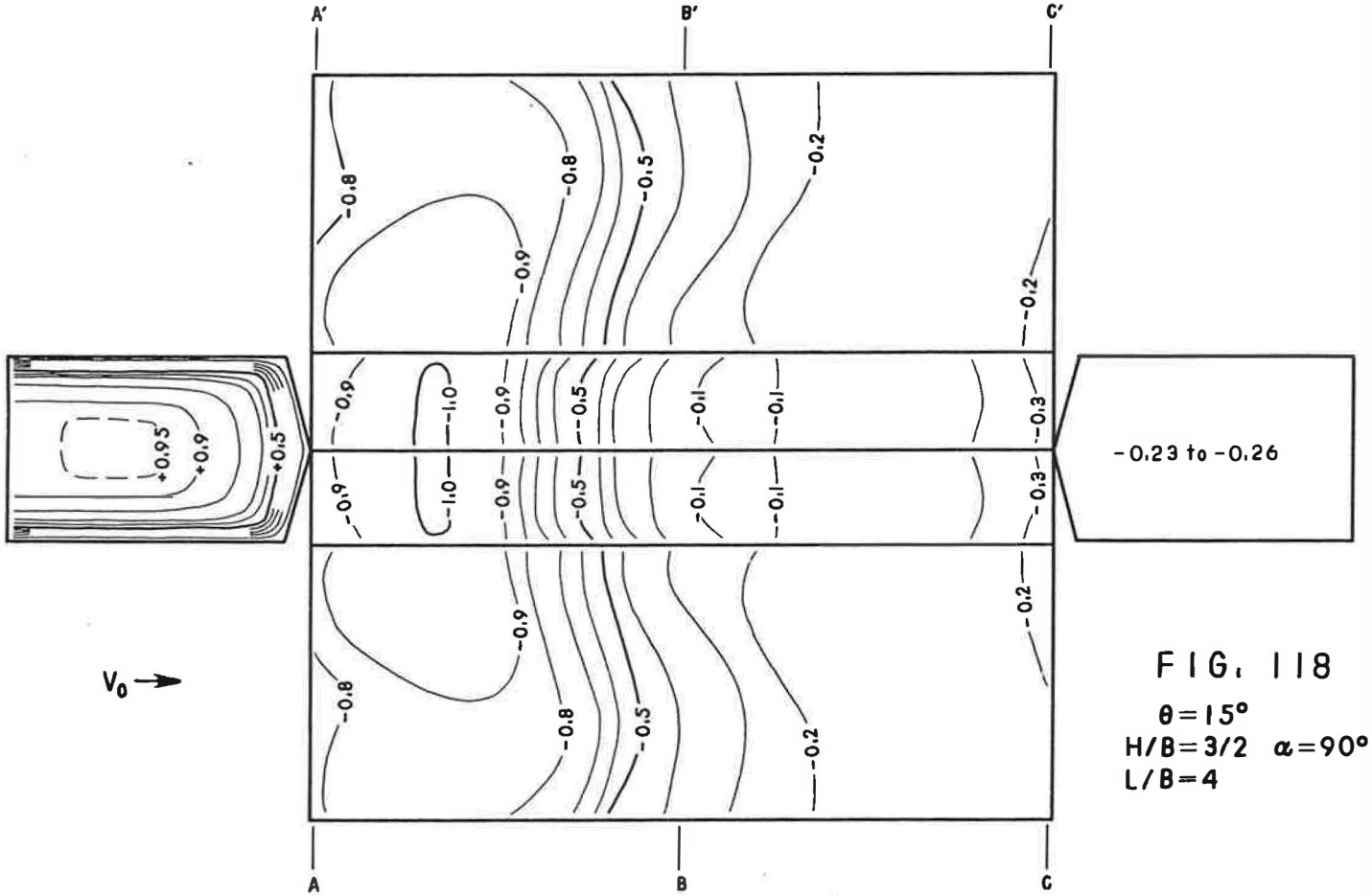

FIG. 118

$\theta = 15°$
$H/B = 3/2 \quad \alpha = 90°$
$L/B = 4$

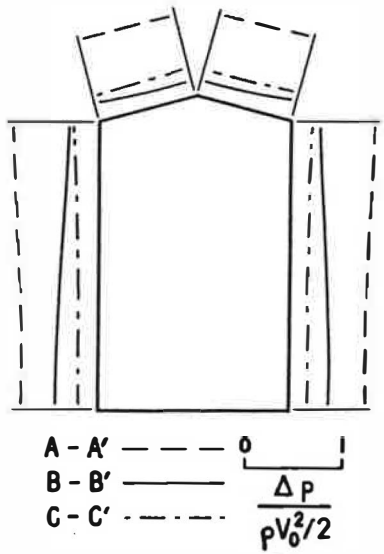

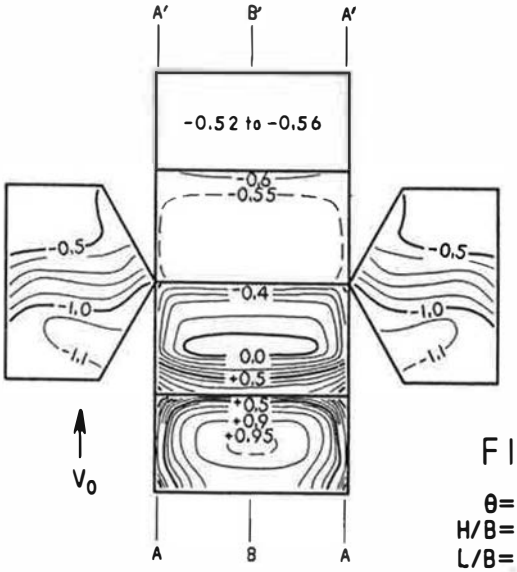

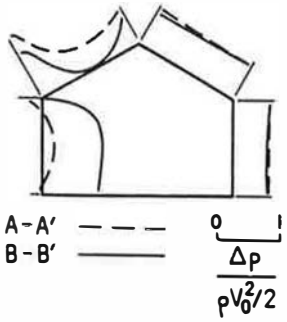

FIG. 119

θ=30°
H/B=1/2 α=0°
L/B=1

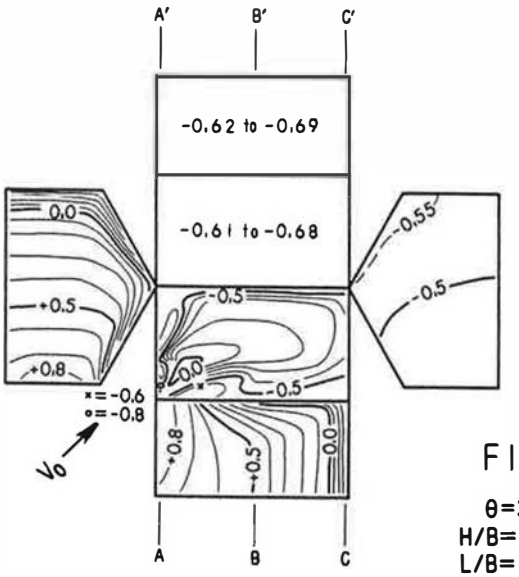

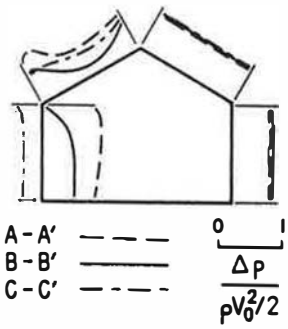

FIG. 120

θ=30°
H/B=1/2 α=45°
L/B=1

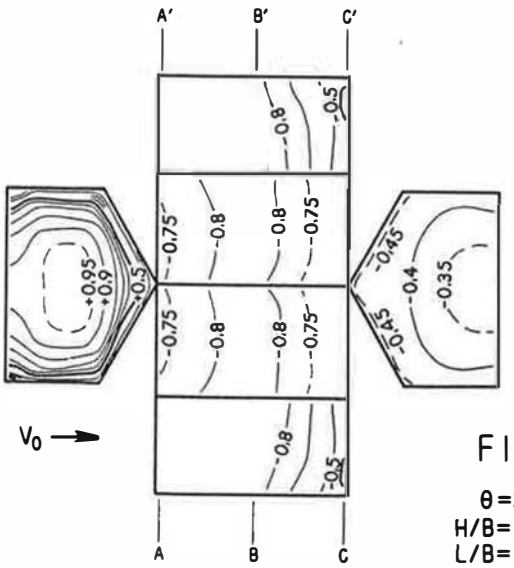

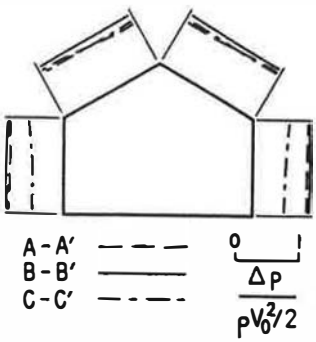

FIG. 121

θ=30°
H/B=1/2 α=90°
L/B=1

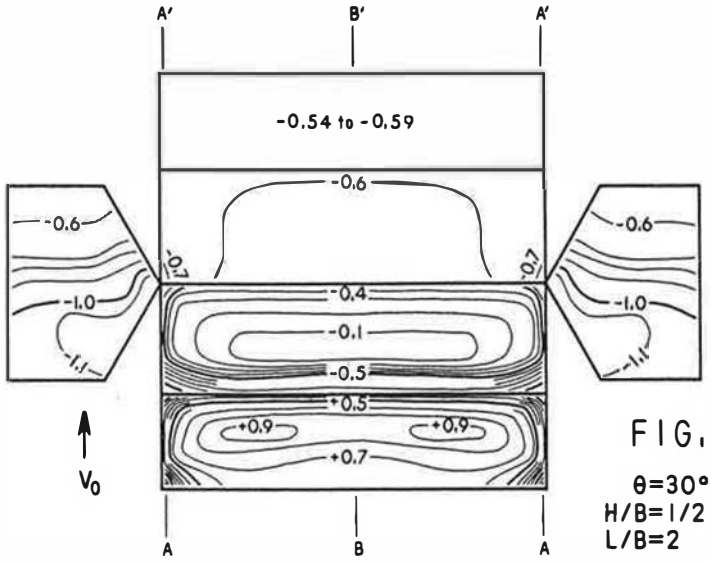

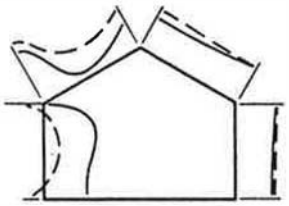

FIG. 122

θ=30°
H/B=1/2 α=0°
L/B=2

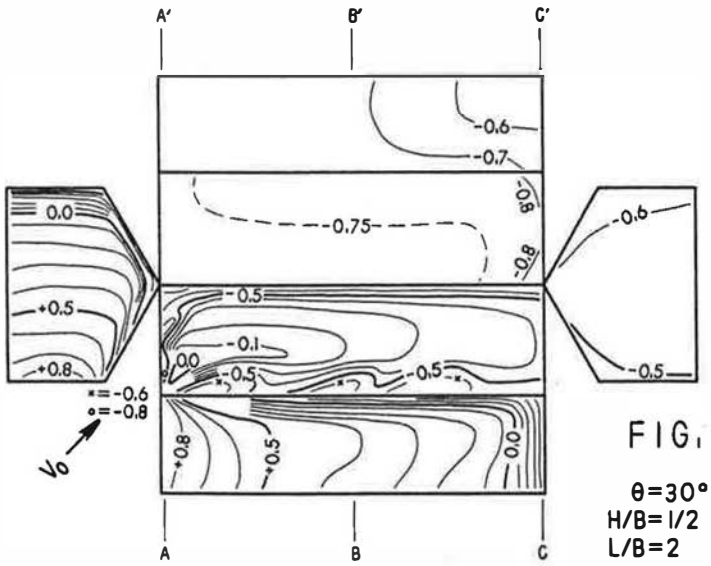

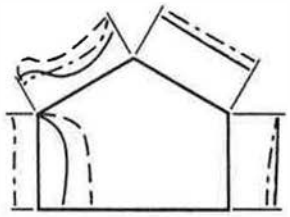

FIG. 123

θ=30°
H/B=1/2 α=45°
L/B=2

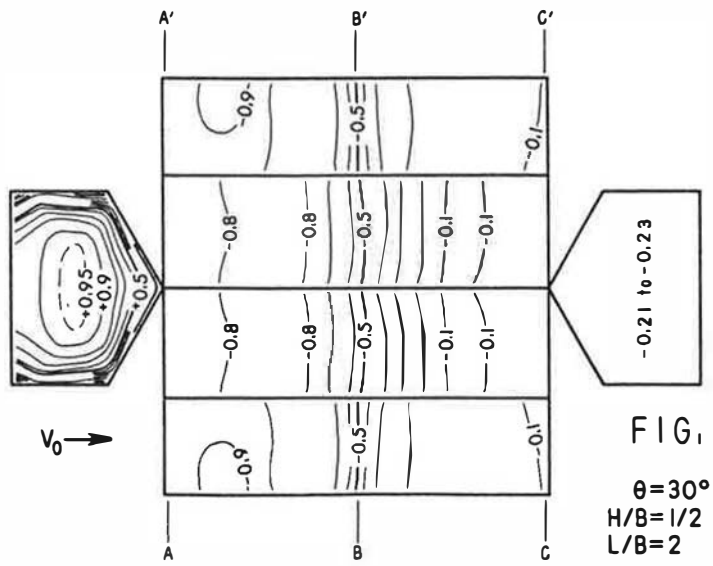

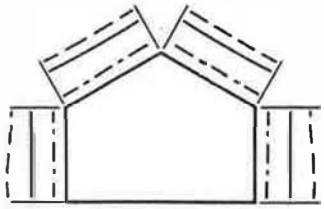

FIG. 124

θ=30°
H/B=1/2 α=90°
L/B=2

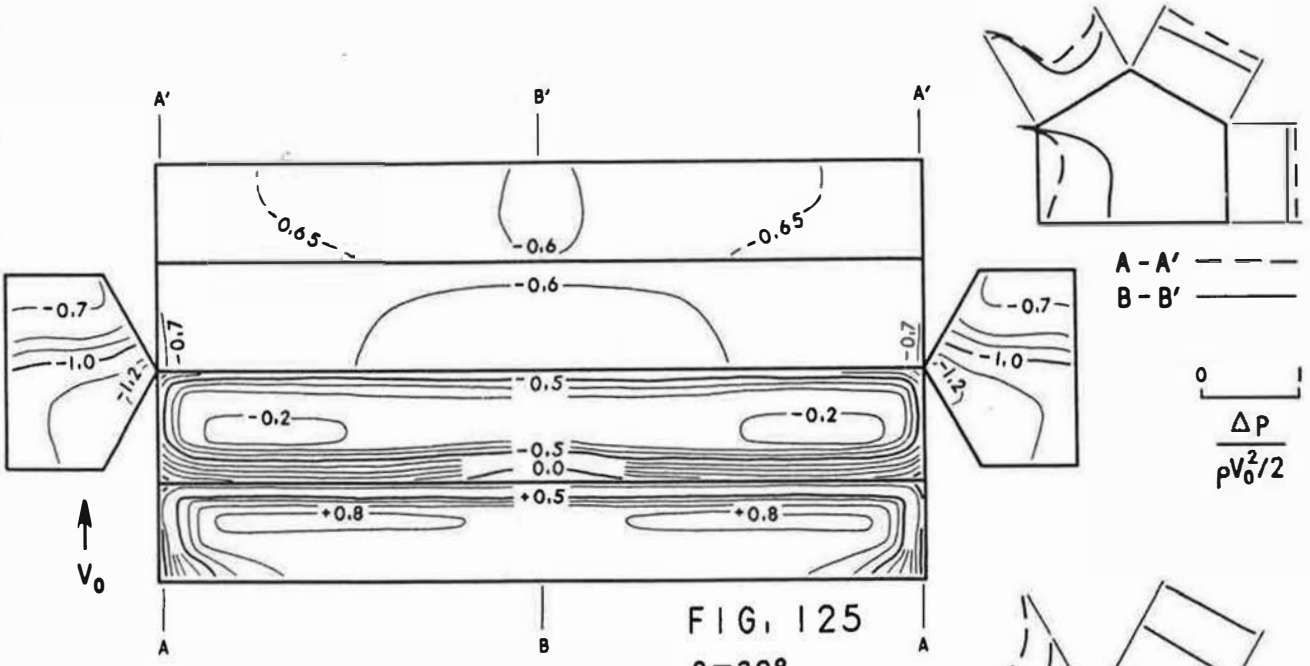

FIG. 125

θ=30°
H/B=1/2 α=0°
L/B=4

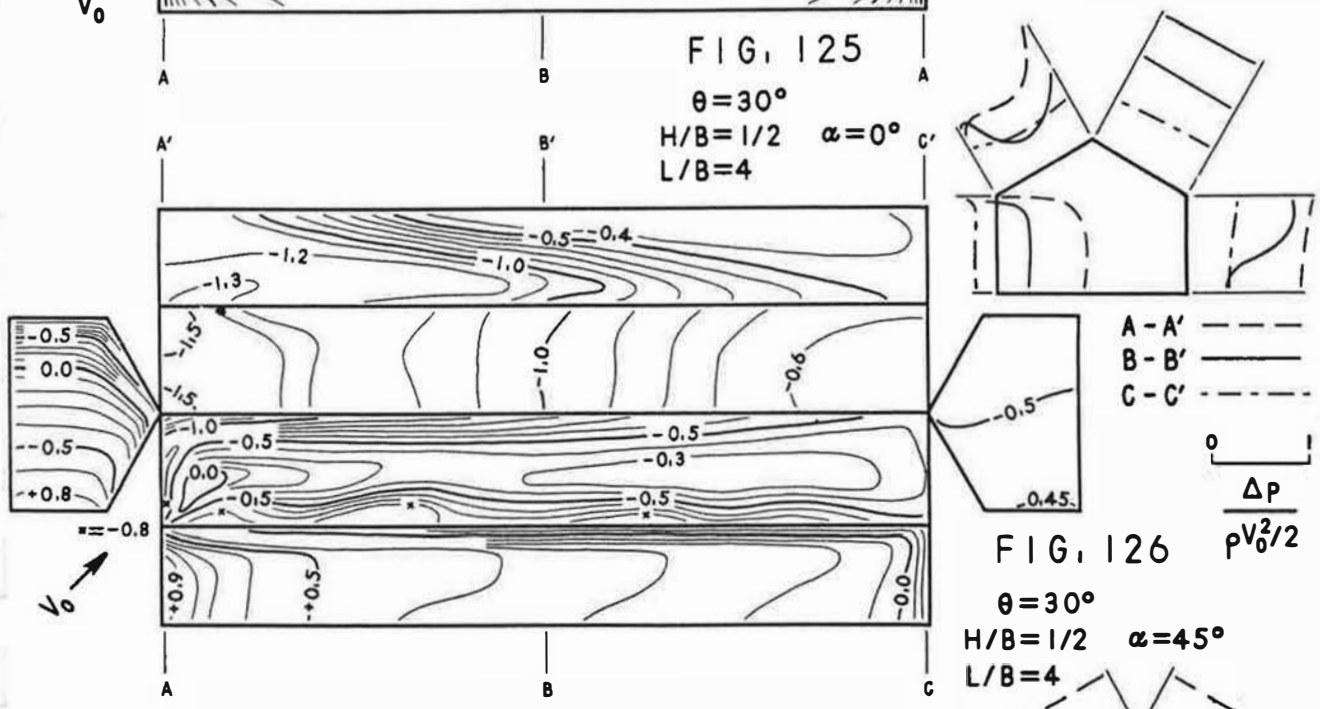

FIG. 126

θ=30°
H/B=1/2 α=45°
L/B=4

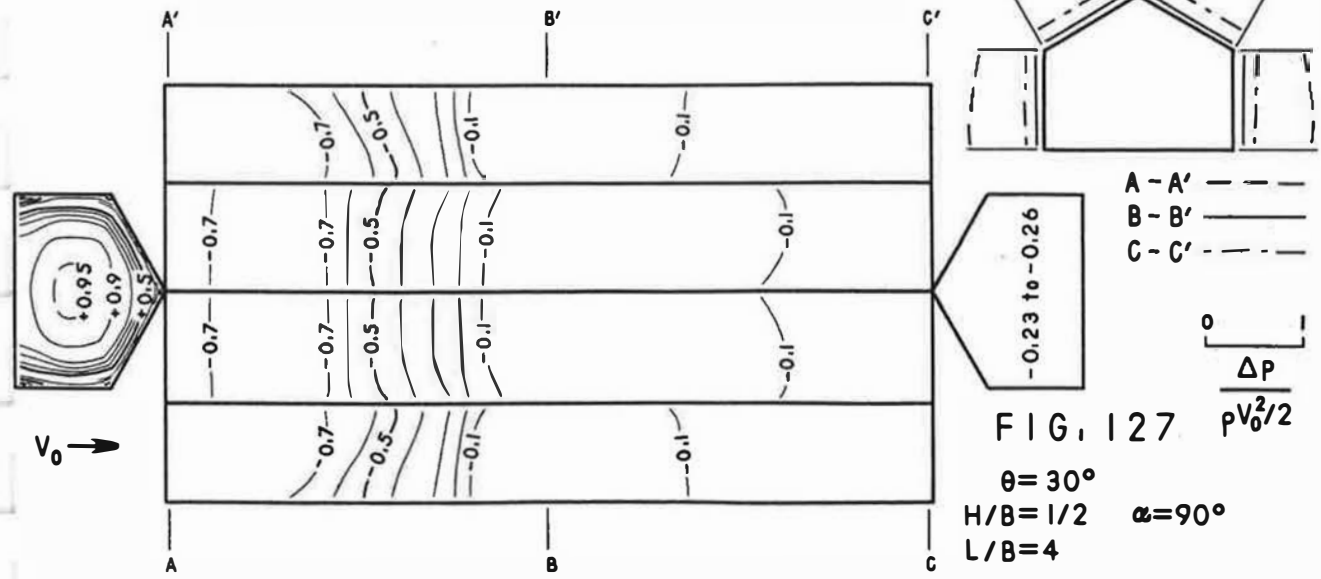

FIG. 127

θ=30°
H/B=1/2 α=90°
L/B=4

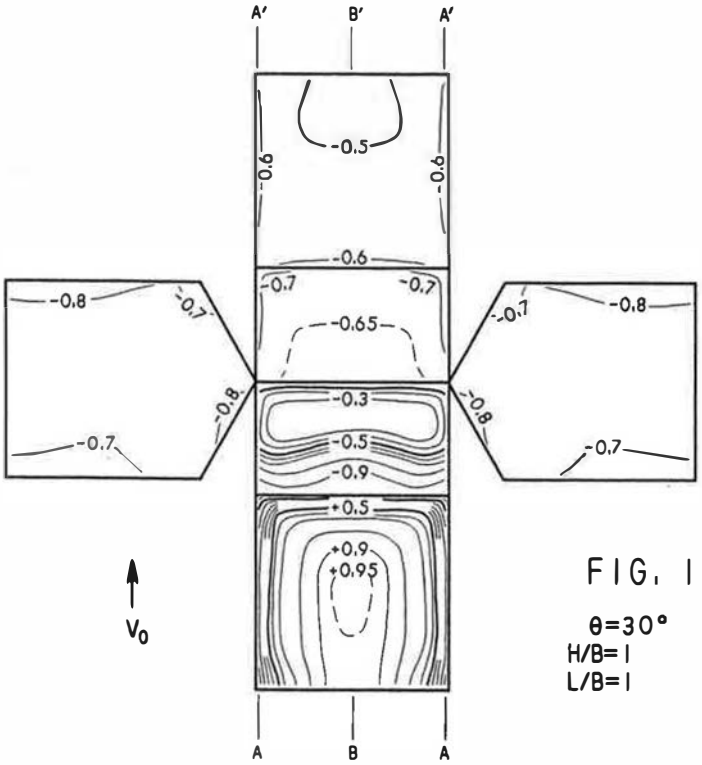

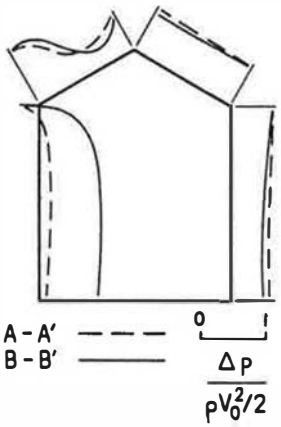

FIG. 128

θ=30°
H/B=1 α=0°
L/B=1

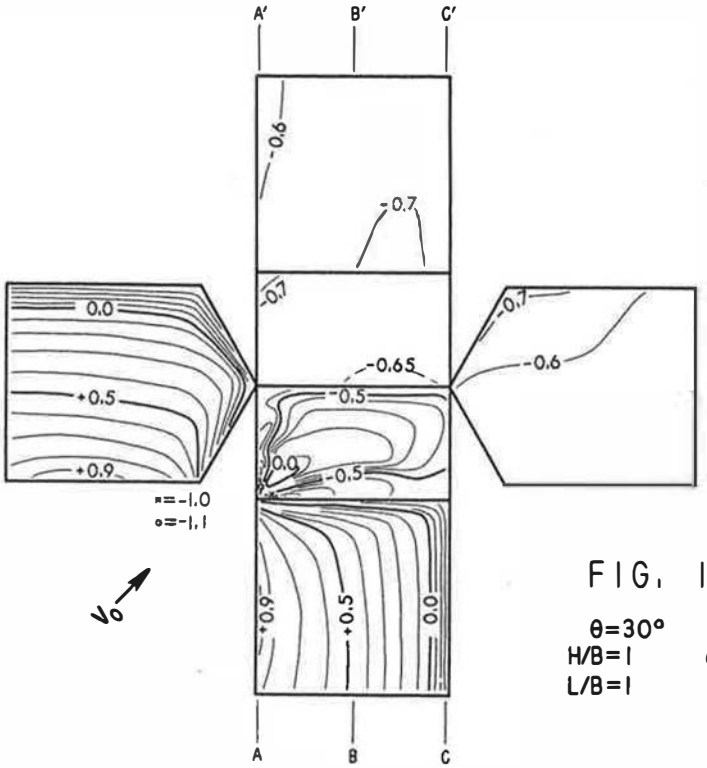

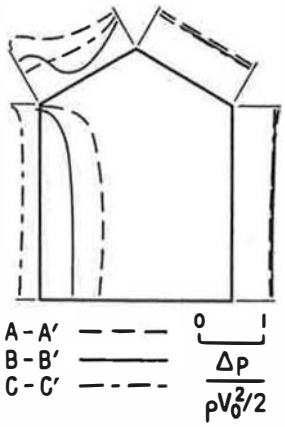

FIG. 129

θ=30°
H/B=1 α=45°
L/B=1

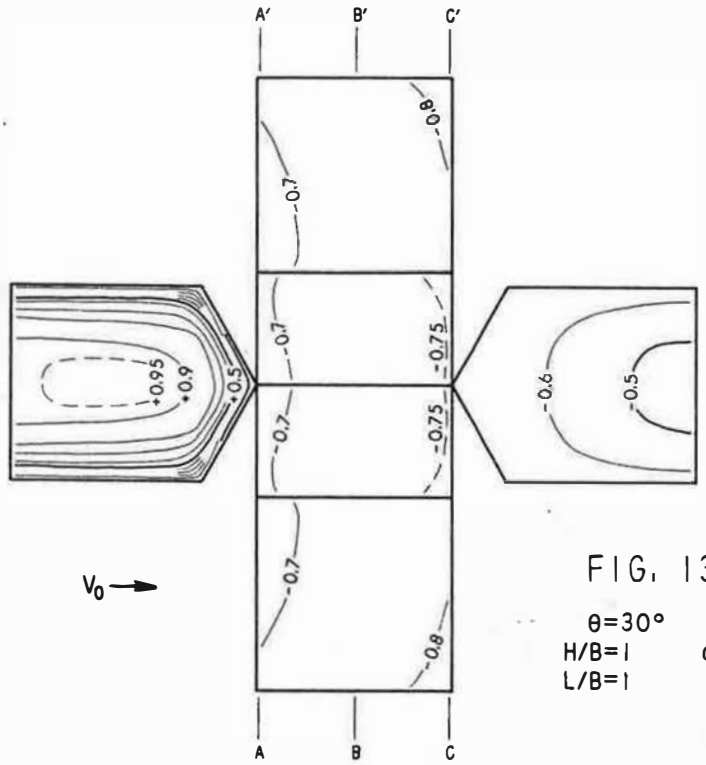

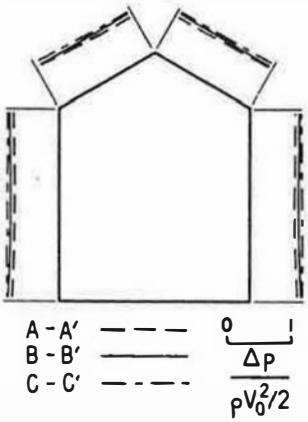

FIG. 130

θ=30°
H/B=1 α=90°
L/B=1

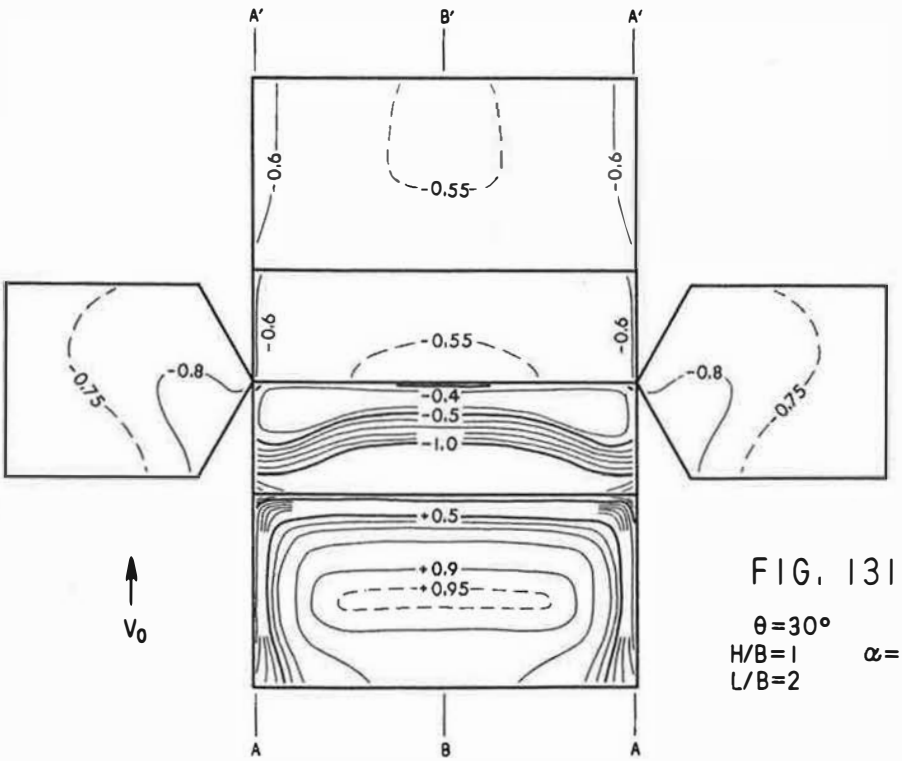

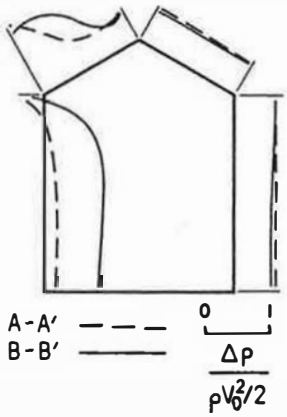

FIG. 131

θ=30°
H/B=1 α=0°
L/B=2

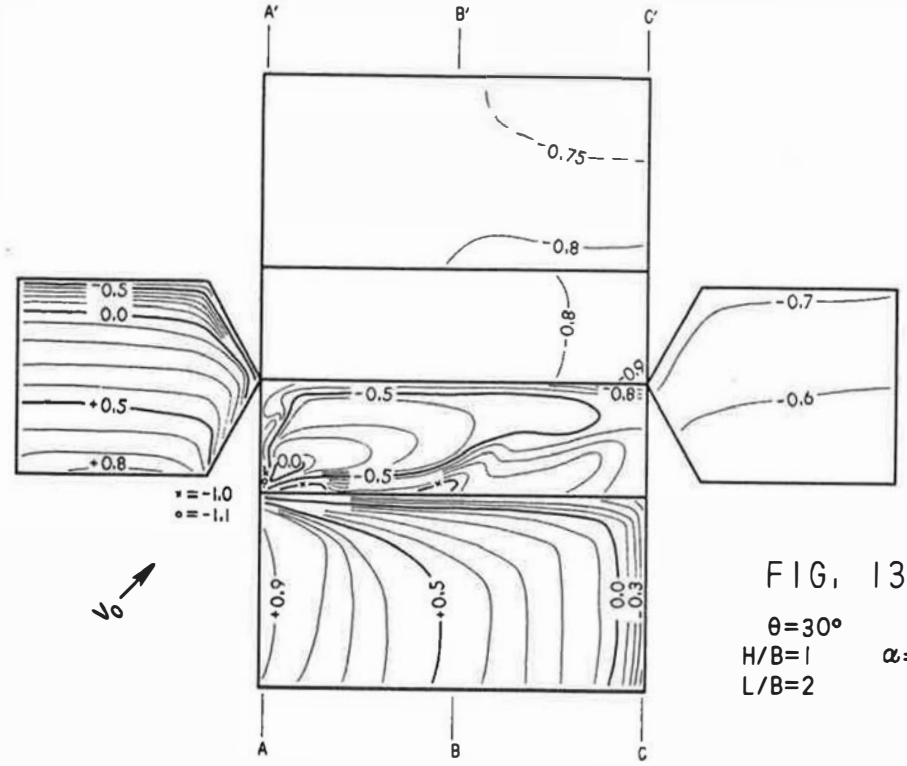

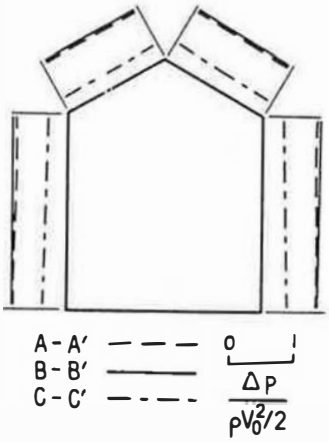

FIG. 132

θ=30°
H/B=1 α=45°
L/B=2

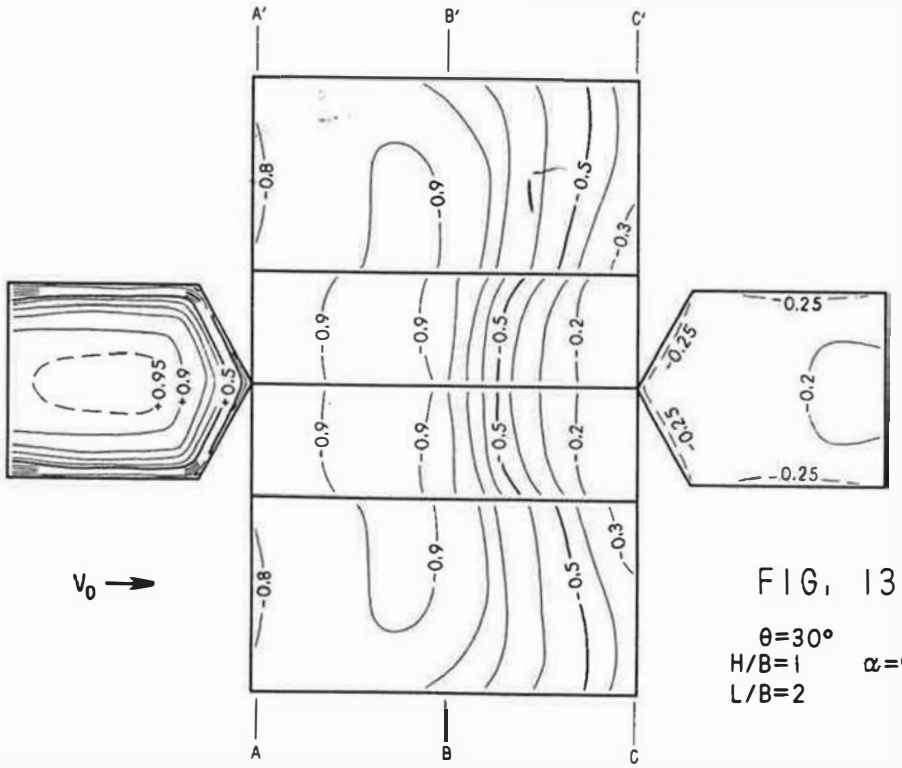

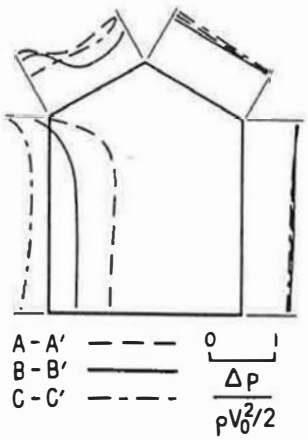

FIG. 133

θ=30°
H/B=1 α=90°
L/B=2

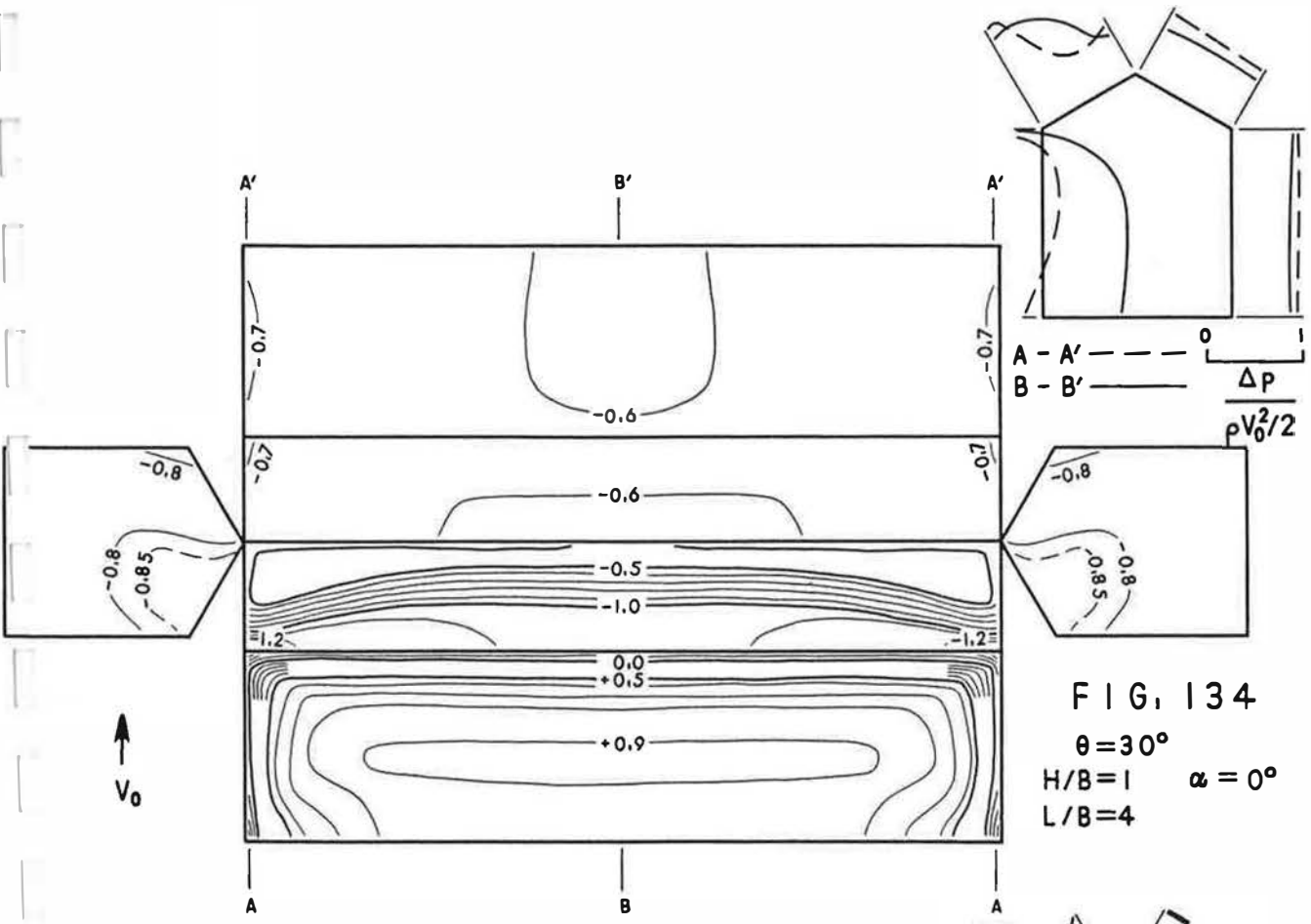

FIG. 134

θ=30°
H/B=1 α = 0°
L/B=4

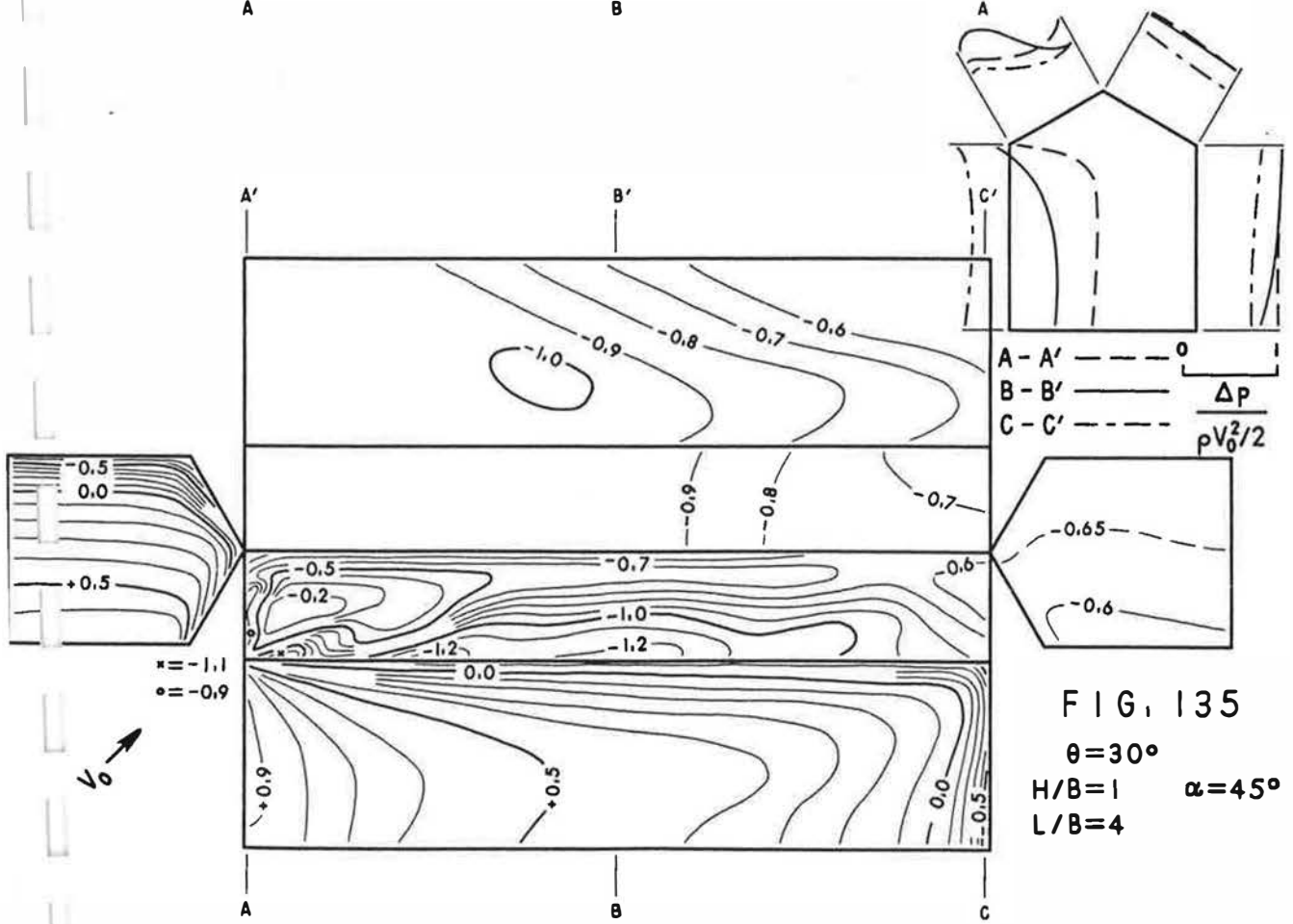

FIG. 135

θ=30°
H/B=1 α=45°
L/B=4

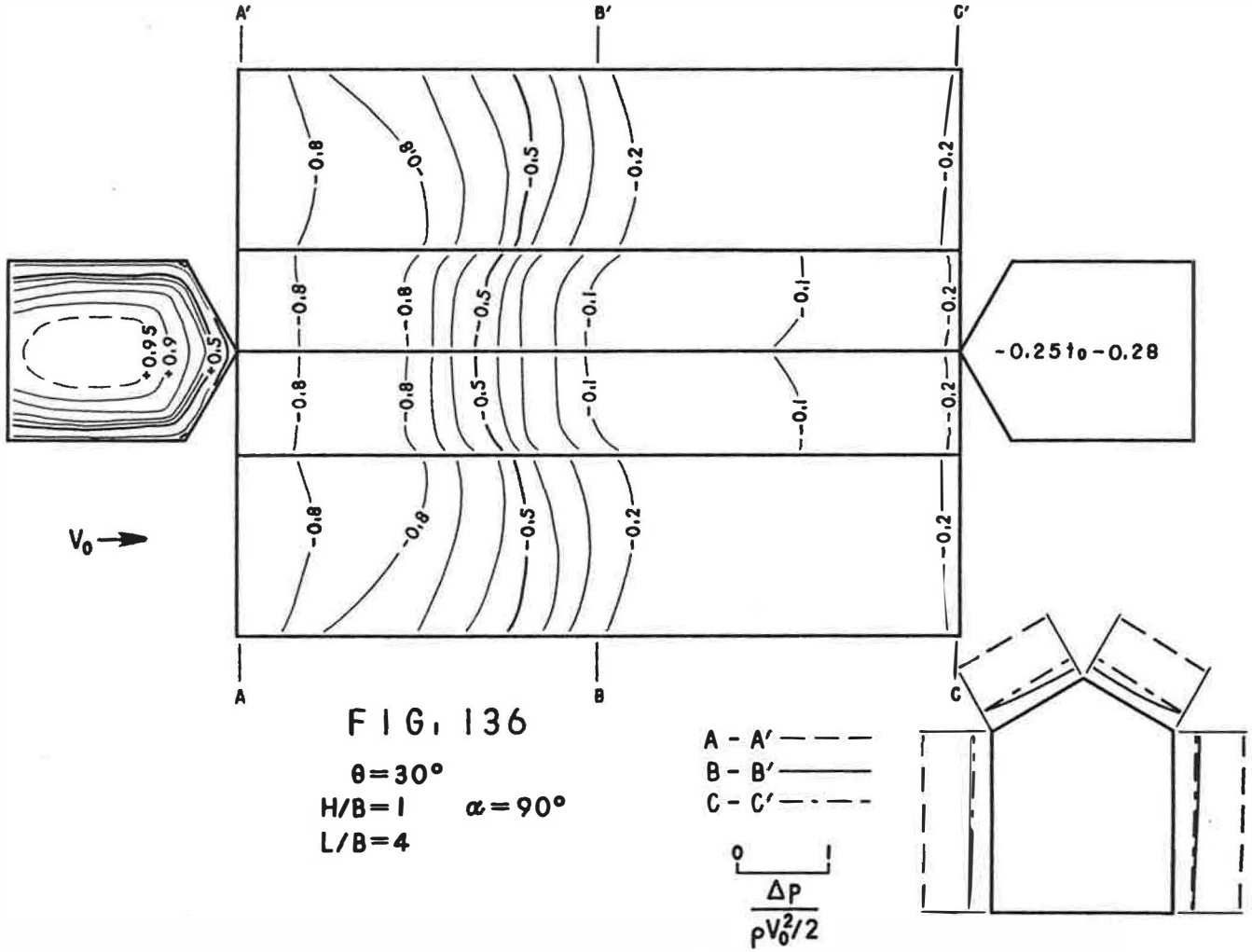

FIG. 136

θ=30°

H/B=1 α=90°

L/B=4

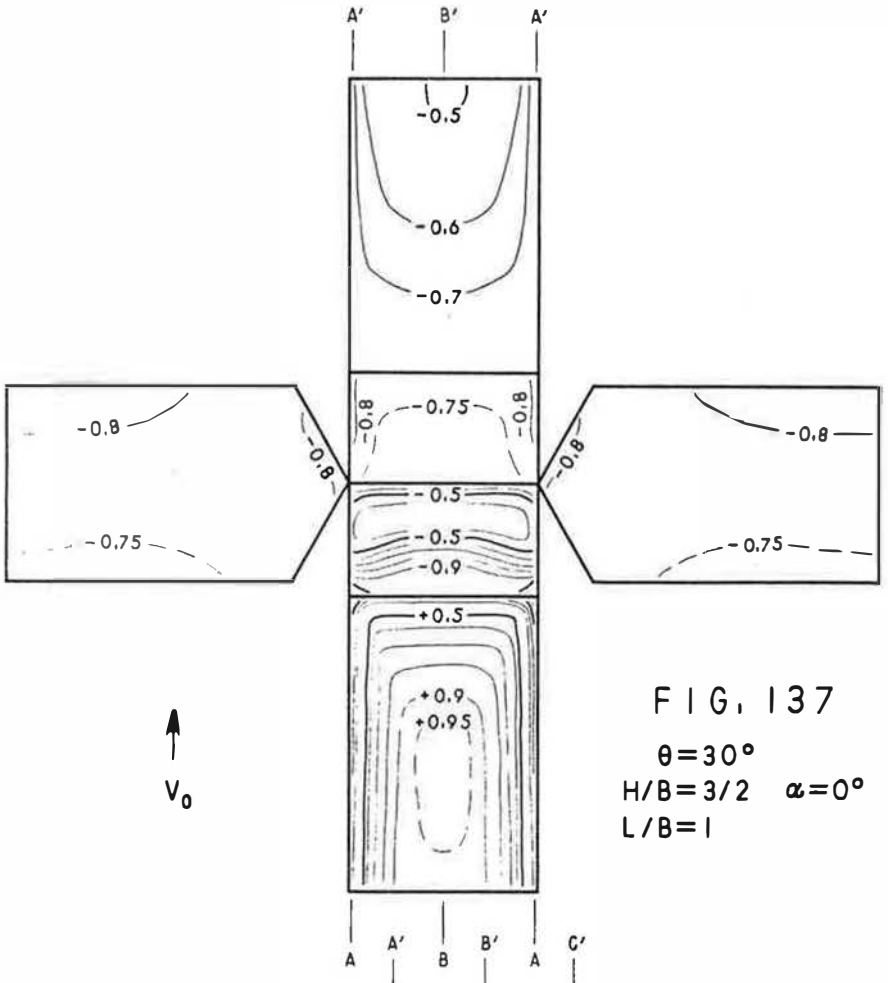

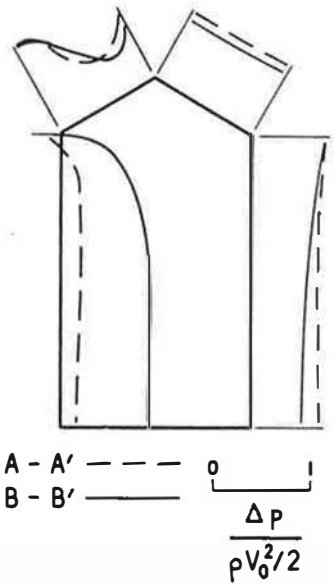

FIG. 137

θ=30°
H/B=3/2 α=0°
L/B=1

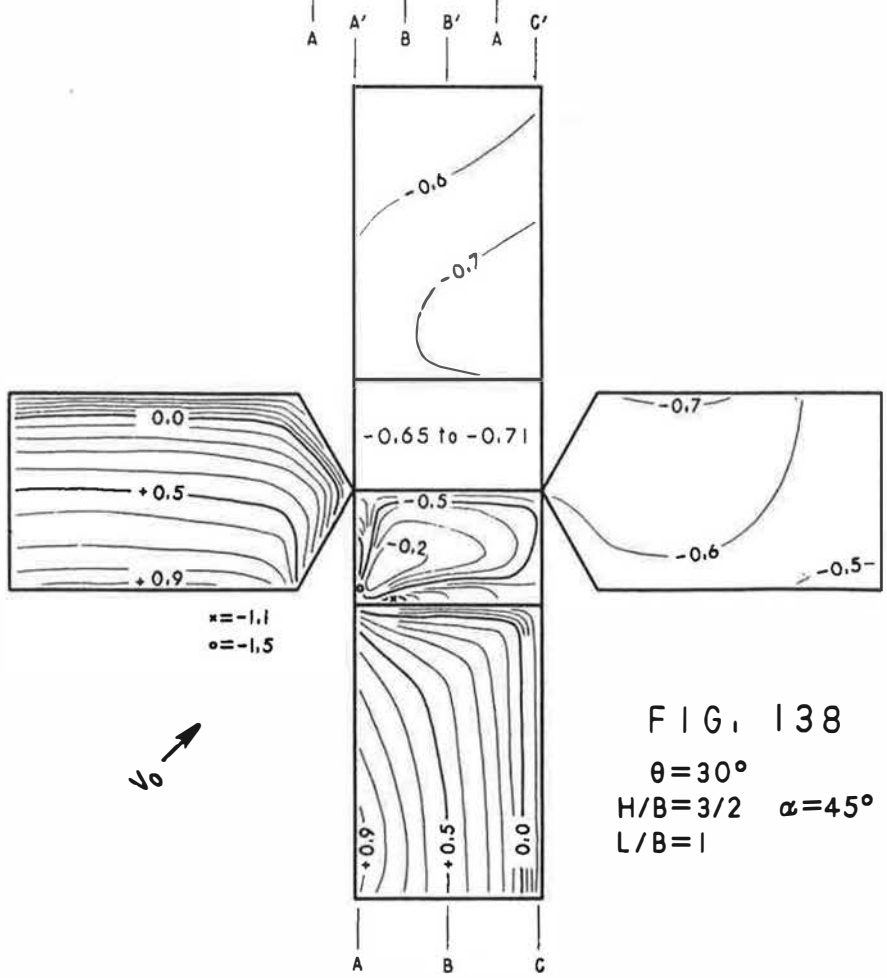

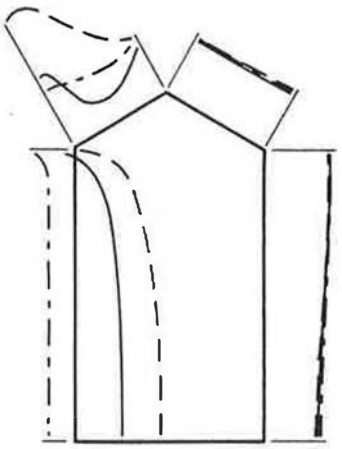

FIG. 138

θ=30°
H/B=3/2 α=45°
L/B=1

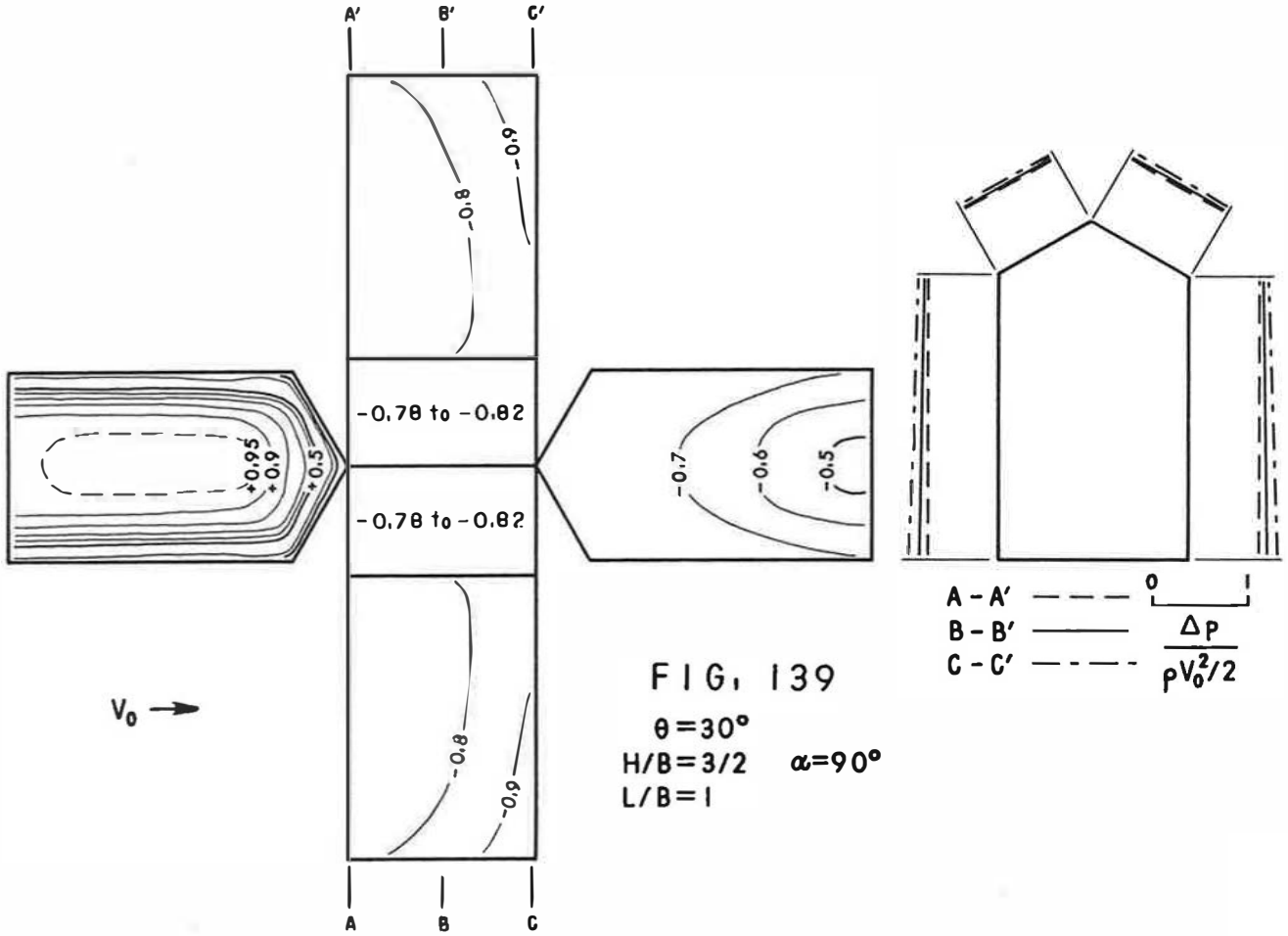

FIG. 139

$\theta = 30°$

$H/B = 3/2$ $\quad \alpha = 90°$

$L/B = 1$

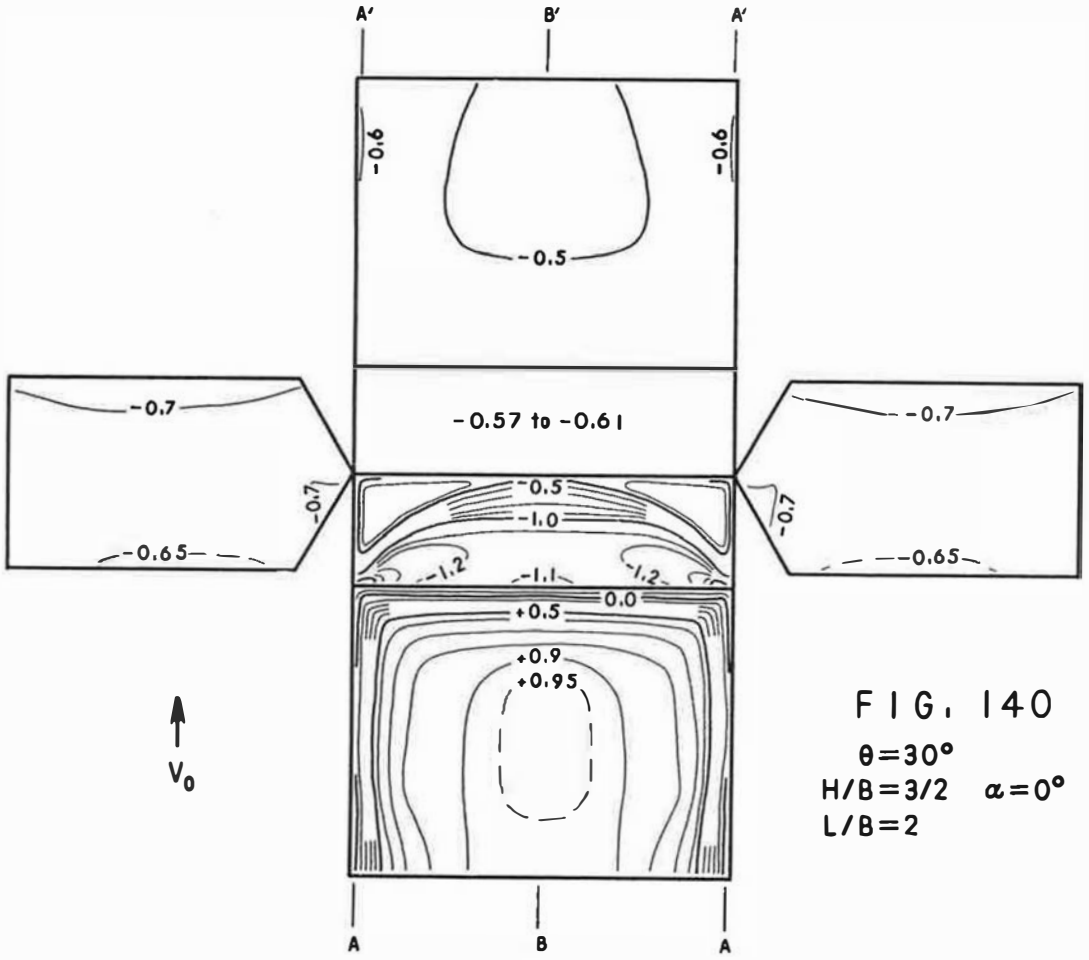

FIG. 140

θ=30°
H/B=3/2 α=0°
L/B=2

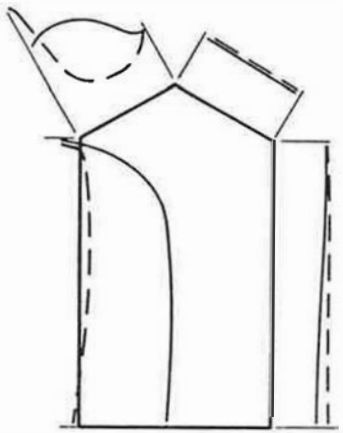

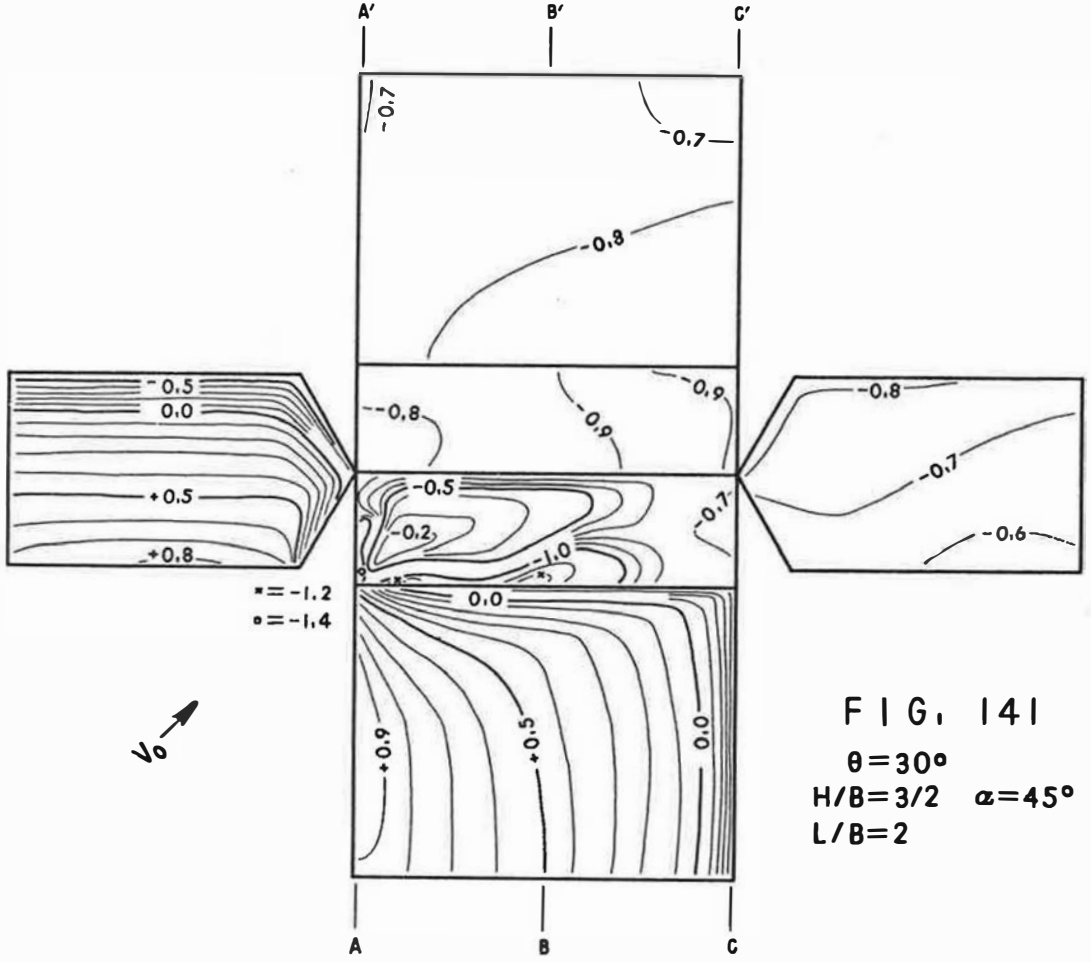

FIG. 141

θ=30°
H/B=3/2 α=45°
L/B=2

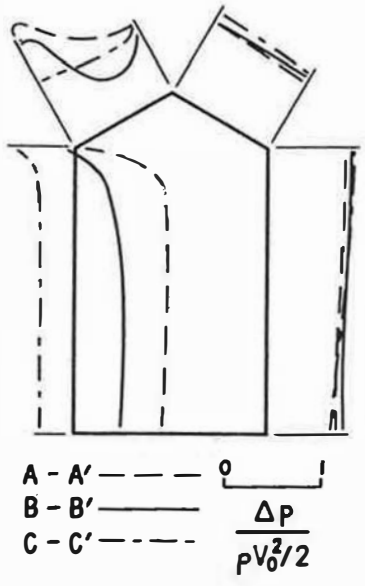

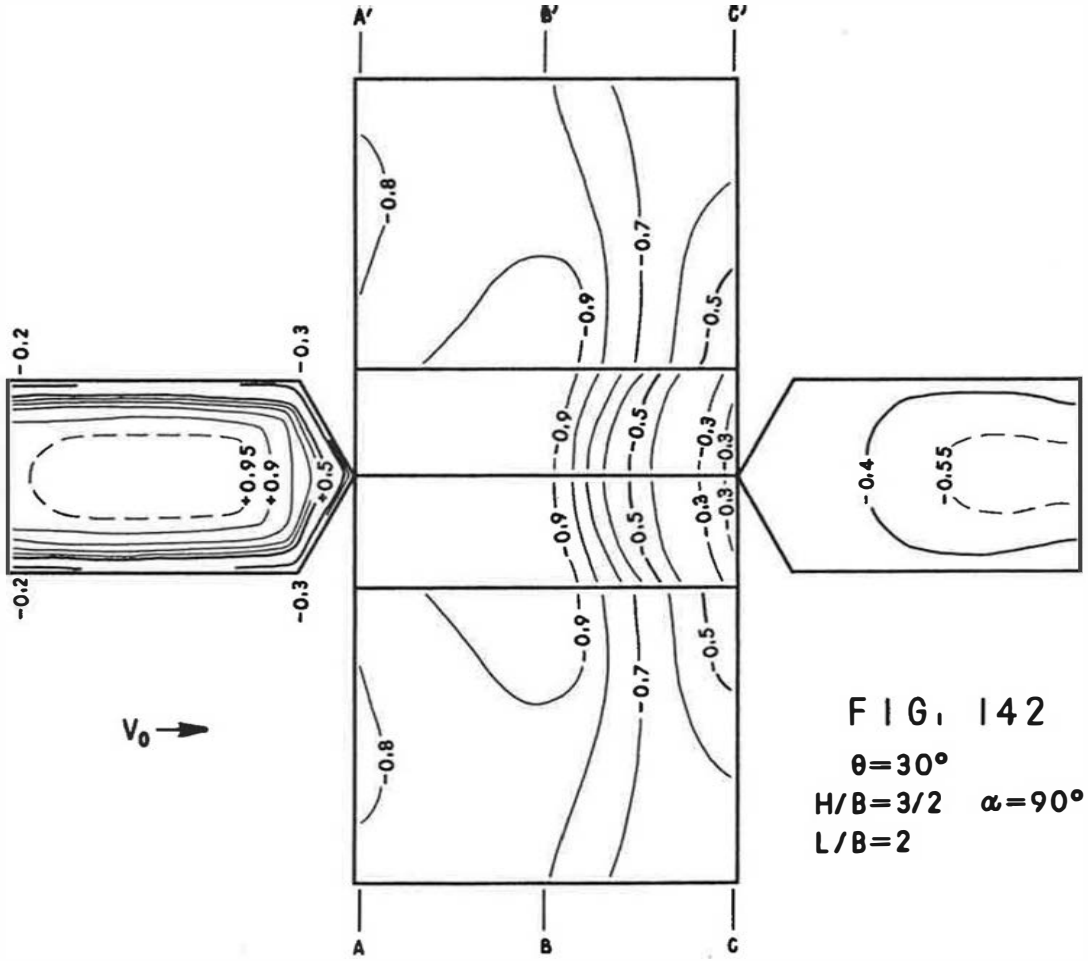

FIG. 142

θ=30°

H/B=3/2 α=90°

L/B=2

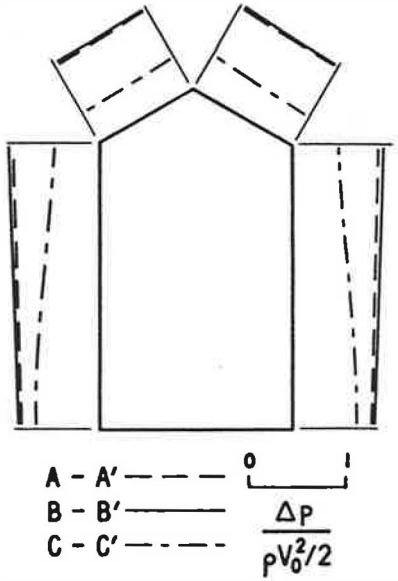

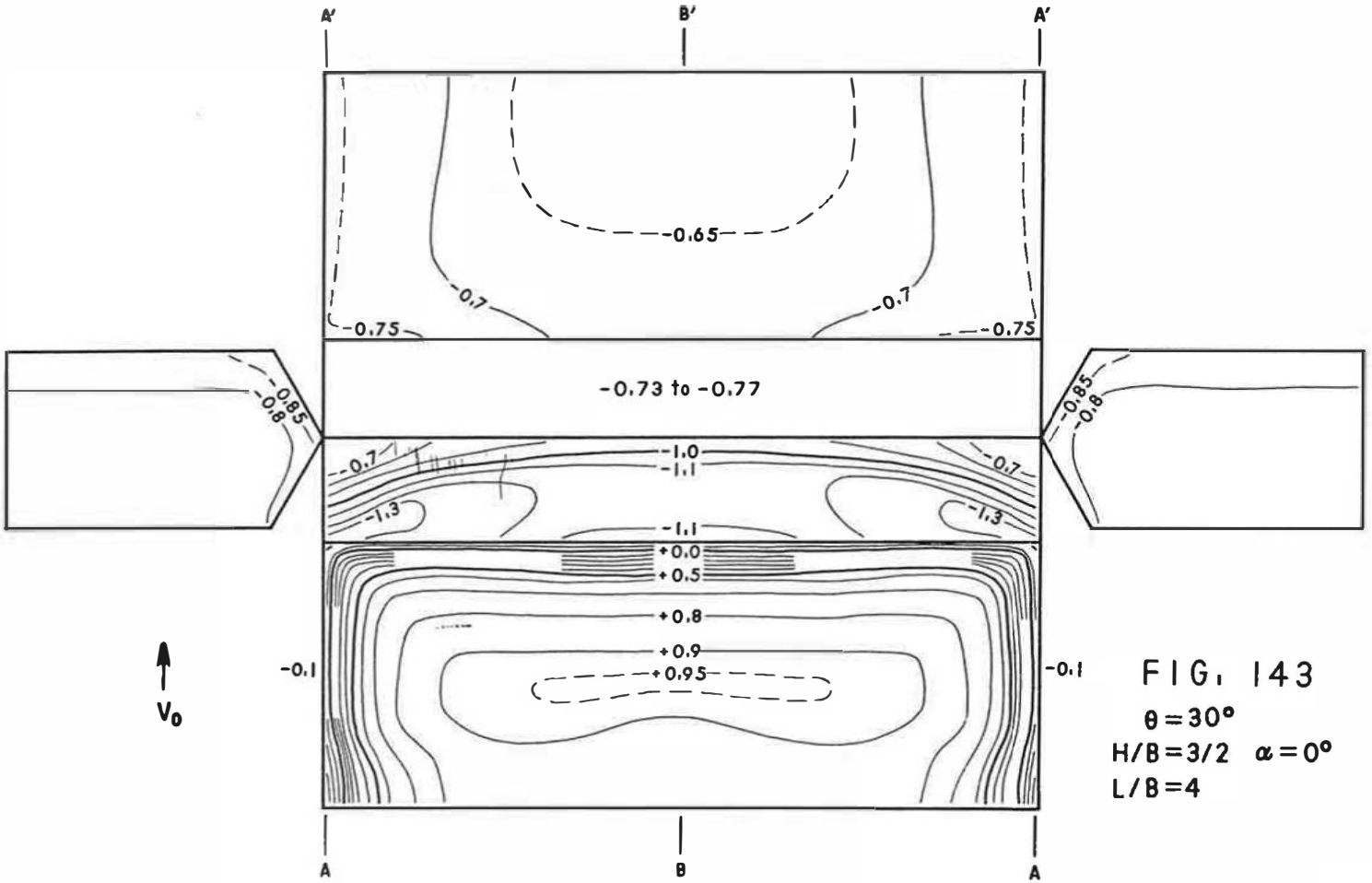

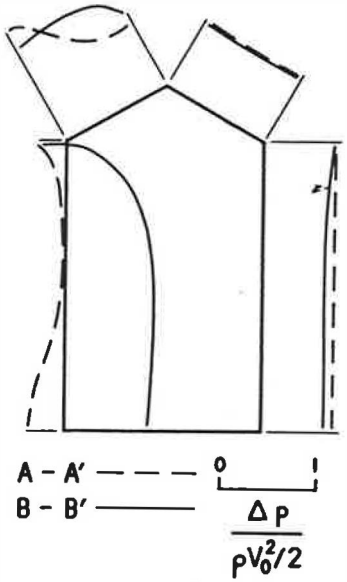

FIG. 143

$\theta = 30°$

$H/B = 3/2 \quad \alpha = 0°$

$L/B = 4$

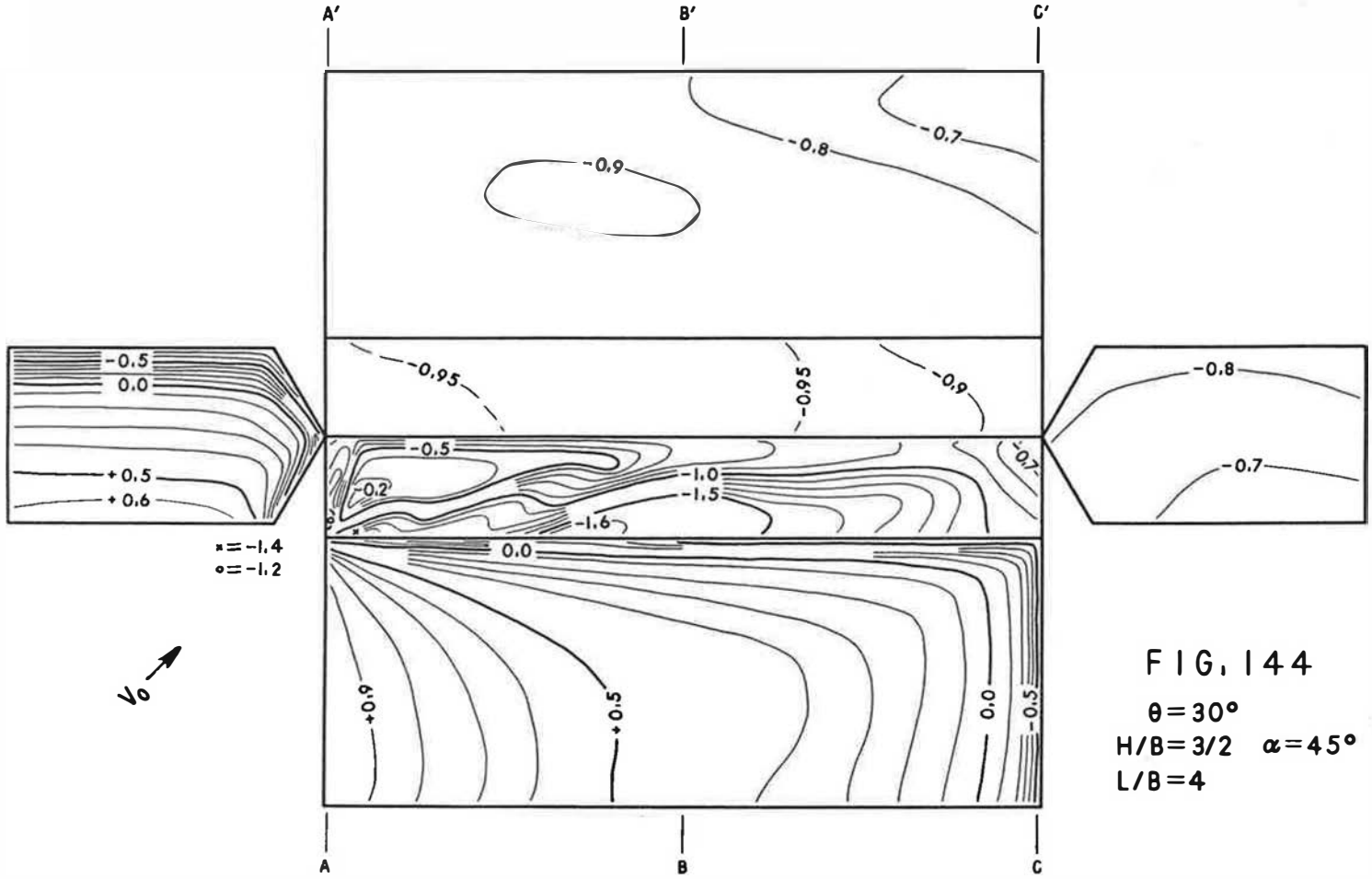

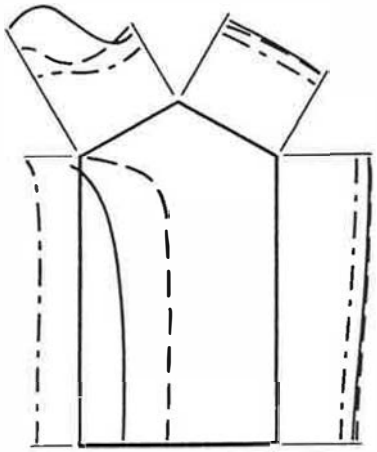

FIG. 144

θ=30°
H/B=3/2 α=45°
L/B=4

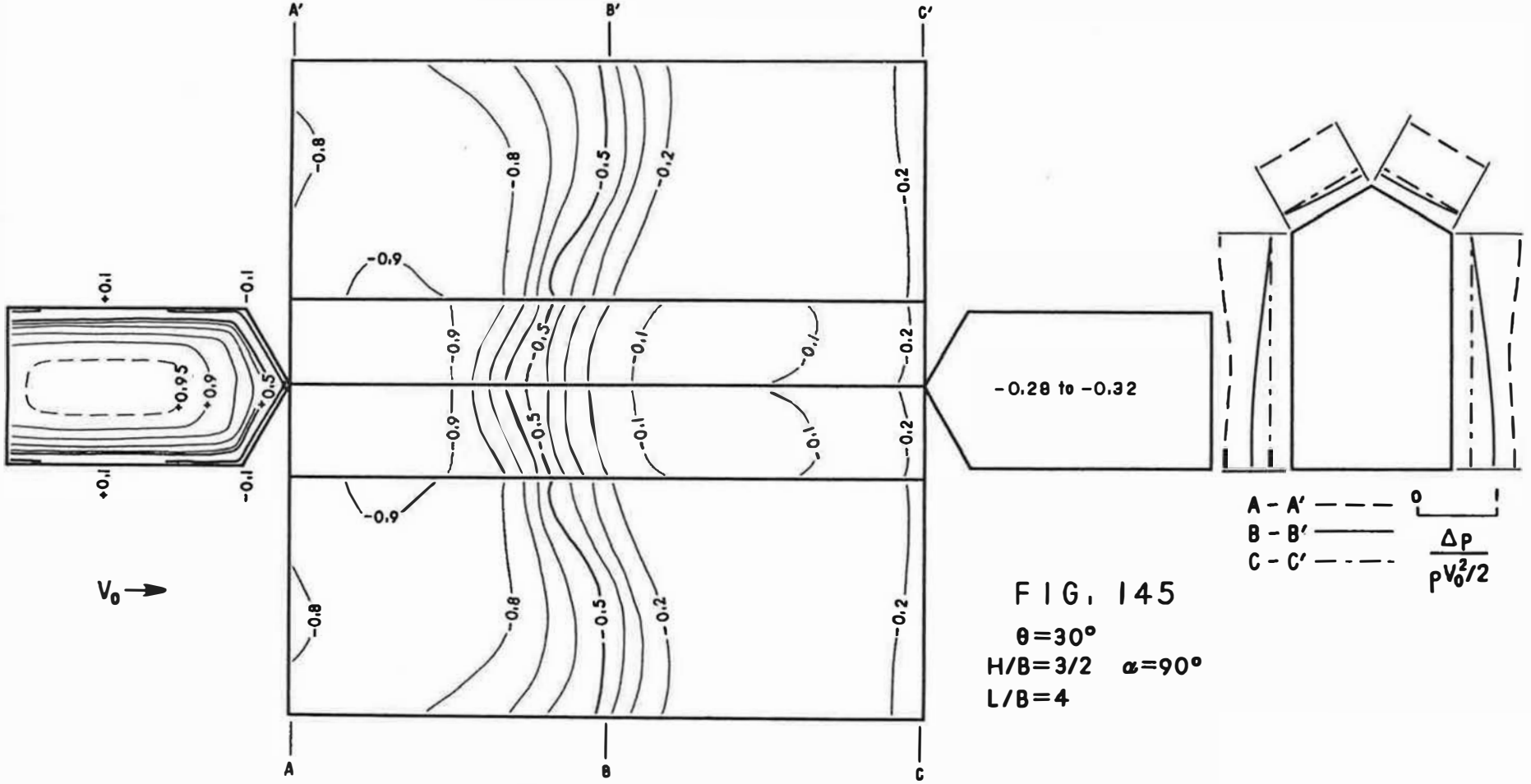

FIG. 145

θ=30°
H/B=3/2 α=90°
L/B=4

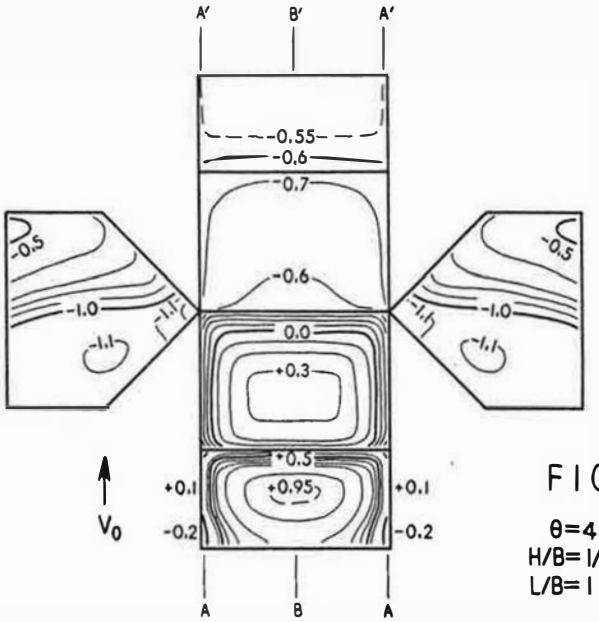

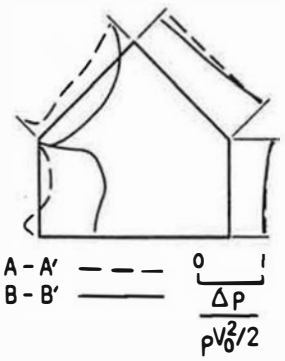

FIG. 146

θ=45°
H/B=1/2 α=0°
L/B=1

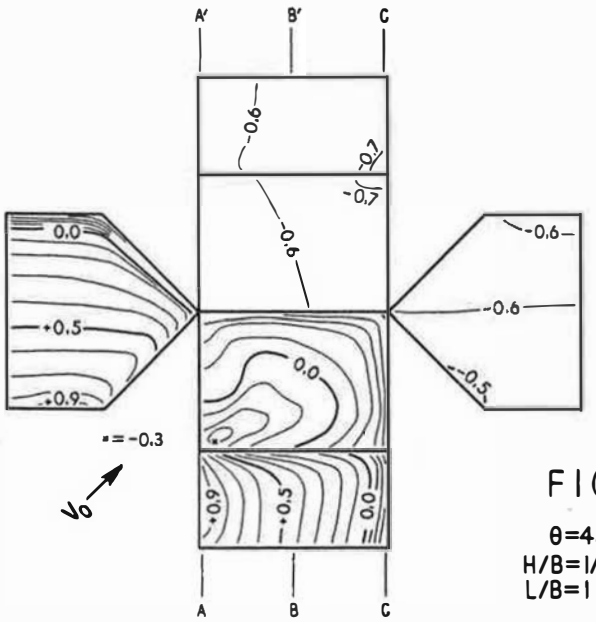

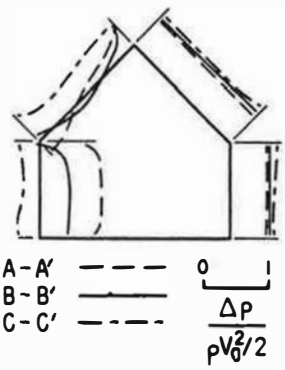

FIG. 147

θ=45°
H/B=1/2 α=45°
L/B=1

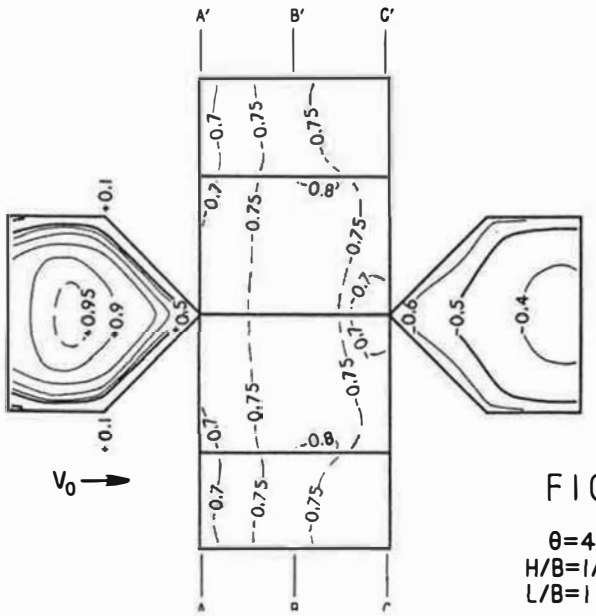

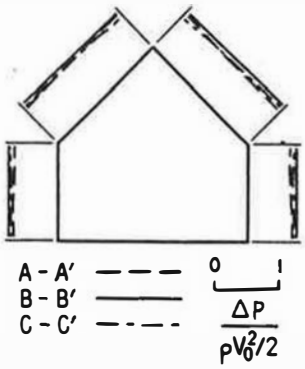

FIG. 148

θ=45°
H/B=1/2 α=90°
L/B=1

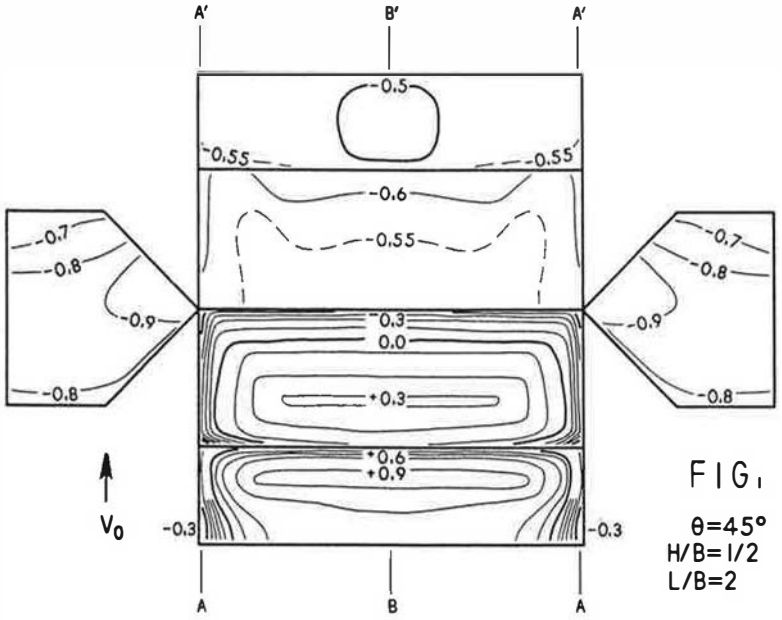

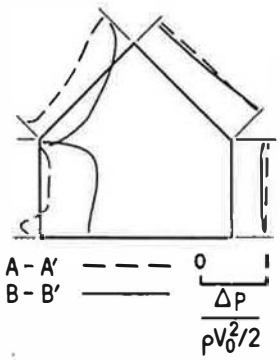

FIG. 149

θ=45°
H/B=1/2 α=0°
L/B=2

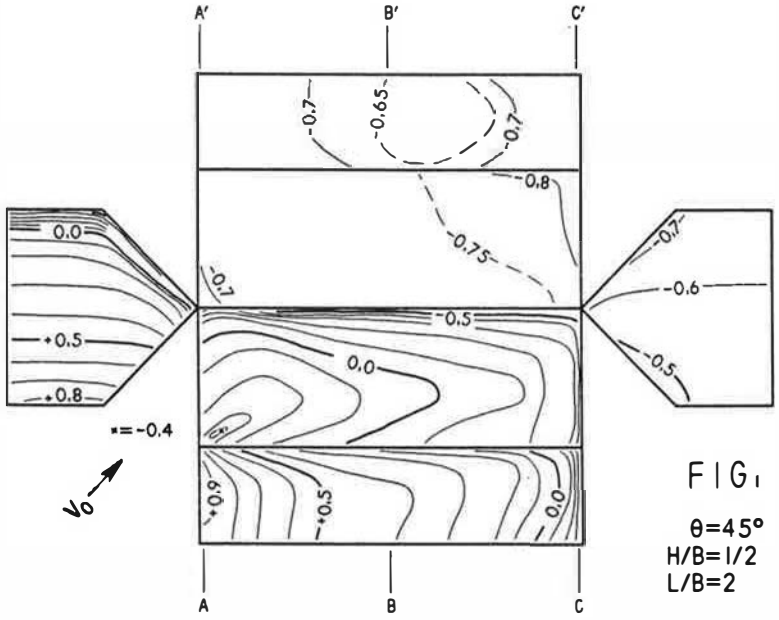

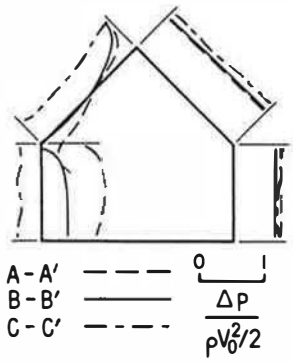

FIG. 150

θ=45°
H/B=1/2 α=45°
L/B=2

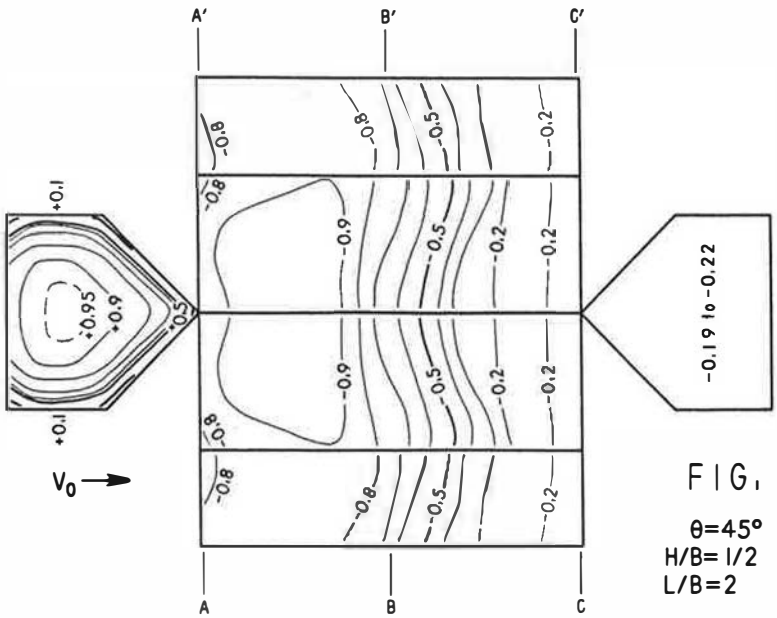

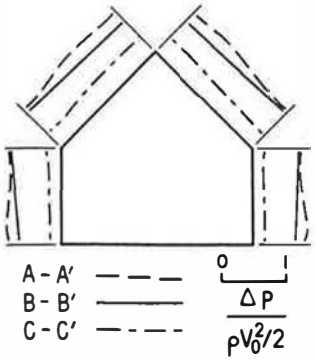

FIG. 151

θ=45°
H/B=1/2 α=90°
L/B=2

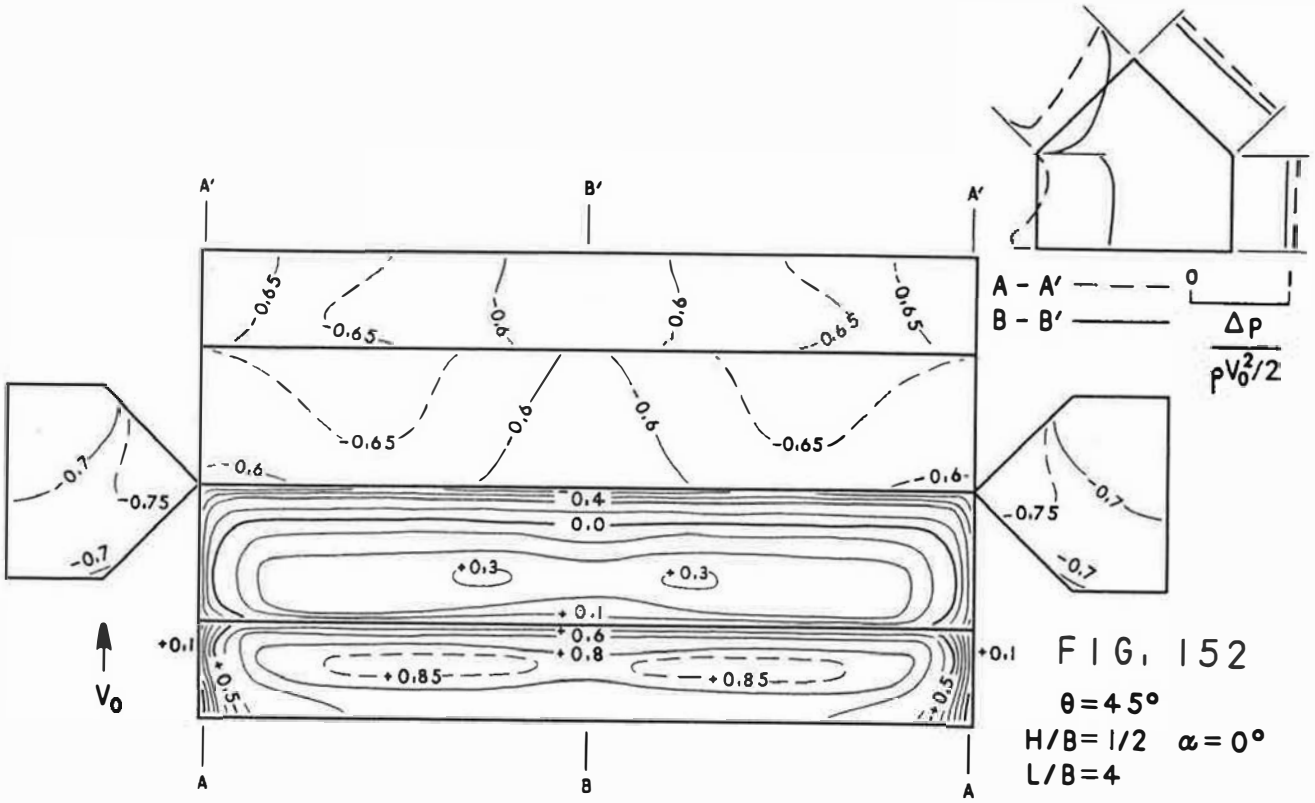

FIG. 152

θ=45°
H/B=1/2 α=0°
L/B=4

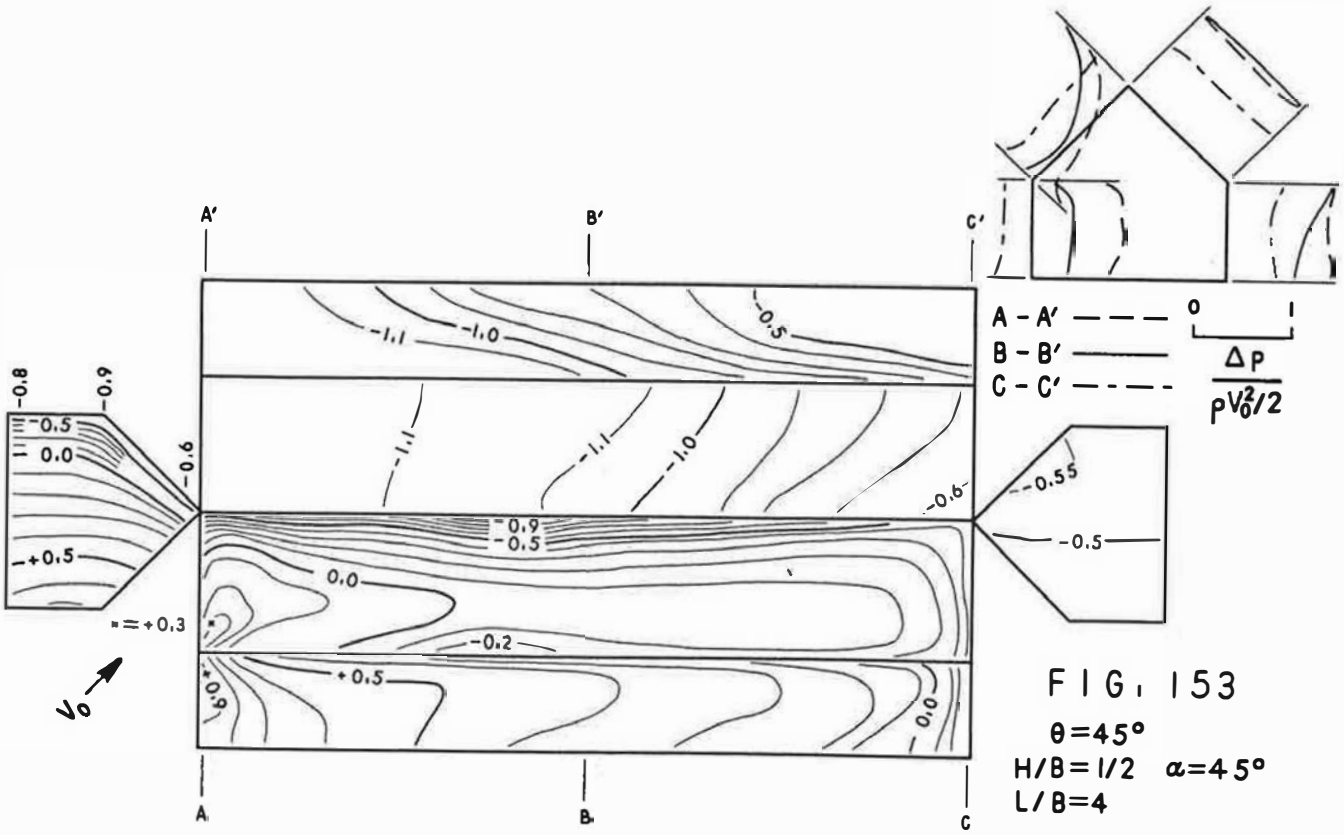

FIG. 153

θ=45°
H/B=1/2 α=45°
L/B=4

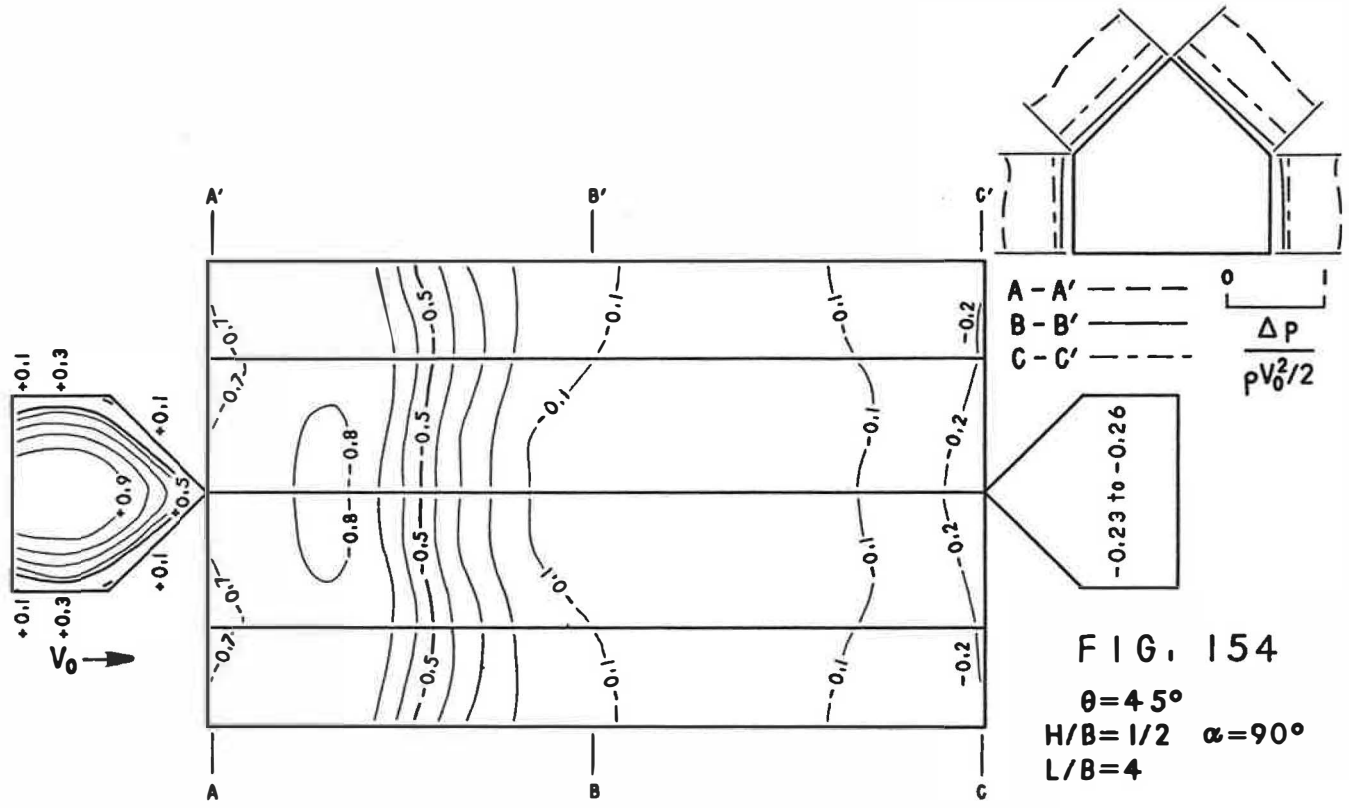

FIG. 154

θ=45°
H/B=1/2 α=90°
L/B=4

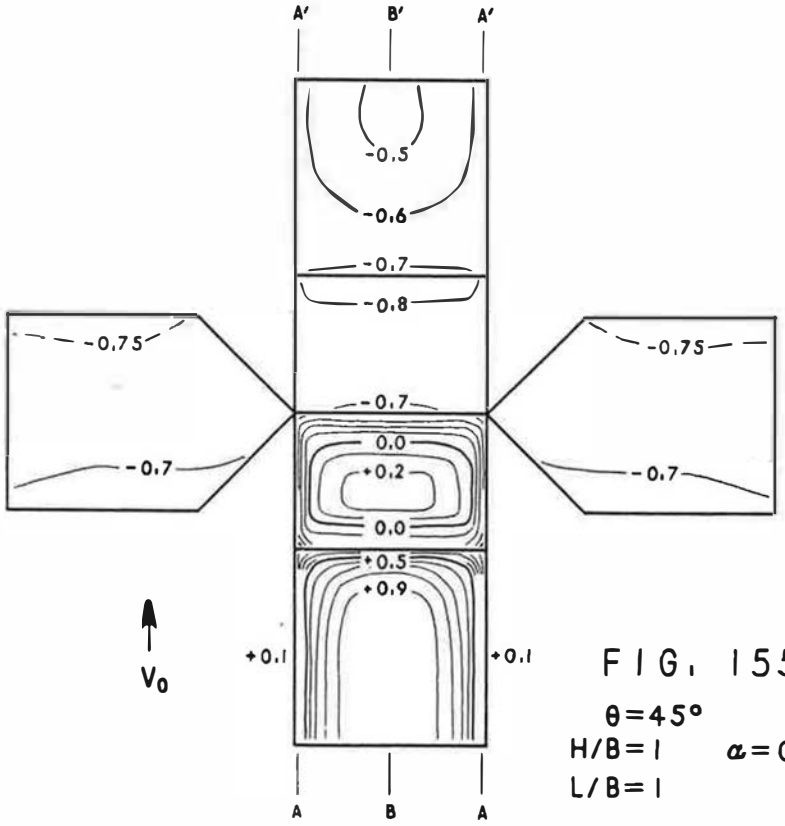

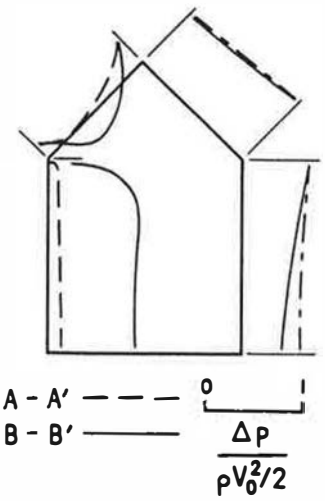

FIG. 155

$\theta = 45°$

H/B = 1 $\quad \alpha = 0°$

L/B = 1

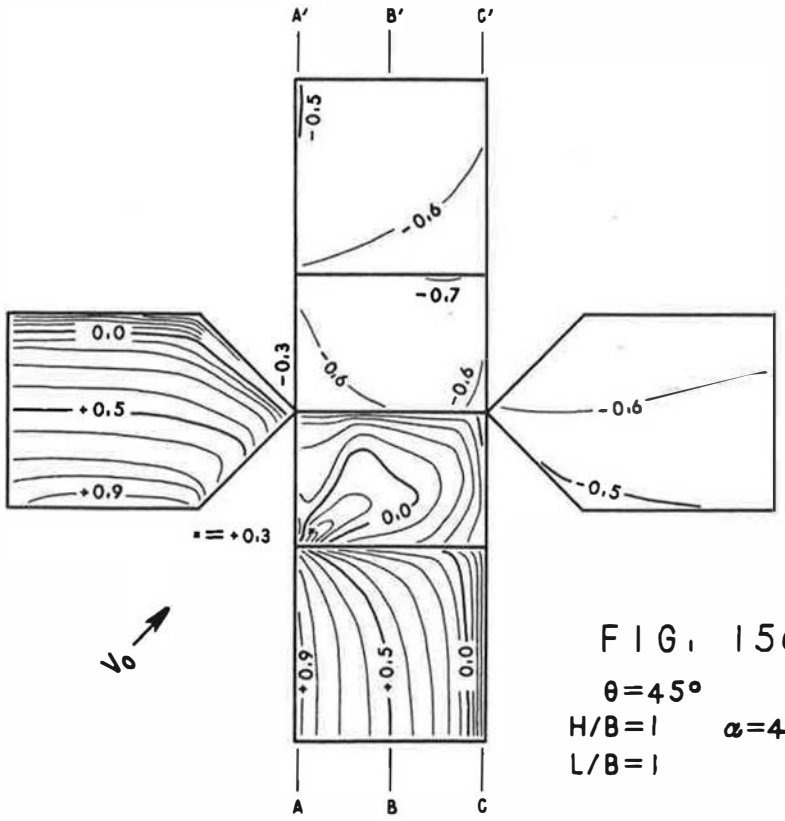

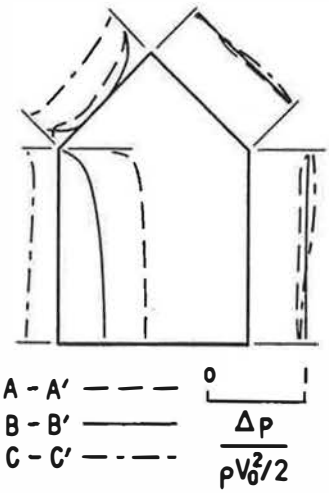

FIG. 156

$\theta = 45°$

H/B = 1 $\quad \alpha = 45°$

L/B = 1

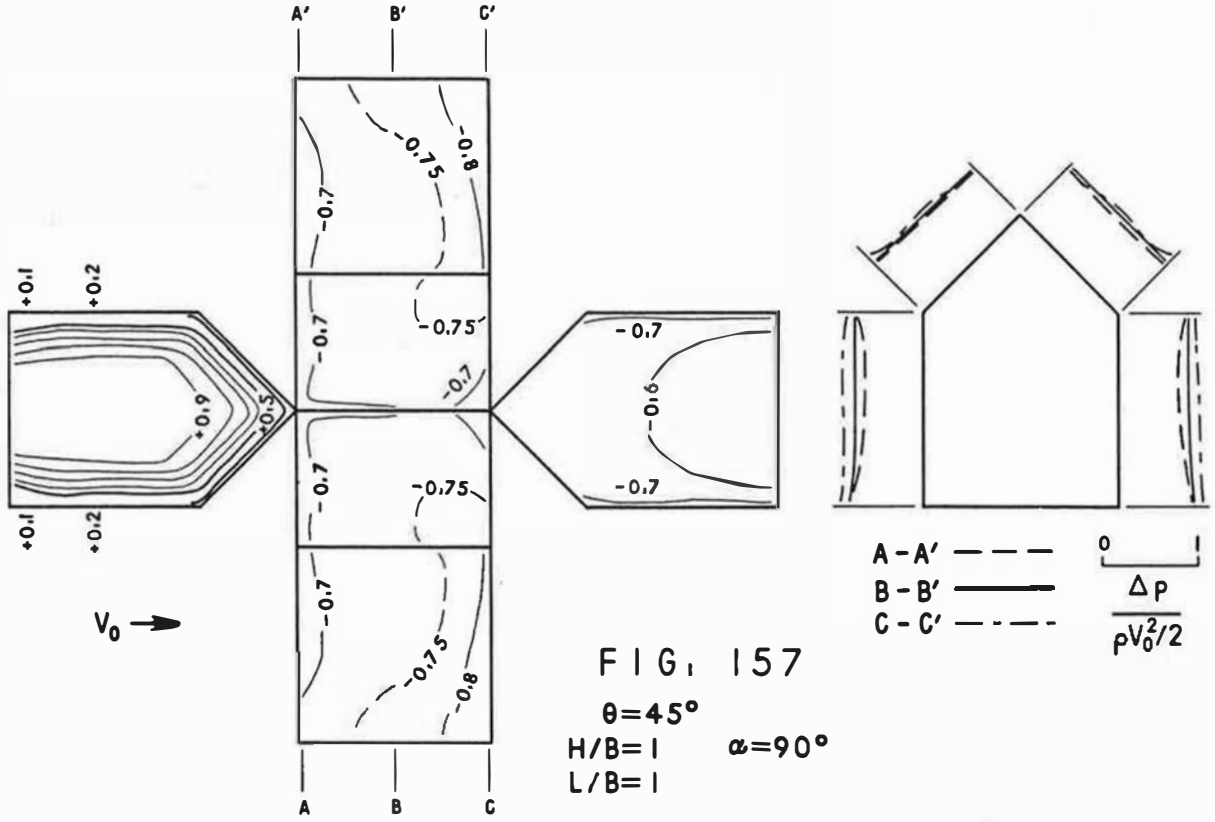

FIG. 157

θ=45°
H/B=1 α=90°
L/B=1

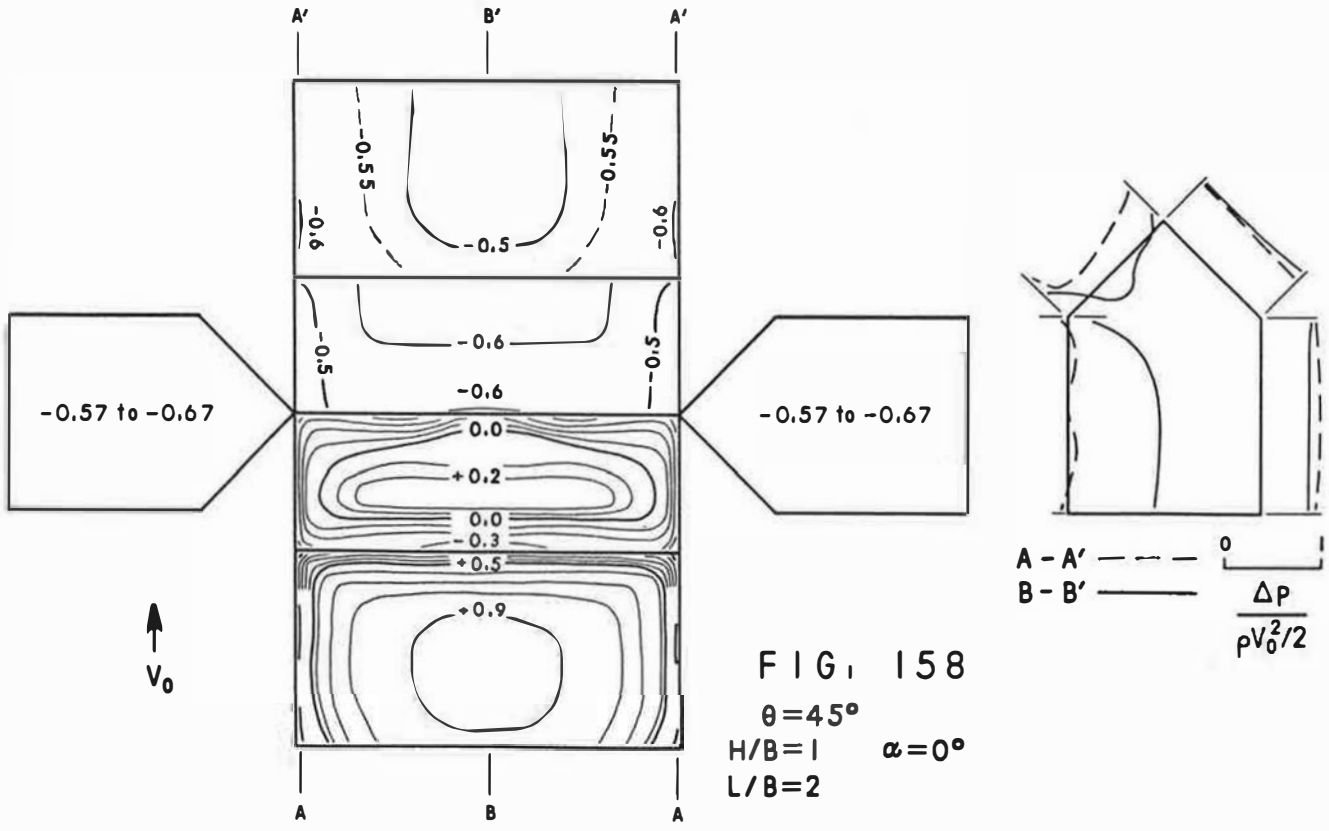

FIG. 158

θ=45°
H/B=1 α=0°
L/B=2

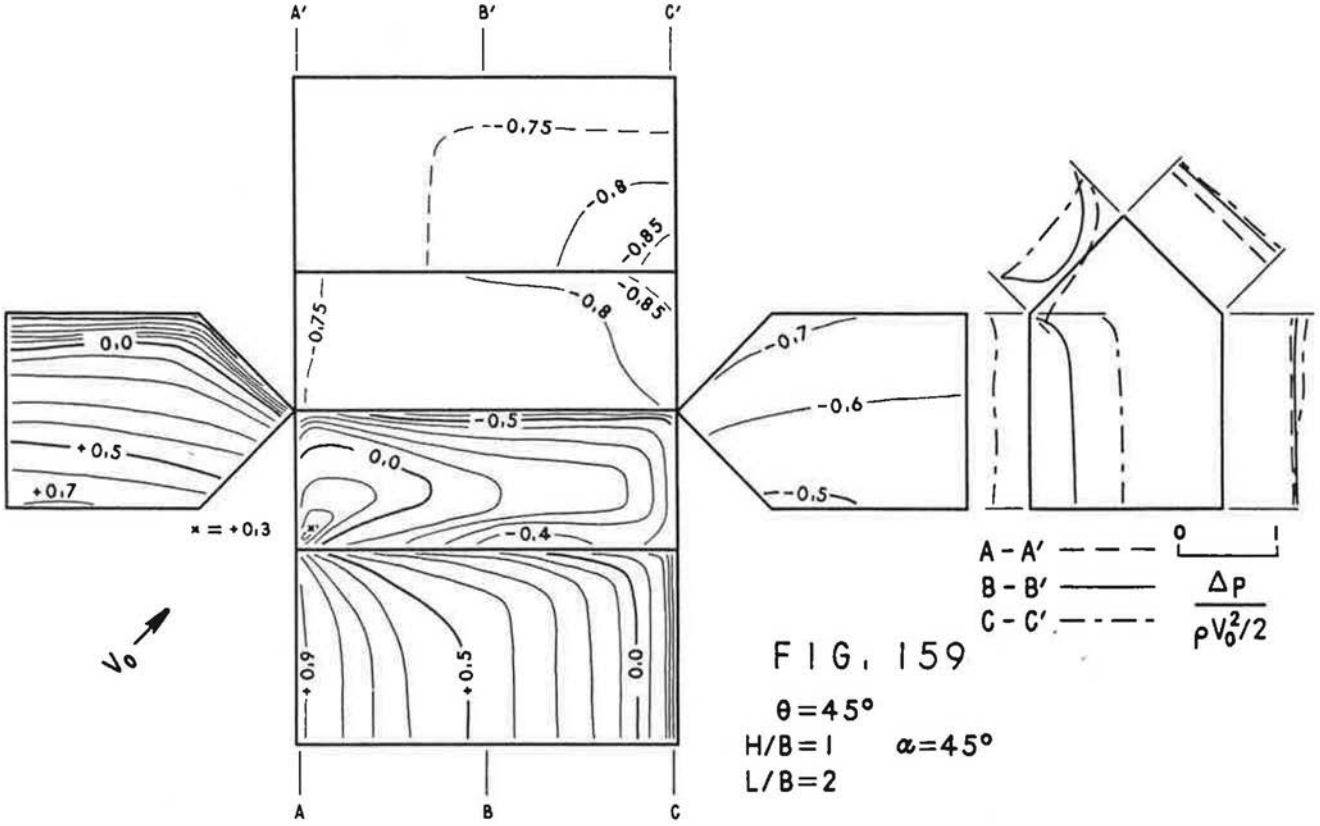

FIG. 159

θ=45°
H/B=1 α=45°
L/B=2

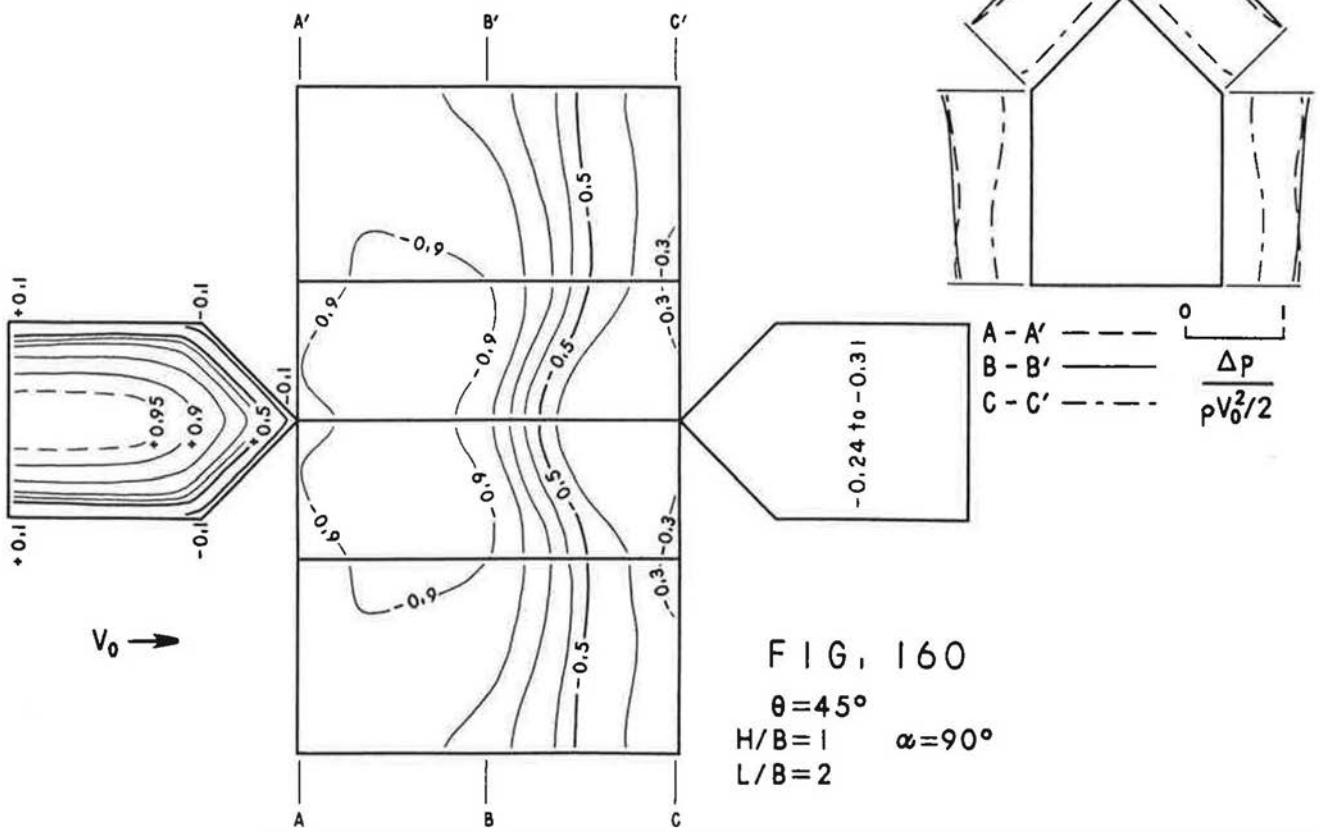

FIG. 160

θ=45°
H/B=1 α=90°
L/B=2

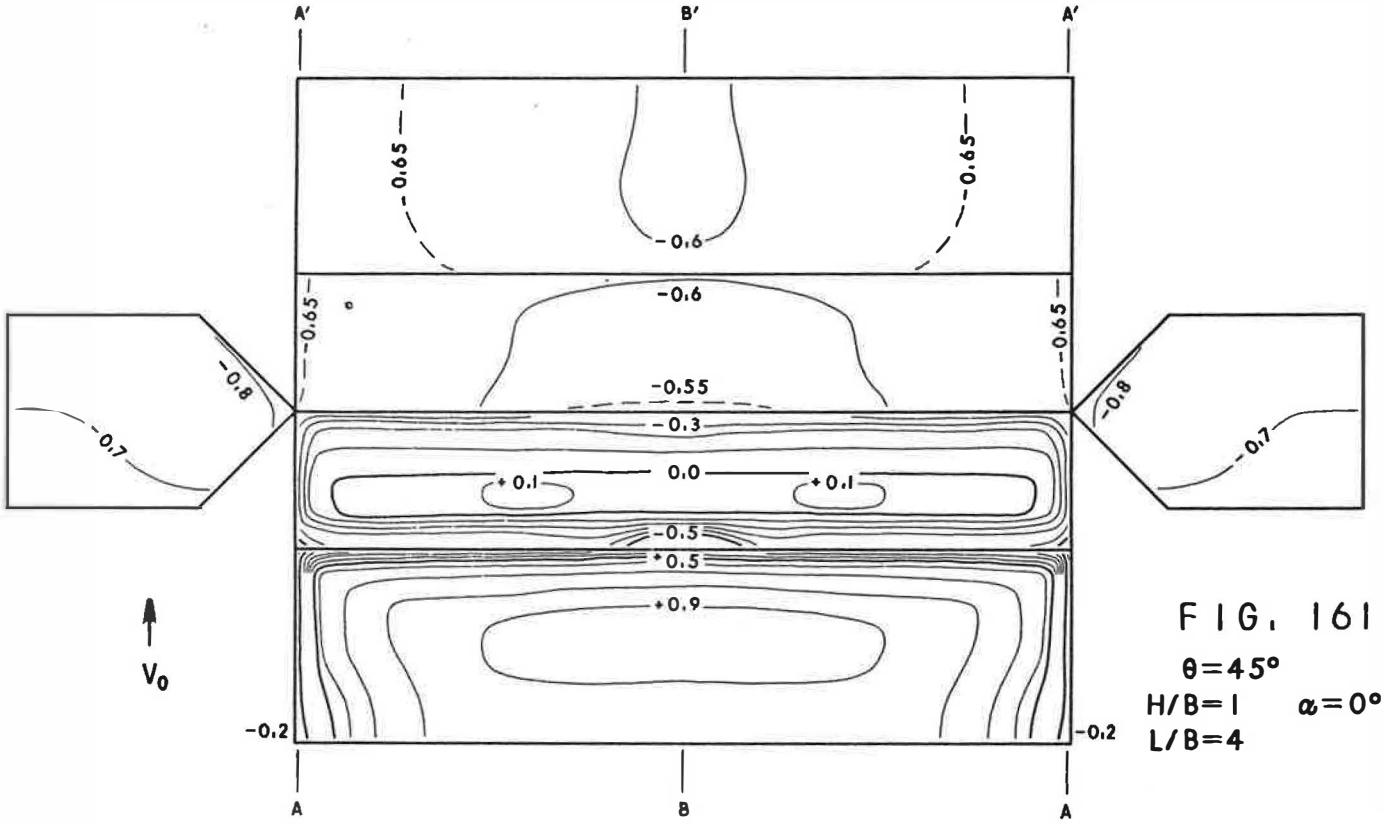

FIG. 161

$\theta = 45°$

$H/B = 1$ $\quad \alpha = 0°$

$L/B = 4$

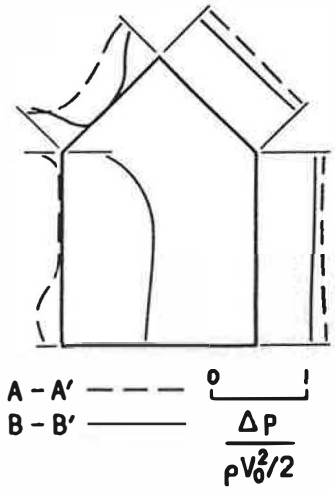

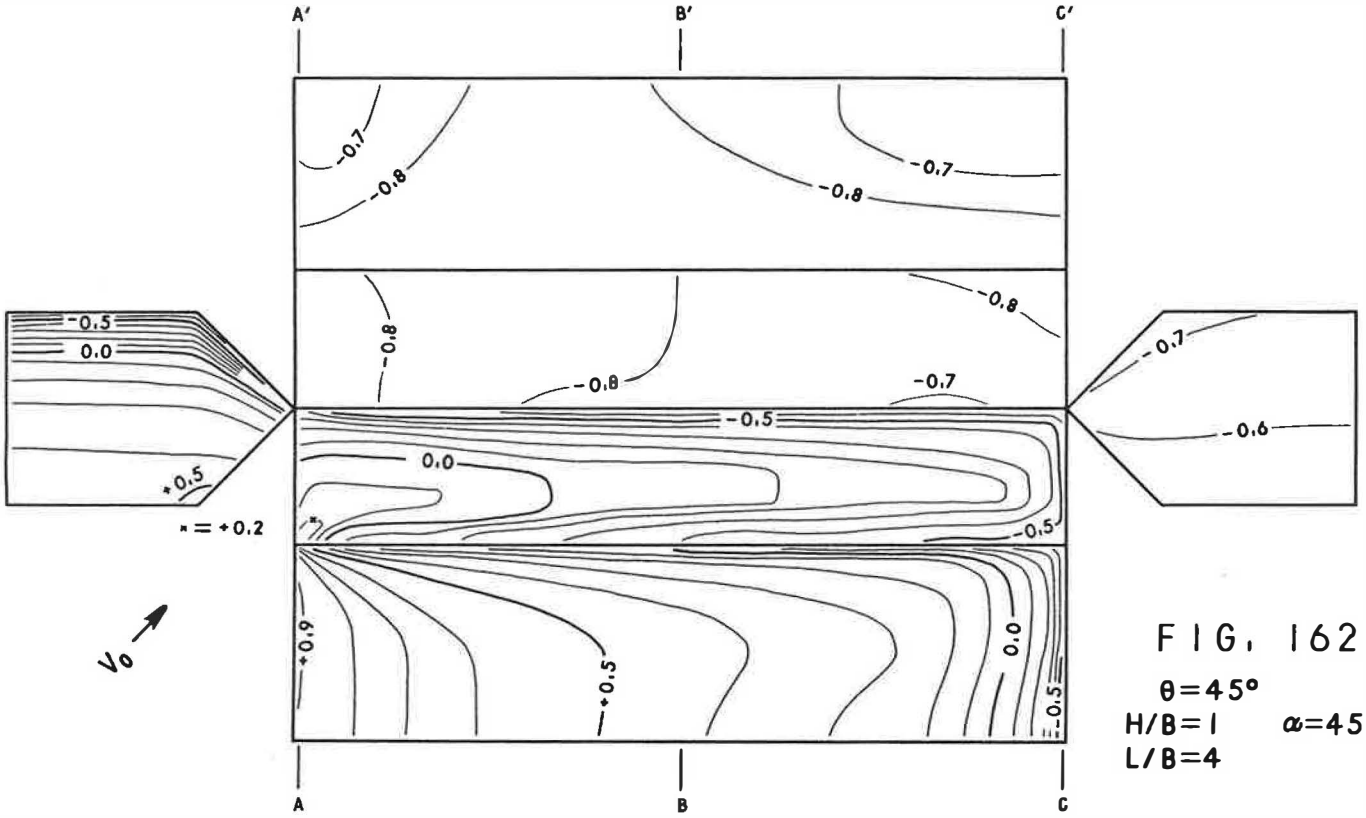

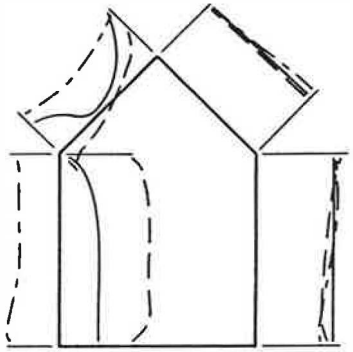

FIG. 162

θ=45°
H/B=1 α=45°
L/B=4

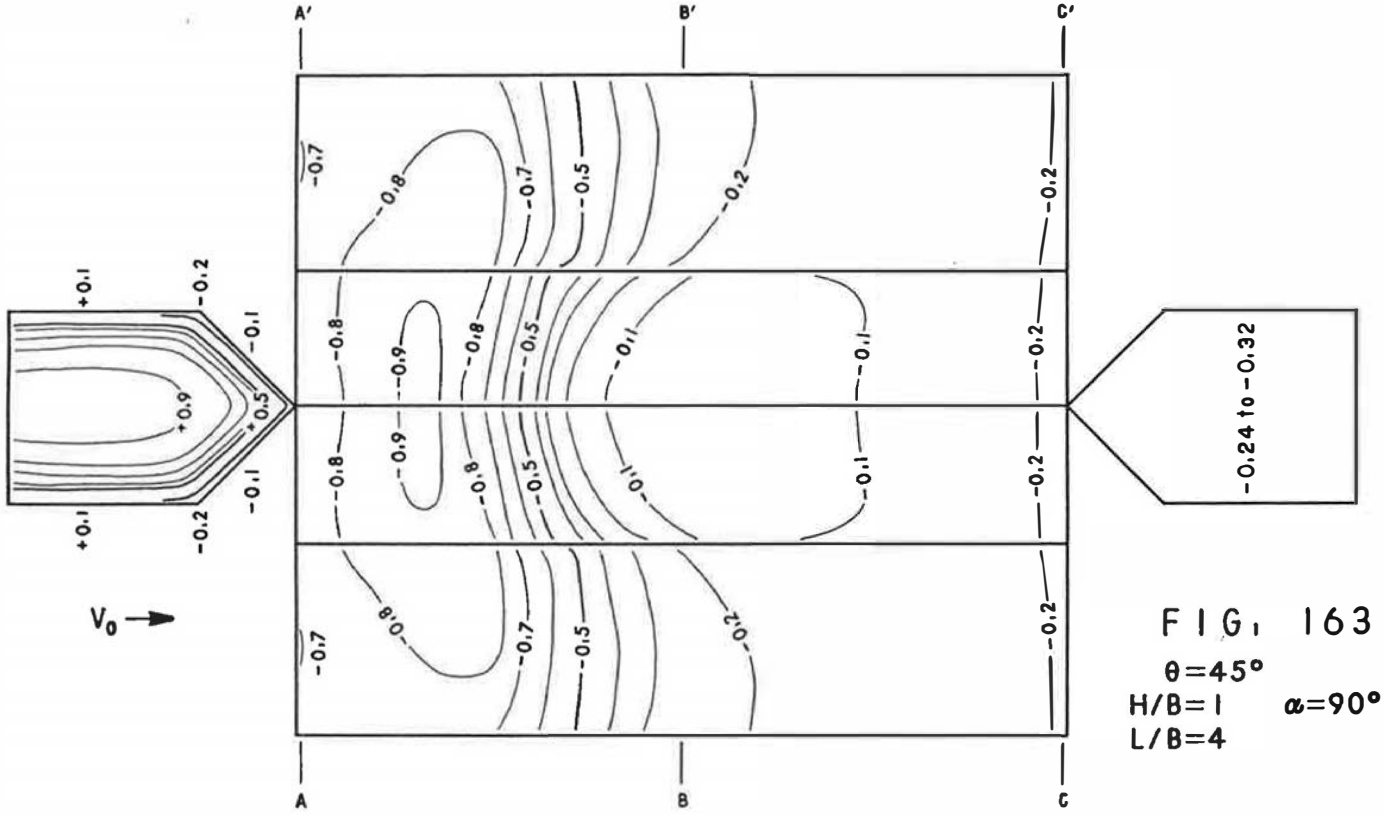

FIG. 163

θ=45°
H/B=1 α=90°
L/B=4

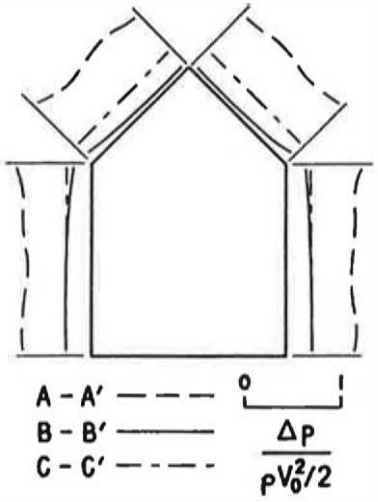

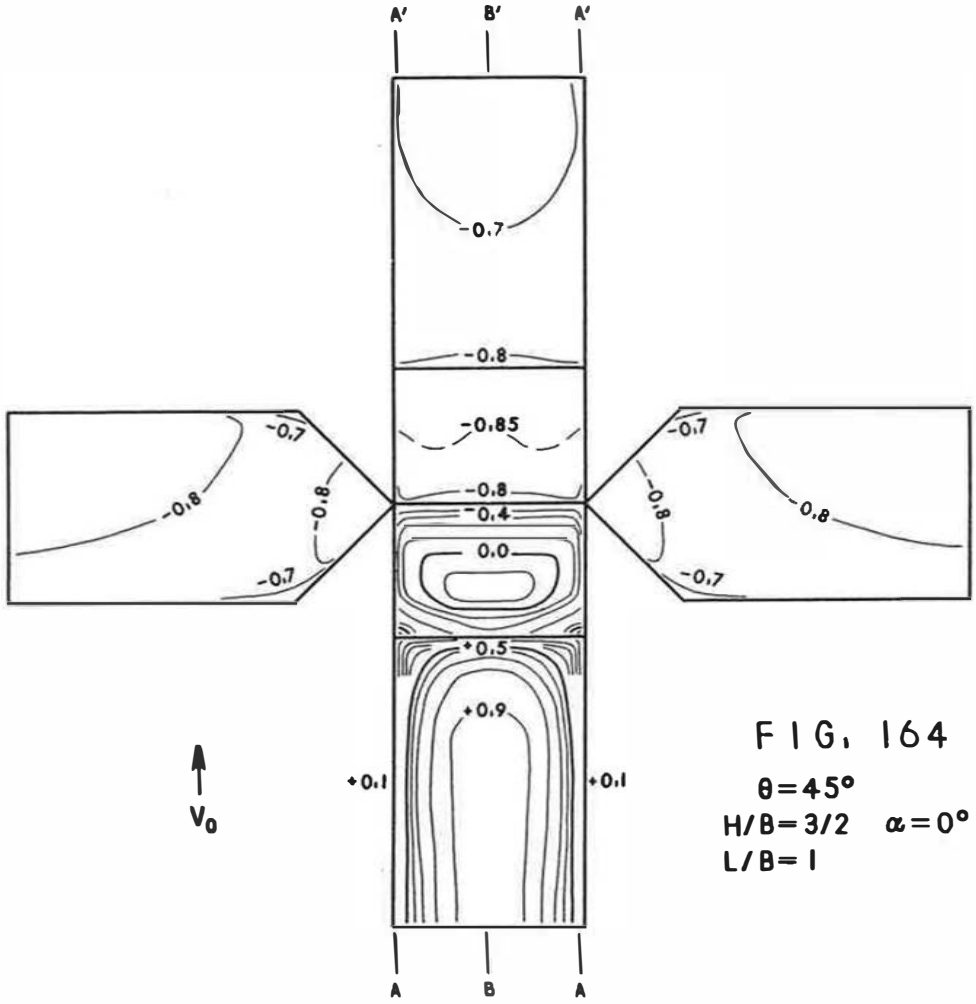

FIG. 164

$\theta = 45°$

$H/B = 3/2 \quad \alpha = 0°$

$L/B = 1$

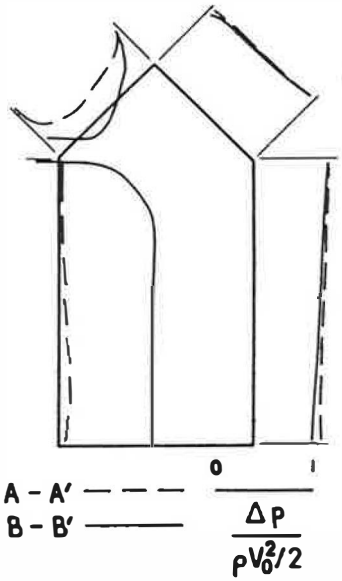

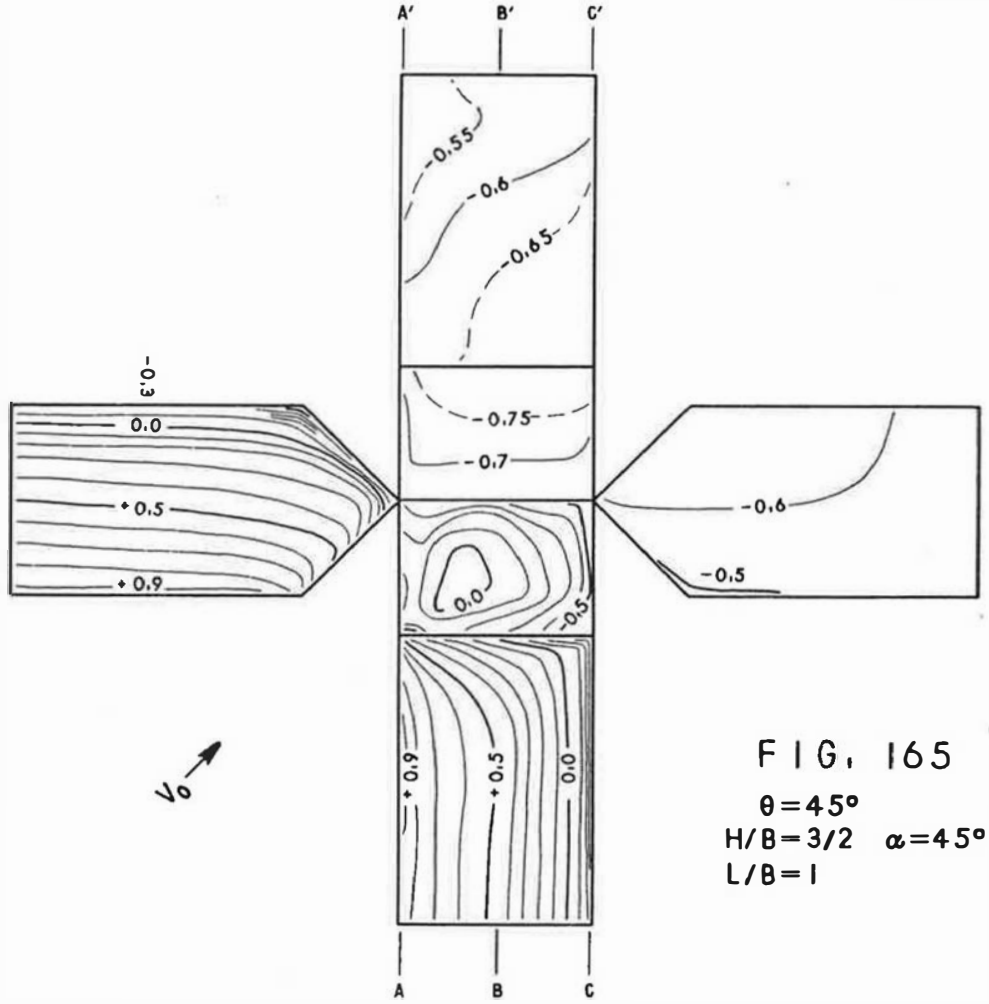

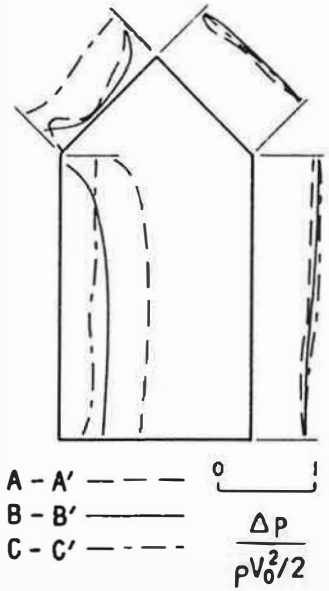

FIG. 165

$\theta = 45°$

$H/B = 3/2 \quad \alpha = 45°$

$L/B = 1$

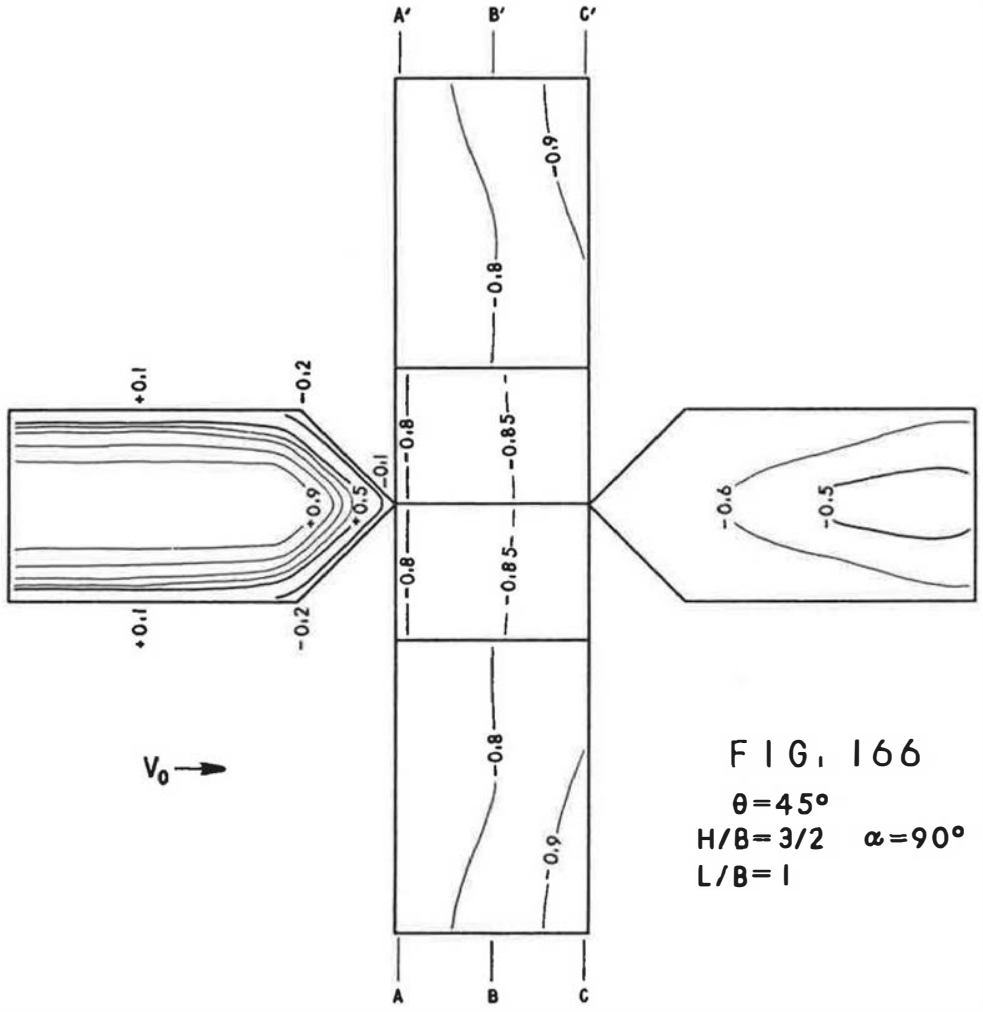

FIG. 166

$\theta = 45°$

$H/B = 3/2 \quad \alpha = 90°$

$L/B = 1$

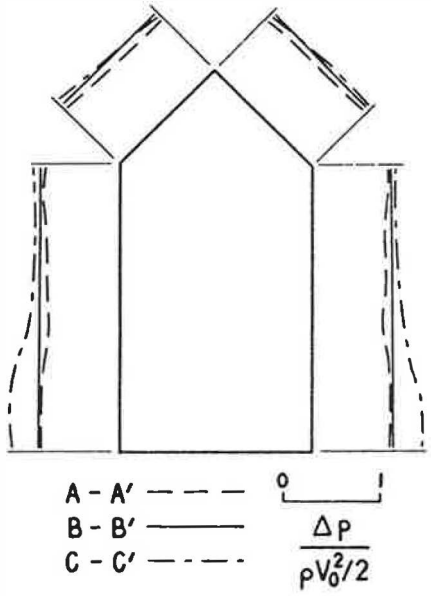

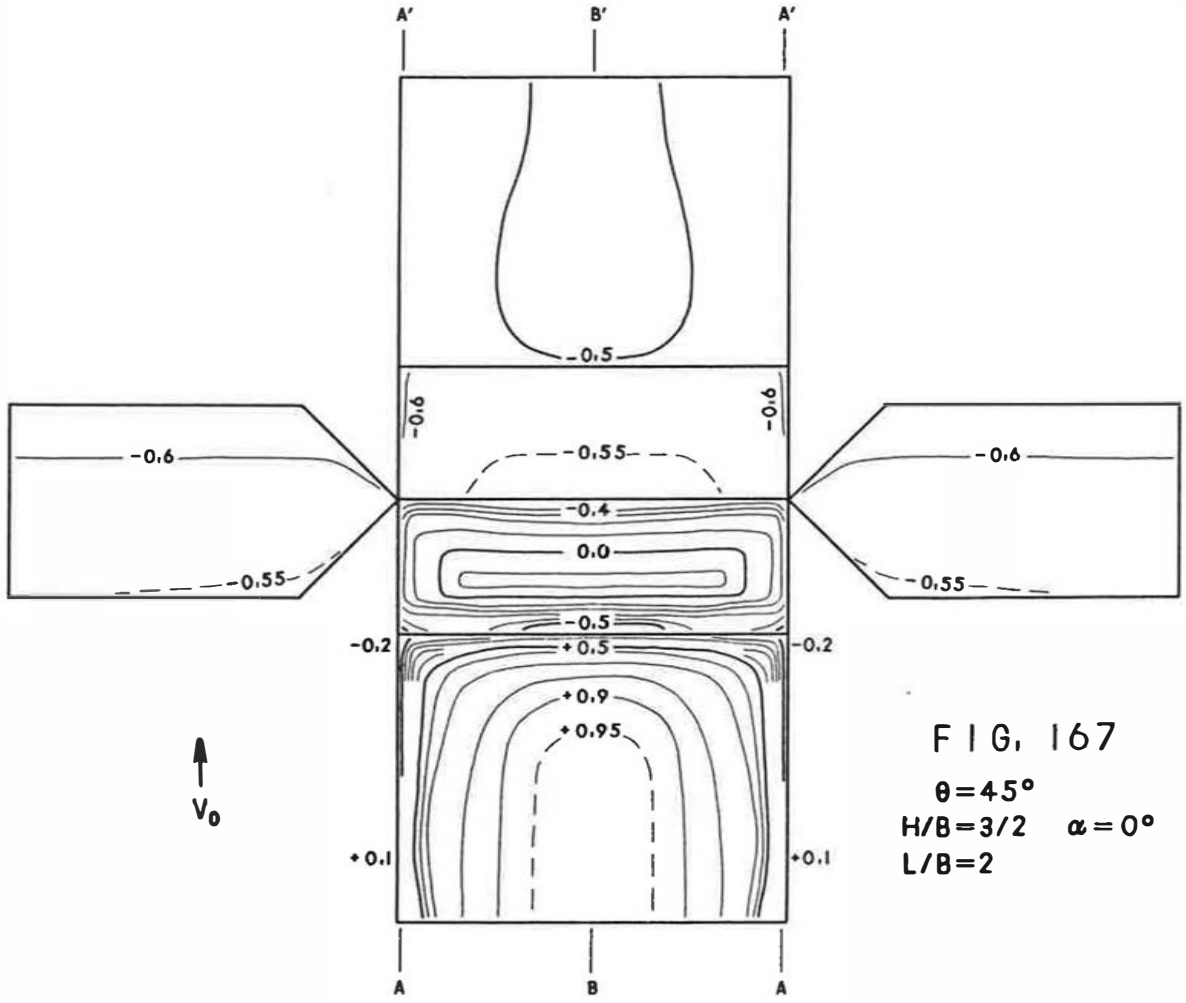

FIG. 167

θ=45°
H/B=3/2 α=0°
L/B=2

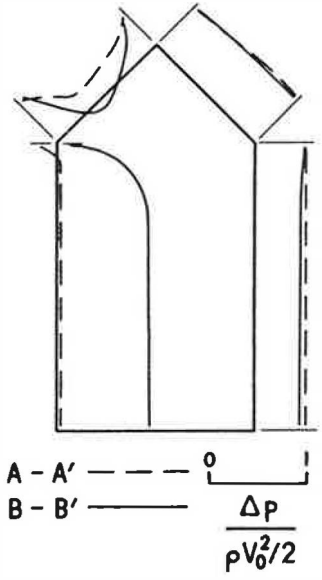

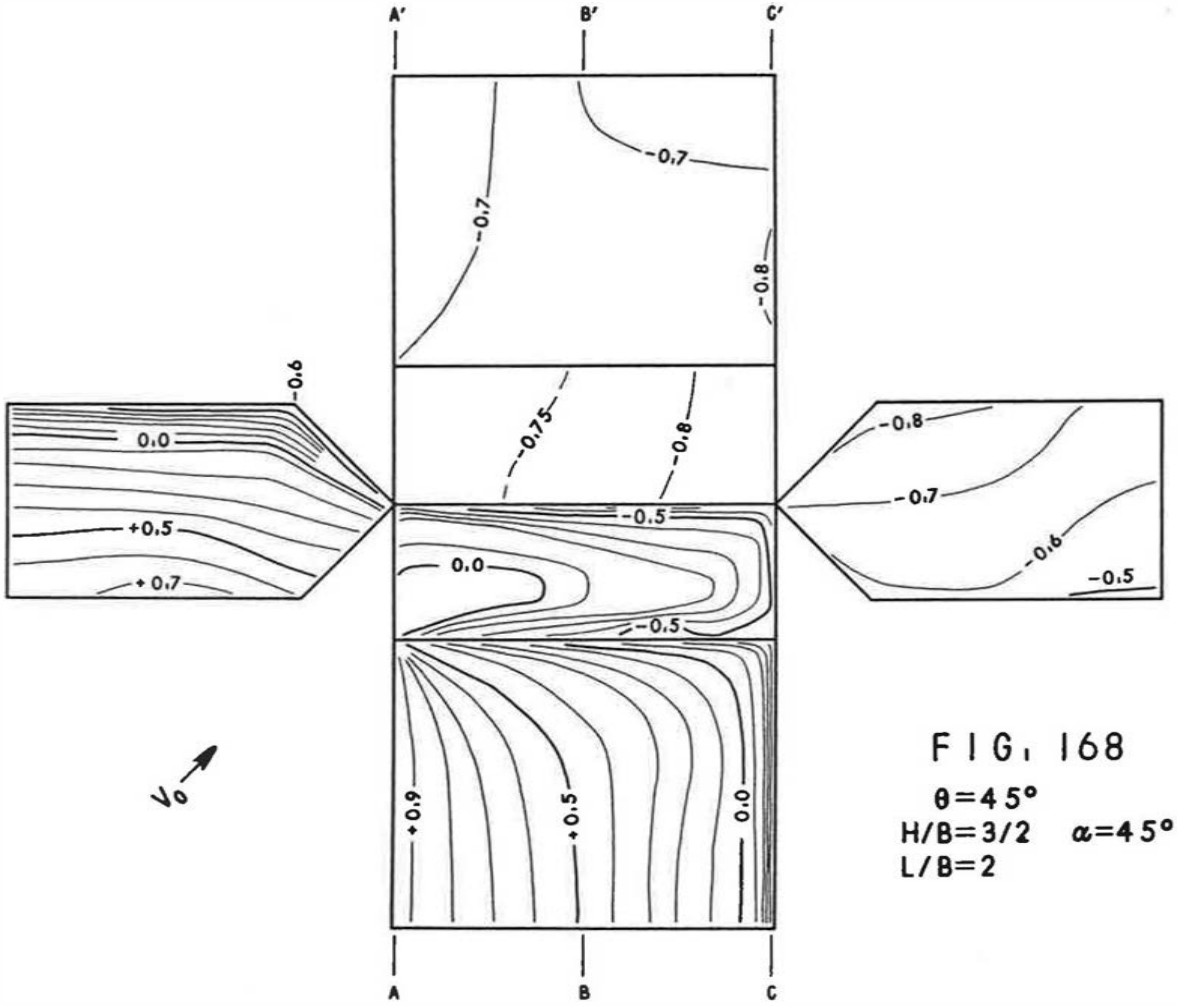

FIG. 168

θ=45°
H/B=3/2 α=45°
L/B=2

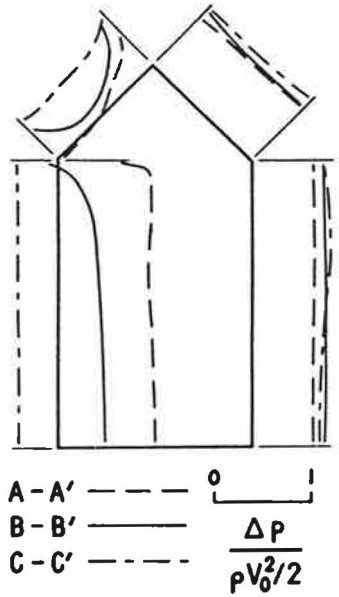

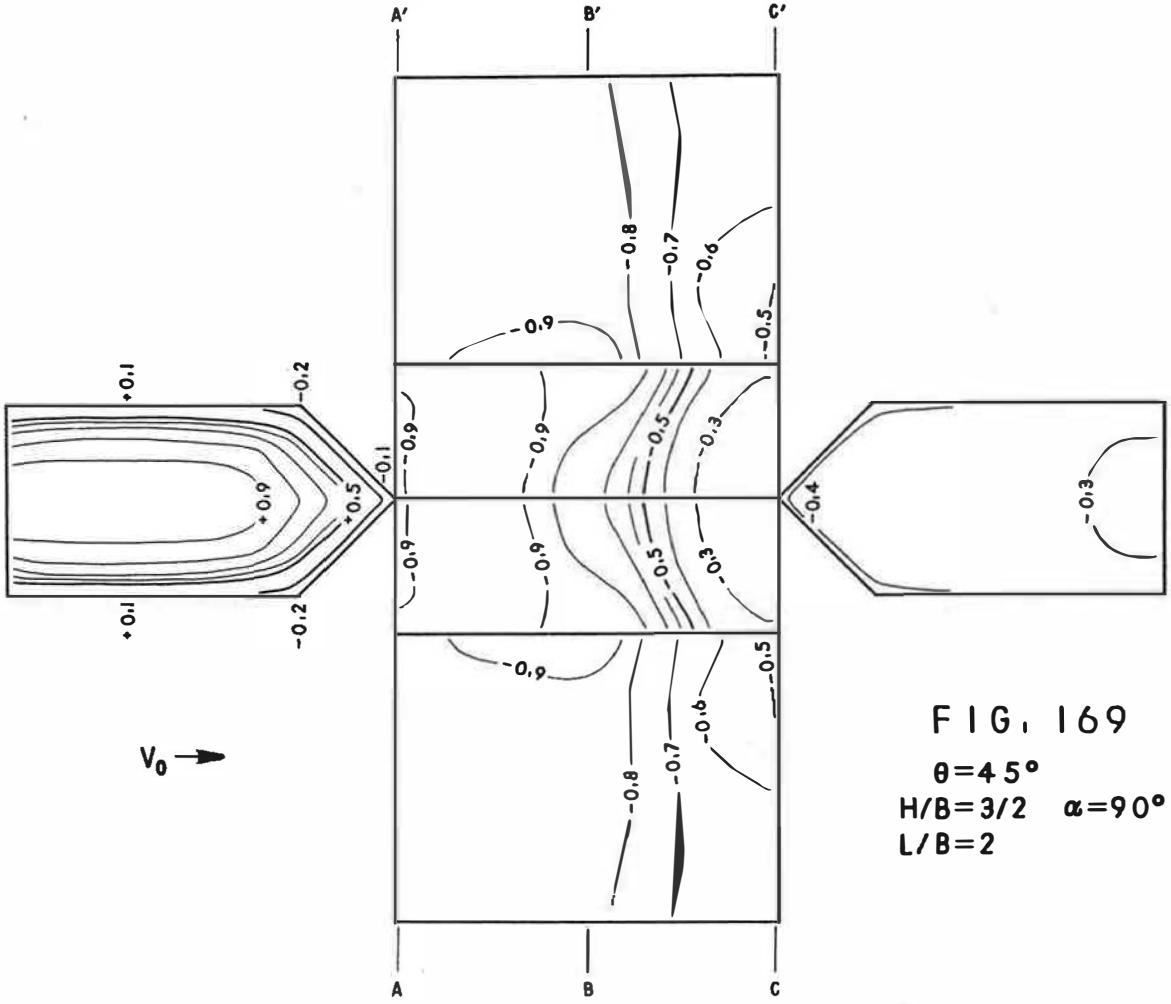

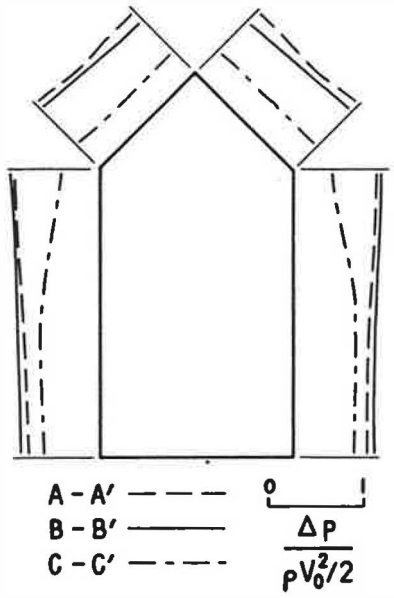

FIG. 169

θ=45°
H/B=3/2 α=90°
L/B=2

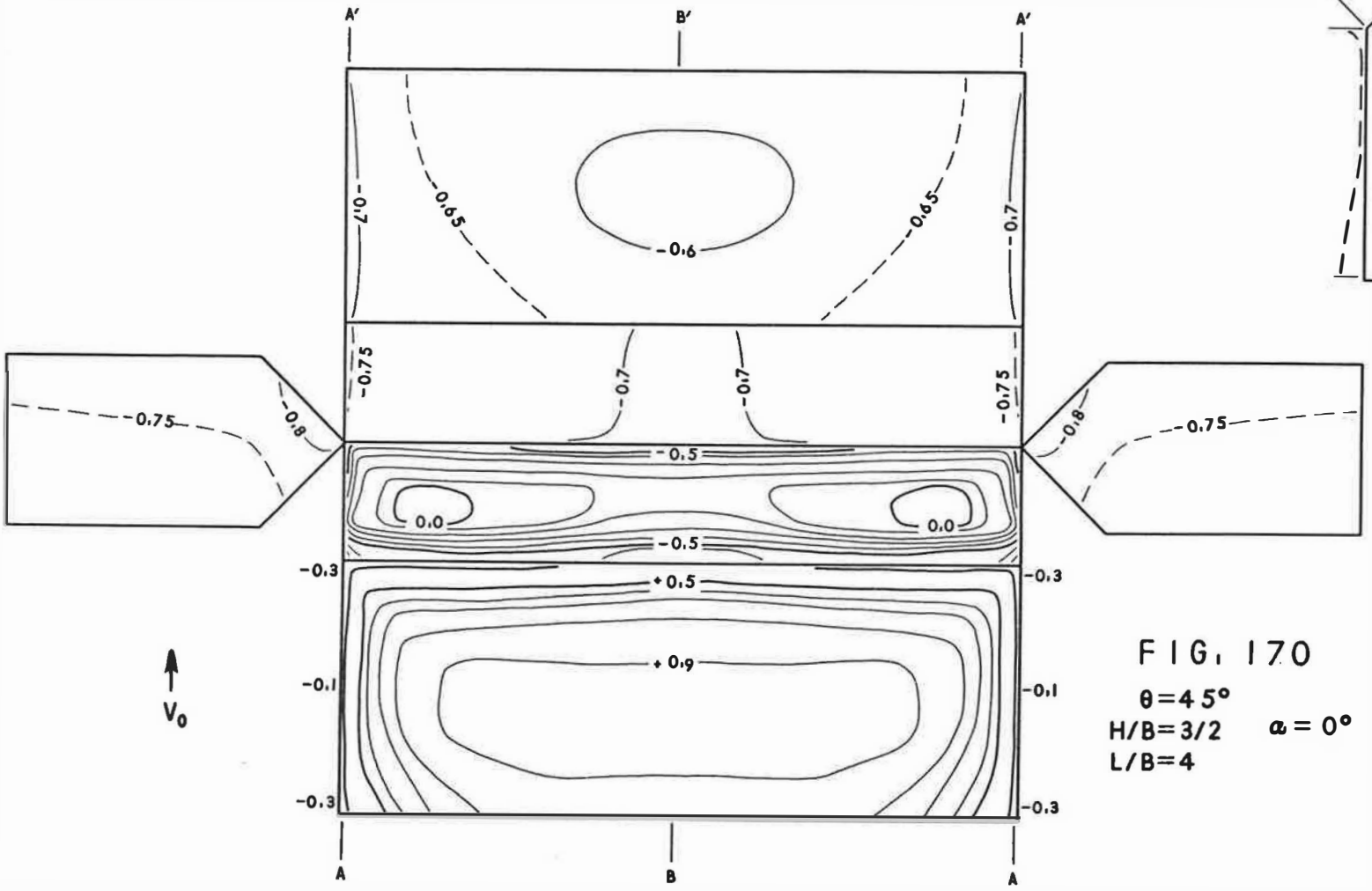

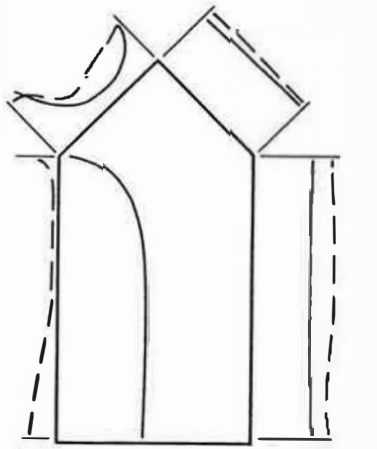

FIG. 170

$\theta = 45°$

H/B = 3/2 $\quad \alpha = 0°$

L/B = 4

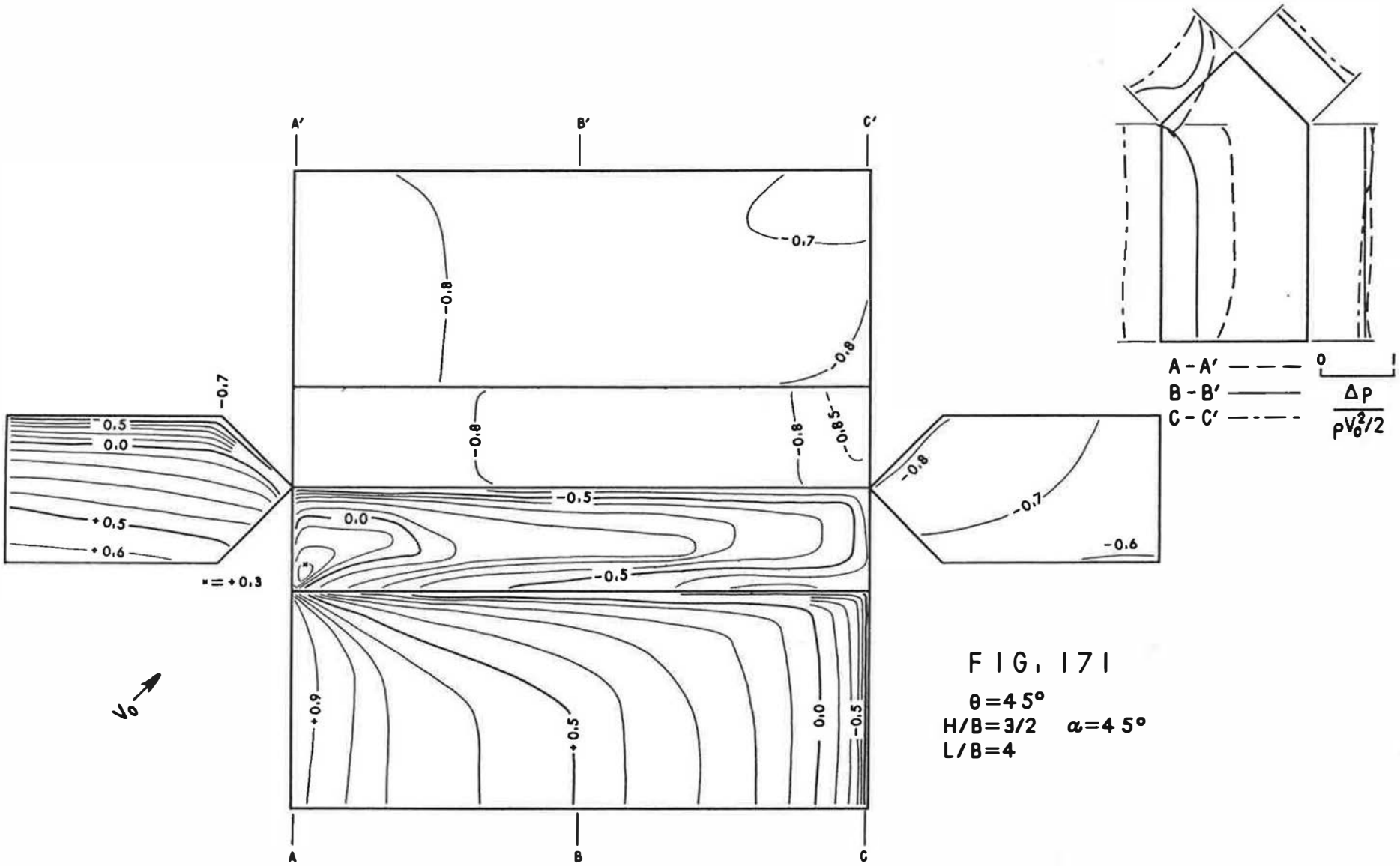

FIG. 171

θ=45°
H/B=3/2 α=45°
L/B=4

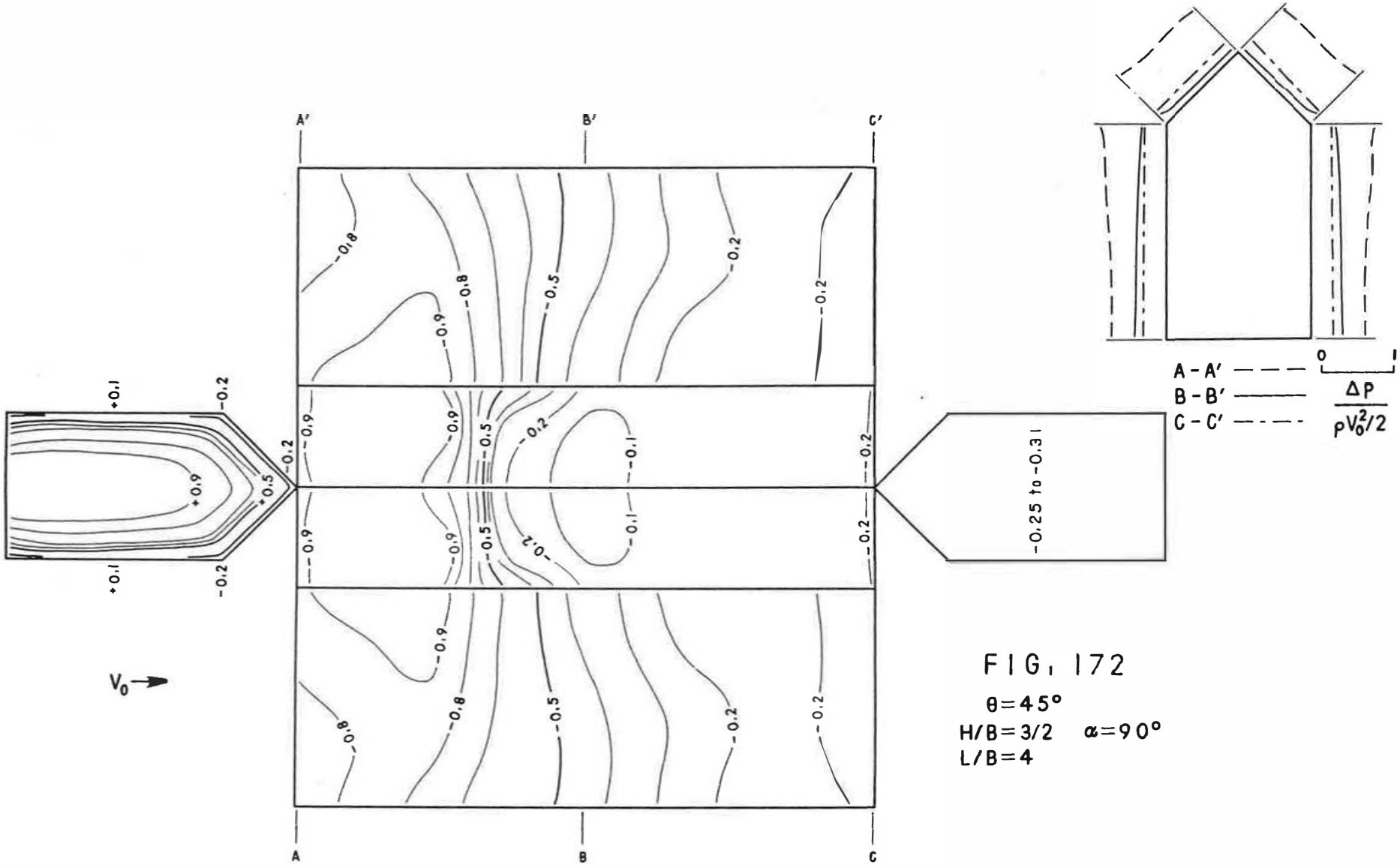

FIG. 172

$\theta = 45°$

$H/B = 3/2 \quad \alpha = 90°$

$L/B = 4$

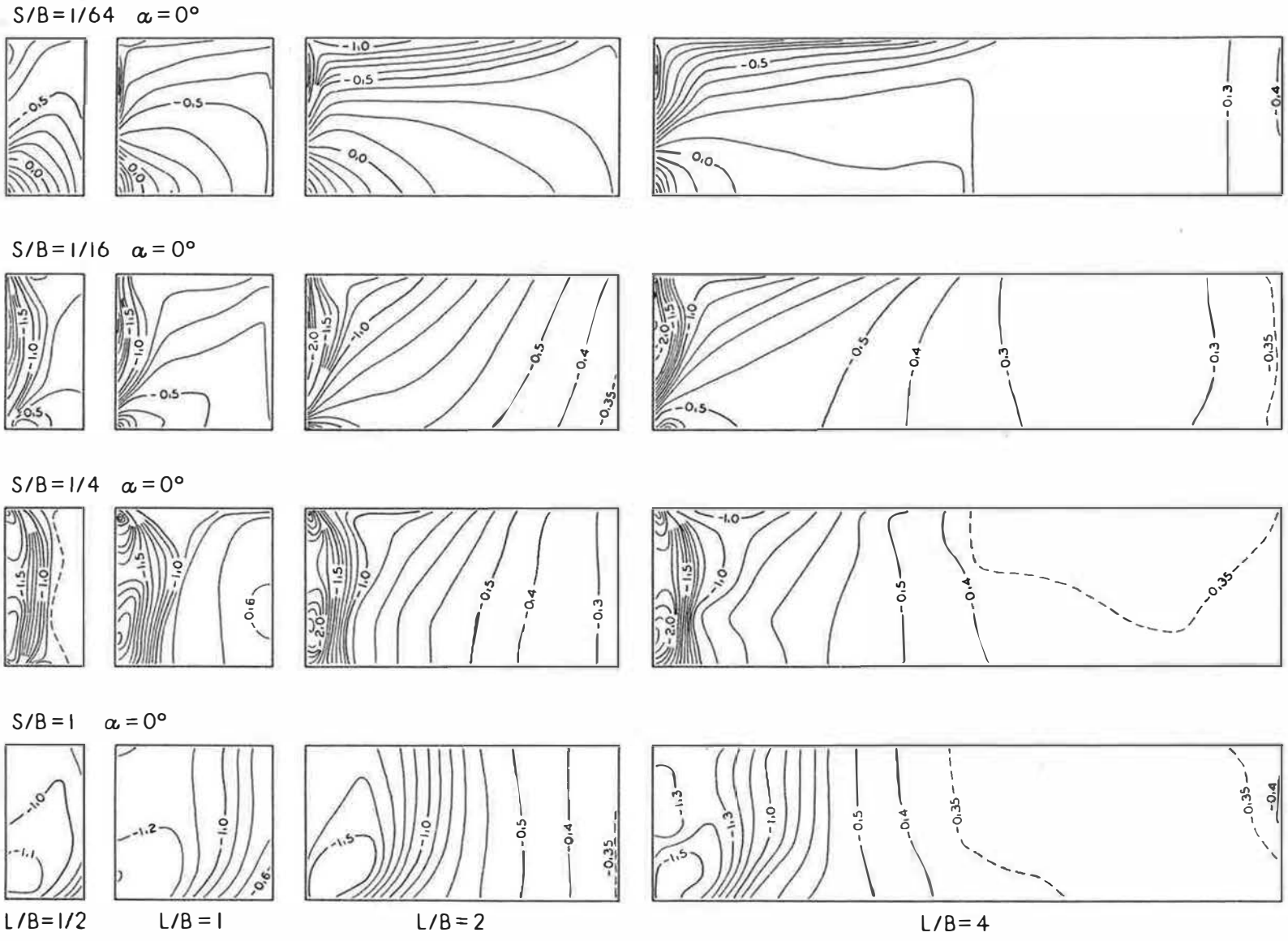

FIG. 173 Typical Pressure Distributions $\frac{\Delta p}{\rho V_0^2/2}$ on Facing Walls of Two Parallel Identical Flat-Roofed Rectangular Buildings (B=H) at Various Degrees of Separation S/B

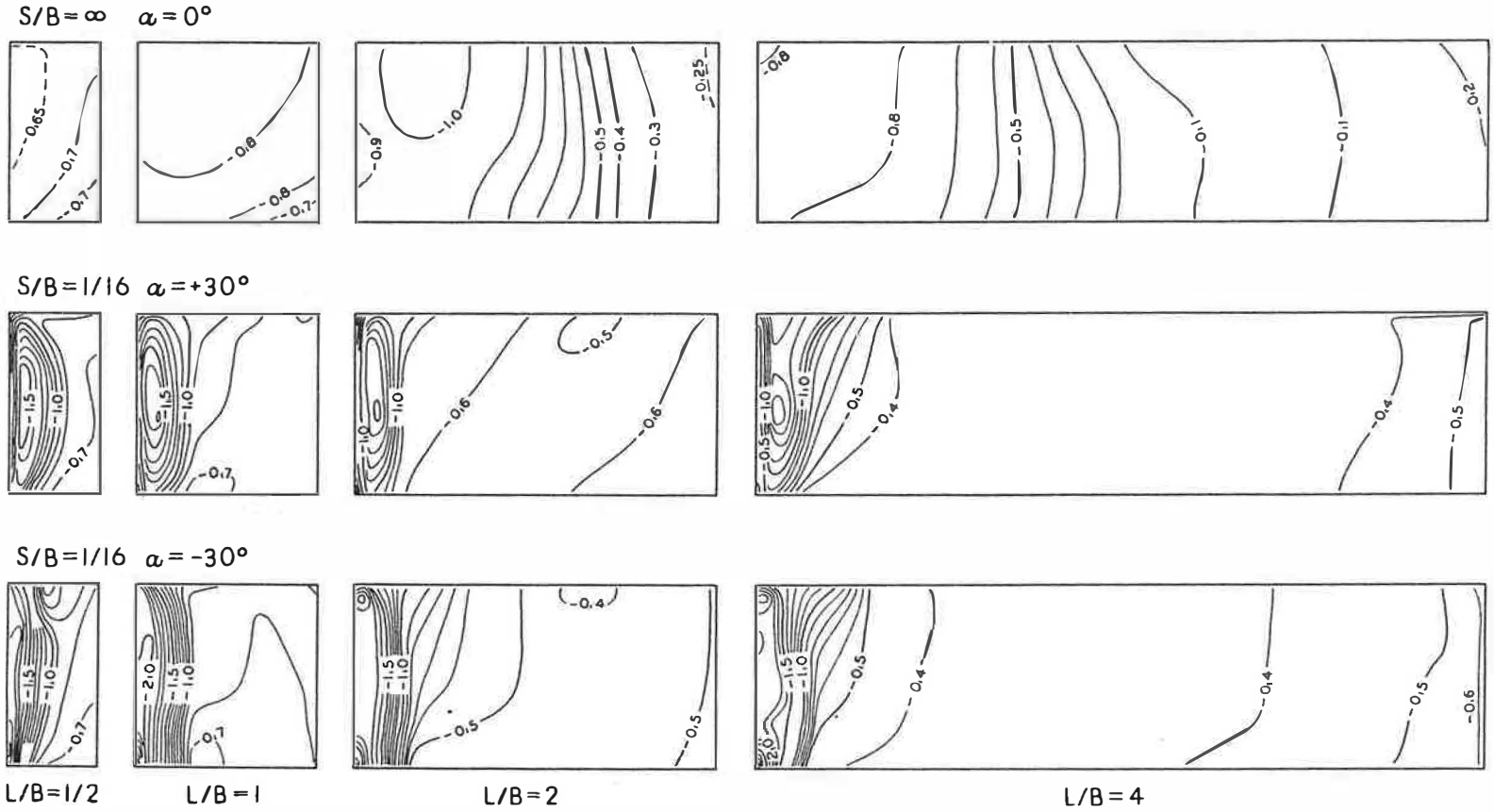

FIG. 173 (Continued)